Unraveling the potential of cold-water carbonates as geochemical archives for paleoceanographic reconstructions

Proxies, vital effects and parasites

Dissertation zur Erlangung des Doktorgrades der Naturwissenschaften

vorgelegt beim Fachbereich 11 der Goethe Universität in Frankfurt am Main

von Nicolai Schleinkofer aus Groß-Umstadt

Frankfurt am Main, 2021

vom Fachbereich 11 der Goethe Universität als Dissertation angenommen.

Dekan: Prof. Dr. Georg Rümpker

Gutachter: PD. Dr. Jacek Raddatz, Goethe Universität Frankfurt am Main, Deutschland

und

Prof. Dr. André Freiwald, Senkenberg am Meer Wilhelmshaven, Deutschland

Datum der Disputation:

Table of content

List of figures

List of tables

List of equations and reactions

List of abbreviations

CWC	Cold-water coral
WWC	Warm-water coral
MIS	Marine isotopic stage
ROV	Remotely operated vehicle
POM	Particulate organic matter
POC	Particulate organic carbon
XANES	X-ray absorption near-edge structure spectroscopy
ECF	Extracellular calcifying fluid
DIC	Dissolved inorganic carbon
CAM	Crassulaceen Acid Metabolism
MS	Mass spectrometer
EI	Electron impact ionization
ICP-OES	Inductively coupled plasma optical emission spectroscopy
LA-ICP-MS	Laser ablation inductively coupled mass spectrometer
GS-MS	Gas source mass spectrometer
sp. nov.	Species nova = new species
XRD	X-ray diffraction
INL	Intermediate nepheloid layer
VE water	Deionized water
MQ water	MilliQ Water = Ultrapure water
PPM	Parts per million
PPB	parts per billion
D_E	Distribution coefficient of element E (Mg, Na, Sr, etc.)

Abstract

Deutsch

Geochemische Untersuchungen an biogenen Karbonaten werden häufig verwendet um Umweltparameter in der Vergangenheit zu rekonstruieren. Diese Untersuchungen werden durch „Vital Effekte" erschwert, die durch biologische Prozesse der untersuchten Organismen ausgelöst werden. Erkennung und Quantifizierung dieser Effekte ist eine Voraussetzung für zuverlässige Rekonstruktionen. Um das Verständnis über den derzeitigen Klimawandel zu erweitern sind entsprechende Untersuchungen unerlässlich, aber auch um die Verteilung bestimmter Organismengruppen in der Vergangenheit zu untersuchen. Aus diesen Informationen können Strategien zum Schutz dieser Organismen abgeleitet werden. In Kapitel drei haben wir untersucht wie Mg/Ca, Na/Ca und Sr/Ca Verhältnisse in Kaltwasser Korallen auf Umwelteinflüsse und biologische Prozesse regieren. Eine Beeinflussung von Mg/Ca oder Sr/Ca Verhältnissen durch Temperatur, Salinität oder pH-Wert konnte nicht festgestellt werden. Dagegen konnte eine inverse Korrelation zwischen Na/Ca Verhältnissen und Temperatur nachgewiesen werden. Diese Korrelation existiert in ähnlicher Form in der Warmwasser Koralle *Porites* sp. als auch in der Bivalve *Mytilus edulis.* Allerdings erschwert die große Variabilität eine sinnvolle Nutzung als Temperaturproxy. Die gefundene Korrelation könnte durch temperaturabhängige Natriumpumpen erklärbar sein, was wir mit verschiedenen Modellen untersuchen.

Neben der Kaltwasser Koralle *Desmophyllum pertusum,* ist die Bivalve *Acesta excavata* häufig in Kaltwasser Korallenriffen anzutreffen. Durch multiple lineare Regressionsanalyse konnte gezeigt werden, dass bis zu 79 % der Variabilität der Mg/Ca, Sr/Ca und Na/Ca Verhältnisse in *A. excavata* durch Temperatur und Salinität erklärbar sind. Jedoch, verhindern Vitaleffekte, ausgelöst durch variable Wachstumsraten und möglicherweise Stress, die Verwendung als Proxy. Weiterhin können organische Ablagerungen im Karbonat die Elementverhältnisse stark beeinflussen. Eine oxidative Entfernung dieser Ablagerungen durch H_2O_2 war nicht möglich. Jedoch wurden die Na/Ca Verhältnisse durch diese Behandlung verringert.

Die beiden untersuchten Spezies *D. pertusum* und *A. excavata* werden häufig von der parasitären Foraminifere *Hyrrokkin sarcophaga* befallen. In Kapitel Fünf haben wir untersucht wie die Geochemie dieser Foraminiferen von der Wirt-Spezies abhängig ist. Erhöhte Sr/Ca Verhältnisse in Foraminiferen, die auf *D. pertusum* parasitierten konnten festgestellt werden. Dies wird wahrscheinlich durch die Aufnahme von Sr-reichem Aragonit aus der Koralle ausgelöst. Weiterhin konnten erhöhte Mn/Ca Verhältnisse in Foraminiferen gemessen werden, die auf *A. excavata* parasitierten aber noch nicht die Schale durchbohrt hatten. Dies ist durch einen Wechsel der Ernährungsstrategie der Foraminiferen zu erklären.

Ohne Zugang zum inneren Weichkörper der Muschel müssen sich die Foraminiferen aus einer anderen Quelle ernähren, wie z.B. durch das Mn und Fe reiche Periostracum auf der Außenseite der Muschelschale. Neben den Elementverhältnissen konnte auch eine Beeinflussung der Sauerstoff- und Kohelstopffisotopie nachgewiesen. Auch dies könnte durch die Aufnahme des spezifischen Karbonates vom Wirt ausgelöst werden oder durch verschiedene pH-Werte der durch *H. sarcophaga* aufgenommenen Flüssigkeiten aus dem Wirt. Dadurch kann die Rate der Hydroxilations-/Hydrationsreaktion beeinflusst werden. Ungenaue Bestimmung der Wirt-spezies von *H. sarcophaga* könnte somit zu falschen Rekonstruktionen mithilfe von Sauerstoffisotopen, Sr/Ca und Mn/Ca Verhältnissen führen.

Veränderungen der Chemischen Zusammensetzung von marinen Karbonaten kann nicht nur durch Vitaleffekte ausgelöst werden, sondern auch Lagerungstechniken nach der Beprobung. Lagerung in Ethanol wird häufig verwendet um den Weichkörper und DNA zu erhalten. Jedoch verursacht diese Lagerung bereits nach 45 Tagen eine Reduktion von Mg/Ca und Na/Ca Verhältnissen. Sr/Ca Verhältnisse dagegen werden nicht verändert.

Neben Temperatur und Salinität ist auch die Nährstoffkonzentration von großer Bedeutung um Zusammenhänge zur Verteilung der verschiedenen Spezies zu untersuchen. In Kapitel sieben ergänzen wir unsere Untersuchung an *A. excavata* um Ba/Ca, P/Ca und Mn/Ca Verhältnisse. Dabei konnten regelmäßige Abfolgen von Peaks in Ba/Ca, Mn/Ca und P/Ca Verhältnissen nachweisen, die wahrscheinlich durch sequentielle Blüten verschiedener Algen, Diatomeen und anderer Mikroorganismen ausgelöst werden. Weiterhin vermuteten wir, durch P/Ca Verhältnisse, eine einfache Erkennung von Wachstumsinkrementen zu erreichen. Diese Theorie musste jedoch verworfen werden.

Die Untersuchung an *H. sarcophaga* konnten durch die Messung von B/Ca Verhältnissen und der Bor Isotopie erweitert werden um die Theorie der Aufnahme von Flüssigkeiten mit verschiedenen pH-Werten zu überprüfen. Jedoch konnten keine signifikanten Unterschiede in der Bor Isotopie zwischen *H. sarcophaga* von verschiedenen Hosts festgestellt werden. Dies schließt jedoch nicht zwangsläufig aus, dass der oben genannte Transfer von Flüssigkeiten stattfindet, da verschiedene Mechanismen wie die Diffusion von Borsäure zu einer Angleichung der pH-Werte führen kann.

English

Geochemical investigations on biogenic carbonates are commonly conducted to reconstruct the environmental conditions of the past. However, different carbonate producers incorporate elements to varying degrees, due to biological vital effects. Detecting and quantifying these effects is crucial to produce reliable reconstructions. These paleoreconstructions are of great importance to evaluate the consequences of our recent climate change and identify control mechanisms on the distribution of endangered species such as *Desmophyllum pertusum.* In chapter three we tested Mg/Ca, Sr/Ca and Na/Ca ratios on this species, among other cold-water scleractinians, to test if they provide reliable proxy information. The results reveal no apparent control of Mg/Ca or Sr/Ca ratios through seawater temperature, salinity or pH. Na/Ca ratios appear to be partly controlled by the seawater temperature, which is also true for other aragonitic organisms such as warm-water corals and the bivalve *Mytilus edulis*. However, a large variability complicates possible reconstructions by means of Na/Ca. In addition, we explore different models to explain the apparent temperature effect on Na/Ca ratios based on temperature sensitive Na and Ca pumping enzymes.

The bivalve *Acesta excavata* is commonly found in cold-water coral reefs among the North Atlantic, together with *D. pertusum*. Multiple linear regression analysis, presented in chapter four, indicates that up to 79% of the elemental variability in Mg/Ca, Sr/Ca and Na/Ca is explainable with temperature and salinity as independent predictor variables. Vital effects, for instance growth rate effects, are evident and make paleoreconstructions not feasible. Furthermore, organic material embedded in the shell, as well as possible stress effects can drastically change the elemental composition. Removal of these organic matrices from bulk samples for LA-ICP-MS (laser ablation inductively coupled mass spectrometer) measurements by means of oxidative cleaning is not possible, but Na/Ca ratios decrease after this cleaning. This is presumably an effect of leaching and not caused by the removal of organic matrices.

Interesting biogeochemical relations were found in the parasitic foraminifera *H. sarcophaga.* We report Mg/Ca, Sr/Ca, Na/Ca and Mn/Ca ratios measured in *H. sarcophaga* from two different host species (*A. excavata* and *D. pertusum*) in chapter five. Sr/Ca ratios are significantly higher in foraminifera that lived on *D. pertusum*. This could indicate that dissolved host material is utilized in shell calcification of *H. sarcophaga*, given the naturally higher strontium concentration in the aragonite of *D. pertusum*. Mn/Ca ratios are highest in foraminifera that lived on *A. excavata* but did not fully penetrate the host's shell. Most likely, this represents a juvenile stadium of the foraminifera during which it feeds on the organic periostracum of the bivalve, which is enriched in Mn and Fe. The isotopic compositions are similarly affected, both $\delta^{18}O$ and $\delta^{13}C$ values are significantly lower in foraminifera that lived

on *D. pertusum* compared to specimen that lived on *A. excavata*. Again, this might represent the uptake of dissolved host material or different pH regimes in the calcifying fluid of the hosts (bivalve < 8, coral > 8) that control the extent of hydration/hydroxylation reactions. Temperature reconstructions are possible using stable oxygen isotopes on this foraminifera species; however, the results are only reliable if the foraminifera lived on *A. excavata*. Samples of *H. sarcophaga* from *D. pertusum* would lead to overestimations of the seawater temperature due to the lower $\delta^{18}O$ values.

Apart from biological vital effects, storage and preservation methods can significantly change the geochemical composition of different marine biogenic carbonates. In chapter six this is presented on the example of ethanol preservation, a common technique to allow extended storage of biogenic samples. The investigation reveals a significant decrease of Mg/Ca and Na/Ca ratios even after only 45 days storage in ultrapure ethanol. Sr/Ca ratios on the other hand are not influenced.

Besides temperature, salinity and pH further environmental parameters are important such as nutrient availability, especially for the distribution of cold-water corals. In chapter seven we extend the investigations on *A. excavata* by including the elemental ratios Ba/Ca, Mn/Ca and P/Ca. We expected P/Ca to be helpful in the otherwise difficult process of identifying growth increments. Based on our observations we had to refute this theory. P/Ca ratios are not systematically enriched in the vicinity of growth lines. Instead, we found a regular sequence of peaks of Ba/Ca, P/Ca and Mn/Ca. This sequence as well as the peaks in general are potentially caused by sequential blooms of different algae, diatoms and other planktonic organisms.

We also extended the investigations on *H. sarcophaga* with B/Ca and boron isotope measurements to test if the foraminifera record signals of different pH environments in the calcifying fluid of the host species. Significant differences in B/Ca ratios are evident, depending on the host species, but no differences in the boron isotopic composition were observable. The missing response in the boron isotopic composition does not necessarily exclude the possibility of different pH-regimes based on the host species. Gagnon et al., (2021) described a mechanism based on boric acid diffusion that can explain the missing response of boron ratios despite different pH regimes

1 Introduction

1.1 Aim of this study

Paleoenvironmental and -climatic reconstructions are the focus of many geoscientific studies. Understanding the ancient climate and the link to biological and geological processes are mandatory for the reconstruction of past ecosystem. Knowledge about the climate of the past allows us to study the effects of a changing climate on different ecosystems and construct preservation strategies. Furthermore, precise reconstructions of the past climate generates valuable data that can be used to train machine learning models and consequently predict the future climate. This is essential to understand the consequences of the recent climate change we are facing and create strategies to alleviate these consequences.

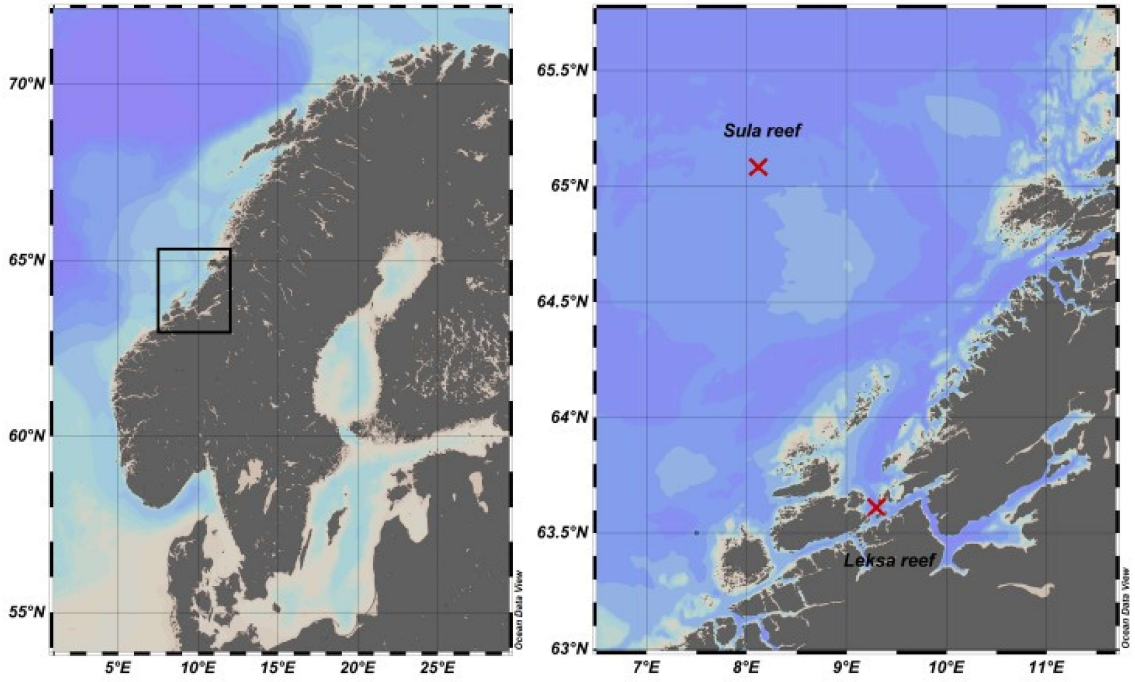

Figure 1-1 Map of the investigated area and main sampling locations

A considerable amount of information we have about the past climate is derived from geochemical investigations of marine calcium-carbonate material. Marine organisms such as foraminifera, corals or bivalves build their shells from aragonite/calcite and provide valuable archives from which we can extract environmental data using the right techniques.

For reconstructions in surface waters, a lot of potential archives are available, that can provide reliable results. Deep-water ecosystems such as cold-water coral (CWC) reefs are less well studied despite their importance as biodiversity hotspots that are comparable to tropical coral reefs (Jensen and Frederiksen, 1992; Rogers, 1999; Roberts et al., 2009;

Henry and Roberts, 2017). The recent climate change greatly threatens these sensitive ecosystems through the combined effects of ocean warming and ocean acidification (McCulloch et al., 2012b; Büscher et al., 2017; Raddatz et al., 2016; Levin and Bris, 2015).

CWC reefs provide habitat and shelter for a wide variety of different carbonate producers such as corals, bivalves and foraminifera that are potentially usable as proxy archives. Bivalves such as *Acesta excavata* that are associated with CWC reefs could provide a valuable tool to reconstruct environmental parameters such as temperature and salinity. In contrast to other archives like foraminifera, bivalves allow us to reconstruct these parameters on a seasonal basis. This is beneficiary for the investigation of corals as seasonality possible contributes a control on the distribution of CWC (Freiwald, 2002; Naumann et al., 2011; Brooke and Järnegren, 2013; Babcock et al., 1994).

Foraminifera provide no seasonal resolved archive. However, they excel in other characteristics such as the comparably well understood biomineralization mechanism (Nehrke et al., 2013; Toyofuku et al., 2017; de Nooijer et al., 2014) and wide distribution patterns (sen Gupta, 2003). The parasitic foraminifera *H. sarcophaga* allows us to research how parasitic relationships can potentially alter paleoreconstructions.

The aim of this study can be summed up to test a wide variety of different proxies on different cold-water carbonate producers to test their applicability to paleoreconstructions and potentially detect and characterize vital effects and other caveats that might influence geochemical reconstructions. To accomplish this, we measured E/Ca ratios, stable isotopic composition of oxygen and carbon isotopes as well as boron isotopic data measured on the bivalve *A. excavata*, the coral *D. pertusum* and the foraminifera *H. sarcophaga* from two contrasting Norwegian CWC reefs (Fig. 1). *In-situ* environmental data was gathered with two landers that were deployed in close proximity to the investigated reefs. This data is used to compare our geochemical data to.

1.2 Sample material (*Acesta excavata*)

1.2.1 Recent and fossil distribution

The species *Acesta excavata* was first described in 1779 by Fabricius, who was a student of Carolus Linnaeus. *A. excavata* is a suspension feeder that lives attached to hard substrates along the continental shelf-break (López Correa et al., 2005).

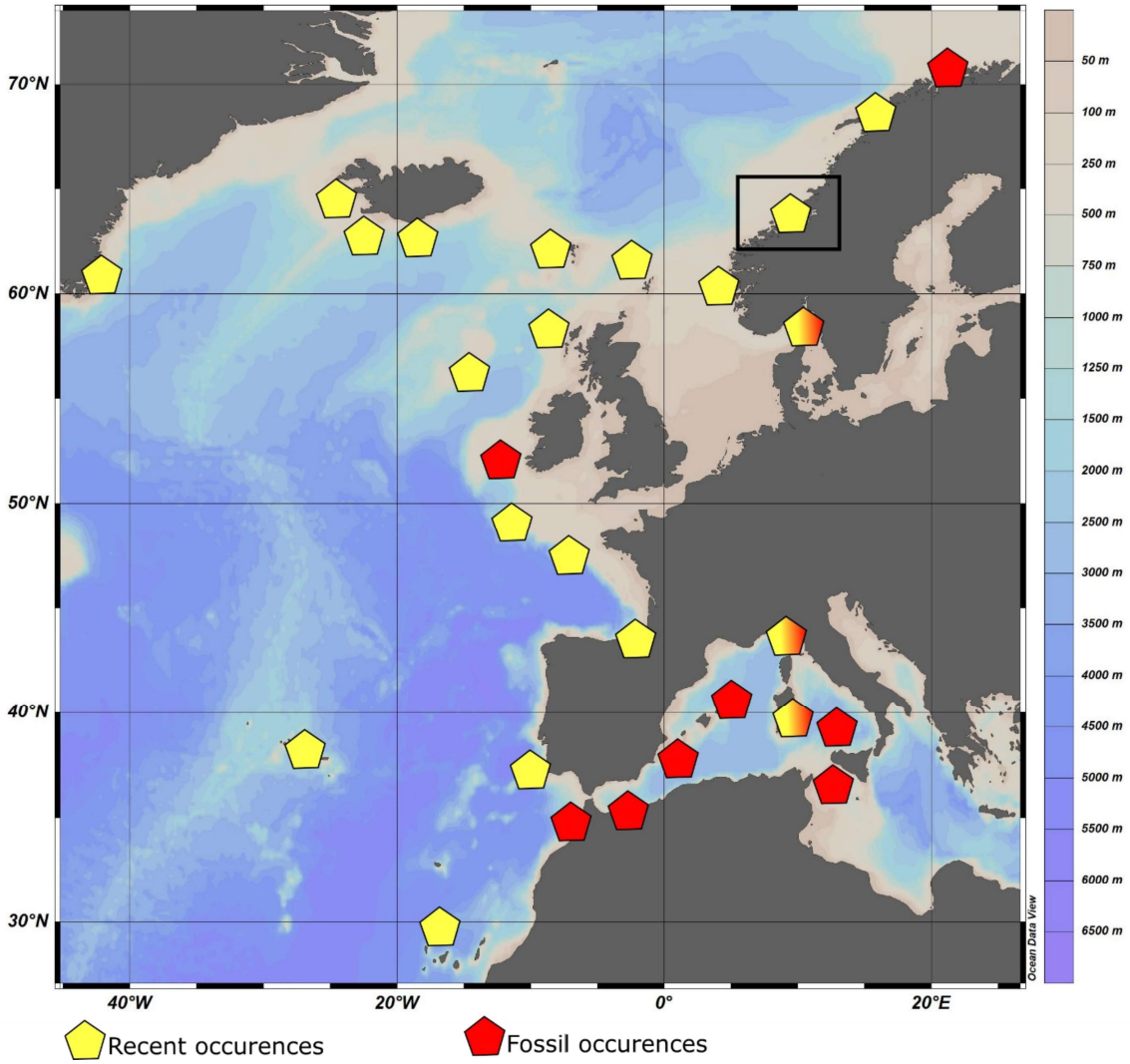

Figure 1-2 Recent distribution (yellow diamonds) of *A. excavata* after López Correa et al., 2005. Red diamonds show submerged subfossil to late Pleistocene sites. The black rectangle shows the main study area with the Leksa reef in the Trondheimsfjord and the Sula reef.

Its recent distribution (Fig. 2) spans along the shelf of the north-east Atlantic Ocean from Norway to Mauretania (López Correa et al., 2005; Bourcier and Zibrowius., 1970; Poppe and Goto, 1991; Madsen, 1949), southern Iceland (Madsen, 1949) and south-west Greenland (Lamy, 1913). Occurrences in the western Atlantic are known from Newfoundland (Gagnon and Haedrich, 2003; Haedrich and Gagnon, 1991). *A. excavata* was widespread in the Mediterranean Sea during the last glacial period (Malatesta and Zarlenga, 1986), but today only few occurrences are known from north of Corsica and the Tyrhennian sea (Ghisotti, 1979; Carcassi, 1983; Terreni and Voliani, 1995; Rocchini, 1983).

Uplifted sections from the Pliocene-Pleistocene period of Rhodes and Sicily are the oldest known occurrences of *A. excavata* (Seguenza, 1880, 1873). Besides numerous fossil sites in

the Mediterranean Sea, cores from the shelf of Mauretania show an association of *D. pertusum* and *A. excavata* with a maximum age of 192 ka corresponding to MIS5 (Wienberg et al., 2018).

Today, a total of 30 fossil species is attributed to *Acesta* (López Correa et al., 2005). While older fossil sites containing the species *A. excavata* are currently unknown, the Genus *Acesta* was present since the Mesozoic era with the oldest specimen deriving from late Jurassic (Callovian) deposits of western India (Kanjilal, 1990). Interestingly, all known Mesozoic *Acesta* localities are from the southern hemisphere of the Gondwana supercontinent (López Correa et al., 2005)

The suitable habitats, for the occurrence of *A. excavata*, span from 40 m to 3200 m, but they are mostly found in depths from 200 m to 800 m especially along the shelf area (López Correa et al., 2005). The suitable temperature and salinity range is 3 to 13°C and 33.4 ‰ to 38.5 ‰ (Malatesta and Zarlenga, 1986; Ghisotti, 1979; Bourcier and Zibrowius., 1970). Mandatory for the occurrence of *A. excavata* is a solid hard ground for settlement. This hardground is often provided by co-occurring CWC such as *D. pertusum* or *Madrepora occulata*. The bivalves are then usually found attached with their byssus filaments to the dead part of the coral framework, just below the living zone, with their shell openings protruding into the open water column (López Correa et al., 2005). While corals and bivalves rely on a constant current that provides particles, *A. excavata* potentially prefers lower current speeds. Fan shaped corals such as *Paragorgia arborea* or *Primnoa resedaeformis* displayed a characteristic pattern, groups of *A. excavata* were always attached to the leeward side of the fan shape (pers. obs. Nicolai Schleinkofer, 2018 and 2020). This is also evident when *D. pertusum* grows in thin, fan-shaped structures.

1.2.2 Species description

Table 1-1 Systematic and classification of *Acesta excavata* (WoRMS - World Register of Marine Species - Acesta excavata (Fabricius, 1779), 2020)

Class	Bivalvia	Linnaeus, 1758
Subclass	Autobranchia	Beuerlen, 1944
Infraclass	Pteriomorphia	Beuerlen, 1944
Order	Limoida	Waller, 1978
Superfamily	Limoidea	Rafinesque, 1815
Family	Limidae	Rafinesque, 1815
Genus	Acesta	H. and A. Adams, 1858
Species	*Acesta excavata*	Fabricius, 1779

Within the family Limidae (Table 1), the genus *Acesta* is rather special. It comprises relatively large species up to 25 cm and mostly deep-water bivalves whereas other genus from this family (*Lima, Limaria, Limatula, Limea, Ctenoides*) tend to be mostly small and shallow water inhabitants (Mikkelsen and Bieler, 2003; Hall-Spencer and Moore, 2000).

The shells of *A. excavata* can grow up to 25 cm in length, shell thickness attributes to 1mm. The shells are inequilateral, equivalved and moderately inflated. The dorsal end is characterized by a prominent auricle, the ventral side displays a smooth and straight commissure. The hinge is straight and characterized by a triangular ligament grove, teeth are missing. The shell surface is white to brown in appearance, caused by a very thin periostracum. The periostracum is often abraded during lifetime which gives the shell a more whitish appearance (López Correa et al., 2005). This appears to happen more often in samples derived from the Sula reef. Samples from the Leksa reef are usually more brownish in appearance. The exterior shell surface displays fine radial ribs, originating from the umbo. These ribs are interrupted by major growth lines in regular increments. In large adult specimens these growth lines get increasingly crowded and difficult to distinguish.

Figure 1-3 Cluster of *A. excavata* specimens on *D. pertusum* framework (4). The mantle cavity (1) and mantle folds (2) are well visible when the bivalves open the shell and protract their tentacles (3).

The soft body is of orange color (Fig. 3) with long tentacles. A siphon is not present. The pallial line is close to the shell margin and non-sinuate. Two muscle imprints are visible on the posterior shell side, one large adductor muscle and a smaller foot muscle. These muscles can be fused in old specimens (López Correa et al., 2005). The foot allows the bivalve in combination with the strong byssus threads to crawl. The byssus threads protrude from the lunular field and additionally allow the bivalve to firmly attach to hard grounds.

1.2.3 Biology of *Acesta excavata*

Acesta excavata feeds on particulate organic matter (POM) through filtration. This feeding type is dominant in animals that inhabit areas with dynamic flow regimes like shelf and continental slope areas (Gage, 2003; Järnegren and Altin, 2006). As the food availability in the deep-sea is scarce, bivalves inhabiting these zones are often specially adapted. Some bivalves have elongated guts to extract a maximum of nutrients from the ingested particles (Allen, 1983). Other adaptation strategies are an increased efficiency of food capture and a reduction of required food through decreasing body size (Oliver, 1979). *A. excavata* adapted to the low food supply by increasing the gill size and therefore the efficiency of food uptake (Järnegren and Altin, 2006). The gill size and clearing rate are the second highest measured in bivalves. This allows the bivalve to efficiently use the low food concentrations in the deep sea (Järnegren and Altin, 2006).

Seasonal food cycles have been proposed as a major factor for the synchronization of reproductive cycles in the deep sea (Järnegren et al., 2007). This is, however, not the case for the genus *Acesta*. *A.* sp. nov. and *A. excavata* do not show differences in their reproductive cycle despite having vastly different food availabilities (Järnegren et al., 2007). In general, *A. excavata* is a gonochoristic broadcast spawner. The reproductive cycle starts with a first spawning in May/June followed by a semi-continuous spawning beginning in August and lasting for the rest of the year (Järnegren et al., 2007). *A. excavata* is a sequential hermaphrodite, during their life cycle they often change their sex from male to female. This usually happens at a size of 77- 90 mm (Järnegren et al., 2007), corresponding to an age of 16-20 years (López Correa et al., 2005). Not all specimens undergo this sex-change as large males >100mm can also be found. (López Correa et al., 2005)

Sampled shells often display a large number of organisms on the shell surface. Most of these organisms are parasitic foraminifera of the species *Hyrrokin sarcophaga* (Cedhagen, 1994) which will be further discussed in a following section.

1.2.4 Shell mineralogy

The shells of A. excavata consist of two different calcium carbonate polymorphs, determined by use of Feigl solution (Feigl et al., 1973) and XRD scanning, aragonite and calcite (López Correa et al., 2005). The hinge area and the interior shell area is entirely constructed from aragonite. In juvenile specimens only a very thin layer of calcite covers the aragonite. With ongoing ontogeny, the calcite layer grows thicker towards the ventral side, where it makes up to 70% of the shell. The calcitic layer itself can be divided in two subunits distinguishable by their mineral form and size (López Correa et al., 2005). The uppermost fibrous layer is composed of 50 µm long and 5 – 10 µm wide fibers which are approximately orientated

orthogonal to the closest growth line. The prisms show a well-defined boundary towards the underlying microgranular layer.

The granules that build the 150 to 250 µm thick microgranular layer are usually less than 1 µm in diameter. Towards the aragonite border these granules become increasingly elongated and more fiber-like (López Correa et al., 2005). Within the microgranular layer a white band is observable in microscopic images of thin sections. This band runs parallel to the aragonitic layer and is discontinued in the young, ventral shell section.

The aragonitic shell layer exhibits a characteristic stripped pattern and makes up ≈50% of the shell thickness in medial shell parts. The stripped pattern is caused by crossed lamellae that are 10 to 25 µm wide (López Correa et al., 2005) .

1.3 Sample material (*Desmophyllum pertusum*)

1.3.1 Species description

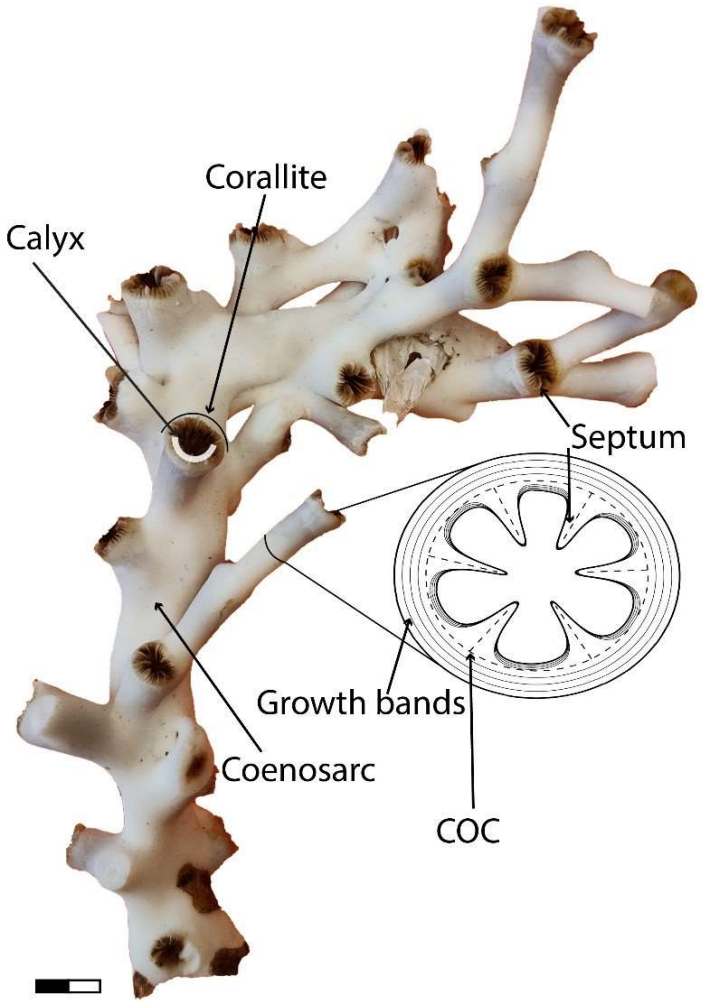

Figure 1-4 Picture of *D. pertusum* and sketch of corallite cross-section. COC = centers of calcification. Scalebar is 10 mm long.

Table 1-2 Systematic and classification of *Desmophyllum pertusum* (WoRMS - World Register of Marine Species - Desmophyllum pertusum (Linnaeus, 1758), 2021)

Class	Anthozoa	Hatschek, 1888
Subclass	Hexacorallia	Haeckel, 1894
Order	Scleractinia	Bourne, 1900
Family	Caryophylliidae	Dana, 1846
Genus	*Desmophyllum*	Ehrenberg, 1834
Species	*Desmophyllum pertusum*	Linnaeus, 1758

The coral *Desmophyllum pertusum* can be found all over the world with mayor occurences in the Northern Atlantic. The distribution pattern is approximately equal to the distribution of *A. excavata* (Fig. 2) as these two species are often co-existing. The coral forms large, three-dimensional frameworks that consist of thousand individual coral polyps. Large CWC reefs and coral mounds are the result of a healthy growth (Roberts et al., 2009). The constructed reefs provide habitat for a high diversity of different fish and invertebrates (Roberts et al., 2009). Suitable temperature and salinity envelopes for the occurrence of these corals are between 4-14°C and 32 – 38 ‰ (Roberts et al., 2009). More critical are specific density layers and the aragonite saturation of the surrounding water, as in an undersaturated environment, calcification processes are greatly limited. The reason for the importance of the mentioned density envelope of 27.35 – 27.65 kg/m³ (Dullo et al., 2008) is not entirely resolved but might be connected to either larval transport or the occurrence of so-called intermediate nepheloid layers (INL) (Kiriakoulakis et al., 2005, 2007; Dullo et al., 2008). These layers provide an important source for particulate organic matter (POM) on which the corals depend as an important nutrient source (Kiriakoulakis et al., 2005, 2007).

Desmophyllum pertusum is gonochoric with two sexes and external fertilization. Asexuell reproduction is possible by fragmentation but also sexual reproduction is possible (Waller and Tyler, 2005). Gametogenesis might be triggered by plankton blooms, as observed in the Porcupine Seablight (Lampitt et al., 2001). Spawning of larvae happens in January/February, which are planula type, planctotrophic active swimmers (Waller and Tyler, 2005).

After settlement the larvae start growing with high growth rates of up to 27.5 mm/a (Gass and Roberts, 2011). The growing corallites are trumpet-shaped and consist of aragonite. Within the theca wall, growth bands are observable that are caused by overgrowth of young polyps. Close to the septs, a light band is observable in the theca wall, the centers of calcification. These give the first framework for longitudinal and lateral growth and are geochemically and isotopically distinct from the fibrous deposits that make up the majority of the theca wall (Cuif and Dauphin, 1998).

1.4 Sample material (*Hyrrokkin sarcophaga*)

1.4.1 Species description

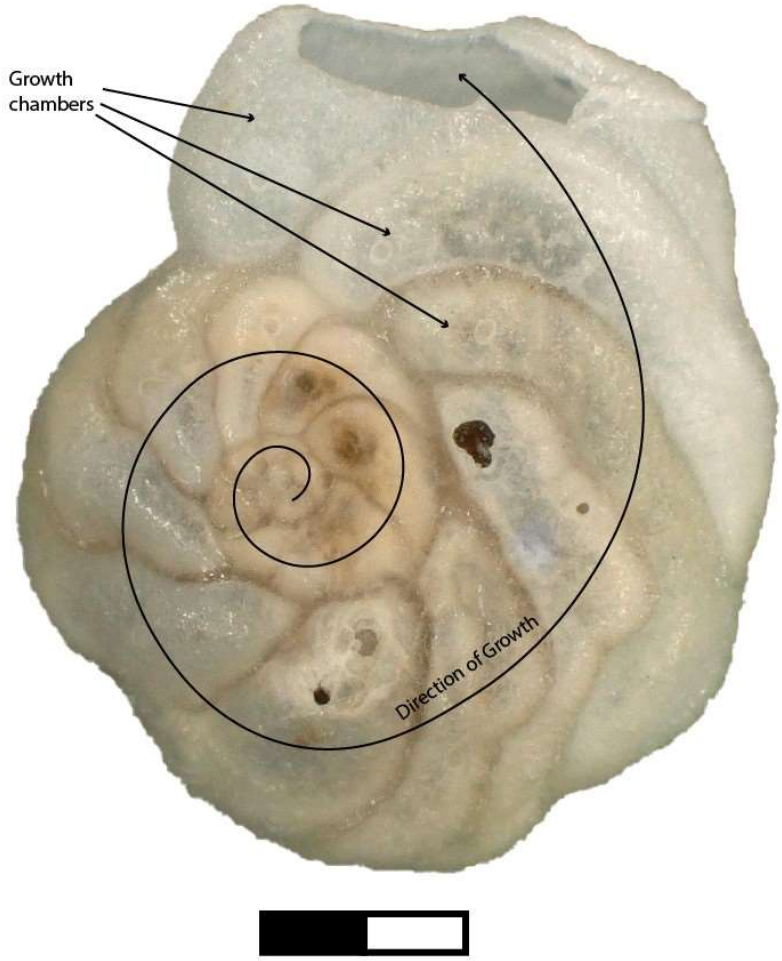

Figure 1-5 Picture of *H. sarcophaga*. Scalebar is 1mm long.

Table 1-3 Systematic and classification of *H. sarcophaga* (WoRMS - World Register of Marine Species - Hyrrokkin Cedhagen, 1994, 2021)

Class	Globothalamea	Pawlowski, Holzmann & Tyszka, 2013
Subclass	Rotaliana	Mikhalevich, 1980
Order	Rotaliida	Delage & Hérouard, 1896
Superfamily	Discorboidea	Ehrenberg, 1838
Family	Rosalinidae	Reiss, 1963
Genus	*Hyrrokkin*	Cedhagen, 1994
Species	*Hyrrokkin sarcophaga*	Cedhagen 1994

The foraminifera *H. sarcophaga* is one of the few species that adapted to a parasitic lifestyle within the Phylum Foraminifera (Walker et al., 2017). *Hyrrokkin sarcophaga* is a common inhabitant of cold-water coral reefs in the North Atlantic. Its recent distribution is equivalent to

the distribution of *A. excavata* (Fig. 2), which is the preferred host species (Beuck et al., 2008). Besides *A. excavata*, *H. sarcophaga* also infests other organisms such as the bivalve *Delectopecten vitreus*, sponges of the family Geodiidae and Ancorinidae, cold-water corals such as *D. pertusum, Madrepora occulata* and *Flabellum japonicum,* as well as other foraminiferans (Beuck et al., 2008; Cheng and Dai, 2016). Rare occurrences on rocks show that it can survive without a host, at least for a limited time period (Cedhagen, 1994). The calcitic tests of *H. sarcophaga* can grow rather large, up to 6 mm in diameter, which are sinistrally coiled, show concave umbilical sides and evolute, convex apical sides (Cedhagen, 1994). The general form of the foraminifera is also found on its host, where an attachment etching is produced that mirrors the tests outline (Cedhagen, 1994). These etchings serve to reduce the risk of removal by the host and possibly satisfy calcium requirements for test precipitation (Cedhagen, 1994). These etchings can occur in high amounts on *A. excavata*, where large specimen showed over 100 attachment etchings on a single shell. From this etched pit, *H. sarcophaga* etches a canal through the shell of its host to get access to the host's soft body. These channel etchings however, are not reported from specimen that infested *D. pertusum* (Beuck et al., 2008; Cedhagen, 1994). Through this canal, the foraminifera can protrude the pseudopodia into the inner shell cavity and feed on the host's soft tissue (Cedhagen, 1994) or ingest calcifying fluid, which is rich in nutritious amino acids (Alexander and Delaca, 1987; Schweizer et al., 2012). The feeding on the bivalve's soft body is supported by the high amount of cell nuclei in the infected areas (Cedhagen, 1994). In infested *D. pertusum* specimen no etched channels are observable, instead multiple filaments protrude into the host's carbonate skeleton and serve an anchoring function (Beuck et al., 2008)

1.4.2 Host defence mechanisms

The channel that is etched through the shell of *A. excavata* poses a threat for the bivalve. Primarily, the foraminifera feeds on the bivalve's soft tissue (Cedhagen, 1994; Beuck et al., 2008). Furthermore, the open canal in the shell allows pathogens to attack the bivalve as well as it allows water to permeate into the extrapallial fluid. Bivalves have to actively concentrate Calcium and carbonate in the calcifying space in order to reach saturation levels that allow the precipitation of calcite or aragonite (Wheeler, 2020). A dissolution with seawater might prevent this concentration of Ca-ions and therefore prevent calcification. Consequently, the bivalve has to utilize mechanisms to stop the boring and seal the canal. This is accomplished by calcifying over the canal and building a thick callus on the inside of the bivalve's shell (Cedhagen, 1994; Beuck et al., 2008).

1.5 Sampling locations

The samples used in this work derive mostly from two reefs on the Norwegian shelf, the Sula reef and the Nord-Leksa reef (Fig. 1). Sample investigated in chapter five were mostly collected during scientific cruise SO275 around Iceland.

1.5.1 Sula reef

The Sula Ridge lies on the Mid-Norwegian shelf, a northeastward-plunging spur from 240 to 340 m water depth (Freiwald et al. 1999). It is built by paleogenic sandstones (Bugge et al. 1984) which form the asymmetric shape with a steep southeastern flank and a smooth northwestern flank. In the northeastern part of the Sula Ridge is the Sula reef complex (64°06.57 N, 08°07.12 E), which describes a cluster of individual coral frameworks. The main reef tracts are located along the southeastern crest of the Sula Ridge and extends up to 14 km in SW-NE direction with widths between 200 and 350 m. The reef systems on the gently sloping northwestern flank are generally smaller and more scattered. The reefs elevate above the surrounding seabed by 5 to 35 m, with 15m in average. The reefs are aligned with an average deviation of 20° to the orientation of the Sula ridge. This is caused by the collapsing Fennoscandian ice dome. The released icebergs frequently hit the Sula ridge, leaving deeply incised furrows, flanked by hard substrates, which are suitable for the colonization of sessile organisms (e.g. *D. pertusum*) (Freiwald et al. 1999). The hydrographic regime in this area is controlled by a branch of Atlantic water that brings water with a temperature that varies from 6.3°C to 7.5°C and salinities from 35.1 to 35.2 ‰ (Freiwald et al., 2002, Personal observation). In combination with tidal motion, the current leads to high velocities of 7 to 44 cm/s. Additionally, the fertile surface water leads to zooplankton blooms and provides many nutrients for the corals and co-occurring bivalves (Eide, 1979).

1.5.2 Nord-Leksa reef

The Nord-Leksa reef is located 90 km east of the Sula reef (63°36.46 N, 09°22.89 E) (Fig.1). The reef is composed of very densely packed *Desmophyllum pertusum* domes forming one large (500 × 200 m) and two smaller patch reefs on a north-eastward trending sub-marine ridge (Mortensen et al., 2001). Due to the location of the reef at the entrance to the Trondheimsfjord, this reef experiences more variety in the environmental parameters due to strong tidal and compensatory currents (Form et al., 2014). Temperature and salinity in this reef amount to 7.4 °C and 35 PSU (Büscher, 2018; Personal Observation, 2018). The reef consists of three summits on which the corals grow. The seabed between these summits conists mostly of sand (Fosså et al., 2006).

2.5.3. Environmental data

In order to compare the measured geochemical data to environmental data such as salinity and temperature, two landers were deployed in close proximity to the investigated reefs (Form et al., 2015). These landers were equipped with temperature, salinity and pH-sensors and recorded the environmental information for 14 months. Unfortunately, the pH-meter failed shortly after the lander deployment. The recorded data (Temperature, salinity, current velocity) is presented in more details in chapter 4.

1.6 Proxy overview

1.6.1 Mg/Ca

Elemental proxies such as Mg/Ca are commonly used in paleoenvironmental reconstructions (Gray and Evans, 2019; Lear et al., 2000; Nürnberg et al., 1996; D'Olivo et al., 2018; Takesue and van Geen, 2004). Mg/Ca ratios are regularly used as a temperature proxy, especially with foraminifera as the used archive (Kristjánsdóttir et al., 2007; McKenna and Prell, 2004; Sadekov et al., 2009; Cléroux et al., 2008; Tripati et al., 2003). Mg^{2+} ions are incorporated into calcite through substitution with Ca^{2+} ions (Mucci and Morse, 1990), forming a solid solution. As this is an endothermic reaction, the substitution is expected to increase with rising temperature (Glover and Sippel, 1967; Katz, 1973). Based on thermodynamic considerations, a sensitivity of 3% per °C was proposed (Lea et al., 1999), which is consistent with several inorganic precipitation experiments (Oomori et al., 1987; Rosenthal and Katz, 1989; Mucci and Morse, 1990). These experiments also showed that the incorporation of Mg^{2+} is basically independent of precipitation rate, however this is only true for inorganic precipitated carbonate. Biologically mediated processes on the other hand are rarely at thermodynamic equilibrium (Hillaire-Marcel and De Vernal, 2007).

The general consent is that Mg/Ca ratios in bivalves are a poor choice for paleoenvironmental reconstructions using bivalves as an archive material (Takesue and van Geen, 2004; Schöne et al., 2010; Freitas et al., 2008; Elliot et al., 2009; Freitas et al., 2006; Wanamaker et al., 2008; Wanamaker and Gillikin, 2019; Poulain et al., 2015). This is caused by biologically mediated processes that cause disequilibrium effects, known as "vital effects" (Urey et al., 1951). While an early study discovered a strong temperature control on Mg/Ca ratios in *Mytilus trossulus* (Klein et al., 1996), these results were never repeated. Following studies on *Pinna nobilis* conclude that temperature reconstructions using Mg/Ca are possible on this particular species, but only during the first four years of the specimen's life. After this timeframe variations through ontogenetic effects mask the temperature signal (Freitas et al., 2005). Results from X-ray Absorption Near Edge Spectroscopy (XANES) on Arctica islandica indicated that a large part of Mg^{2+} ions in bivalve aragonite is not substituted but hosted by a disordered phase such as the organic matrix (Foster et al., 2008). The influence of organic

material on Mg/Ca ratios was confirmed on several species, both aragonitic and calcitic (Freitas et al., 2009; Tanaka et al., 2018; Schöne et al., 2010, 2011). However not all studies agree with the hypothesis that organic material causes significant Mg/Ca variation. Microprobe investigation on *Ruditapes phillipinarum* showed that Mg was not associated with Sulphur, a proxy for organic material (Poulain et al., 2015). Furthermore, Marali et al., 2017 showed that Mg/Ca ratios in bivalves ,from the same location, are highly reproducible, indicating some sort of external forcing. Still though, while most studies recognize a temperature sensitivity of Mg/Ca ratios, the general consent is, that they are not usable for reconstruction due to vital effects (Ullmann et al., 2013; Schöne et al., 2011; Tynan et al., 2017; Wanamaker et al., 2008). The discussed vital effects include: presence of organic material (Tanaka et al., 2018; Schöne et al., 2010), crystal size and orientation (Freitas et al., 2009), changes of transportation rate of Mg^{2+} and Ca^{2+} ions to the calcification space (Foster et al., 2008) , ion-zoning in the calcification fluid (Tanaka et al., 2018) and organisms suffering from stress and consequent metabolic changes (Lorens and Bender, 1980; Wanamaker and Gillikin, 2019).

Similar to the studies on bivalves, studies on CWC show that Mg/Ca is not systematically controlled by the calcification temperature (Rollion-Bard and Blamart, 2015; c. Instead, significant influences of growth rate changes and the presence of organic material and ACC is expected to control the incorporation of Mg into the corals aragonite skeleton (Finch and Allison, 2008). CWC display higher ratios of Mg/Ca in the centers of calcification (COC), consistent with the distribution of organic matter and possibly ACC in the coral (Rollion-Bard et al., 2010; Cuif et al., 2003). Further controls on Mg/Ca are predicted through the precipitation rate by the surface entrapment model (Gabitov et al., 2014c). Surface entrapment happens when the crystal growth rate is faster than the diffusion of Mg^{2+} ions. This causes Mg^{2+} ions, that are adsorbed to the crystal surface, to be overgrown by calcite before equilibration can happen (Watson, 1996).

In foraminifera, Mg/Ca ratios serve as reliable recorders of seawater temperatures (Nürnberg et al., 1996; Rosenthal et al., 2006; Lear et al., 2002; Lea et al., 1999).However, species-specific effects are observable, therefore it remains speculative if *H. sarcophaga* can be used for temperature reconstructions (Lear et al., 2002). Potential further controls are changes in growth rate, crystal size and morphology, salinity and pH (Rosenthal et al., 2006; Lea et al., 1999). However, salinity and pH presumably do not represent independent effects but instead influences Mg/Ca ratios through alteration of the growth rate (Lea et al., 1999).

An important effect of Mg incorporation into calcite is the distortion it introduces into the crystal lattice due to its small ionic-radius. This distortion increases the size of certain lattice

positions and consequently increases the incorporation of larger ions such as Sr and Na (Mucci and Morse, 1983)

1.6.2 Sr/Ca

In contrast to Mg/Ca ratios, Sr/Ca ratios show no temperature sensitivity in calcite. However, Sr/Ca ratios measured in aragonite show a weak inverse, exponential temperature dependence. Similar to Mg^{2+} in calcite, the incorporation of Sr^{2+} in aragonite is a substitution with Ca^{2+} (Kinsman and Holland, 1969). This incorporation causes the enthalpy of the product to decrease relative to the enthalpy of the educt (exotherm), which explains the inverse temperature sensitivity (Kinsman and Holland, 1969). Sr/Ca ratios are mainly used in corals, both WWC and CWC (de Villiers et al., 1994, 1995; Mitsuguchi et al., 2003; Raddatz et al., 2013).

Similarly, to Mg/Ca ratios, Sr/Ca ratios in bivalves are considered to be bad temperature proxies/proxies in general due to strong vital effects. Early studies on Sr/Ca ratios measured on *Mytilus edulis,* did reveal a positive correlation with temperature in the calcitic shell layer and a negative correlation in the aragonitic nacreous layer (Dodd, 1965). While the underlying mechanisms were not understood it was already proposed that actually growth rate controls the Sr/Ca ratio in the calcitic layer instead of calcification temperature (Dodd, 1965). These results were confirmed by Klein et al., 1996, who predicted the metabolic activity and the salinity of the surrounding water masses to possess the highest predictive power on Sr/Ca ratios in biogenic calcite. Similar results were provided by Purton et al., 1999 who discovered increasing Sr/Ca ratios throughout the ontogeny of the aragonitic bivalve *Venericardia planicosta*, which was attributed to changes in the metabolic activity and changes of the calcification rate (Purton et al., 1999). This is contradicted by results from inorganic precipitated aragonite where no effect on the precipitation rate was found (Kinsman and Holland, 1969) indicating that this might be a mainly biological effect. On the other hand, precipitation rate effects were found in inorganically precipitated calcite (Gabitov et al., 2014a; Lorens, 1981; Morse and Bender, 1990). This effect is explained with the surface entrapment model.

Similar studies to Dodd, 1965 were conducted often on different bivalve species but the temperature sensitivity of Sr/Ca was not reproducible in these consecutive studies. Kinetic effects such as alterations through calcification rate changes are mostly proposed to explain the observable variability in Sr/Ca ratios (Schöne et al., 2013; Wanamaker and Gillikin, 2019; Schöne et al., 2011; Poulain et al., 2015; Lorrain et al., 2005; Freitas et al., 2005; Takesue and van Geen, 2004). Additionally, organic material might also control Sr/Ca ratios in bivalves as strontium has a great adsorption potential to organic material (Khani et al., 2012; Kunioka et al., 2006; Schöne et al., 2010).

In foraminifera, Sr/Ca ratios increase with increasing temperature, salinity and pH (Lea et al., 1999). However, all these effects are explainable with covariations of temperature, salinity and pH with calcification rate (Lea et al., 1999; Lorens, 1981; Morse and Bender, 1990; Bijma et al., 1999). Effects of seawater Sr/Ca ratios are not evident (Lea et al., 1999). As previously stated, incorporation of Mg-ions can also increase the incorporation of Sr into calcite (Mucci and Morse, 1983)

1.6.3 Na/Ca

Na^+ ions are incorporated into aragonite and calcite substituting for Ca^{2+} despite the difference in charge (Okumura and Kitano, 1986; Kitano et al., 1975; Yoshimura et al., 2017). This is possible because Na^+ ions have a similar ionic radius as Ca^{2+} ions but lattice defects such as CO_3^{2-} vacancies are mandatory to account for these charge differences (Mucci and Morse, 1990; White, 1977; Yoshimura et al., 2017). As these lattice defects are a function of the calcification rate, a control of Na/Ca ratios through it is likely. Besides a possible control through calcification rate, a salinity control was proposed early by several researches on atlantic oysters (Rucker and Valentine, 1961), barnacles (Gordon et al., 1970) and inorganically precipitated calcite (Ishikawa and Ichikuni, 1984). Even though this would have filled an important niche, as there was and still is no independent salinity proxy it took until 2013, when Wit et al. presented the first calibration on *Amonia tepida*, a benthic foraminifer. Similar studies were conducted on different species, which came to similar results, indicating that Na/Ca ratios in foraminiferal calcite are mainly controlled by the sodium activity in the surrounding medium and can therefore be used for salinity reconstructions. Other studies however contradict these results and propose that Na/Ca ratios in foraminiferal calcite are more controlled by the Na/Ca ratio in the surrounding water (Hauzer et al., 2018).

Na/Ca measurements in bivalves are scarce in the literature. Results from the freshwater bivalve *Elliptio complanate* indicate that Na/Ca ratios can serve to reconstruct the Na content of streams. However, this is only possible for large scale effects. Intraannual changes due to road-salt use in winter were not traceable (O'Neil and Gillikin, 2014). Results from Zhao et al., 2017 indicate that Na/Ca ratios might be controlled through the acid/base and ionic regulation mechanisms of the bivalve. The underlying mechanism is supposed to be the Na^+/H^+ exchanger which reduced the inner-cellular H^+ concentration, to ease calcification, in exchange for Na^+-ions (Zhao et al., 2017a). Interestingly, this effect is traceable through different generations. When specimens of *Ruditapes phillipinarum* are subjected to low-pH environments, their descendants show significantly lower Na/Ca ratios then specimens with no history of acidified conditions (Zhao et al., 2017b). This effect could indicate mechanisms of adaption to low pH environments and showcase the resilience of bivalves to ocean acidification (Zhao et al., 2017b). A strong influence through internal effects is also proposed by Marali et al., 2017 who did not find reproducible Na/Ca time series in shells of *Arctica*

islandica, that were sampled from the same environmental setting (Marali et al., 2017b). While this result indicates, that Na/Ca ratios are mainly controlled through internal effects, the authors stress that higher resolved measurements could improve the usability of Na/Ca ratios. This is due to the fact that it reduces “signal smearing” (Marali et al., 2017a). Internal effects are also suggested by Ballesta-Artero et al., 2018 who found a significant relation between both food supply, temperature and Na/Ca ratios. The author proposes metabolic effects as an explanation, as these covary with temperature and food supply (Ballesta-Artero et al., 2018). A temperature control on Na/Ca ratios was, however, also proposed by Rollion-Bard and Blamart, 2015 in *Desmophyllum pertusum* as well as by Schleinkofer et al., 2019 for *Desmophyllum pertusum* but also calcitic organisms such as *Mytilus edulis* and different foraminifera species.

1.6.4 Ba/Ca

Ba/Ca ratios in bivalves are rather well researched and show potential to reconstruct phytoplankton dynamics and oceanic Ba/Ca concentrations (which are also correlated to salinity)(Poulain et al., 2015). However, the different internal and external forcing mechanisms are not fully understood. In general Ba/Ca ratios in bivalves are characterized by stable background levels (Putten et al., 2000; Lazareth et al., 2003; Gillikin et al., 2008; Chauvaud et al., 2009; Barats et al., 2009; Gillikin et al., 2006a) ,that are controlled by the aqueous Ba/Ca ratio (Gillikin et al., 2006a), with sharp, intense maxima. These maxima appear to be correlated to phytoplankton blooms (Stecher et al., 1996; Lazareth et al., 2003; Putten et al., 2000) but further research revealed that they cannot be used as a direct proxy for seawater Ba/Ca or phytoplankton activity (Gillikin et al., 2006a, 2008). The Ba/Ca signal in the bivalve calcite/aragonite does not appear to derive from ingested phytoplankton, instead is a product of processes that happen during the phytoplankton decay (Gillikin et al., 2006a). Besides phytoplankton dynamics as an external forcing mechanism, biological factors that control Ba/Ca ratios in bivalves are evident. Interestingly bivalves show similar Ba/Ca ratios regardless if the shell is built from aragonite or calcite indicating that the D_{Ba} is predominantly controlled by biological or chemical effects within the extrapallial fluid (Elliot et al., 2009). Additionally, in other organisms such as the zooxanthelate coral *Porites lutea*, stress is discussed as a factor controlling Ba/Ca ratios (Chen et al., 2011). Similar effects are also known from bivalves regarding Mg/Ca ratios (Lorens and Bender, 1980; Wanamaker and Gillikin, 2019).

Ba/Ca ratios in foraminifera have been shown to correlate with the seawater barium concentration (Lea and Boyle, 1989, 1991). Refractory nutrients (silica, alkalinity) are similarly correlated with seawater Ba concentrations, allowing Ba/Ca ratios in foraminifera to be used for reconstructing the distribution of these refractory nutrients in the past (Lea and Boyle, 1991; Hall and Chan, 2004a, b). Still, species specific effects are evident. Species of

Globorotalia, for instance, are enriched in Ba/Ca possibly as an effect of different habitats and shell precipitation modes (Lea and Boyle, 1991). Barium enrichment in the water is also controlled by changes of the glacial-interglacial circulation pattern and can serve to identify meltwater events, which is utilized in the Northern Atlantic to reconstruct glacier fluctuations with *D. pertusum* as the proxy archive (Raddatz et al., 2016)

1.6.5 Mn/Ca

Manganese in aquatic settings is mainly controlled by the change between its two oxidation states of Mn, Mn^{2+} and Mn^{4+}, with the latter being insoluble in water (Statham and Burton, 1986; Hydes et al., 1986). The transformation between these two redox states is mainly controlled by the redox conditions (and therefore the oxygen concentration) and the pH conditions (Glasby and Schulz, 1999). The main fluxes for Mn into the ocean are through freshwater input and aeolian dust (Bender et al., 1977). In the ocean Mn^{4+} oxides can be reduced through bacterial activity which makes the Mn bioavailable for other organisms such as bivalves and allows for an incorporation of Mn^{2+} ions into the carbonate shell(Klinkhammer and McManus, 2001; Burnett et al., 2003). This covariance with bacteria causes Mn^{2+} to be stronger concentrated in benthic environments during summer months as a result of increased biological activity and consequent increased input of organic material and reduced oxygen concentrations (Berelson et al., 2003; Dehairs et al., 1989). The ability to monitor manganese levels in the ocean through proxy archives would therefore provide valuable information about the redox conditions in oceanic environments.

Nevertheless, only few studies have measured Mn/Ca ratios in bivalves in order to relate them to environmental or biological mechanisms. Mn/Ca ratios in *Isognomon ehippium*, from a mangrove setting, were suggested to be related to phytoplankton blooms caused by increased riverine discharge (Lazareth et al., 2003). Shell Mn/Ca in *Mytilus edulis* from the Netherlands showed a seasonal cyclicity with high values in late spring. That was also considered to be related to primary productivity (Putten et al., 2000). Phytoplankton blooms in the Menai Street (Great Britain) however, preceded the Mn/Ca maxima and therefore cannot constitute the major control. Instead, it is proposed that shell Mn/Ca ratios reflect the seawater Mn concentration (Freitas et al., 2006). A correlation with phytoplankton activity is still plausible since the amount of dissolved Mn in the ocean is controlled by the redox conditions (Landing and Bruland, 1987) and decaying organic matter from phytoplankton could consume oxygen and therefore change the redox potential.

In foraminifera, Mn/Ca ratios are regularly used to reconstruct redox conditions in the past due to the mechanisms outlined above (Koho et al., 2015; Groeneveld and Filipsson, 2013; Glock et al., 2012; Guo et al., 2019)

1.6.6 P/Ca

P/Ca ratios are barely researched, despite the importance of phosphor in nearly every biological process. In particular, I am not aware of a single study that measured P/Ca ratios in bivalves. In corals the usability of P/Ca as a nutrient proxy and potential use to reconstruct water mass dynamics is discussed (Anagnostou et al., 2011; LaVigne et al., 2010). In bivalves, this has not been researched but P/Ca ratios might also be useful to locate organic rich growth lines (Cusack et al., 2008). This is also possible using Mutvei's solution (Schöne et al., 2005) but some bivalves such as the investigated species *Acesta excavata* do not show good visible growth lines after Mutvei's treatment. Additionally, the Mutvei's solution possibly destroys the sample for further geochemical investigations due to the influence of Alcian blue and glutaraldehyde. Therefore, P/Ca ratios might constitute a way to locate growth lines in bivalves with bad growth line visibility and without potentially destroying the sample.

Results from foraminifera show that P/Ca ratios are unaffected by oxidative cleaning procedures, indicating that P is hosted in the calcite and not loosely bound to organic material. The authors propose that PO_4 substitutes with CO_3 and might serve as a possible proxy for seawater phosphate chemistry (Newton et al., 2007). This effect was used in a study aimed at quantifying the effects of fish-farms on heavy metal and phosphorous pollution (Oron et al., 2021)

1.6.7 Stable oxygen isotopes ($\delta^{18}O$)

At the time of writing this section, stable oxygen isotopes are the only reliable proxy for temperature reconstructions (Urey et al., 1951; Urey, 1947; Epstein et al., 1953) in bivalves. Almost all investigated species of bivalves are known to precipitate their shells in oxygen isotopic equilibrium with the ambient water (Mook and Vogel, 1968; Hallmann et al., 2009; Surge and Schöne, 2015; Surge et al., 2001; Elliot et al., 2002, 2009). Exceptions include *Pecten maximus,* attributed to differences in carbonate chemistry of the extracellular calcifying fluid (ECF)(Owen et al., 2002), larvae of *Placopecten magellanicus* and adult specimen of *Panopea abrupta,* attributed to stress during growth (Owen et al., 2008; Hallmann et al., 2008) and *Eurhomalea exalbida* attributed to a pH increase during ontogeny (Yan et al., 2012). As bivalves mostly precipitate their shell in isotopic equilibrium with the surrounding water, changes in $\delta^{18}O$ can be attributed to temperature changes and changes in the $\delta^{18}O$ signal of the ambient water (Urey, 1947; Epstein et al., 1953). If the temperature can be inferred from another technique than $\delta^{18}O$ ratios can also be used to estimate salinity variations (Ingram et al., 1996). $\delta^{18}O$-ratios also provide a way to investigate the growth characteristics of bivalves and confirm the annual character of growth lines (Jones et al., 1983).

Similarly, stable oxygen isotopes measured in foraminifera provide a reliable method to reconstruct paleotemperatures and hydrological changes. Caveats for this method include vital effects and diagenesis. Especially planktonic foraminifera have to be treated cautiously due to their photosymbionts. These photosymbionts lower the pH and increase carbonate ion concentration (Rink et al., 1998). Isotopic fractionation between the dissolved inorganic carbon species can occur (Zeebe, 1999) and shift the incorporation of the isotopes towards disequilibrium. The use of benthic foraminifera suffers from similar problems, caused by the habitat and ontogeny stage. Infaunal species experience a different pH than epifaunal species, again leading to disequilibrium fractionation (Bemis et al., 1998). Additional ontogeny effects are evident, indicated by a slight negative offset in young/small specimens. These are presumably caused by higher amounts of metabolic CO_2 during calcification (Barras et al., 2010; Filipsson et al., 2010).

CWC display a similar mechanism of pH-regulation to facilitate calcification (McCulloch et al., 2012b). This mechanism manifests itself in the isotopic difference between the COC and fibrous deposits(Rollion-Bard et al., 2010; Blamart et al., 2005). These vital effects hinder the usage of stable oxygen isotopes for paleoreconstructions but allow a more detailed view into calcification mechanisms(Adkins et al., 2003).

In general, decreasing $\delta^{18}O$-ratios indicate increasing temperatures. Due to modern mass spectrometry techniques, small samples gathered by Micromilling can be sampled and analyzed with an external precision of less than 0.08‰ (Fiebig et al., 2005). This allows temperature reconstructions with a precision of 0.34°C when the $\delta^{18}O$-ratio of the ambient water is known or can be inferred. This is the biggest problem as the water $\delta^{18}O$-ratio is rarely know for prehistoric environments (Schöne and Surge, 2012).

1.6.8 Stable carbon isotopes ($\delta^{13}C$)

Compared to stable oxygen isotopes, stable carbon isotopes are far more complicated. Theoretically, stable carbon isotopes can provide information about the $\delta^{13}C$ ratio of the dissolved inorganic carbon (DIC) and can therefore be used to gain information on primary production (Mook and Vogel, 1968). In general, plants preferentially use the lighter ^{12}C during photosynthesis. This leads to more positive $\delta^{13}C$ ratios during times of high primary productivity. On the contrary oxidation of organic matter causes decreasing $\delta^{13}C_{DIC}$ ratios and consequently decreasing $\delta^{13}C_{shell}$ ratios (Schöne and Surge, 2012). Additionally, different plants use different forms of CO^2 fixation (C3, C4, Crassulaceen Acid Metabolism (CAM)). During this fixation, kinetic fractionation of carbon isotopes occurs which leads to characteristic $\delta^{13}C$ ratios for the different forms of carbon dioxide fixation (Chikaraishi et al., 2004; O'Leary, 1988). In proximal settings shell derived $\delta^{13}C$-ratios can therefore also give information about the dominating plants in the region. This is due to the fact that C4 plants

generally have a higher $\delta^{13}C$-ratio (Chikaraishi et al., 2004; Goewert et al., 2007). Unfortunately, bivalves do not precipitate in isotopic equilibrium with DIC and kinetic effects play important roles ((Mcconnaughey and Gillikin, 2008; Chauvaud and Thébault, 2011; De Ridder et al., 2004; Gillikin et al., 2006b). Bivalves do not solely take up carbon through food but they also incorporate metabolic CO_2 into their shell. Additionally, the amount of metabolic CO_2 is dependent on the stage of ontogeny (Mcconnaughey and Gillikin, 2008). In most bivalves the amount of metabolic carbon in the shell is less than 10% (McConnaughey et al., 1997) but can be as high as 40% (Gillikin et al., 2006b, 2007). This metabolic effect however does not necessarily prevent $\delta^{13}C$ ratios from being useful for reconstruction purposes. One field of application could be the quantification of metabolic rates in different specimens (Lorrain et al., 2004). This data could be used to quantify the effects of metabolic changes on E/Ca ratios such as Mg/Ca and Sr/Ca. Gillikin et al., 2006b investigated *Mytilus edulis* that were transferred from a marine setting to a brackish setting. The experiment revealed a shift of $\delta^{13}C$ ratios towards lower values. This was attributed to salinity changes and changes of the metabolic rate, but the sensitivity was too low to allow for precise salinity reconstructions (Gillikin et al., 2006b). Future research should focus on precisely determining the metabolic contribution to account for this effect (Yan et al., 2014).

Similar to oxygen isotopes, carbon isotopes in CWC are characterized by significant differences between COC's and fibrous deposits. Fibers are systematically enriched compared to the COC in addition to a general equilibrium offset of 3-4‰ (Blamart et al., 2005). The offset corresponds to an isotopic shift associated with the organism's respiration (Blamart et al., 2005). Differences between the skeleton sections (COC, fibrous deposits) can be explained with the calcification model of Adkins et al.,2003: The authors suggested a model with two distinct pools, CO_2 (aq) and seawater DIC. CO_2 diffuses passively through the calicoblastic cells, activated by a pH-gradient that is maintained by Ca-ATPase (Adkins et al., 2003). Depending on the internal pH-regulation and metabolic activity the two reservoirs contribute with changing ratios to the internal calcification pool, thereby altering the isotopic signal recorded in the aragonite (Adkins et al., 2003).

Carbon isotopes in foraminifera are similarly influenced as oxygen isotopes. Respirated, light CO_2 can decrease both carbon and oxygen isotope signals (Rohling and Cooke, 1998; Mackensen and Bickert, 1999). Microhabitat effects (infaunal vs. epifaunal) with different pH regimes, as well as different ontogeny stages and photosymbionts can cause disequilibrium effects through combined effects of influence of metabolic CO_2 and different pH regimes (Rohling and Cooke, 1998). Still, when these effects are carefully considered, carbon isotopes measured in foraminifera can provide interesting insights in water mass transport and hydrological changes as well as precipitation, runoff information and information about the flora on land (Rohling and Cooke, 1998)

1.6.9 Clumped isotopes (Δ^{47} & Δ^{48})

The biggest caveat of stable oxygen isotopes for temperature reconstruction is the necessity to know the $\delta^{18}O$-value of the ambient water. This is however, hardly measurable and must be estimated, which can lead to wrong temperature reconstructions. This problem can be overcome by using new techniques such as clumped isotopes. Molecules such as CO_2, that are made up by elements with multiple isotopes can vary in their isotopic composition. These molecules of different mass are called isotopologues. Carbonate minerals contain many carbonate isotopologues of which four constitute 99.99% of the carbonate content of these minerals and control stable oxygen and carbon isotopic signals (Ghosh et al., 2006). Interesting for clumped isotopes however are the remaining 16 isotopologues which constitute the highest diversity. Exchange reactions between the different isotopologues can be expressed as:

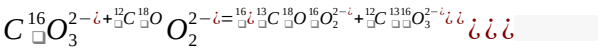

Equation 1-1 Echange reaction between different CO_2 isotopologues

The thermodynamics of the reaction shown above have been thoroughly investigated and show that equilibrium constants for such reactions are dependent on the calcification temperature (Urey, 1947; Wang et al., 2004; Bigeleisen and Mayer, 1947). Following these thermodynamic rules, the equilibrium constant of equation 1 should be 1 at very high temperatures and increase with decreasing temperature. This would shift the equilibrium to the right side of the reaction causing an increasing amount of multiple substituted isotopologues (Ghosh et al., 2006). Therefore, the equilibrium constant from reactions like reaction 1 can be used as a temperature proxy in thermodynamically equilibrated carbonates (Ghosh et al., 2006). This technique is restricted by our current analytical methods (Schöne and Surge, 2012). Currently 10 aliquots á 10 mg are needed for temperature reconstructions with an uncertainty of ± 1°C (Affek et al., 2008; Eiler, 2007; Came et al., 2007). However, the techniques are rapidly improving. With newer devices such as the KIEL IV, only 100 µg in 15 – 20 aliquots are necessary per sample.

Since clumped isotopes are a relatively new technique, bivalve specific papers are scarce but more common than for instance P/Ca related bivalve papers which showcases the importance of clumped isotopes in geosciences. Eagle et al., 2013 report a robust relationship between Δ47 and calcification temperature in multiple bivalve species including *Mytilus edulis*, *Arctica islandica* and *Pecten maximus* among others. Differences between aragonitic and calcitic species as well as influences through carbonate saturation differences

were not observable (Eagle et al., 2013). No significant kinetic effects are also reported from Wacker et al., 2014 for *Spondylus* sp., but they report differing slopes and y-intercepts from the results of earlier studies (Ghosh et al., 2006; Came et al., 2007; Wacker et al., 2014). The results of Wacker et al. however match with the results from Henkes et al., 2013 on mollusc and brachiopod shells as well as the theoretical calcite calibration by Guo et al., 2009. As the studies show none or very minor vital effects on Δ47 values, clumped isotopes are already commonly used for reconstructions (Tobin et al., 2014; Dennis et al., 2013; De Winter et al., 2018; Van Plantinga and Grossman, 2018)

While Δ47 – temperature relationships were considered a practically vital effect free proxy, this hypothesis had to be refuted for several organism species including cephalopods, corals, echinoids and brachiopods. Both CWC (D. dianthus) and WWC (Porites sp.) exhibited pronounced vital effects either in their $\delta^{18}O$/ $\delta^{13}C$ ratio or an enrichment in ^{13}C-^{18}O clumping during winter growth (Ghosh et al., 2006). Ongoing research stated that the vital effects modulating $\delta^{18}O$/ $\delta^{13}C$ ratios derive from pH changes in CWC have no effect on the clumped isotope signal (Thiagarajan et al., 2011). In contrast to Ghosh et al., 2006 the authors also find no evidence for vital effects in Porites sp. which is attributed to the different sampling strategies utilized by Ghosh et al., 2006 and Thiagarajan et al., 2011. While Ghosh et al. sampled with a seasonal resolution, Thiagarajan et al. used annual mean samples and vital effects appear to be only evident in the thin winter bands of the coral (Thiagarajan et al., 2011; Ghosh et al., 2006). The existence of vital effects in both CWC and WWC was, however, also found in other studies regardless of the sampling strategy. Research on hermatypic corals shows a continuous offset from the expected Δ47 values, leading to temperature underestimations by 8°C while ahermatypic corals generally agree with inorganic calibrations (Saenger et al., 2012). The data suggests that increasing calcification rates also increase these vital effects which might be related to fractionation processes during the hydration/hydroxylation of CO2 within the calcifying space (Saenger et al., 2012). These processes are also discussed as the underlying mechanism for vital effects in brachiopods (Bajnai et al., 2018). These vital effects can be resolved using coupled Δ47 and Δ48 measurements. Simultaneous measurements of Δ47 and Δ48 on a single phase allows to identify carbonates that did not precipitate in equilibrium with their parent solution as well as identifying the responsible kinetic fractionation processes (Bajnai et al., 2020)

1.6.10 Radioactive carbon dating (^{14}C)

Radioactive carbon dating is a technique that is readily used with bivalves for dating purposes up to 50,000 years (Peharda et al., 2019; Kubota et al., 2018; Rixhon et al., 2018; Ambrose et al., 2015; Gordillo et al., 2015; Etayo-Cadavid et al., 2019). The technique is based upon the fact, that dead organism loose ^{14}C after their death due to radioactive decay. With knowledge of the initial ^{14}C concentration we can measure the amount of ^{14}C in the

sample and calculate an age when the organism died. However, several potential problems have to be considered. As already mentioned, vital effects can have tremendous effects on elemental ratios and isotopic system alike. Transport of carbon through the different biological pathways can cause isotopic fractionation due to different reaction rates and bonding strengths of different molecular species (Pigati, 2002). However, bivalves do generally incorporate oxygen and carbon isotopes in equilibrium with the ambient water (Mook and Vogel, 1968). When the samples are rich in conchiolin (organic matter) reconstructed ages might be erroneous, as the conchiolin is depleted in ^{14}C relative to the shell material (Hadden et al., 2018).

1.6.11 Boron isotopes ($\delta^{11}B$)

The reconstruction of CO_2 concentrations is a field of growing interest with regards to the climate change we are recently facing. An independent pH proxy, that could be utilized to reconstruct CO_2 concentrations in the past is not available. The measurement of boron isotopes is an emerging technique that could be used for this purpose. Boron exists in the oceans in two forms, boric acid ($B(OH)_3$) and borate-ions ($B(OH)_4^-$). The concentration of these two species is dependent on the seawater pH, where $B(OH)_3$ is dominant in low pH environments and $B(OH)_4^-$ is dominant in high pH environments. Measuring the boron isotopic composition in marine carbonates can therefore give us information about the calcification pH. However, this method relies on a critical assumption, that only borate is incorporated into the carbonate. Measurements on several different biogenic carbonate producers revealed isotopic compositions that are remarkably close to the isotopic composition of borate in seawater (Hemming and Hanson, 1992) which is an indicator that indeed only borate is incorporated into carbonate. A following study, however measured far higher values, which are not explainable if only borate is incorporated (Gaillardet and Allègre, 1995), although it is the general consent.

Boron isotopes measured in bivalves, corals and foraminifera can therefore serve to reconstruct pH in the seawater. However, several caveats have to be monitored. An important factor is the pH-regulation of the organism. Foraminifera, corals and bivalves control their internal pH in order to facilitate calcification or keep cellular gradients up for transport processes (McCulloch et al., 2012a, b; de Nooijer et al., 2014; Hammer et al., 2011). Therefore, the question remains what pH value we are actually reconstructing, the seawater pH or the internal pH of the organisms calcifying fluid. Foraminifera, for instance elevate their internal pH by 0.5 – 1 unit above the ambient seawater (De Nooijer et al., 2009; Bentov et al., 2009). Despite this pH elevation, $\delta^{11}B$ values in most foraminifera are consistent with seawater borate at seawater pH (Rae et al., 2011; Henehan et al., 2016; Foster, 2008). The mechanisms behind this phenomenon are not resolved yet, but possible explanations include: active borate transport, pH elevation only occurring during the initial

chamber formation, pH elevation being countered by carbon concentration and/or carbonate precipitation and pH elevation being less pronounced in the natural environment compared to culture setups (Rae, 2018). On the contrary, corals who display a similar mechanism to regulate their internal pH, imprint this regulation in their $\delta^{11}B$ values (McCulloch et al., 2012b; Anagnostou et al., 2012). Bivalves also alter their internal pH, but different to the aforementioned organisms, they decrease their internal pH, presumably as an effect of metabolic CO_2 (Gillikin et al., 2007). However, calcification still presumes even in undersaturated environments (Crenshaw, 1972; Heinemann et al., 2012). In experiments, the bivalve *Mytilus edulis* showed no variation in $\delta^{11}B$ values with changing ambient pH, indicating $\delta^{11}B$ values in bivalves reflect the internal calcifying fluid pH (Heinemann et al., 2012).

A further explanation for $\delta^{11}B$ values being unaffected by biological pH regulation mechanisms is transmembrane diffusion of boric acid. Boric acid could diffuse through biologic membranes into the calcifying space where rapid equilibration with borate ions occurs. This consequently leads to calcifying space borate isotope values that are consistent with the ambient seawater despite the pH regulation (Gagnon et al., 2021). Based on this mechanism a two-endmember model was proposed. The two endmembers are rapid membrane diffusion of boric acid and consequent equilibration of the calcifying fluid borate isotope composition to seawater values and a slow diffusion endmember where the diffusion of boric acid is negligible (Gagnon et al., 2021). Applying this model to foraminifera, corals and bivalves, foraminifera would show rapid diffusion, whereas corals and bivalves would display negligible boric acid diffusion.

1.7 Selected methods

1.7.1 Inductively coupled plasma optical emission spectrometry (ICP-OES)

Multielement analysis using ICP-OES is a common measuring technique in geosciences (Schöne et al., 2010; Schleinkofer et al., 2019; Schöne et al., 2011; Yan et al., 2013; Alfonso et al., 2008; Lazareth et al., 2003; Hédouin et al., 2011).

ICP-OES is used for measuring elemental concentrations in a wide variety of different materials (carbonate, water, ethanol). The machine uses a hot plasma in which the fluid samples are sprayed. Due to the high energy in the plasma, electrons are excited leading to a shift to higher energy orbitals. When the electrons revert to their original state characteristic radiation is released. This radiation is measured in the spectrometer and used to quantify the calibration of the measured elements.

One of the main advantages of the ICP-OES is the high excitation reached by the ICP, compared to other excitation methods like graphite furnaces. The higher temperature of the

ICP increase the emission intensity by seven magnitudes. The high excitation also allows for several elements being measured simultaneously. Due to the large signal magnitude and relatively low background noise the detection limit is low (ppb or less for some elements) (Olesik, 1991). Additionally, all elements are measured simultaneously in the ICP-OES, which makes it a very fast technique for sample characterization in comparison to atom-absorption spectrometry.

1.7.2 Mass spectrometry

Mass spectrometry is another commonly used technique in geosciences for the determination of the isotopic and elemental composition of sample material. A mass spectrometer generally consists of three parts, the ion source, the analyzer and the detector. In the ion source the analyte is transferred to a gas phase and ionized. Ionization can be accomplished using different techniques. In this work, we used a Finnigan MAT 253 mass spectrometer which is equipped with electron impact ionization technique (EI). A heated metallic filament produces electrons which are accelerated and directed to collide with the vaporized sample (El-Aneed et al., 2009). After ionization, the ions are guided through an electric field and separated according to their mass to charge ratio. The separated ions are then detected in an electron multiplier. In the here presented studies, we used mass spectrometry mainly for the determination of the isotopic composition of carbonate samples but also for elemental characterization as explained in the next section.

1.7.3 Laser ablation inductively coupled plasma mass spectrometry (LA-ICP-MS)

On major drawback of the aforementioned measuring techniques is its limitation regarding the sampling process. As it is a wet-chemical technique, dissolvable samples are needed, mostly in the form of powder. The minimum possible sampling resolution is therefore determined by the tool, that is used for sampling. Common sampling techniques include handheld power tools (micro drilling), similar to dentist tooling (“Dremel”) or CNC controlled mills that are equipped with additional microscopes, so called “Micromills”. Micro drilling with dentist tooling allows for a minimal sampling resolution of 1 mm whereas Micromilling allows for a finer resolution of 0.1 mm. Micromilling has been proven as a reliable way to sample carbonate materials with high spatial resolution (Spötl and Mattey, 2006)

Table 1-4 Comparison of different sampling techniques

	Spatial resolution	Element analysis	Isotope analysis	Speed	Sample preparation	Sample impact
Micro drilling	500-1000 µm	+	+	Medium	None	High
Micromilling	100 µm	+	+	Low	Surface should be approximately flat	High

Laser ablation	10 µm	+	+	High	Surface should be approximately flat	Low

Laser-ablation uses finely focused, pulsed laser with high fluence to rapidly heat and consequently ablate small quantities of sample material. This technique offers an increased spatial resolution up to few µm in combination with high sampling speeds. Coupled to a mass spectrometer, laser ablation offers fast sampling with minimal preparation, low detection limits (sub ng/g) and high precision measurements (Müller and Fietzke, 2016)

The high spatial resolution that is offered by laser ablation is very beneficial for the investigation of high-resolution proxy archives such as bivalves, especially with slow growing cold-water species. Fast growing species such as *Pecten maximus* with a daily growth rate of 250 µm/d (Lorrain et al., 2005) can potentially be sampled with an hourly resolution.

1.7.4 Electron probe micro analysis (EPMA)

EPMA offers an even lower spatial resolution of 1 µm (Müller and Fietzke, 2016). The basic principle of an EPMA is based on electrons emitted from an electron source, accelerated and collimated through lenses to form an electron beam that is targeted at the sample surface. When the electron beam hits the sample surface electrons are removed from low energy orbitals of the atom. These electrons are replaced by electrons from higher energy orbitals causing an emission of different electromagnetic radiations such as x-rays, secondary electrons and backscattered electrons. The wavelength of the emitted x-rays is equivalent to energy difference of the involved orbitals. As these energy levels are unique among the different elements the investigation of the emitted wavelengths allows us to identify and quantify the elemental concentrations in the sample of interest. Two types of analysis are used with EPMA: wavelength dispersive (WDX) and energy dispersive (EDX) x-ray spectroscopy. WDX uses diffraction of the emitted x-rays to accomplish a spectral analysis. Since the spectroscope always analyses a certain wavelength range only a few elements can be measured simultaneously (Thomas and Gemming, 2013). The benefit of WDX is a higher precision especially with light elements. EDX is based on the characteristic energy that the released electrons emit. With EDX all elements can be measured simultaneously but with lower sensitivity than WDX (Thomas and Gemming, 2013). Another important feature of the EPMA is the ability to produce semi-quantitative element maps, which can greatly help us to understand biomineralization processes (see chapter 5)

1.7.5 ^{14}C Sample preparation

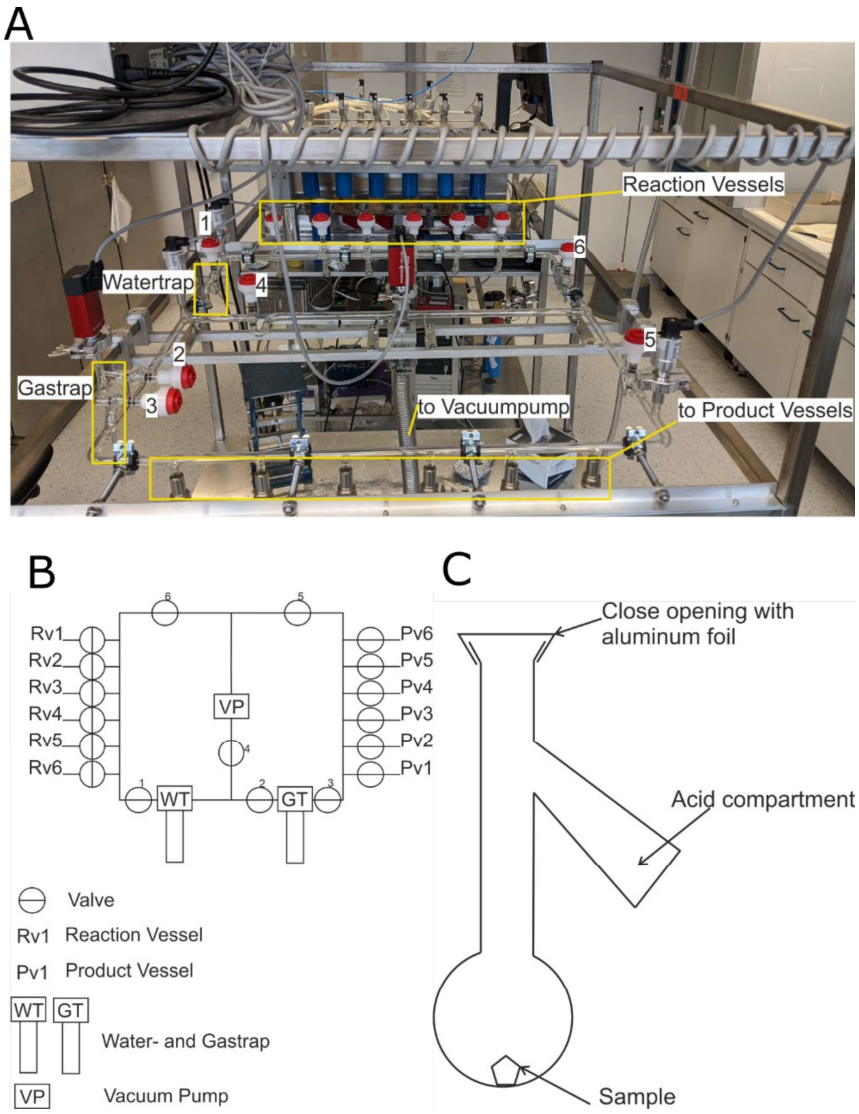

Figure 1-6 Overview and schematic model of the apparatus used for ^{14}C sample preparation. A: Picture of the apparatus (important features are marked in yellow rectangulars), B: Schematic model of the apparatus, C: Model of the reaction vessel

The investigation on the fossil samples is not completed therefore no ^{14}C data is included in this thesis, however I want to give a brief introduction into the preparation of samples for ^{14}C measurements because it is a rather interesting process.

In order to measure calcium carbonate as sample material, the sample material has to be prepared to extract the carbon from it. For a ^{14}C measurement around 1mg carbon is needed which corresponds to around 10 mg of calcium carbonate. Some material is lost during the preparation process, therefore a sample size of ≈ 20 mg iss advisable.

The preparation starts with leaching of the samples, which are best provided as solid samples and not as powder. The leaching process cleans the sample from possible

contamination. The samples are submerged in 4% HCL for at least 1 minute (depending on initial sample size). Afterwards they are washed with VE/MQ water. Optimally, each sample should weigh around 10 mg after the leaching process. After the leaching process the samples are air dried in an oven for 2 hours at 65°C. After the drying process all sample should be weighed and transferred into the reaction vessels which are closed with aluminum foil (Fig 6/C).

The process can be explained as follows:

$$CaCO_3 + HCL = CO_2 + H_2O + Ca\,Cl_2$$

Equation 1-2 Reaction of carbonate with acid to CO_2 and $CaCl_2$

The calcium carbonate reacts with hydrochloric acid to carbon dioxide (wanted product), water and calcium chloride. The water and calcium chloride are unwanted byproducts which are removed in the water trap.

The extraction process is explained on the example of the extraction facility located in the institute for environmental physics in Heidelberg. The facility consists of six reaction vessel and six product vessels that are connected to a bi-circular vacuum glass system (Fig 6/A + B).

Before the extraction process starts, the whole system should be evacuated for an extended period of time. The vacuum should be around 5^{-5} – 10^{-5} mbar. For this all the valves should be open. A cold mixture of Acetone and dry ice (solid CO_2) (slushy consistency) must be prepared in a Dewar vessel and a Dewar vessel with liquid nitrogen must be prepared.

Before the first extraction begins, all pressure sensors should be checked and the pressures inside the system should be noted.

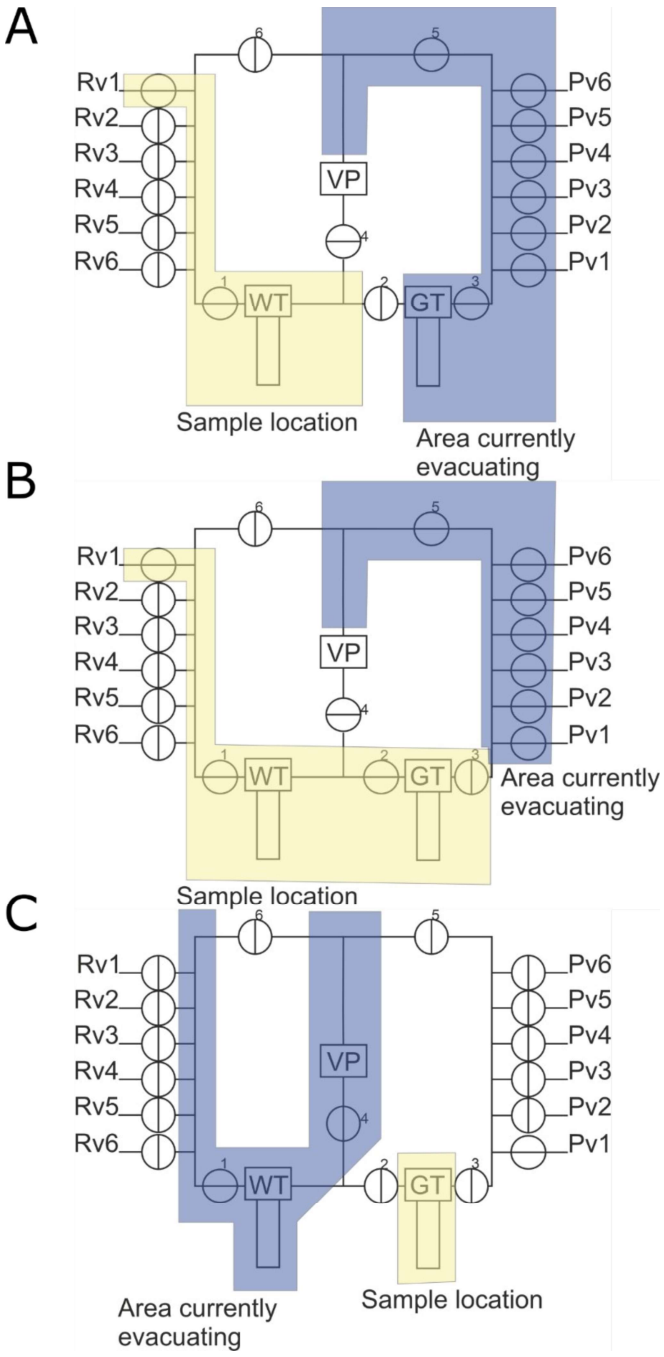

Figure 1-7 Overview of the carbon extraction process. A: Sample transfer from reaction vessel to water trap, B: Sample transfer to gas trap, C: Sample transfer to product vessel. The sample location is marked by the yellow area, the areas that are currently evacuated are marked by the blue areas.

The process of extracting carbone from carbonate samples includes the following steps:

1. Fill the acid compartment in the reaction vessel (Fig.6/C) with 0.5 ml of 3M HCL. Use a Syringe

2. Attach the reaction vessel to position 1 of the device. Keep valves closed.

3. Close all valves necessary (2,3,4,5,6)

4. Place Dewar vessel with acetone – dry ice mixture under the water trap.

5. Open the valve to the reaction vessel. Air is now in the system and needs to be removed. However, the vacuum pump cannot handle that much air, therefore we need to divide the pressure. This is done by closing Valve 1. Afterwards we can open valve 4 and half of the air is evacuated (vacuum pump will audibly work harder). Valve 1 can be opened when the sound of the vacuum pump normalized. The air from the reaction vessel should be evacuated at least 5 minutes.

6. Close valves 2 and 4, open Valve 3 and 5 so the parts not in use will be further evacuated. Valve 6 stays always closed.

7. Place liquid nitrogen under the gas trap

8. Let the reaction begin by turning the reaction vessel so the acid drips onto the sample. Keep reaction vessel valve closed, so nothing spills into the device.

9. Open the reaction vessel valve. Valves 2,4,5 are closed.

10. Wait a few minutes so the water gets frozen in the water trap

11.Close valve 3 and open Valve 2. The carbon dioxide should become visible in the gas trap as a silver line. Wait until the pressure stop decreasing (Fig. 7/B).

12. Close Valve 2 and Rv1. The carbon dioxide is now completely in the gas trap.

13. Remove the liquid nitrogen and heat the finger of the gas trap with a heat gun. The pressure will rise to 100-200 mbar. Note that value.

14. Valve 4 and 1 can be opened. Valve 5 and Pv2-6 should be closed.

15. Place liquid nitrogen under the freeze finger of the product vessel. Open valve Pv1 and 3. Carbon dioxide will liquify in the freeze finger of the product vessel (Fig. 7/C).

16. Close Pv1. The sample is now ready. When all samples are prepared, graphitization is the next step.

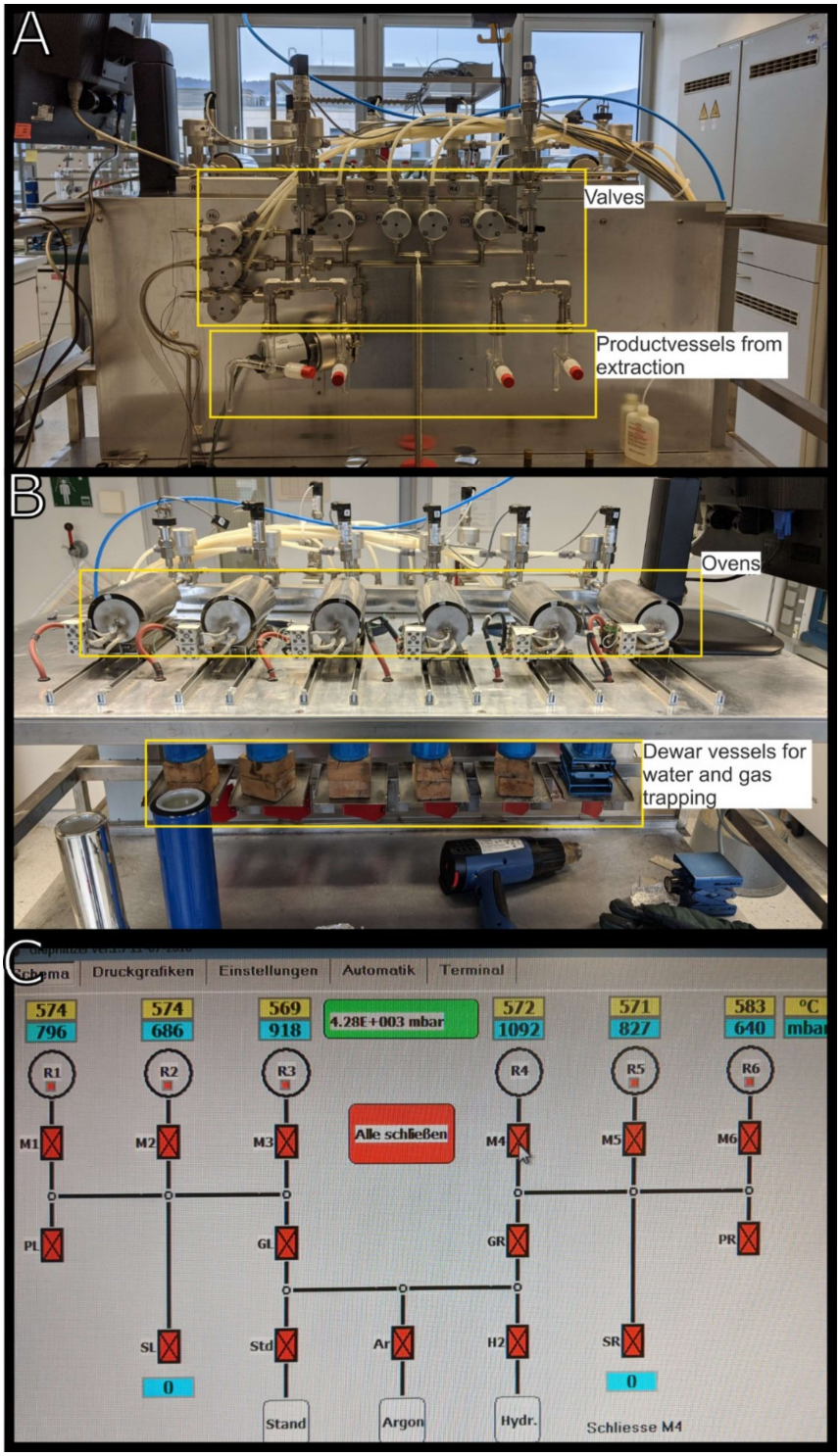

Figure 1-8 Picture of the device used for graphitization and UI of the controls. A: Valve system and location for product vessel from carbon extraction, B: Ovens for the graphitization process, C: UI of the control system

During the graphitization the carbon dioxide gathered during extraction is reduced using H_2 and Fe to C.

$$CO_2 + H_2 + Fe = C + Fe + H_2O$$

Equation 1-3 Reduction of CO_2 to C with Fe as a catalyst

The iron acts as a catalyst to increase reaction speed. The H_2 acts as a reducing agent and is oxidized to water.

The device consists of six Reactors (Fig. 8/B) with ovens which are connected through a system of valves and hoses to 4 Product vessels from the extraction process (Fig. 8/A). The device is divided into a left and right part. The sites are alternated after every sample. After 2 samples, new product vessels have to be connected.

1. The reactors have to be loaded with 3 mg of Fe (note weight). The Fe has to be conditioned, which means that it is repeatedly oxidized and reduced again. This process is automated and takes about 3 hours. Prior to conditioning the iron should be erected with a magnet to increase the surface area.

2. Put liquid nitrogen under the freeze finger of reactor 1 to determine the target.

3. Open the product vessel valve. If the pressure sensor und SL (Fig. 8/C) displays more than 50 mbar, the pressure has to be divided by closing the valve again.

4 Open Valve M1 and SL. The sample travels into the reactor.

5. Close all valves again (M1, SL, Product vessel)

6. Remove liquid nitrogen and heat the freeze finger with a heat gun.

7.Read the pressure (Blue square over reactor). It should be around 200 – 300 mbar.

8. Place the liquid nitrogen under the freeze finger again.

9. Calculate the amount of H_2 needed by multiplying the pressure from step 7 with 2.2 and 0.74.

10. Open valve M1, GI and Hydr. H_2 will flow into the reactor. Close Hydr. Valve when needed pressure is reached.

11. Remove liquid nitrogen again and heat freeze finger to note Pges.

12. Place Acetone – Dry ice mixture under the freeze finger and start reaction by rolling the oven (575°C) over the reactor.

13. Repeat with further sample, alternating sides.

14. When the reaction is finished, evacuate the whole system again.

15. Fill the reactor with argon by opening all reactor (M1-6), open valve GL and Gr and Argon until pressure reads around 700 mbar. Close all valves

16. When pumping the Argon out of the system, pressure division is very necessary. Open GL and close again followed by PL open. Repeat several times.

1.8 Structure of this thesis

This thesis consists of six manuscripts, of which three were published in peer-reviewed scientific journals. One chapter is currently in submission. Two additional chapters give preliminary results about the latest projects.

In Chapter three we researched the environmental and biological controls of Na/Ca ratios in different CWC species. The manuscript was published in Biogeosciences on 20.09.2019 under the DOI 10.5194/bg-16-3565-2019

Chapter four is a geochemical investigation on *Acesta excavata.* We measured Mg/Ca, Sr/Ca and Na/Ca ratios and compared the results with in-situ gathered environmental information to explore if the measured element ratios can be used for paleoreconstructions. The Manuscript was published in PlosONE on 30.04.2021 under the DOI 10.1371/journal.pone.0245605

In chapter five we explore the parasite-host relation of *Hyrrokkin sarcophaga* with *Desmophyllum pertusum* and Acesta excavata on the basis of E/Ca and stable isotope measurements. The Manuscript was published in Biogeosciences on 20.08.2021 under the DOI 10.5194/bg-18-4733-202

Chapter six explores the effects of ethanol preservation on geochemical signatures in different marine carbonates (bivalves, corals, foraminifera). The Manuscript was submitted to Limonology and Oceanography: Methods on 27.09.2021

Chapter seven aims to extend the results from chapter four. with measurements of P/Ca, Mn/Ca and Ba/Ca to possibly reconstruct plankton dynamics. This manuscript was presented at EGU 2020.

Chapter eight presents preliminary results that extend the research started in chapter five. We used boron isotopes and B/Ca ratios to further explore parasite/host interactions with regards to pH-regulation mechanisms that are utilized by the host and possibly alter the

isotopic composition of the parasites. This manuscript was presented at the Boron Isotope Short Course at Goldschmidt Conference 2021.

2 Environmental and biological controls on Na/Ca ratios in scleractinian cold-water corals

Nicolai Schleinkofer[1,2], Jacek Raddatz[1,2], André Freiwald[3,4], David Evans[1,2], Lydia Beuck[3], Andres Rüggeberg[4], Volker Liebetrau[5]

[1]Institute of Geosciences, Goethe University Frankfurt, Altenhöferallee 1, 60438 Frankfurt am Main, Germany

[2]Frankfurt Isotope and Element Research Center (FIERCE), Goethe University Frankfurt, Altenhöferallee 1, 60438 Frankfurt am Main, Germany

[3]Senckenberg am M0eer, Marine Research Department, Südstrand 40, 26382 Wilhelmshaven, Germany

[4]MARUM (Zentrum für Marine Umweltwissenschaften), Bremen University, Leobener Str. 8, 28359 Bremen, Germany

[5]Department of Geosciences, Faculty of Science and Medicine, University of Fribourg, Chemin du Musée 6, CH-1700 Fribourg, Switzerland

[6]GEOMAR Helmholtz Centre for Ocean Research Kiel, Wischhofstr. 1-3, D-24148 Kiel, Germany

Published in Biogeosciences on 20.09.2019 under the DOI 10.5194/bg-16-3565-2019

(https://bg.copernicus.org/articles/16/3565/2019/)

2.1 Abstract

Here we present a comprehensive attempt to correlate aragonitic Na/Ca ratios from *Desmophyllum pertusum* (formerly known as *Lophelia pertusa*), *Madrepora oculata* and a caryophylliid cold-water coral (CWC) species with different seawater parameters such as temperature, salinity and pH. Living CWC specimens were collected from 16 different locations and analyzed for their Na/Ca ratios using solution-based inductively coupled plasma-optical emission spectrometry (ICP-OES) measurements.

The results reveal no apparent correlation with salinity (30.1–40.57 g/kg), but a significant inverse correlation with temperature (-0.31 ± 0.04 mmol/mol/°C). Other marine aragonitic organisms such as *Mytilus edulis* (inner aragonitic shell portion) and *Porites* sp. exhibit similar results highlighting the consistency of the calculated CWC regressions. Corresponding Na/Mg ratios show a similar temperature sensitivity to Na/Ca ratios, but the combination of two ratios appear to reduce the impact of vital effects and domain-dependent geochemical variation. The high degree of scatter and elemental heterogeneities between the different skeletal features in both Na/Ca and Na/Mg however limit the use of these ratios as a proxy and/or make a high number of samples necessary. Additionally, we explore two models to explain the observed temperature sensitivity of Na/Ca ratios for an open and semi-enclosed calcifying space based on temperature sensitive Na and Ca pumping enzymes and transport proteins that change the composition of the calcifying fluid and consequently the skeletal Na/Ca ratio.

2.2 Introduction

Sodium to calcium ratios (Na/Ca) has been proposed as a new tool in paleoceanography to reconstruct seawater salinities. Cultured benthic and planktonic foraminifera as well as living planktonic foraminifera from the Red Sea showed the potential of calcitic Na/Ca ratios as a salinity proxy (Mezger et al., 2016; Wit et al., 2013)

Independent proxies are needed to reconstruct the environment in which CWC lived in the past to better understand their temperature/salinity/pH tolerances and to study the influence

of parameters on their spatial distribution. This would also help to better locate new unknown sites of CWC occurrences. For temperature and pH, different geochemical proxies can be used to calculate these parameters in the geological past. Sr/Ca and Li/Mg ratios serve as temperature proxies (Cohen et al., 2006; Gagnon et al., 2007; Mitsuguchi et al., 1996; Raddatz et al., 2013; Rollion-Bard and Blamart, 2015; Shirai et al., 2005; Montagna et al., 2014; Raddatz et al., 2014a)

Reconstructing past salinities can be accomplished with several different techniques, e.g. diatom and dinoflagellate species composition(Zonneveld et al., 2001)

The influence of seawater salinity on Na/Ca ratios are known from Atlantic oysters (Rucker and Valentine, 1961), barnacle shells (Gordon et al., 1970) as well as inorganically precipitated calcium carbonate (Ishikawa and Ichikuni, 1984). Recently it has been shown that Na incorporation in calcitic planktonic and benthic foraminifera appears to be at least partly controlled by seawater salinity (Allen et al., 2016 (only in *Globigerinoides ruber*); Mezger et al., 2016; Wit et al., 2013). According to Wit et al. (2013), the incorporation of Na in calcite depends on the activity of Na in the seawater which is a function of salinity. There is strong evidence that Na substitutes for Ca in biogenic aragonite despite its charge difference (Okumura and Kitano, 1986; Yoshimura et al., 2017). However, since Na and Ca compete for the same lattice positions, the calcium concentration and Na/Ca activity ratio of the surrounding seawater might also control the amount of sodium incorporation (Ishikawa and Ichikuni, 1984; White, 1977). Over longer periods of geological time, when concentrations of some elements in seawater have varied, this would inhibit the use of Na/Ca ratios as a salinity proxy but might prove useful to reconstruct oceanic calcium concentrations. Recent studies also show that the Na/Ca ratio in foraminiferal calcite is also mainly controlled by seawater Na/Ca ratios (Hauzer et al., 2018).

In this study, we investigate the impact of different seawater parameters on the incorporation of Na in the aragonitic skeleton of the scleractinian cold-water coral *D. pertusum, M. oculata* and a caryophylliid species from the Red Sea. The corals were collected alive from a variety

of locations to cover a broad range of temperatures (5.9–21.6°C) and salinities (30.1–40.6 g/kg).

2.3 Materials & methods

2.3.1 Study area and sample collection

Table 2-1 Na/Ca, Sr/Ca, Mg/Ca mean values measured with ICP-OES, standard deviation and sample number. Values relate to certain salinity and temperature envelopes.

	Na/Ca			Sr/Ca			Mg/Ca		
Temperature [°C]	mmol/mol	n	SD	mmol/mol	n	SD	mmol/ mol	n	SD
6.23 ± 0.31	26.30	12	2.88	10.16	12	0.23	4.09	12	1.27
7.94 ± 0.41	25.30	15	2.48	10.13	15	0.24	3.90	14	0.74
9.83 ± 0.46	24.96	5	3.26	10.18	5	0.21	3.83	5	1.49
13.56 ± 0.09	25.33	5	1.43	10.01	6	0.27	4.15	6	0.62
21.64 ± 0.02	21.13	4	0.82	9.94	5	0.34	3.97	5	0.8
	Na/Ca			Sr/Ca			Mg/Ca		
Average Salinity [g/kg]	mmol/mol	n	SD	mmol/mol	n	SD	mmol/ mol	n	SD
30.1	23.42	2	2.25	10.06	2	0.09	4.15	2	2.75
31.2	23.70	5	3.06	10.14	5	0.31	3.74	4	0.73
35.22 ± 0.21	26.18	25	2.46	10.16	25	0.22	3.99	25	1.01
38.67 ± 0.07	25.33	5	1.43	10.01	6	0.27	4.16	6	0.62
40.56 ± 0.01	21.13	4	0.82	9.94	5	0.34	3.97	5	0.8

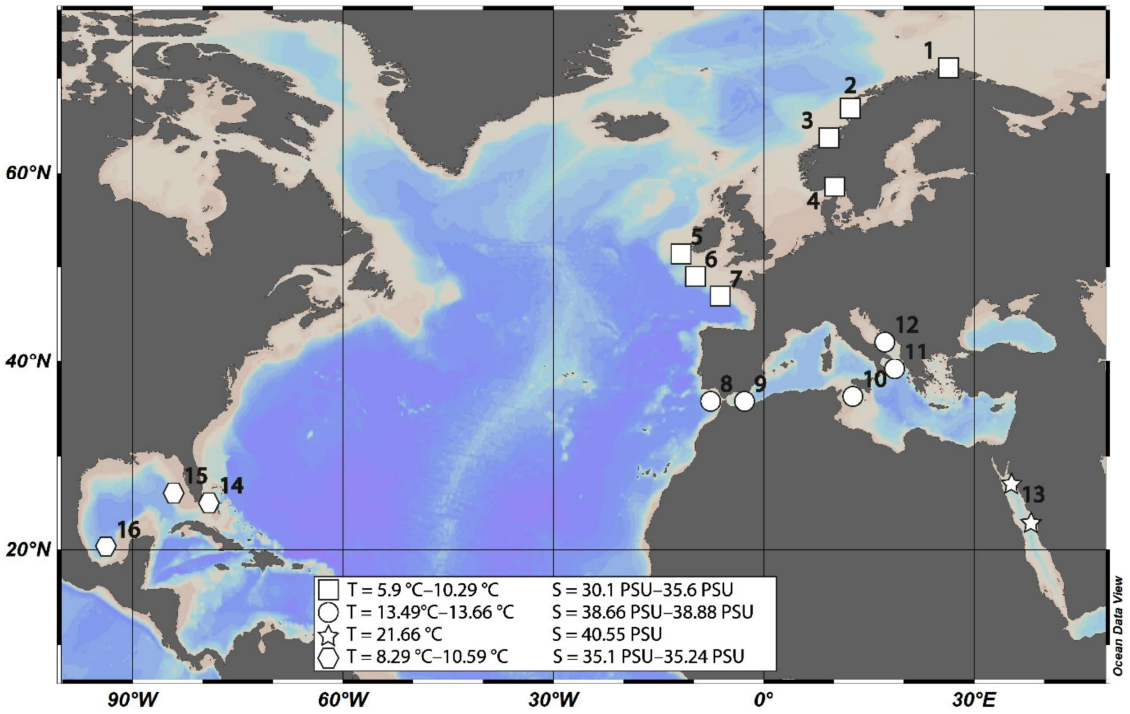

Figure 2-1 Map of sampling locations. Locations are grouped in four areas with similar physical parameters. 1: Lopphavet, Sotbakken, Stjernsund; 2: Traenadjupet; 3: Sula, Nordleksa, Tautra, Røberg; 4: Oslofjord; 5: Galway Mound, 6: Whittard Canyon; 7: Guilvinec Canyon; 8: Meknes Carbonate Mound Province 9: El Idrissi Bank; 10: Urania Bank; 11: Santa Maria di Leuca (SML) Province, 12: Bari Canyon; 13: Red Sea; 14: Great Bahama Bank; 15: Southwest Florida; 16: Campeche Bank

The samples were taken from 45 different coral specimens collected from 16 different locations (Table. 1). Most of the samples (n=25) were collected during different cruises from the Norwegian margin. The other samples derive from the Irish Margin and Bay of Biscay (n=4), the Mediterranean Sea and Gulf of Cadiz (n=7), the Gulf of Mexico and Great Bahama Bank (n=4) and the Red Sea (n=5) (Fig. 1). Conductivity-Temperature-Depth (CTD) downcast data for water parameters was available for all locations except the Red Sea and the Gulf of Mexico. Where no CTD data was available, the water parameters were retrieved from annual averaged data from World Ocean Atlas 2013 (Locarnini et al., 2013; Zweng et al., 2013). Where available, comparison of *in-situ* CTD and WOA13 data, revealed an agreement within 0.15°C in Santa Maria de Leuca and 0.04°C in the Bay of Biscay respectively. The seawater carbonate system data such as pH was taken from the associated cruise report (Flögel et al., 2014) or in case of the Red Sea and the western

Atlantic from Mezger et al., (2016) and CARINA. Flögel et al., 2014 used a WTW Multi 350i compact precision hand- held meter to determine pH (Flögel et al., 2014), pH in the Red Sea was calculated from DIC and TA, measured during PELAGIA 64PE158 (Mezger et al., 2016), using CO2SYS (Lewis and Wallace, 1998). pH values are reported using the total scale.

We took 31 samples from different coral colonies and three different species (*D. pertusum, M. oculata,* Caryophylliidae) that were collected during different cruises. The samples were taken from the uppermost calices after physically cleaning them with a dental drill tool to remove secondary overgrowths. We avoided further cleaning or rinsing with water because studies suggest that structurally substituted Na is readily leached even by distilled water (Ragland et al., 1979). It is possible that organic contents inside the skeleton bias the results as shown in foraminifera (Branson et al., 2016). However, the study on foraminifera shows that the Na/Ca ratio only significantly varies at POS (primary organic sheet) regions. In corals the COC (centers of calcification) would be an equivalent structure, which we avoided during the sampling process. Furthermore, it has been suggested that these regions only significantly affect bulk sample elemental ratios in very thin-walled foraminifera (Branson et al., 2016). In corals the area of COC is larger (20% of the total skeleton radius (Rollion-Bard and Blamart, 2015)) but the Na/Ca ratio does not increase in the COC as strong as it does in the POS areas of foraminifera (Rollion-Bard and Blamart, 2015; Branson et al., 2016). Avoiding the COC areas in bulk samples only reduces the mean Na/Ca ratio by 0.18 mmol/mol ($0.18\,mmol/mol = \overline{Na/Ca}_{inc.COC}^{Sample\,1-i} - \overline{Na/Ca}_{exc.COC}^{Sample\,1-i}$), additional cleaning of organic material is therefore not necessary. An additional 14 samples (*D. pertusum*) were prepared as longitudinal slices through the coral's calice, glued on metal plates. In order to identify elemental heterogenities within the theca wall, subsamples were taken using a Micromill (Merchantec MM-000-134).

2.3.2 ICP-OES Analyses

Elemental ratios were measured by inductively coupled plasma optical emission spectrometry (ICP-OES). The ICP-OES analysis was carried out with a Thermoscientific iCap 6300 dual viewing at Goethe University/Frankfurt. This machine is both capable of measuring

axially and radially. Alkali metals (Na) were measured radially on line 589.59 nm whereas earth-alkali metals (Mg, Sr) were measured axially on lines 279.55 nm and 421.55 nm respectively. The sample powder (≈ 140 µg) was dissolved in 500 µl HNO_3 (2%) and 300 µl aliquots were separated. Subsequently 1500 µl of 1.2 mg/l yttrium solution was added to each aliquot as an internal standard resulting in 1 mg/l. The intensity data was background subtracted and standardized internally to Y and normalized to Ca. External standards were mixed from single element standard solutions to match the typical element concentrations of cold-water corals (cf. Rosenthal et al., 1988). The coral standard JCp-1 (Hathorne et al., 2013a; Okai et al., 2002) was measured after every tenth sample to allow for drift correction and monitor measurement quality.

Relative precision of the Element/Ca measurements was based on the international calcium-carbonate standard JCp-1 (20 replicates) and amounts to 20.47 ± 0.68 mmol/mol Na/Ca (19.8 ± 0.14 mmol/mol (Okai et al., 2002)), 4.09 ± 0.11 mmol/mol Mg/Ca (4.199 ± 0.065 mmol/mol (Okai et al., 2002; Hathorne et al., 2013)) and 9.36 ± 0.07 mmol/mol Sr/Ca (8.838 ± 0.042 mmol/mol (Okai et al., 2002; Hathorne et al., 2013)). Measurements were conducted in two sessions lasting ten and five hours.

2.3.3 Data processing

Before calculations of correlations or applying statistics outliers were removed from the raw data. Outliers were identified by the average ±1.5 SD per oceanic region (Norwegian margin, Bay of Biscay/Irish Margin, Mediterranean Sea, Red Sea, Gulf of Mexico/Bahamas). The threshold was chosen to eliminate data points <15 mmol/mol and >35 mmol/mol cover a range from 15 to 35 mmol/mol which is roughly 5 mmol/mol higher and lower than the reported range from a similar study (Rollion-Bard and Blamart, 2015). The profiled samples were additionally checked for values that derive from the COC, which are identifiable through a positively correlating increase in Mg/Ca and Na/Ca. The chosen threshold was the mean of the profiled sample + 2SD of JCp-1. Statistical calculations were conducted with the ORIGIN Pro software suite.

2.4 Results

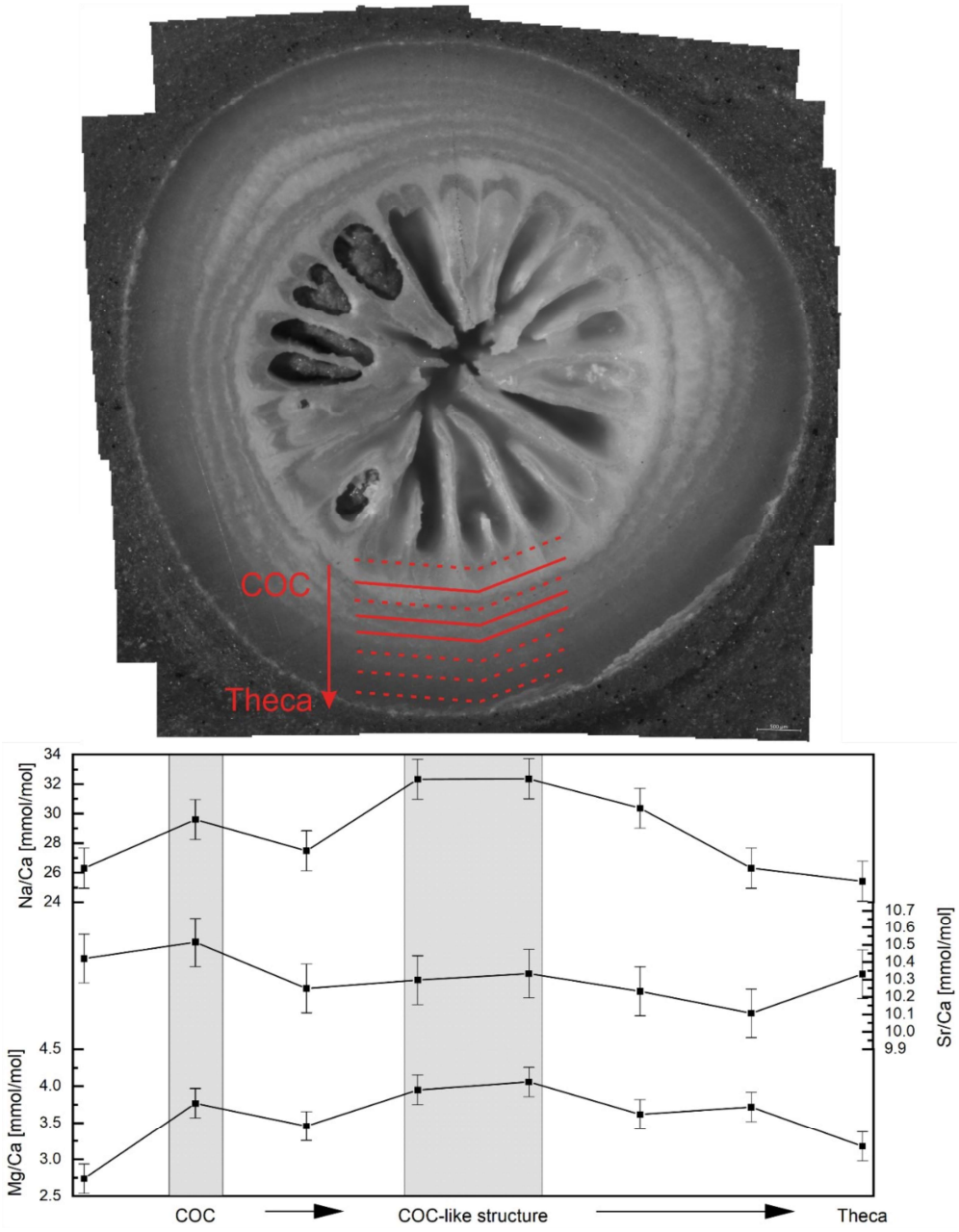

Figure 2-2 Intra-individual element heterogeneities of one sample from Lopphavet (D. pertusum). Shaded-grey areas indicate COC and COC-like structures (solid lines in sample picture). Error bars indicate 2SD of the JCp-1 mean. Within the uncertainty Sr/Ca ratios show no significant changes throughout the coral, whereas Mg/Ca and Na/Ca show variations of 1.25 mmol/mol and 6 mmol/mol respectively.

Spatial distribution patterns show great variations in Na/Ca ratios through the coral's skeleton (Fig. 2). In the COC and COC-like structures (structures that geochemically correspond to COC but morphologically to fibrous deposits) Na/Ca ratios show significant increases but the

amount of increase relative to the mean is not uniform in the sample. Increases range from +2 to +10 mmol/mol. Mg/Ca is positively correlated with Na/Ca in the COC structures but mostly independent from each other in the fibrous deposits (FD). Similar to Na/Ca, the amplitude of Mg/Ca in the COC-structures is very variable in their amount and ranges from +0.5 to +3 mmol/mol. Both sodium and magnesium are often enriched in the outermost parts of the theca. Sr/Ca ratios are mostly stable throughout the theca and seem to be independent from the different skeletal structures. In some samples, co-variances between Sr/Ca and Mg/Ca; Na/Ca are present but in general they do not appear to be controlled by the skeletal morphology in the same way as Mg/Ca and Na/Ca as shown by their independency from the different skeletal structures.

2.4.1 Element/Ca ratios of scleractinian cold-water corals

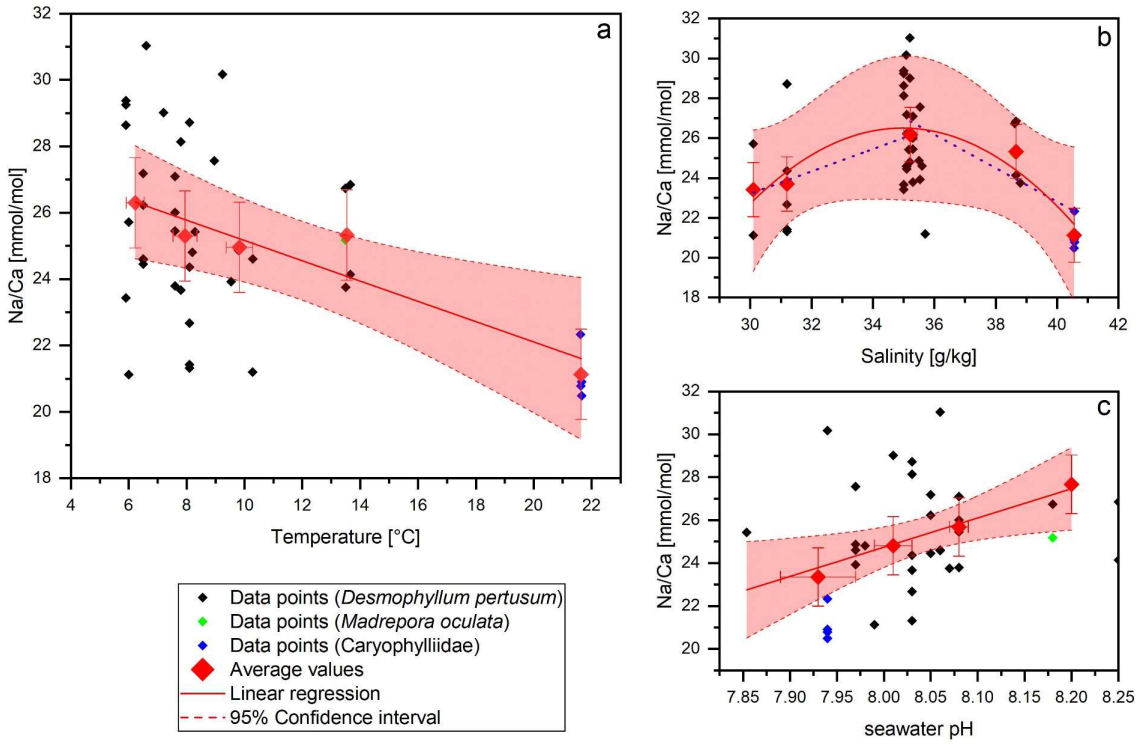

Figure 2-3 Na/Ca data (without COC) plotted against water temperature, salinity and pH. Red diamonds indicate averaged values for temperature ranges. Temperature ranges are 5–7°C, 7–9°C, 9–11°C, 13–15°C and 21–23°C. X-Error relates to the SD of the temperature/salinity mean. Y- Error bars indicate 2SD of the JCp-1 mean. Red lines are linear regressions of the averaged values with the 95 % confidence interval shaded. Blue dotted lines indicate linear regressions for different salinity ranges.

Na/Ca ratios vary between 20.49 ± 1.36 (1SD) mmol/mol in the Red Sea and 31.04 ± 1.36 mmol/mol in the Norwegian reefs with a mean at 25.22 mmol/mol and a standard deviation of 2.8 mmol/mol (Fig. 3). The values are in accordance to previous studies on *D. pertusum* (21.94–28.11 mmol/mol (Rollion-Bard and Blamart, 2015)), but 5 mmol/mol higher than reported for zooxanthellate corals (Amiel et al., 1973; Busenberg and Niel Plummer, 1985; Mitsuguchi et al., 2001; Ramos et al., 2004; Swart, 1981). Significant deviations between *D. pertusum (n=38)*, *M. oculata* (n=2) and Caryophylliidae (n=5) are not observable. A linear correlation between salinity and Na/Ca over the whole salinity range is not observable, but the present dataset is best described with a second order polynomial function. Accordingly, there is a positive trend from 30.1–35 g/kg followed by a negative trend from 35–40.5 g/kg. Linear regressions equal: $f(S_{30.1\text{-}35}) = 6.4 + 0.56 * S$ ($R^2 = 0.99$, $P = 0.072$) and $f(S_{35\text{-}40.5}) = 56.61 - 0.84 * S$ ($R^2 = 0.66$, $P = 0.4$). As the *P*-values show a significant slope is missing in all these regressions. In the case of the polynomial fit the *P*-value shows that the fit is not significantly superior to $f(S_{30,1\text{-}40,5}) = \text{constant}$.

Na/Ca and temperature show a significant negative correlation, which is however mainly driven by the samples from the highest temperature (Red Sea). The linear regression equals:

$$f^{\square}_{T6-22\,^{\circ}C} = 28.2 \pm 0.9 - 0.31 \pm 0.07 \times T \left(R^2 = 0.87, P = 0.02 \right)$$

Equation 2-4 Linear regression between Na/Ca and seawater temperature

Temperature and salinity show a positive correlation; accordingly, this negative correlation cannot be caused by covariances between salinity and temperature. Corals from the Mediterranean Sea are slightly elevated in their Na/Ca ratio, but within error they still fit the correlation with both salinity and temperature. Distribution coefficients ($K_d^{Na} = Na/Ca_{carbonate}/ Na/Ca_{seawater}$) at specific temperatures for several different species, including the scleractinian cold-water corals from this study, *Porites* sp. and *M. edulis*, show similar values. K_d^{Na} from this study amounts to $K_d^{Na}{}_{(6.2°C)} = 5.73*10^{-4}$, $K_d^{Na}{}_{(7.9°C)} = 5.51*10^{-4}$, $K_d^{Na}{}_{(9.8°C)} = 5.44*10^{-4}$, $K_d^{Na}{}_{(13.5°C)} = 5.62*10^{-4}$, $K_d^{Na}{}_{(21.6°C)} = 4.73*10^{-4}$. Distribution coefficients for *Porites* sp. and *M. edulis* are $K_d^{Na}{}_{(26.03°C)} = 4.6*10^{-4}$ (Mitsuguchi et al., 2001) and $K_d^{Na}{}_{(12.5°C)} = 5.25*10^{-4}$ (Lorens and

Bender, 1980) respectively. For comparison, the inorganic distribution coefficient is with $4.00*10^{-4}$ at 15°C, about 20% lower (Kinsman, 1970). The results from White (1977) show that the composition of the solution affects the elemental ratios in the precipitate, but in the study from Kinsman (1970) the precipitation happened from seawater. Therefore, it is reasonable to use this data for comparison. A combined regression using the data from this study, the *D. pertusum* data from Rollion-Bard and Blamart (2015), *M. edulis* data from Lorens and Bender (1980) and *Porites* sp. data from Ramos et al. (2004) and Mitsuguchi et al. (2001) equals:

$$f^{\square}_{T6-27.63\,^{\circ}C} = 28.03 \pm 0.7 - 0.31 \pm 0.04 \times T \left(R^2 = 0.9, P < 0.0001\right)$$

Equation 2-5 Combined regression between Na/Ca and seawater temperature with data from other authors

Na/Ca also shows a significant positive correlation with pH of the ambient seawater. Linear regression equals: f(pH) = - 84.26 ± 40.15 + 13.63 ± 5.49 * pH (R^2 = 0.14, *P*= 0.017). A negative trend between pH and temperature is visible.

2.4.2 Mg/Ca & Sr/Ca

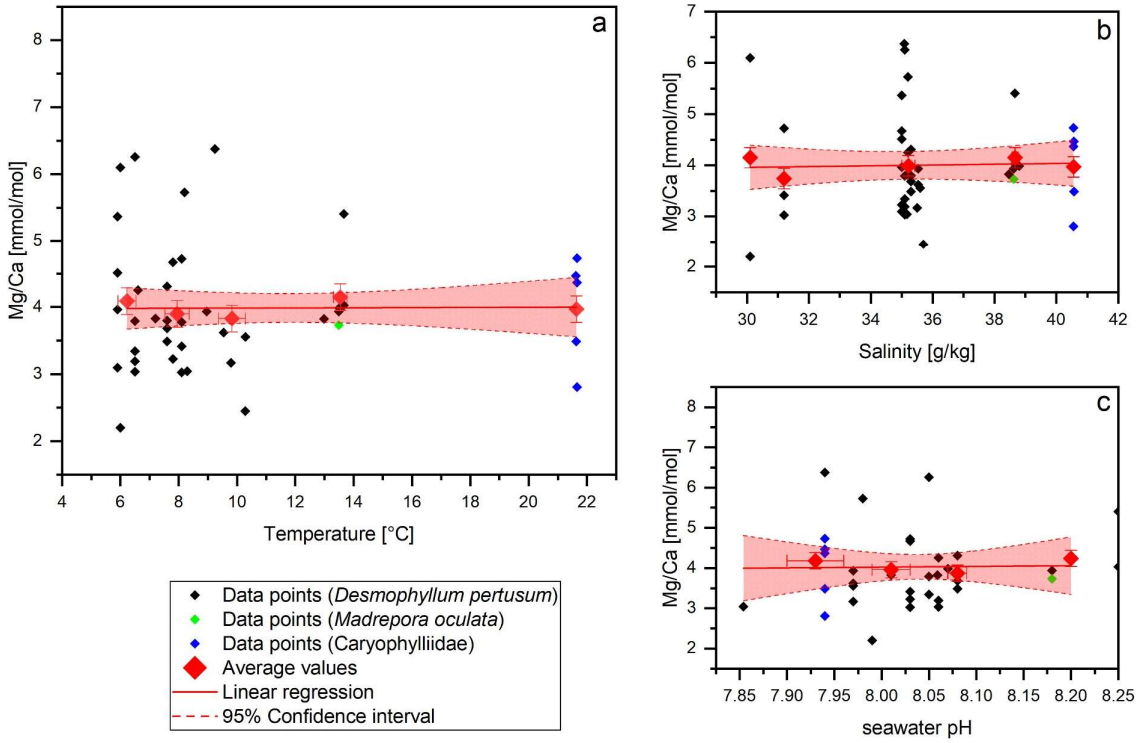

Figure 2-4 Mg/Ca data (without COC) plotted against water temperature, salinity and pH. Red diamonds indicate averaged values for temperature ranges. Temperature ranges are 5–7°C, 7–9°C, 9–11°C, 13–15°C and 21–23°C. X-Error relates to the SD of the temperature/salinity mean Y- Error bars indicate 2SD of the JCp-1 mean. Red lines are linear regressions of the averaged values with the 95 % confidence interval shaded.

Mg/Ca values vary between 2.2 ± 0.2 mmol/mol in the Red Sea and 6.38 ± 0.2 mmol/mol in the Mediterranean Sea with a mean of 3.99 mmol/mol and a standard deviation of 0.97 mmol/mol (Fig. 4). Maximum values are higher than literature states for *D. pertusum* (2.99–4.72 mmol/mol (Raddatz et al., 2013; Rollion-Bard and Blamart, 2015; Cohen et al., 2006;

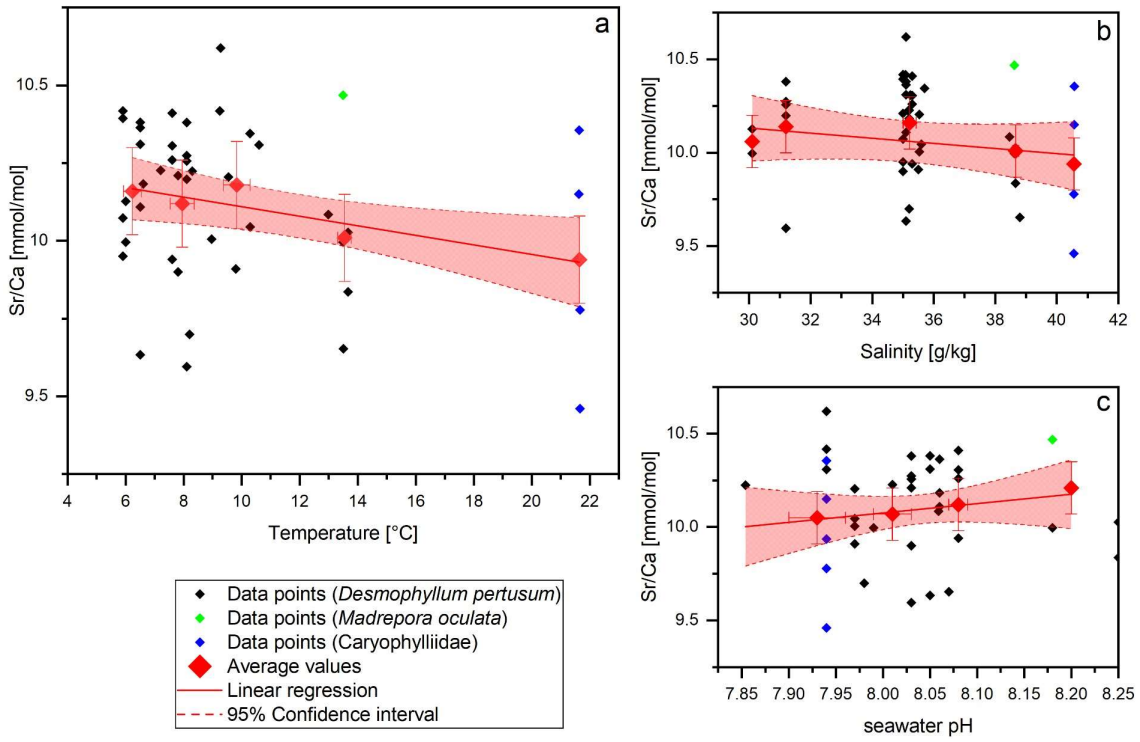

Gagnon et al., 2007)) but the mean values are well inside the range of literature. Significant deviations between *D. pertusum*, *M. oculata* and Caryophylliidae are not observable, although there are limited published data *M. oculata* and Caryophylliidae. Seawater parameters such as temperature, salinity and pH have no significant effect on Mg/Ca ratios in the skeleton.

Figure 2-5 Sr/Ca data (without COC) plotted against water temperature, salinity and pH. Red diamonds indicate averaged values for temperature ranges. Temperature ranges are 5–7°C, 7–9°C, 9–11°C, 13–15°C and 21–23°C. X-Error relates to the SD of the temperature/salinity mean. Y- Error bars indicate 2SD of the JCp-1 mean. Red lines are linear regressions of the averaged values with the 95 % confidence interval shaded.

Sr/Ca values vary between 9.46 ± 0.14 and 10.46 ± 0.14 mmol/mol with a mean of 10.1 ± 0.14 mmol/mol and a standard deviation of 0.25 mmol/mol (Fig. 5). Both maximum and minimum values derive from corals that grew in reefs that are located in the Trondheimfjord. The values are in accordance to previous studies on *D. pertusum* (9.27–10.05 mmol /mol (Raddatz et al., 2013; Cohen et al., 2006; Gagnon et al., 2007)). Significant deviations between *D. pertusum*, *M. oculata* and Caryophylliidae are not observable. Despite the known temperature effect on Sr/Ca ratios this effect is not pronounced in this dataset. The correlation shows a strongly deviating slope of -0.015 mmol/mol/°C in comparison to that given in literature (-0.083 ± 0.017 mmol/mol/°C (Raddatz et al., 2013)). Linear regressions equal: f(T) = 10.26 ± 0.05 – 0.015 ± 0.004 * T (R^2 = 0.83, *P* = 0.03). Sr/Ca vs. salinity values show a distribution pattern similar to that of Na/Ca vs. salinity values with the maximum at 35 g/kg and descending values at lower and higher salinities but an AIC and a F-Test confirm that a linear fit is better suited. The Linear regression equals f(S) = 10.58 ± 0.03 – 0.015 ± 0.01 * S (R^2 = 0.52, *P* = 0.17). *P*-values show that the correlation is not significant.

2.4.3 Element concentrations in the extracellular calcifying fluid (ECF)

Based on the assumption of a semi-enclosed ECF with seawater-leakage and a consequent $[Na]_{ECF}$ similar to $[Na]_{Seawater}$ it is possible to calculate $[Ca]_{ECF}$ and $[Mg]_{ECF}$ using skeletal Na/Ca and Mg/Ca data. Assuming $[Na]_{Seawater} = [Na]_{ECF}$ = 455 mmol/l (Turekian et al., 2010) and an invariant Na distribution coefficient, $[Ca]_{ECF}$ can be calculated with the following equation:

$$[Ca]_{ECF} = \frac{[Na]_{ECF} * K_d^{Na}}{\frac{Na}{Ca}_{Coral}}$$

Equation 2-6 Equation to calculate the concentration of Ca in the ECF

In order to do so, knowledge of K_d^{Na} is required. White (1977) reports 1.8 – 4.1*10^{-4} for inorganic aragonite in the four experiments with solution Na/Ca closest to the natural seawater ratio (~45 mol/mol), which would result in predicted aragonite Na/Ca ratios of 8 – 18 mmol/mol, slightly lower than the coral aragonite values we measure. Because this difference may be explained via differences in (e.g.) inorganic and coral aragonite growth rates (Mucci, 1988; White, 1977; Yoshimura et al., 2017) or the presence of organics (Cuif et al., 2003; Stolarski, 2003; Amiel et al., 1973), we adjust our data so that the predicted aragonite Na/Ca ratios fit our measured ratios by using K_d^{Na}=5.37*10^{-4} calculated from the coral samples presented here. As such we cannot presently constrain absolute $[Ca]_{ECF}$ values using this method, however the aim here is simply to explore whether differences in $[Ca]_{ECF}$ can explain the variance in both our Na/Ca and Mg/Ca data. An improved understanding of the inorganic distribution coefficient may enable both precise and accurate ECF reconstructions in the future. Using the method outlined above, we calculate $[Ca]_{ECF}$ values ranging from 7.9 mmol/l to 12.3 mmol/l with a mean of 9.9 mmol/l. This range is in good agreement with the microsensor studies on *Galaxea fascicularis* conducted by Al-Horani et al., (2003)(9-11 mmol/l). By substituting these data into the equation:

$$[Mg]_{ECF} = \frac{\frac{Mg}{Ca}_{Coral} * [Ca]_{ECF}}{K_d^{Mg}}$$

Equation 2-7 Equation to calculate the concentration of Mg in the ECF

With K_d^{Mg}=7.9*10^{-4}, calculated from the coral samples presented here, $[Mg]_{ECF}$ can also be calculated. Resulting values range from 32.8 mmol/l to 104.7 mmol/l and a mean of 51.5 mmol/l and a median of 46.5 mmol/l. Results show that the Mg-concentration in the ECF is constant with changing Ca-concentration.

2.5 Discussion

2.5.1 Heterogeneities of elemental ratios in scleractinian corals

Ninety percent of the sodium in corals is located in the aragonitic mineral phase, the remaining sodium is bound to organic material and exchangeable sites (Amiel et al., 1973). Magnesium, which co-varies with sodium, is not located in the aragonitic phase but either organic material (20–30%) and a highly disordered inorganic phase such as amorphous calcium carbonate (ACC) (70–80%) (Amiel et al., 1973; Finch and Allison, 2008) or nanodomains of Mg-bearing carbonate occluded in the aragonite (Finch and Allison, 2008). A small percentage seems to be also trapped along the (001) surface (Ruiz-Hernandez et al., 2012). Elemental heterogeneities are particularly visible when comparing COC and fibrous deposits (Fig. 2). COC are both chemically and morphologically distinct from the fibrous deposits. While the COC are built by sub-micron sized granular crystals (Constantz, 1989), the fibers that build the fibrous zones are not single orthorhombic crystals but elongated composite structures with very fine organo-mineral alternations (Cuif and Dauphin, 1998). Reasons for the different chemical composition are still under debate and include: (1) pH variations in the calcifying fluid (Adkins et al., 2003; Holcomb et al., 2009), (2) Rayleigh fractionation (Cohen et al., 2006; Gagnon et al., 2007), (3) kinetic fractionation (McConnaughey, 1989; Sinclair et al., 2006), (4) mixed ion transport through direct seawater transport and ionic pumping (Gagnon et al., 2012), and (5) precipitation from different compartments (Meibom et al., 2004; Rollion-Bard et al., 2010, 2011).

The missing co-variance between Sr/Ca and Mg/Ca or Na/Ca ratios excludes Rayleigh fractionation as the main mechanism responsible for the large variances of elemental ratios (Rollion-Bard and Blamart, 2015), as well as mixed ion transport for similar reasons (Rollion-Bard and Blamart, 2015). pH variations and consequent changes in the saturation of the calcifying fluid have been shown to alter Mg/Ca ratios in corals and abiogenic aragonite (Holcomb et al., 2009) and therefore, could potentially alter Na/Ca ratios as well. While the pH-elevation at the COC is supported by several studies (McCulloch et al., 2012b; Sinclair et al., 2006; Raddatz et al., 2014b), Tambutté et al. (2007) propose that the nanometer-sized

spaces between the skeleton and the calicoblastic ectoderm does not allow a modification of the saturation state. Also, studies based on $\delta^{11}B$ measurements show that the COC might be an area of lower pH-values compared to the fibrous zones (Rollion-Bard et al., 2011; Blamart et al., 2007; Jurikova et al., 2019). Our data may be explained by different calcification compartments (Meibom et al., 2004; Rollion-Bard et al., 2010, 2011) in combination with kinetic effects caused by rapid calcification rates. Additionally, we propose changing organic contents as a further mechanism that controls elemental ratio differences in the different skeletal parts, visible in the covariance of Mg/Ca and Na/Ca ratios throughout the skeleton. However, it is not clear in what way the different precipitation regions are distinct from each other, for example whether they are characterized by different cell types or different modes of the same cell types (Rollion-Bard et al., 2010). So far, only calicoblasts and desmocytes are known from the aboral ectoderm of corals (Allemand et al., 2011; Tambutté et al., 2007) but calicoblasts show differences in their morphology, ranging from very thin, long and flat to thick and cup like (Tambutté et al., 2007). A major controlling factor on the cell shape is the calcification activity, with flat calicoblasts corresponding to low calcification activity and thick calicoblasts to high calcification activity (Tambutté et al., 2007). These different cell morphologies might be the reason for different types of precipitation, ACC, a proposed precursor phase of aragonite (Von Euw et al., 2017; Rollion-Bard et al., 2010), and granular crystals in the COC regions or organo-mineral fibers in the fibrous deposits. The precipitation of ACC in the COC would certainly explain the enrichment of Mg in these areas, as it is necessary to stabilize the otherwise unstable ACC (Von Euw et al., 2017), however, the relevance of ACC to coral calcification has been questioned as it has so far not been possible to form ACC under carbonate system conditions thought to characterize the calcification space (Evans et al., 2019). Alternatively, the COC are known to be rich in organic material (Cuif et al., 2003; Stolarski, 2003), which would also explain the enrichment of Mg as well as explaining a slight enrichment of Na. However, the amount of Na bound to organic material is not high enough (Amiel et al., 1973) that the enrichment in the COC can be solely explained by high organic contents. Kinetic effects, due to rapid calcification rates

are more likely to be the main control for Na variations in COC and fibrous deposits. Since Na is incorporated in the aragonite lattice by direct substitution with Ca (Okumura and Kitano, 1986; Yoshimura et al., 2017), charge differences occur due to the exchange of divalent Ca with monovalent Na. These charge differences need to be compensated by lattice defects (CO_3^{2-} vacancies), which occur more often at higher precipitation rates (White, 1977; Mucci, 1988; Yoshimura et al., 2017). Growth rate effects are also known for the incorporation of Mg into inorganic aragonite, albeit these effects more likely result from crystal surface entrapment of Mg by new formed aragonite (Gabitov et al., 2008, 2011; Watson, 1996).

Sr/Ca ratios in the warm-water coral *Pocillopora damicornis* seems to be largely unaffected by growth rate changes over a range of one to over 50 µm/day (Brahmi et al., 2012), at least when comparing different skeletal architectures (Fig. 2). This is supported by our data as the observed Sr/Ca ratios show no significant decrease in the COC or COC-like areas as would be expected from the results of de Villiers et al. (1994) despite the significantly different growth rates in these areas (COC > 50–60 µm/day, FD = 1–3 µm/day (Brahmi et al., 2012)). In fact, an increase in the COC is more often but still not regularly visible (Cohen et al., 2006). Consequently, a significant effect of the different skeletal architectures on Sr/Ca ratios in coralline aragonite can be excluded. Slight increases in the COC however can be explained with the great adsorption potential of Sr to organic matter (Chen, 1997; Khani et al., 2012; Kunioka et al., 2006)

2.5.2 Environmental control on coral Na/Ca ratios

2.5.2.1 Salinity

Recently, Na/Ca ratios in foraminiferal calcite have been suggested as a potential salinity proxy (Allen et al., 2016; Bertlich et al., 2018; Mezger et al., 2016; Wit et al., 2013). Ishikawa and Ichikuni (1984) proposed that the activity of Na in seawater is the primary controlling factor for the incorporation of Na in calcite. However, more recent studies have shown that Na/Ca in foraminiferal calcite is mainly driven by the seawater Na/Ca ratio instead of the Na

activity when this is the dominant variable (Hauzer et al., 2018; Evans et al., 2018a). Species-specific offsets make further biological controls highly plausible.

In this study, no correlation between salinity and Na/Ca ratios is present (Fig. 3). The positive trend up to 35 g/kg followed by a negative trend after 35 g/kg can be explained by growth rate changes due to the changing salinity. To our knowledge no studies on the effect of salinity on growth rates have been conducted on *D. pertusum* but it is plausible that it shows reduced growth rates in salinities diverging from the biological optimum similar to other marine organisms (e.g. *M. edulis* (Malone and Dodd, 1967)). A specific osmoregulation is probably not needed for CWC in the mostly salinity stable habitats they live in (Roberts et al., 2009). Reduced growth rates consequently lower the amount of lattice defects and the amount of possible incorporation sites for sodium (Mucci, 1988; White, 1977; Yoshimura et al., 2017), if bulk extension-rates are indeed related to crystal growth rates.

If Na/Ca ratios in corals are controlled by calcification rates, a calcification rate proxy could be used to correct this effect. Sr/Ca ratios have been discussed as a possible growth rate proxy (de Villiers et al., 1994) and may be used to determine changes in growth rate. However, our data shows that the Sr/Ca ratios remain constant with changing salinities. Accordingly, concluding from the results of de Villiers et al. (1994) the calcification rate would remain constant over the whole salinity range. It should be noted that higher growth rates do not necessarily imply higher calcification rates or vice versa. Higher growth rate can also be caused by higher organic deposits in the skeleton (Stolarski, 2003). Therefore, a change in calcification cannot necessary be inferred from changing Sr/Ca ratios. Still, the effects that growth or calcification rate changes and the different skeletal architectures have on Sr/Ca ratios in corals is still discussed. There is evidence for positive and negative correlation of Sr/Ca with growth and calcification rate as well as the different skeletal architectures (Allison and Finch, 2004; Cohen et al., 2006; Kunioka et al., 2006; Raddatz et al., 2013). It still remains unknown why there is no persistent Sr/Ca variation between the differential skeletal architectures (COC, fibrous deposits) in this study despite being visible in several other studies (Cohen et al., 2006; Gagnon et al., 2007; Raddatz et al., 2013). An explanation could

be the low sampling resolution in the profiled samples and possible mixing of COC and fibrous zone material. Further research is needed to evaluate the effects of growth and calcification rates on Sr/Ca ratios in biogenic carbonates.

2.5.2.2 Temperature

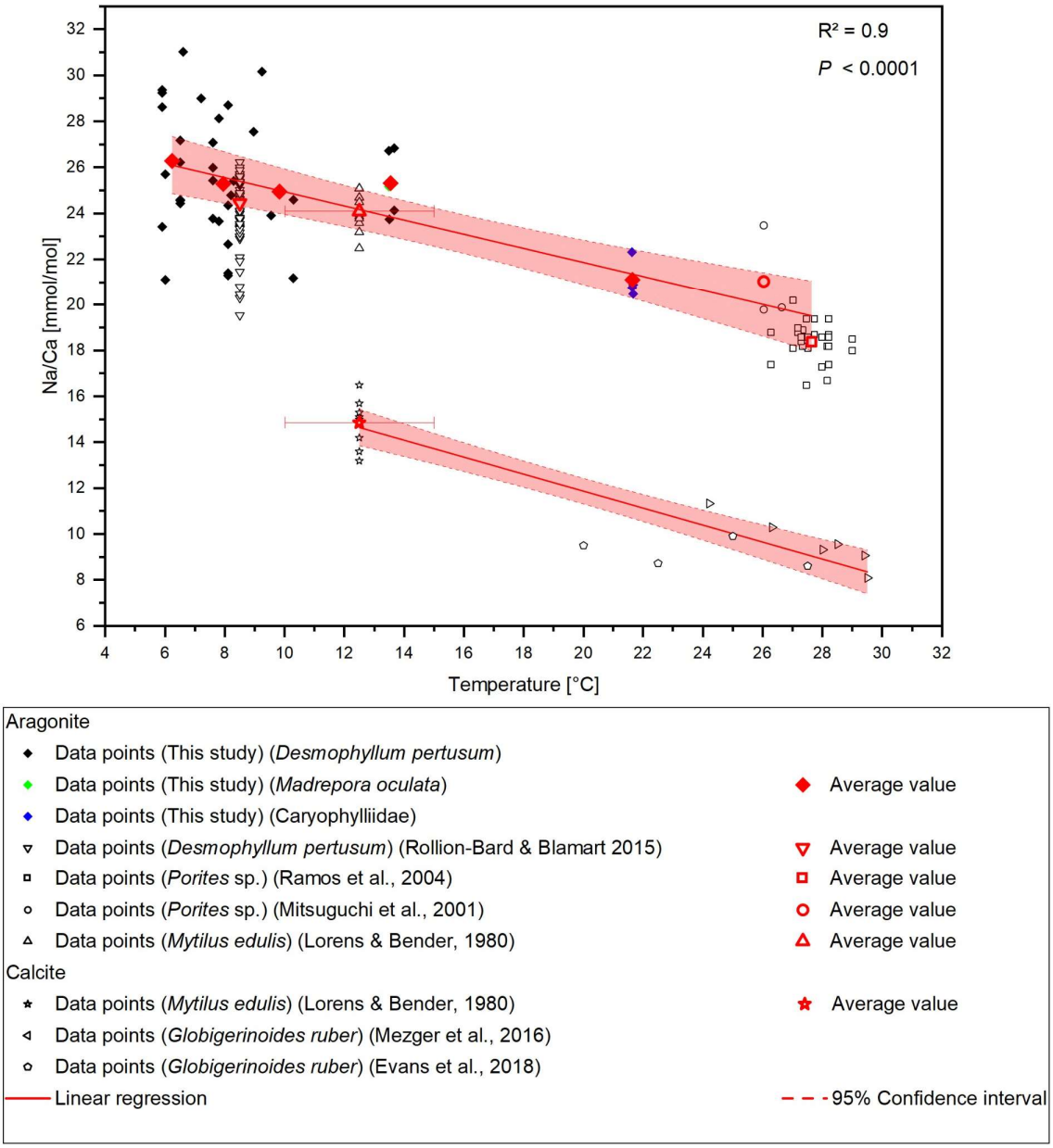

Figure 2-6 Compiled Na/Ca ratios from different studies. D. pertusum, M. oculata, M. edulis and Porites sp. show a negative linear relation with water temperature. R² relates only to the aragonitic samples Calcitic samples from M. edulis and Globigerinoides ruber show the same sensitivity, albeit with an offset of 10 mmol/mol. Temperature for the data from Lorens & Bender amounts to the average temperature of the tank the corals were cultivated in while the error bars show maximum and minimum values.

A temperature control on Na/Ca ratios has been shown in inorganic precipitated aragonite (White, 1977) and in the planktonic foraminifera *G. ruber* and *G. sacculifer* (Mezger et al., 2016), although temperature and salinity covary in that study. Furthermore, Rollion-Bard and Blamart (2015) suggest a possible temperature control on Na/Ca ratios in the CWC *D. pertusum* and the warm-water coral *Porites* sp. However, the temperature sensitivity in inorganically precipitated aragonite is far lower compared to the biogenic aragonite from CWC including a systematic offset of $K_d^{Na}{}_{(15°C)}$= $1.17*10^{-4}$. Interestingly, other marine carbonates (*Porites* sp., *M. edulis*) also fit in the calculated temperature sensitivity. This holds true for biogenic aragonite and biogenic calcite, where *M. edulis* fits into the temperature sensitivity found by Mezger et al. (2016). A combined regression using the data from Evans et al. (2018), Mezger et al. (2016) and Lorens and Bender (1980) reveals a temperature sensitivity of -0.37 mmol/mol/°C which is strikingly similar to the sensitivity in aragonite of -0.31 mmol/mol/°C (Fig. 6). The samples that Mezger et al. (2016) used in their study derive from the Red Sea, where a negative correlation between the seawater salinity and seawater temperature exists. They conclude that the salinity effect on Na/Ca ratios and the covariance between salinity and temperature cause the temperature sensitivity of Na/Ca ratios. However, it is also possible that the salinity sensitivity is caused by a temperature effect.

The apparent offset between inorganically precipitated aragonite and biogenic carbonates further implies a biological control on Na incorporation. In contrast to other elements such as Lithium (Montagna et al., 2014), the high correlation between *D. pertusum, M. oculata*, Caryophylliidae, *Porites* sp. and *M. edulis* implies that the Na/Ca variance introduced by these possibly occurring vital effects appear to be similar for all these species. We suggest that similar Na pathways into the calcifying space exist in foraminifera, mussels and scleractinian warm-water as well as cold-water corals and temperature exerts a strong control on the activity of these pathways, altering the sodium availability during calcification. Further controls are possibly contributed by temperature dependent solubility variations of $CaCO_3$ and Na_2CO_3 and an exothermic Na incorporation mechanism.

Bertlich et al. (2018) proposed that lower temperatures increase the solubility of calcium carbonate and increase the amount of free Ca, leading to higher Na/Ca ratios at lower temperatures. Yet such a solubility-controlled temperature effect on calcite and aragonite is rather small, whereas the sensitivity to pressure changes is much more pronounced (Pytkowicz and Conners, 1964; Zeebe and Wolf-Gladrow, 2001). Accordingly, the Na/Ca ratio should also decrease with water depth. Here we do observe a relationship between Na/Ca ratios and water depth, but at constant temperatures (7.2°C – 7.8°C) there is no effect of water depth (160 m – 280 m) on Na/Ca ratios. The relationship between depth and Na/Ca ratios is therefore presumably caused by the positive correlation between water temperature and water depth. A decrease in Na/Ca ratios with temperatures could also be explained by solubility effects similar to the effects that are discussed to cause the temperature effects on Li/Ca ratios (Marriott et al., 2004). The solubility of Na_2CO_3 increases with increasing temperature (Haynes et al., 2016). Again, this would result in decreasing Na/Ca ratios with increasing temperature, because the solubility of Na_2CO_3 decreases relative to calcium carbonate (Haynes et al., 2016), making it thermodynamically less favorable to incorporate Na. The effects of pressure on the solubility of Na_2CO_3 cannot be quantified at the moment due to the lack of studies.

Moreover, the temperature effect can also be caused by an exothermic substitution mechanism of Na into the aragonite lattice, similar to the incorporation of Mg in calcite (Mucci and Morse, 1990). If the substitution between Ca and Na is exothermic, consequently the incorporation of Na is favored at lower temperatures. However, there is to our knowledge, no study available that contains enthalpy data for this reaction. While the proposed mechanism by Bertlich et al., (2018) can be excluded as an explanation for the temperature sensitivity of Na/Ca ratios, the other explanations are equally plausible in terms of the existing studies. Still, the differences in the temperature sensitivity between inorganic precipitated aragonite and biogenic aragonite requires further biological controls to explain this deviation.

As an alternative, we explore whether temperature dependent Na membrane pathways can explain temperature effects on aragonitic Na/Ca ratios. There are several enzymes and ion

pumps known that constitute sodium pathways through the membrane of the calcifying space. Na^+/K^+-ATPase are known from the tropical coral *Galaxea fascicularis* (Ip and Lim, 1991), Na/Ca ion pumps are suggested to exist in *Galaxea fascicularis* and *Tubastraea faulkneri* (Marshall, 1996). Na^+/K^+-ATPase was found in the bivalve species *M. edulis* and *Limecola balthica* (Pagliarani et al., 2006; Wang and Fisher, 1999) as well as Na/Mg ion pumps in *Ruditapes philippinarum* and *Mytilus galloprovincialis* (Pagliarani et al., 2006). Whether these enzymes exist in *D. pertusum* is unknown, but since corals possess a nervous system (Chen et al., 2008) and *D. pertusum* shows reaction to electrical stimulation (Shelton, 1980) at least the existence of Na^+/K^+-ATPase must be assumed. However, it remains unclear if this enzyme participates in the modification of the calcifying fluid. The participation of Na/Ca ion pumps is also plausible, since it would result in higher Ca-concentrations in the calcifying space which would aid the calcification process due to the high transport capacity (Carafoli et al., 2001). Membrane calcium pumps on the other hand are better suited to transport Ca from a compartment with low Ca-concentrations, which is not applicable when considering seawater as the source compartment (Wang et al., 1992). Since the activity of enzymes is a function of temperature (Sizer, 2006), a temperature control of the ion concentration in the calcifying fluid has to be considered. Rising temperatures would increase the activity of the particular enzyme following the Arrhenius equation (Arrhenius, 1896) and consequently lower the Na-concentration in the calcifying space. Unfortunately, it is impossible to quantify these effects from the data at hand, because the optimum temperature and activation energy is not enzyme specific, but further controlled by enzyme and substrate purity and the presence of inhibitors or activators. Specific research is needed to identify the particular enzyme in these corals as well as determine the rate of ion-exchange, although we note that an enzymatic control on aragonitic Na/Ca ratios does not necessarily imply a temperature control. In addition, besides a temperature control, there is also a pH control on enzyme activity (Trivedi and Danforth, 1966). While a positive correlation between Na/Ca and seawater pH is present in the samples utilized here, it is not possible to determine if this is caused by pH-controlled enzymatic activity or due to an

increased calcification rate. Higher seawater pH would cause higher calcification fluid pH which would consequently also increase the aragonite saturation in the calcifying fluid (McCulloch et al., 2012b). The degree of pH elevation in the coral calcifying space would therefore decrease, ultimately conserving energy (≈ 10 % / -0.1 pH_{SW}) which can be used for ATP-dependent transport proteins, pumping more Ca or CO_3^{2-}, leading to faster calcification (McCulloch et al., 2012b). It is also possible that the apparent sensitivity of Na/Ca to pH changes is caused by the negative covariance of pH and temperature

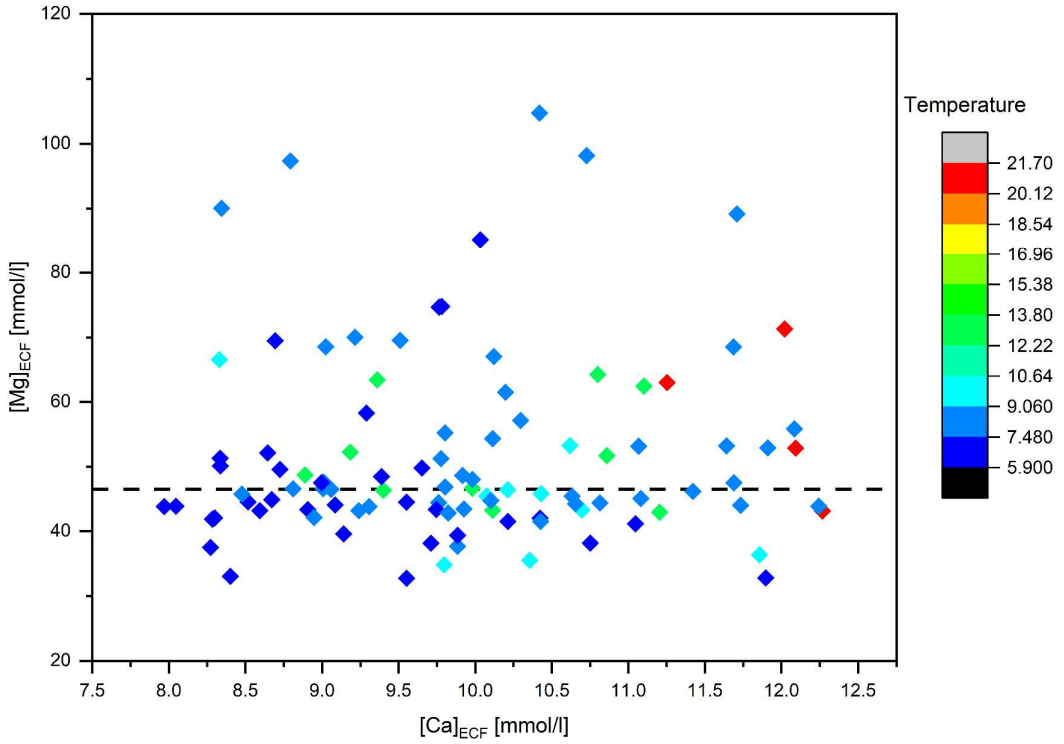

Figure 2-7 Calcium and Magnesium concentration in the ECF of the investigated corals. The color of the data points indicates the ambient water temperature, which is increasing with increasing Ca-concentrations. The dashed line indicates the median of the Mg-concentration in the ECF.

Admittedly, the above discussion is only viable under the assumption of a closed calcifying space with a much lower $[Na]_{ECF}$ than $[Na]_{Seawater}$. In the case of an open or semi-enclosed calcifying space with $[Na]_{ECF}$ close or equal to $[Na]_{Seawater}$ the amount of Na removed by enzymes or other ion-pumps is far too low to cause any significant changes in the composition of the calcifying fluid with regards to Na. In combination with the low distribution

coefficient, changes in the Na-concentration of the ECF cannot cause the high variability of the skeletal Na/Ca ratios. Since there is evidence for an at least semi-enclosed calcifying space (Tambutté et al., 2011) we also consider this option. As described in Sec. 3.3 it is possible to calculate the Mg-concentration of the ECF under the assumption of seawater leakage into the calcifying space (Adkins et al., 2003; Gagnon et al., 2012) and a resulting approximately constant Na-concentration. Based on this hypothesis, and the calculations defined in Eq. 3 and 4, we show that the Mg-concentration in the ECF is constant, but with changing Ca-concentration (Fig. 7). There is a large degree of scatter in the $[Mg]_{ECF}$ reconstructions (Fig. 7), which we suggest is unlikely to represent real changes in the ECF [Mg] as it is difficult to envisage a purpose for elevating $[Mg]_{ECF}$ above the of seawater given that it plays an inhibitory role in calcium carbonate precipitation by acting antagonistic to the calcium transport (OKAZAKI, 1956; Swart, 1981; Yamazato, 1966). It may be that the scatter above seawater values is derived from the presence of organic material, as a small positive bias in measured coral Mg/Ca would result in a large overestimation of $[Mg]_{ECF}$. Crucially however, we find that $[Mg]_{ECF}$ does not change as a function of $[Ca]_{ECF}$, with the implication that in this model changing skeletal Mg/Ca and Na/Ca ratios are not caused by changes of the Mg or Na-concentration of the ECF but rather are entirely explicable through changes in the Ca-concentration. Again, this might be caused by temperature-dependent enzyme or ion-pump activity. Higher temperatures would then cause a higher exchange capacity (Elias et al., 2001), leading to higher Ca- (Fig. 7) and marginally lower Na-concentrations in the ECF and consequently lower Mg/Ca and Na/Ca ratios. An elevation of [Ca] in the ECF and the calcifying front is also supported by recent studies from Decarlo et al., (2018) and Sevilgen et al., (2019), who conducted Raman spectroscopic, $\delta^{11}B$ and microsensor measurements on *Pocillopora damicornis, Acropora youngei* and *Stylophora pistilla*. The results furthermore indicate the involvement of transcellular pathways to elevate the Ca-concentration in the ECF (Sevilgen et al., 2019).

Even though a clear correlation between temperature and Na/Ca is present, the usefulness of Na/Ca ratios is greatly reduced due to the large intraspecies variability. At 6°C Na/Ca

ratios vary by up to 20% and even up to 10 % in a single polyp. There are several possible reasons for this variability. One is the insufficient removal of the COC during the sampling process. Due to the high growth rate and high organic content in the COC, elements, such as Mg, Na and Li are enriched whereas others like U are depleted (Gagnon et al., 2007; Raddatz et al., 2014b, 2013a; Rollion-Bard and Blamart, 2015; Robinson et al., 2014; Rollion-Bard and Blamart, 2014). This effect would also explain the high Na/Ca values in corals from the Mediterranean Sea (T=13.56°C). It is possible that during the sampling process a larger amount of the fibrous deposits was removed in comparison to the other samples. This would cause a greater effect of the enriched COC material and therefore cause higher Na/Ca ratios. It is therefore preferable to use in-situ techniques (laser ablation, EPMA, SIMS) instead of solution-based chemistry and profile measurements through the theca wall instead of bulk samples, because it allows for a better recognition and removal of values that derive from COC or COC-like structures. Seasonality could be also a factor responsible for a percentage of the variation, but the sampled corals originate from depths where seasonality presumably only plays a minor role. An estimated seasonal temperature change of 4°C only suffices to explain 1 mmol/mol variation but not the observed variation of 10 mmol/mol. From this, it can be inferred that there must be other controls on Na/Ca ratios besides water temperature. Diurnal temperature fluctuations caused by internal waves as found for example in the Rockall Trough are also not high enough (3°C) to explain these variations (Mienis et al., 2007). As mentioned in Sec 4.1, calcification rates constitute a major control on Na/Ca ratios by controlling the amount of incorporation sites for Na (Kitano et al., 1975; Mucci, 1988; White, 1977; Yoshimura et al., 2017). Therefore, numerous second order control factors could cause variations in the Na/Ca ratios by controlling the calcification rate. These second order controls include nutrient availability and supply, changes in the carbonate system, coral fitness and many more. Some of these controls (nutrient supply, coral fitness) have the potential to vary with a high spatial resolution and consequently cause great variations in Na/Ca ratios even if the samples derive from the same colony.

2.5.3 Na/Mg ratios to overcome vital effects

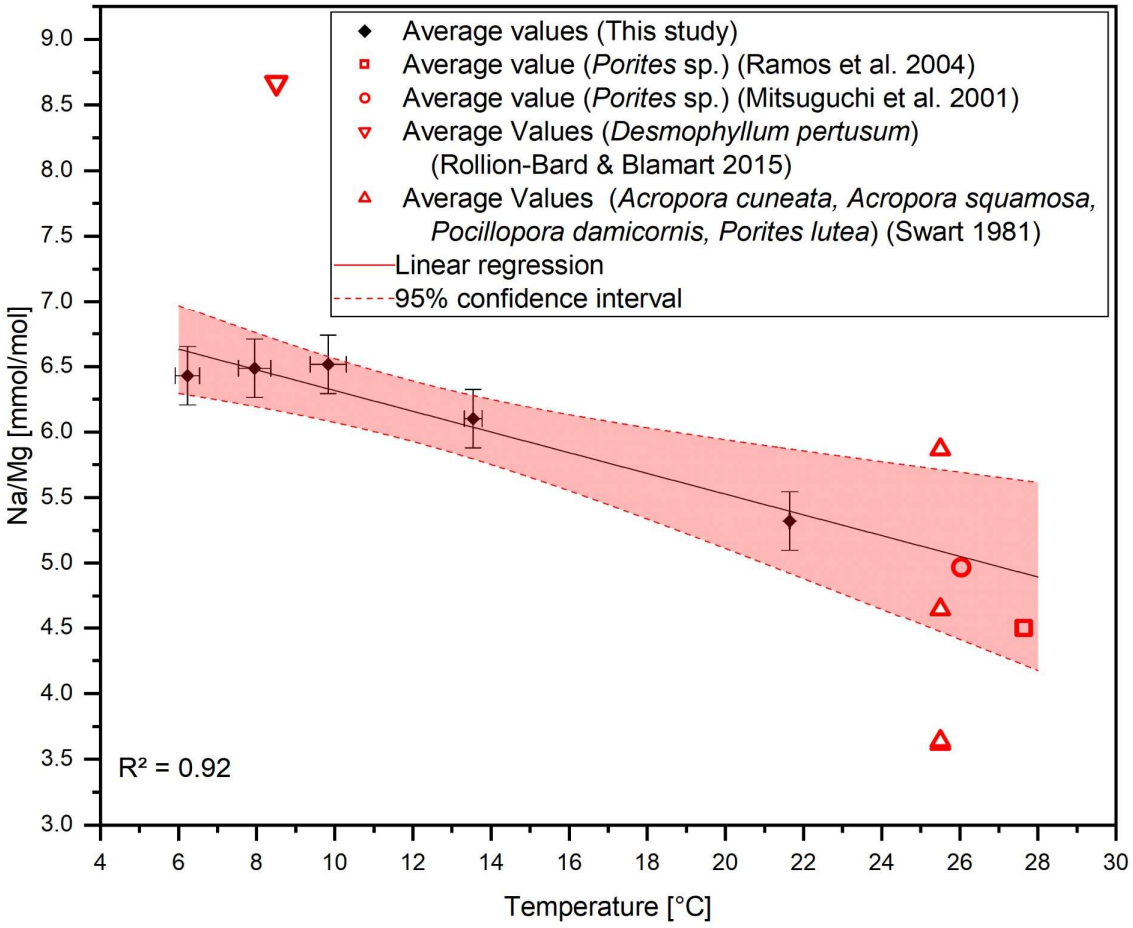

Figure 2-8 Na/Mg ratios from this study vs. water temperature. Na/Mg ratios can be used to correct for the sampling of varying proportions of different domains. Y-Error bars relate to 2SD of the JCp-1 measurements. X-Error bars relate to 1SD of the temperature mean for the chosen temperature ranges.

Even though a good correlation of R^2=0.9 between Na/Ca and temperature is observable in our data, the samples from the Mediterranean Sea (T=13.54°C) show slightly elevated Na/Ca ratios. Reasons for this are discussed in Sec. 4.2. Rollion-Bard and Blamart (2015) proposed Na/Mg ratios to overcome these effects. The basis for this is that Na/Ca and Mg/Ca ratios could be controlled by similar vital effects such as growth rate and the amount of organic content. Combining Na/Ca and Mg/Ca ratios reduces the impact of these effects, though the temperature sensitivity of Na/Ca ratios is preserved as Mg/Ca ratios show no apparent correlation with temperature (Fig. 8). The resulting regression between Na/Mg and temperature yields the following equation:

$$f^{\square}_{T6-22\,°C} = 7.1 \pm 0.17 - 0.07 \pm 0.01 \times T \left(R^2 = 0.92, P = 0.009 \right)$$

Equation 2-8 Linear regression between Na/Mg and seawater temperature

The application of Na/Mg in this study does not significantly improve the regression, as it removes the inverse correlation between 6 and 10°C. This might be caused by covariance between sodium and magnesium. It was shown that magnesium in the parent solution reduces the amount of incorporated sodium (Okumura and Kitano, 1986). However, utilizing Na/Mg ratios removes the striking irregularity at 13.54 °C. The large scatter, however, is not significantly reduced which implies further vital effects that cannot be resolved with this technique. To overcome this the mean of at least 10 analyzed samples should be used to obtain reliable results. If these prerequisites are fulfilled, Na/Mg and Na/Ca could provide a means of reconstructing temperature. This could prove useful especially for temperature reconstructions in deep time on organisms that are extinct today. In this case the nearest living relative principle is used, which potentially introduces large errors. Further research on different aragonitic and calcitic organisms is necessary to detect further species that show the same temperature sensitivity. If it is shown that Na/Ca and/or Na/Mg ratios show no species-specific variations, empirical calibrations could be applied to extinct species for which proxy calibrations are not possible. Still though, when using Na/Ca for temperature reconstructions changes in seawater have to be considered that would lead to an underestimation of temperature at high pH. However, Na/Mg show no sensitivity to changes in seawater pH, so by combining Na/Ca and Mg/Ca ratios this effect can be ignored.

2.6 Conclusion

The data at hand does not support the utility of Na/Ca in cold-water corals as a salinity proxy as proposed by Wit et al., (2013) and Mezger et al., (2016) for biogenic calcite. While there is a positive trend between Na/Ca and salinity when excluding data from the Red Sea samples, it is not statistically significant.

A significant inverse correlation between temperature and Na/Ca ratios is present, which cannot be explained by a co-variance of temperature and salinity (c.f. Mezger et al., 2016).

Two additional organisms, *Porites* sp. (Mitsuguchi et al., 2001; Ramos et al., 2004) and *M. edulis* (Lorens and Bender, 1980) fit in this regression too. The mechanism of sodium incorporation therefore appears to be consistent between these three species. We propose temperature-dependent activity in Na-ion or Ca-ion transport proteins as the underlying mechanism behind the observable correlation. While the intraspecies and intraindividual variation is large, Na/Ca can be well correlated to environmental variables when based on the averages of several specimens. Therefore, Na/Ca ratios might provide a temperature-proxy that is usable for a wide variety of aragonitic organisms and maybe even calcitic organisms. As proposed by Rollion-Bard and Blamart (2015), Na/Mg ratios can be used to correct for inconsistencies during the sampling process.

2.7 Author contribution

Jacek Raddatz and Nicolai Schleinkofer designed the experiments and conducted the measurements. Jacek Raddatz, Andre Freiwald, Lydia Beuck, Andres Rüggeberg and Volker Liebetrau provided samples and environmental data. Nicolai Schleinkofer prepared the manuscript with contributions from all co-authors.

2.8 Acknowledgements

We are grateful to all cruise captains, crew members and cruise participants of research cruises POS325, POS391, POS455, POS 385, M61, POS625, B10-17a/b, 64PE284, M70/1, COR2, MSM20-4, KRSE2013 and RV Gunnerus. Ship time of RV Belgica was provided by BELSPO and RBINS–OD Nature. Cruise POS391 was realized by DFG Project RI 598/4-1. JR acknowledges funding from DFG project ECHO RA 2516-1. AR acknowledges support from Swiss National Science Foundation, SNF project number 200021_149247.

FIERCE is financially supported by the Wilhelm and Else Heraeus Foundation, which is gratefully acknowledged. This is FIERCE contribution No. 002

2.9 References

Adkins, J. F., Boyle, E. A., Curry, W. B. and Lutringer, A.: Stable isotopes in deep-sea corals and a new mechanism for “vital effects,” Geochim. Cosmochim. Acta, 67(6), 1129–1143, doi:10.1016/S0016-7037(00)01203-6, 2003.

Al-Horani, F. A., Al-Moghrabi, S. M. and De Beer, D.: The mechanism of calcification and its relation to photosynthesis and respiration in the scleractinian coral Galaxea fascicularis, Mar. Biol., 142(3), 419–426, doi:10.1007/s00227-002-0981-8, 2003.

Allemand, D., Tambutté, É., Zoccola, D. and Tambutté, S.: Coral Calcification, Cells to Reefs, in Coral Reefs: An Ecosystem in Transition, pp. 119–150, Springer Netherlands, Dordrecht., 2011.

Allen, K. A., Hönisch, B., Eggins, S. M., Haynes, L. L., Rosenthal, Y. and Yu, J.: Trace element proxies for surface ocean conditions: A synthesis of culture calibrations with planktic foraminifera, Geochim. Cosmochim. Acta, 193, 197–221, doi:10.1016/j.gca.2016.08.015, 2016.

Allison, N. and Finch, A. A.: High-resolution Sr/Ca records in modern Porites lobata corals: Effects of skeletal extension rate and architecture, Geochemistry, Geophys. Geosystems, 5(5), doi:10.1029/2004GC000696, 2004.

Amiel, A. J., Friedman, G. M. and Miller, D. S.: Distribution and nature of incorporation of trace elements in modern aragonitic corals*, Sedimentology, 20(1), 47–64, doi:10.1111/j.1365-3091.1973.tb01606.x, 1973.

Anagnostou, E., Sherrell, R. M., Gagnon, A., LaVigne, M., Field, M. P. and McDonough, W. F.: Seawater nutrient and carbonate ion concentrations recorded as P/Ca, Ba/Ca, and U/Ca in the deep-sea coral Desmophyllum dianthus, Geochim. Cosmochim. Acta, 75(9), 2529–2543, doi:10.1016/j.gca.2011.02.019, 2011.

Anagnostou, E., Huang, K. F., You, C. F., Sikes, E. L. and Sherrell, R. M.: Evaluation of boron isotope ratio as a pH proxy in the deep sea coral Desmophyllum dianthus: Evidence of physiological pH adjustment, Earth Planet. Sci. Lett., 349–350(July 2015), 251–260, doi:10.1016/j.epsl.2012.07.006, 2012.

Arrhenius, S.: XXXI. On the influence of carbonic acid in the air upon the temperature of the ground, London, Edinburgh, Dublin Philos. Mag. J. Sci., 41(251), 237–276, doi:10.1080/14786449608620846, 1896.

Bertlich, J., Nürnberg, D., Hathorne, E. C., De Nooijer, L. J., Mezger, E. M., Kienast, M., Nordhausen, S., Reichart, G. J., Schönfeld, J. and Bijma, J.: Salinity control on Na

incorporation into calcite tests of the planktonic foraminifera Trilobatus sacculifer - Evidence from culture experiments and surface sediments, Biogeosciences, 15(20), 5991–6018, doi:10.5194/bg-15-5991-2018, 2018.

Bett, B. J.: UK Atlantic Margin Environmental Survey: Introduction and overview of bathyal benthic ecology, Cont. Shelf Res., 21(8–10), 917–956, doi:10.1016/S0278-4343(00)00119-9, 2001.

Blamart, D., Rollion-Bard, C., Meibom, A., Cuif, J. P., Juillet-Leclerc, A. and Dauphin, Y.: Correlation of boron isotopic composition with ultrastructure in the deep-sea coral Lophelia pertusa: Implications for biomineralization and paleo-pH, Geochemistry, Geophys. Geosystems, 8(12), 1–11, doi:10.1029/2007GC001686, 2007.

Bollmann, J., Herrle, J. O., Cortés, M. Y. and Fielding, S. R.: The effect of sea water salinity on the morphology of Emiliania huxleyi in plankton and sediment samples, Earth Planet. Sci. Lett., 284(3–4), 320–328, doi:10.1016/j.epsl.2009.05.003, 2009.

Brahmi, C., Kopp, C., Domart-Coulon, I., Stolarski, J. and Meibom, A.: Skeletal growth dynamics linked to trace-element composition in the scleractinian coral Pocillopora damicornis, Geochim. Cosmochim. Acta, 99, 146–158, doi:10.1016/j.gca.2012.09.031, 2012.

Branson, O., Bonnin, E. A., Perea, D. E., Spero, H. J., Zhu, Z., Winters, M., Hönisch, B., Russell, A. D., Fehrenbacher, J. S. and Gagnon, A. C.: Nanometer-Scale Chemistry of a Calcite Biomineralization Template: Implications for Skeletal Composition and Nucleation, Proc. Natl. Acad. Sci., 113(46), 12934–12939, doi:10.1073/pnas.1522864113, 2016.

Büscher, J. V., Form, A. U. and Riebesell, U.: Interactive Effects of Ocean Acidification and Warming on Growth, Fitness and Survival of the Cold-Water Coral Lophelia pertusa under Different Food Availabilities, Front. Mar. Sci., 4(April), 1–14, doi:10.3389/fmars.2017.00101, 2017.

Busenberg, E. and Niel Plummer, L.: Kinetic and thermodynamic factors controlling the distribution of SO32− and Na+ in calcites and selected aragonites, Geochim. Cosmochim. Acta, 49(3), 713–725, doi:10.1016/0016-7037(85)90166-8, 1985.

Carafoli, E., Santella, L., Branca, D. and Brini, M.: Generation, control, and processing of cellular calcium signals, Crit. Rev. Biochem. Mol. Biol., 36(2), 107–260, doi:10.1080/20014091074183, 2001.

Chen, E., Stiefel, K. M., Sejnowski, T. J. and Bullock, T. H.: Model of traveling waves in a coral nerve network, J. Comp. Physiol. A Neuroethol. Sensory, Neural, Behav. Physiol., 194(2), 195–200, doi:10.1007/s00359-007-0305-z, 2008.

Chen, J.-P.: Batch and Contunuous Adsorption of Stontium by Plant Root Tissues, Bioresour. Technol., 60, 185–189, doi:10.1016/S0960-8524(97)00021-7, 1997.

Cohen, A. L., Gaetani, G. A., Lundälv, T., Corliss, B. H. and George, R. Y.: Compositional variability in a cold-water scleractinian, Lophelia pertusa: New insights into “vital effects,” Geochemistry, Geophys. Geosystems, 7(12), doi:10.1029/2006GC001354, 2006.

Constantz, B. R.: Skeletal Organization in Caribbean Acropora Spp. (Lamarck), in Origin, Evolution, and Modern Aspects of Biomineralization in Plants and Animals, pp. 175–199, Springer US, Boston, MA., 1989.

Cuif, J.-P. and Dauphin, Y.: Microstructural and physico-chemical characterization of ’ centers of calcification ’ in septa of some Recent scleractinian corals, Paläontologische Zeitschrift, 72(November), 257–270, doi:10.1007/BF02988357, 1998.

Cuif, J. P., Dauphin, Y. Y., Doucet, J., Salome, M. and Susini, J.: XANES mapping of organic sulfate in three scleractinian coral skeletons, Geochim. Cosmochim. Acta, 67(1), 75–83, doi:10.1016/S0016-7037(02)01041-4, 2003.

Decarlo, T. M., Comeau, S., Cornwall, C. E. and McCulloch, M. T.: Coral resistance to ocean acidification linked to increased calcium at the site of calcification, Proc. R. Soc. B Biol. Sci., 285(1878), doi:10.1098/rspb.2018.0564, 2018.

Druffel, E. R. M.: Geochemistry of corals: Proxies of past ocean chemistry, ocean circulation, and climate, Proc. Natl. Acad. Sci., 94(16), 8354–8361, doi:10.1073/pnas.94.16.8354, 1997.

Dullo, W. C., Flögel, S. and Rüggeberg, A.: Cold-water coral growth in relation to the hydrography of the Celtic and Nordic European continental margin, Mar. Ecol. Prog. Ser., 371, 165–176, doi:10.3354/meps07623, 2008.

Elderfield, H. and Ganssen, G.: Past temperature and δ18O of surface ocean waters inferred from foraminiferal Mg/Ca ratios, Nature, 405(6785), 442–445, doi:10.1038/35013033, 2000.

Elderfield, H., Ferretti, P., Greaves, M., Crowhurst, S. J., McCave, I. N., Hodell, D. a and Piotrowski, A. M.: Evolution of ocean temperature, Science (80-.)., 337(August), 704–709, doi:10.1594/PANGAEA.786205, 2012.

Elias, C. L., Xue, X. H., Marshall, C. R., Omelchenko, A., Hryshko, L. V. and Tibbits, G. F.: Temperature dependence of cloned mammalian and salmonid cardiac Na(+)/Ca(2+) exchanger isoforms., Am. J. Physiol. Cell Physiol., 281(3), C993–C1000, doi:10.1111/j.1432-1033.1984.tb08031.x, 2001.

Von Euw, S., Zhang, Q., Manichev, V., Murali, N., Gross, J., Feldman, L. C., Gustafsson, T., Flach, C., Mendelsohn, R. and Falkowski, P. G.: Biological control of aragonite formation in stony corals, Science (80-.)., 356(6341), 933–938, doi:10.1126/science.aam6371, 2017.

Evans, D., Müller, W. and Erez, J.: Assessing foraminifera biomineralisation models through trace element data of cultures under variable seawater chemistry, Geochim. Cosmochim. Acta, 236, 198–217, doi:10.1016/j.gca.2018.02.048, 2018.

Evans, D., Webb, P., Penkman, K. E. H., Kroger, R. and Allison, N.: The characteristics and biological relevance of inorganic amorphous calcium carbonate (ACC) precipitated from seawater, Cryst. Growth Des., doi:10.1021/acs.cgd.9b00003, 2019.

Finch, A. A. and Allison, N.: Mg structural state in coral aragonite and implications for the paleoenvironmental proxy, Geophys. Res. Lett., 35(8), 1–5, doi:10.1029/2008GL033543, 2008.

Flögel, S., Dullo, W. C., Pfannkuche, O., Kiriakoulakis, K. and Rüggeberg, A.: Geochemical and physical constraints for the occurrence of living cold-water corals, Deep. Res. Part II Top. Stud. Oceanogr., 99, 19–26, doi:10.1016/j.dsr2.2013.06.006, 2014.

Form, A. U. and Riebesell, U.: Acclimation to ocean acidification during long-term CO2 exposure in the cold-water coral Lophelia pertusa, Glob. Chang. Biol., 18(3), 843–853, doi:10.1111/j.1365-2486.2011.02583.x, 2012.

Freiwald, A.: Reef-Forming Cold-Water Corals, in Ocean Margin Systems, pp. 365–385, Springer Berlin Heidelberg, Berlin, Heidelberg., 2002.

Freiwald, A. and Roberts, J. M., Eds.: Cold-Water Corals and Ecosystems, Springer Berlin Heidelberg, Berlin, Heidelberg., 2005.

Freiwald, A., Beuck, L., Rüggeberg, A., Taviani, M. and Hebbeln, D.: The White Coral Community in the Central Mediterranean Sea Revealed by ROV Surveys, Oceanography, 22(1), 58–74, doi:10.5670/oceanog.2009.06, 2009.

Gabitov, R. I., Gaetani, G. A., Watson, E. B., Cohen, A. L. and Ehrlich, H. L.: Experimental determination of growth rate effect on U6+ and Mg2+ partitioning between aragonite and fluid at elevated U6+ concentration, Geochim. Cosmochim. Acta, 72(16), 4058–4068, doi:10.1016/j.gca.2008.05.047, 2008.

Gabitov, R. I., Schmitt, A. K., Rosner, M., McKeegan, K. D., Gaetani, G. A., Cohen, A. L., Watson, E. B. and Harrison, T. M.: In situ δ 7 Li, Li/Ca, and Mg/Ca analyses of synthetic aragonites, Geochemistry, Geophys. Geosystems, 12(3), n/a-n/a, doi:10.1029/2010GC003322, 2011.

Gagnon, A. C., Adkins, J. F., Fernandez, D. P. and Robinson, L. F.: Sr/Ca and Mg/Ca vital effects correlated with skeletal architecture in a scleractinian deep-sea coral and the role of Rayleigh fractionation, Earth Planet. Sci. Lett., 261(1–2), 280–295, doi:10.1016/j.epsl.2007.07.013, 2007.

Gagnon, A. C., Adkins, J. F. and Erez, J.: Seawater transport during coral biomineralization, Earth Planet. Sci. Lett., 329–330, 150–161, doi:10.1016/j.epsl.2012.03.005, 2012.

Gordon, C. M., Carr, R. A. and Larson, R. E.: the Influence of Environmental Factors on the Sodium and Manganese Content of Barnacle Shells, Limnol. Oceanogr., 15(3), 461–466, doi:10.4319/lo.1970.15.3.0461, 1970.

Hathorne, E. C., Gagnon, A., Felis, T., Adkins, J., Asami, R., Boer, W., Caillon, N., Case, D., Cobb, K. M., Douville, E., DeMenocal, P., Eisenhauer, A., Garbe-Schönberg, D., Geibert, W., Goldstein, S., Hughen, K., Inoue, M., Kawahata, H., Kölling, M., Cornec, F. L., Linsley, B. K., McGregor, H. V., Montagna, P., Nurhati, I. S., Quinn, T. M., Raddatz, J., Rebaubier, H., Robinson, L., Sadekov, A., Sherrell, R., Sinclair, D., Tudhope, A. W., Wei, G., Wong, H., Wu, H. C. and You, C.-F.: Interlaboratory study for coral Sr/Ca and other element/Ca ratio measurements, Geochemistry, Geophys. Geosystems, 14(9), 3730–3750, doi:10.1002/ggge.20230, 2013.

Hauzer, H., Evans, D., Müller, W., Rosenthal, Y. and Erez, J.: Calibration of Na partitioning in the calcitic foraminifer Operculina ammonoides under variable Ca concentration: Toward reconstructing past seawater composition, Earth Planet. Sci. Lett., 497, 80–91, doi:10.1016/j.epsl.2018.06.004, 2018.

Haynes, W. M., Lide, D. R. and Bruno, T. J.: CRC Handbook of chemistry and physics : a ready-reference book of chemical and physical data., 2016.

Henry, L.-A. and Roberts, J. M.: Global Biodiversity in Cold-Water Coral Reef Ecosystems, in Marine Animal Forests, pp. 1–21, Springer International Publishing, Cham., 2016.

Holcomb, M., Cohen, A. L., Gabitov, R. I. and Hutter, J. L.: Compositional and morphological features of aragonite precipitated experimentally from seawater and biogenically by corals, Geochim. Cosmochim. Acta, 73(14), 4166–4179, doi:10.1016/j.gca.2009.04.015, 2009.

Ip, Y. K. and Lim, A. L. L.: Are calcium and strontium transported by the same mechanism in the hermatypic coral Galaxey fascicularis?, J. Exp. Biol., 159, 507–513, 1991.

Ishikawa, M. and Ichikuni, M.: Uptake of sodium and potassium by calcite, Chem. Geol., 42(1–4), 137–146, doi:10.1016/0009-2541(84)90010-X, 1984.

Israelson, C. and Buchardt, B.: Strontium and oxygen isotopic composition of East Greenland rivers and surface waters: Implication for palaeoenvironmental interpretation, Palaeogeogr. Palaeoclimatol. Palaeoecol., 153(1–4), 93–104, doi:10.1016/S0031-0182(99)00068-1, 1999.

Jurikova, H., Liebetrau, V., Raddatz, J., Fietzke, J., Trotter, J., Rocholl, A., Krause, S., McCulloch, M., Rüggeberg, A. and Eisenhauer, A.: Boron isotope composition of the cold-water coral Lophelia pertusa along the Norwegian margin: Zooming into a potential pH-proxy by combining bulk and high-resolution approaches, Chem. Geol., #pagerange#, doi:10.1016/j.chemgeo.2019.01.005, 2019.

Khani, M. H., Pahlavanzadeh, H. and Alizadeh, K.: Biosorption of strontium from aqueous solution by fungus Aspergillus terreus, Environ. Sci. Pollut. Res., 19(6), 2408–2418, doi:10.1007/s11356-012-0753-z, 2012.

Kinsman, D.: Trace cations in aragonite, Abstr. Geol. Soc. Am., 2, 596–597, 1970.

Kiriakoulakis, K., Fisher, E., Wolff, G. A., Freiwald, A., Grehan, A. and Roberts, J. M.: Lipids and nitrogen isotopes of two deep-water corals from the North-East Atlantic: initial results and implications for their nutrition, in Cold-Water Corals and Ecosystems, pp. 715–729, Springer-Verlag, Berlin/Heidelberg., 2005.

Kiriakoulakis, K., Freiwald, A., Fisher, E. and Wolff, G. A.: Organic matter quality and supply to deep-water coral/mound systems of the NW European Continental Margin, Int. J. Earth Sci., 96(1), 159–170, doi:10.1007/s00531-006-0078-6, 2007.

Kitano, Y., Okumura, M. and Idogaki, M.: Incorporation of sodium, chloride and sulfate with calcium carbonate., Geochem. J., 9(2), 75–84, doi:10.2343/geochemj.9.75, 1975.

Kunioka, D., Shirai, K., Takahata, N., Sano, Y., Toyofuku, T. and Ujiie, Y.: Microdistribution of Mg/Ca, Sr/Ca, and Ba/Ca ratios in Pulleniatina obliquiloculata test by using a NanoSIMS: Implication for the vital effect mechanism, Geochemistry, Geophys. Geosystems, 7(12), doi:10.1029/2006GC001280, 2006.

Lear, C., Elderfield, H. and Wilson, P.: Cenozoic {Deep-Sea} Temperatures and Global Ice Volumes from {Mg/Ca} in Benthic Foraminiferal Calcite, Science (80-.)., 287(5451), 269–272, doi:10.1126/science.287.5451.269, 2000.

Lewis, E. and Wallace, D. W.: R: Program developed for CO2 system calculations ORNL/CDIAC-105, Carbon Dioxide Inf. Anal. CentreOak Ridge Natl. Lab. US Dep. Energy, Oak Ridge, Tennessee, 1998.

Locarnini, R. A., Mishonov, A. V, Antonov, J. I., Boyer, T. P., Garcia, H. E., Baranova, O. K., Zweng, M. M., Paver, C. R., Reagan, J. R., Johnson, D. R., Hamilton, M., Seidov 1948-, D. and Levitus, S.: World ocean atlas 2013. Volume 1, Temperature, edited by O. C. L. National Oceanographic Data Center (U.S.) and N. E. S. United States Data, and Information Service, , doi:http://doi.org/10.7289/V55X26VD, 2013.

López Correa, M., Montagna, P., Vendrell-Simón, B., McCulloch, M. and Taviani, M.: Stable isotopes (δ18O and δ13C), trace and minor element compositions of Recent scleractinians and Last Glacial bivalves at the Santa Maria di Leuca deep-water coral province, Ionian Sea, Deep. Res. Part II Top. Stud. Oceanogr., 57(5–6), 471–486, doi:10.1016/j.dsr2.2009.08.016, 2010.

Lorens, R. B. and Bender, M. L.: The impact of solution chemistry on Mytilus edulis calcite and aragonite, Geochim. Cosmochim. Acta, 44(9), 1265–1278, doi:10.1016/0016-7037(80)90087-3, 1980.

Malone, P. G. and Dodd, J. R.: Temperature and salinity effects on calcification rate in Mytilus edulis and its paleoecological implications, Limnol. Oceanogr., 12(3), 432–436, doi:10.4319/lo.1967.12.3.0432, 1967.

Marriott, C. S., Henderson, G. M., Belshaw, N. S. and Tudhope, A. W.: Temperature dependence of δ7Li, δ44Ca and Li/Ca during growth of calcium carbonate, Earth Planet. Sci. Lett., 222(2), 615–624, doi:10.1016/j.epsl.2004.02.031, 2004.

Marshall, A. T.: Calcification in hermatypic and ahermatypic corals, Science (80-.)., 271(5249), 637–639, doi:10.1126/science.271.5249.637, 1996.

McConnaughey, T.: 13C and18O isotopic disequilibrium in biological carbonates: I. Patterns, Geochim. Cosmochim. Acta, 53(1), 151–162, doi:10.1016/0016-7037(89)90282-2, 1989.

McCulloch, M., Trotter, J., Montagna, P., Falter, J., Dunbar, R., Freiwald, A., Försterra, G., López Correa, M., Maier, C., Rüggeberg, A. and Taviani, M.: Resilience of cold-water scleractinian corals to ocean acidification: Boron isotopic systematics of pH and saturation state up-regulation, Geochim. Cosmochim. Acta, 87, 21–34, doi:10.1016/j.gca.2012.03.027, 2012.

van der Meer, M. T. J., Baas, M., Rijpstra, W. I. C., Marino, G., Rohling, E. J., Sinninghe Damsté, J. S. and Schouten, S.: Hydrogen isotopic compositions of long-chain alkenones record freshwater flooding of the Eastern Mediterranean at the onset of sapropel deposition, Earth Planet. Sci. Lett., 262(3–4), 594–600, doi:10.1016/j.epsl.2007.08.014, 2007.

Meibom, A., Cuif, J. P., Hillion, F., Constantz, B. R., Juillet-Leclerc, A., Dauphin, Y., Watanabe, T. and Dunbar, R. B.: Distribution of magnesium in coral skeleton, Geophys. Res. Lett., 31(23), 1–4, doi:10.1029/2004GL021313, 2004.

Mertens, K. N., Ribeiro, S., Bouimetarhan, I., Caner, H., Combourieu Nebout, N., Dale, B., De Vernal, A., Ellegaard, M., Filipova, M., Godhe, A., Goubert, E., Grøsfjeld, K., Holzwarth, U., Kotthoff, U., Leroy, S. A. G., Londeix, L., Marret, F., Matsuoka, K., Mudie, P. J., Naudts, L., Peña-Manjarrez, J. L., Persson, A., Popescu, S. M., Pospelova, V., Sangiorgi, F., van der Meer, M. T. J., Vink, A., Zonneveld, K. A. F., Vercauteren, D., Vlassenbroeck, J. and Louwye, S.: Process length variation in cysts of a dinoflagellate, Lingulodinium machaerophorum, in surface sediments: Investigating its potential as salinity proxy, Mar. Micropaleontol., 70(1–2), 54–69, doi:10.1016/j.marmicro.2008.10.004, 2009.

Mezger, E. M., de Nooijer, L. J., Boer, W., Brummer, G. J. A. and Reichart, G. J.: Salinity controls on Na incorporation in Red Sea planktonic foraminifera, Paleoceanography, 31(12), 1562–1582, doi:10.1002/2016PA003052, 2016.

Mienis, F., de Stigter, H. C., White, M., Duineveld, G., de Haas, H. and van Weering, T. C. E.: Hydrodynamic controls on cold-water coral growth and carbonate-mound development at the SW and SE Rockall Trough Margin, NE Atlantic Ocean, Deep. Res. Part I Oceanogr. Res. Pap., 54(9), 1655–1674, doi:10.1016/j.dsr.2007.05.013, 2007.

Mitsuguchi, T., Matsumoto, E., Abe, O., Uchida, T. and Isdale, P. J.: Mg/Ca thermometry in coral skeletons, Science (80-.)., 274(5289), 961–963, doi:10.1126/science.274.5289.961, 1996.

Mitsuguchi, T., Uchida, T., Matsumoto, E., Isdale, P. J. and Kawana, T.: Variations in Mg/Ca, Na/Ca, and Sr/Ca ratios of coral skeletons with chemical treatments: implications for carbonate geochemistry, Geochim. Cosmochim. Acta, 65(17), 2865–2874, doi:10.1016/S0016-7037(01)00626-3, 2001.

Montagna, P., McCulloch, M., Douville, E., López Correa, M., Trotter, J., Rodolfo-Metalpa, R., Dissard, D., Ferrier-Pagès, C., Frank, N., Freiwald, A., Goldstein, S., Mazzoli, C., Reynaud, S., Rüggeberg, A., Russo, S. and Taviani, M.: Li/Mg systematics in scleractinian corals: Calibration of the thermometer, Geochim. Cosmochim. Acta, 132, 288–310, doi:10.1016/j.gca.2014.02.005, 2014.

Mucci, A.: Manganese uptake during calcite precipitation from seawater: Conditions leading to the formation of a pseudokutnahorite, Geochim. Cosmochim. Acta, 52(7), 1859–1868, doi:10.1016/0016-7037(88)90009-9, 1988.

Mucci, A. and Morse, J.: Chemistry of low-temperature abiotic calcites: Experimental studies on coprecipitation, stability, and fractionation, Rev. Aquat. Sci, 3(2–3), 217–254, 1990.

Neulinger, S. C., Järnegren, J., Ludvigsen, M., Lochte, K. and Dullo, W. C.: Phenotype-specific bacterial communities in the cold-water coral Lophelia pertusa (Scleractinia) and their implications for the coral's nutrition, health, and distribution, Appl. Environ. Microbiol., 74(23), 7272–7285, doi:10.1128/AEM.01777-08, 2008.

Okai, T., Suzuki, A., Kawahata, H., Terashima, S. and Imai, N.: Preparation of a New Geological Survey of Japan Geochemical Reference Material: Coral JCp-1, Geostand. Geoanalytical Res., 26(1), 95–99, doi:10.1111/j.1751-908X.2002.tb00627.x, 2002.

Okazaki, K.: SKELETON FORMATION OF SEA URCHIN LARVAE. I. EFFECT OF CA CONCENTRATION OF THE MEDIUM, Biol. Bull., 110(3), 320–333, doi:10.2307/1538838, 1956.

Okumura, M. and Kitano, Y.: Coprecipitation of alkali metal ions with calcium carbonate, Geochim. Cosmochim. Acta, 50(1), 49–58, doi:10.1016/0016-7037(86)90047-5, 1986.

Pagliarani, A., Bandiera, P., Ventrella, V., Trombetti, F., Pirini, M. and Borgatti, A. R.: Response to alkyltins of two Na+-dependent ATPase activities in Tapes philippinarum and Mytilus galloprovincialis, Toxicol. Vitr., 20(7), 1145–1153, doi:10.1016/j.tiv.2006.02.006, 2006.

Pytkowicz, R. M. and Conners, D. N.: High pressure solubility of calcium carbonate in seawater, Science (80-.)., 144(3620), 840–841, doi:10.1126/science.144.3620.840, 1964.

Raddatz, J., Liebetrau, V., Rüggeberg, A., Hathorne, E., Krabbenhöft, A., Eisenhauer, A., Böhm, F., Vollstaedt, H., Fietzke, J., Correa, M. L., Freiwald, A. and Dullo, W.: Stable Sr-isotope , Sr / Ca , Mg / Ca , Li / Ca and Mg / Li ratios in the scleractinian cold-water coral Lophelia pertusa, Chem. Geol., 352, 143–152, doi:10.1016/j.chemgeo.2013.06.013, 2013.

Raddatz, J., Rüggeberg, A., Liebetrau, V., Foubert, A., Hathorne, E. C., Fietzke, J., Eisenhauer, A. and Dullo, W. C.: Environmental boundary conditions of cold-water coral mound growth over the last 3 million years in the Porcupine Seabight, Northeast Atlantic, Deep. Res. Part II Top. Stud. Oceanogr., 99, 227–236, doi:10.1016/j.dsr2.2013.06.009, 2014a.

Raddatz, J., Rüggeberg, A., Flögel, S., Hathorne, E. C., Liebetrau, V., Eisenhauer, A. and Dullo, W. C.: The influence of seawater pH on U/Ca ratios in the scleractinian cold-water coral Lophelia pertusa, Biogeosciences, 11(7), 1863–1871, doi:10.5194/bg-11-1863-2014, 2014b.

Raddatz, J., Liebetrau, V., Trotter, J., Rüggeberg, A., Flögel, S., Dullo, W. C., Eisenhauer, A., Voigt, S. and McCulloch, M.: Environmental constraints on Holocene cold-water coral reef growth off Norway: Insights from a multiproxy approach, Paleoceanography, 31(10), 1350–1367, doi:10.1002/2016PA002974, 2016.

Ragland, P. C., Pilkey, O. H. and Blackwelder, B. W.: Diagenetic changes in the elemental composition of unrecrystallized mollusk shells, Chem. Geol., 25(1–2), 123–134, doi:10.1016/0009-2541(79)90088-3, 1979.

Ramos, A. A., Inoue, Y. and Ohde, S.: Metal contents in Porites corals: Anthropogenic input of river run-off into a coral reef from an urbanized area, Okinawa, Mar. Pollut. Bull., 48(3–4), 281–294, doi:10.1016/j.marpolbul.2003.08.003, 2004.

Roberts, J. M.: Reefs of the Deep: The Biology and Geology of Cold-Water Coral Ecosystems, Science (80-.)., 312(5773), 543–547, doi:10.1126/science.1119861, 2006.

Roberts, J. M., Wheeler, A., Freiwald, A. and Cairns, S.: Cold-Water Corals, Cambridge University Press, Cambridge., 2009.

Robinson, L. F., Adkins, J. F., Frank, N., Gagnon, A. C., Prouty, N. G., Brendan Roark, E. and de Flierdt, T. van: The geochemistry of deep-sea coral skeletons: A review of vital effects and applications for palaeoceanography, Deep. Res. Part II Top. Stud. Oceanogr., 99, 184–198, doi:10.1016/j.dsr2.2013.06.005, 2014.

Roder, C., Berumen, M. L., Bouwmeester, J., Papathanassiou, E., Al-Suwailem, A. and Voolstra, C. R.: First biological measurements of deep-sea corals from the Red Sea, Sci. Rep., 3(1), 2802, doi:10.1038/srep02802, 2013.

Rollion-Bard, C. and Blamart, D.: SIMS method and examples of applications in coral biomineralization, Biominer. Sourceb., (March), 249–261, doi:10.1201/b16621-20, 2014.

Rollion-Bard, C. and Blamart, D.: Possible controls on Li, Na, and Mg incorporation into aragonite coral skeletons, Chem. Geol., 396, 98–111, doi:10.1016/j.chemgeo.2014.12.011, 2015.

Rollion-Bard, C., Blamart, D., Cuif, J. P. and Dauphin, Y.: In situ measurements of oxygen isotopic composition in deep-sea coral, Lophelia pertusa: Re-examination of the current geochemical models of biomineralization, Geochim. Cosmochim. Acta, 74(4), 1338–1349, doi:10.1016/j.gca.2009.11.011, 2010.

Rollion-Bard, C., Blamart, D., Trebosc, J., Tricot, G., Mussi, A. and Cuif, J. P.: Boron isotopes as pH proxy: A new look at boron speciation in deep-sea corals using11B MAS

NMR and EELS, Geochim. Cosmochim. Acta, 75(4), 1003–1012, doi:10.1016/j.gca.2010.11.023, 2011.

Rosenthal, Y., Field, M. P. and Sherrell, R. M.: Precise Determination of Element/Calcium Ratios in Calcareous Samples Using Sector Field Inductively Coupled Plasma Mass Spectrometry, Anal. Chem., 71(15), 3248–3253, doi:10.1021/ac981410x, 1999.

Rucker, J. B. and Valentine, J. W.: Salinity response of trace element concentration in Crassostrea virginica, Nature, 190(4781), 1099–1100, doi:10.1038/1901099a0, 1961.

Rüggeberg, A., Flögel, S., Dullo, W. C., Hissmann, K. and Freiwald, A.: Water mass characteristics and sill dynamics in a subpolar cold-water coral reef setting at Stjernsund, northern Norway, Mar. Geol., 282(1–2), 5–12, doi:10.1016/j.margeo.2010.05.009, 2011.

Ruiz-Hernandez, S. E., Grau-Crespo, R., Almora-Barrios, N., Wolthers, M., Ruiz-Salvador, A. R., Fernandez, N. and De Leeuw, N. H.: Mg/Ca partitioning between aqueous solution and aragonite mineral: A molecular dynamics study, Chem. - A Eur. J., 18(32), 9828–9833, doi:10.1002/chem.201200966, 2012.

Schouten, S., Ossebaar, J., Schreiber, K., Kienhuis, M. V. M., Langer, G., Benthien, A. and Bijma, J.: The effect of temperature, salinity and growth rate on the stable hydrogen isotopic composition of long chain alkenones produced by Emiliania huxleyi and Gephyrocapsa oceanica, Biogeosciences, 3(1), 113–119, doi:10.5194/bg-3-113-2006, 2006.

Sevilgen, D. S., Venn, A. A., Hu, M. Y., Tambutté, E., de Beer, D., Planas-Bielsa, V. and Tambutté, S.: Full in vivo characterization of carbonate chemistry at the site of calcification in corals, Sci. Adv., 5(1), eaau7447, doi:10.1126/sciadv.aau7447, 2019.

Shelton, G. A. B.: LOPHELIA pertusa (l.): Electrical conduction and behaviour in a deep-water coral, J. Mar. Biol. Assoc. United Kingdom, 60(2), 517–528, doi:10.1017/S0025315400028538, 1980.

Shirai, K., Kusakabe, M., Nakai, S., Ishii, T., Watanabe, T., Hiyagon, H. and Sano, Y.: Deep-sea coral geochemistry: Implication for the vital effect, Chem. Geol., 224(4), 212–222, doi:10.1016/j.chemgeo.2005.08.009, 2005.

Sinclair, D. J., Williams, B. and Risk, M.: A biological origin for climate signals in corals - Trace element “vital effects” are ubiquitous in Scleractinian coral skeletons, Geophys. Res. Lett., 33(17), 1–5, doi:10.1029/2006GL027183, 2006.

Sizer, I. W.: Effects of temperature on enzyme kinetics, in Advances in Enzymology and Related Areas of Molecular Biology, pp. 35–62, Wiley-Blackwell., 2006.

Stolarski, J.: Three-dimensional micro- and nanostructural characteristics of the scleractinian coral skeleton: A biocalcification proxy, Acta Palaeontol. Pol., 48(4), 497–530, doi:Available from: http://www.app.pan.pl/article/item/app48-497.html., 2003.

Swart, P. K.: The strontium, magnesium and sodium composition of recent scleractinian coral skeletons as standards for palaeoenvironmental analysis, Palaeogeogr. Palaeoclimatol. Palaeoecol., 34(C), 115–136, doi:10.1016/0031-0182(81)90060-2, 1981.

Tambutté, E., Allemand, D., Zoccola, D., Meibom, A., Lotto, S., Caminiti, N. and Tambutté, S.: Observations of the tissue-skeleton interface in the scleractinian coral Stylophora pistillata, Coral Reefs, 26(3), 517–529, doi:10.1007/s00338-007-0263-5, 2007.

Tambutté, S., Holcomb, M., Ferrier-Pagès, C., Reynaud, S., Tambutté, É., Zoccola, D. and Allemand, D.: Coral biomineralization: From the gene to the environment, J. Exp. Mar. Bio. Ecol., 408(1–2), 58–78, doi:10.1016/j.jembe.2011.07.026, 2011.

Taviani, M., Remia, A., Corselli, C., Freiwald, A., Malinverno, E., Mastrototaro, F., Savini, A. and Tursi, A.: First geo-marine survey of living cold-water Lophelia reefs in the Ionian Sea (Mediterranean basin), Facies, 50(3–4), 409–417, doi:10.1007/s10347-004-0039-0, 2005.

Trivedi, B. and Danforth, W. H.: Effect of pH on the kinetics of frog muscle phosphofructokinase., J. Biol. Chem., 241(17), 4110–4112, doi:10.2196/jmir.1752, 1966.

Turekian, K. K., Steele, J. H. and Thorpe, S. A.: Marine Chemistry & Geochemistry A DERIVATIVE OF ENCYCLOPEDIA OF OCEAN SCIENCES., 2010.

de Villiers, S., Shen, G. T. and Nelson, B. K.: The Sr/Ca-temperature relationship in coralline aragonite: Influence of variability in (Sr/Ca)Seawater and skeletal growth parameters, Geochim. Cosmochim. Acta, 58(1), 197–208, doi:10.1016/0016-7037(94)90457-X, 1994.

Wang, K., Villalobo, A. and Roufogalis, B.: The plasma membrane calcium pump: a multiregulated transporter, Trends Cell Biol., 2(February), 46–52 [online] Available from: http://www.ncbi.nlm.nih.gov/pubmed/14731526 (Accessed 22 August 2018), 1992.

Wang, W. X. and Fisher, N. S.: Effects of calcium and metabolic inhibitors on trace element uptake in two marine bivalves, J. Exp. Mar. Bio. Ecol., 236(1), 149–164, doi:10.1016/S0022-0981(98)00195-6, 1999.

Watson, E. B.: WATSON - surface enrichment and trace-element uptake during crystal growth, , 60(24), 5013–5020, 1996.

Weldeab, S., Lea, D. W., Schneider, R. R. and Andersen, N.: Centennial scale climate instabilities in a wet early Holocene West African monsoon, Geophys. Res. Lett., 34(24), 1–6, doi:10.1029/2007GL031898, 2007.

White, A. F.: Sodium and potassium coprecipitation in aragonite, Geochim. Cosmochim. Acta, 41(5), 613–625, doi:10.1016/0016-7037(77)90301-5, 1977.

Wit, J. C., De Nooijer, L. J., Wolthers, M. and Reichart, G. J.: A novel salinity proxy based on na incorporation into foraminiferal calcite, Biogeosciences, 10(10), 6375–6387, doi:10.5194/bg-10-6375-2013, 2013.

Yamazato, K.: Calcification in a solitary coral, Fungia scutaria Lamarck in relation to environmental factors, 1966.

Yoshimura, T., Tamenori, Y., Suzuki, A., Kawahata, H., Iwasaki, N., Hasegawa, H., Nguyen, L. T., Kuroyanagi, A., Yamazaki, T., Kuroda, J. and Ohkouchi, N.: Altervalent substitution of sodium for calcium in biogenic calcite and aragonite, Geochim. Cosmochim. Acta, 202, 21–38, doi:10.1016/j.gca.2016.12.003, 2017.

Zeebe, R. E. and Wolf-Gladrow, D. A.: CO2 in seawater : equilibrium, kinetics, isotopes. [online] Available from: http://epic.awi.de/4276/ (Accessed 22 August 2018), 2001.

Zonneveld, K. A. F., P. Hoek, R., Brinkhuis, H. and Helmut Willems: Geographical distributions of organic-walled dinoflagellate cysts in surficial sediments of the Benguela upwelling region and their relationship to upper ocean conditions, Prog. Oceanogr., 48(1), 25–72, doi:10.1016/S0079-6611(00)00047-1, 2001.

Zweng, M. M., Reagan, J. R., Antonov, J. I., Locarnini, R. A., Mishonov, A. V, Boyer, T. P., Garcia, H. E., Baranova, O. K., Johnson, D. R., Seidov 1948-, D., Biddle, M. M. and Levitus, S.: World ocean atlas 2013. Volume 2, Salinity, edited by O. C. L. National Oceanographic Data Center (U.S.) and N. E. S. United States Data, and Information Service, , doi:http://doi.org/10.7289/V5251G4D, 2013.

Zweng, M. M., Reagan, J. R., Antonov, J. I., Locarnini, R. A., Mishonov, A. V, Boyer, T. P., Garcia, H. E., Baranova, O. K., Johnson, D. R., Seidov 1948-, D., Biddle, M. M. and Levitus, S.: World ocean atlas 2013. Volume 2, Salinity, edited by O. C. L. National Oceanographic Data Center (U.S.) and N. E. S. United States Data, and Information Service, , doi:http://doi.org/10.7289/V5251G4D, 2013.

3 Compositional variability of Mg/Ca, Sr/Ca, and Na/Ca in the deep-sea bivalve Acesta excavata (Fabricius, 1779)

Nicolai Schleinkofer[1,2*], Jacek Raddatz[1,2], David Evans[1,2], Axel Gerdes[1,2], Sascha Flögel[3], Silke Voigt[1,2]; Janina Vanessa Büscher[4], Max Wisshak[5]

[1]Goethe University Frankfurt, Institute of Geosciences, Frankfurt am Main, Germany

[2]Goethe University Frankfurt, Frankfurt Isotope and Element Research Center (FIERCE), Frankfurt am Main, Germany

[3]GEOMAR Helmholtz-Centre for Ocean Research, Kiel, Germany

[4]National University of Ireland, Department of Earth and Ocean Sciences, Galway, Ireland

[5]Senckenberg am Meer, Marine Research Department, Wilhelmshaven, Germany

Published in PlosONE on 30.04.2021 under the DOI 10.1371/journal.pone.0245605

(https://journals.plos.org/plosone/article?id=10.1371/journal.pone.0245605)

3.1 Abstract

Acesta excavata (Fabricius, 1779) is a slow growing bivalve from the Limidae family and is often found associated with cold-water coral reefs along the European continental margin. Here we present the compositional variability of frequently used proxy elemental ratios (Mg/Ca, Sr/Ca, Na/Ca) measured by laser-ablation mass spectrometry (LA-ICP-MS) and compare it to *in-situ* recorded instrumental seawater parameters such as temperature and salinity.

Shell Mg/Ca measured in the fibrous calcitic shell section was overall not correlated with seawater temperature or salinity; however, some samples show significant correlations with temperature with a sensitivity that was found to be unusually high in comparison to other marine organisms. Mg/Ca and Sr/Ca measured in the fibrous calcitic shell section display significant negative correlations with the linear extension rate of the shell, which indicates strong vital effects in these bivalves. Multiple linear regression analysis indicates that up to 79% of elemental variability is explicable with temperature and salinity as independent predictor values. Yet, the overall results clearly show that the application of Element/Ca (E/Ca) ratios in these bivalves to reconstruct past changes in temperature and salinity is likely to be complicated due to strong vital effects and the effects of organic material embedded in the shell. Therefore, we suggest to apply additional techniques, such as clumped isotopes, in order to exactly determine and quantify the underlying vital effects and possibly account for these.

We found differences in the chemical composition between the two calcitic shell layers that are possibly explainable through differences of the crystal morphology. Sr/Ca ratios also appear to be partly controlled by the amount of magnesium, because the small magnesium ions bend the crystal lattice which increases the space for strontium incorporation.

Oxidative cleaning with H_2O_2 did not significantly change the Mg/Ca and Sr/Ca composition of the shell. Na/Ca ratios decreased after the oxidative cleaning, which is most likely a leaching effect and not caused by the removal of organic matter.

3.2 Introduction

Cold-water coral (CWC) reefs comprise an important contribution to the marine biodiversity on continental margins that is similar to that of warm-water coral (WWC) reefs (Shannon-index = CWC: 5.5, WWC: 5.09 (Jensen and Frederiksen, 1992; Rogers, 1999; Roberts et al., 2009; Henry and Roberts, 2017; Austin et al., 1980; Spellerberg and Fedor, 2003). The reefs provide shelter for other organisms such as the bivalve *Acesta excavata* (Fabricius, 1779) as one of the key species associated with CWC reefs. These sensitive ecosystems are greatly threatened by the combined effects of ocean acidification and warming (McCulloch et al.,

2012b; Büscher et al., 2017; Raddatz et al., 2016; Levin and Bris, 2015b). Understanding the physiological limits of these ecosystems and their associated organisms in the past may provide important information for conservation strategies. Analyzing the environmental factors that control the distribution of CWCs has therefore been the focus of marine research in the last few decades. Salinity, temperature and aragonite saturation are important factors controlling the distribution of CWC (Freiwald, 2002; Guinotte et al., 2006). Water flow velocity and the effect of changing flow velocities on food supply to the corals also control CWC reef distribution (Mortensen et al., 2001), whilst the degree to which seasonality controls the flourishing state of CWC reefs is poorly constrained. Seasonally fluctuating zooplankton concentrations are an important nutrient source for the corals and might thus be an important controlling factor for the distribution of CWC reefs(Naumann et al., 2011; Freiwald, 2002). Moreover, the synchronization of gamete spawning may also be triggered by seasonal changes in temperature (Brooke and Järnegren, 2013) or changing moon phases (Babcock et al., 1994). However, the reconstruction of past changes in the seasonality at CWC reefs is challenging because reef-forming CWCs, such as *Desmophyllum pertusum* (formerly known as *Lophelia pertusa*) lack well-defined growth patterns. While growth patterns in reef forming CWCs are observable, the timing of their formation is unknown (Gass and Roberts, 2011; Lartaud et al., 2016), making seasonal reconstructions challenging. In addition, commonly used proxies such as Mg/Ca and can be influenced by vital effects (Cohen et al., 2006; Raddatz and Rüggeberg, 2019; Adkins et al., 2003; Raddatz et al., 2013). Other corals such as bamboo corals show more promising results regarding growth patterns and trace element proxies (LaVigne et al., 2011; Sinclair et al., 2011; Hill et al., 2011, 2012) and might therefore provide an alternative archive.

The deep-water bivalve *Acesta excavata* could be an archive for the seasonality of seawater attributes in regions of CWC distribution. A previous study revealed cyclic repetitions of density changes in the shell and regular growth increment spacing, indicating a rhythmic, possibly annual control of shell deposition (López Correa et al., 2005). In general, *A. excavata* displays two growth modes. The first phase lasts until the bivalve has built 18-22 increments (= 18 – 22 years (López Correa et al., 2005)) and reaches a size of approximately 10 cm. The second growth phase is characterized by slower growth and more tightly aligned growth increments(López Correa et al., 2005). The growth increments suggest a typical lifespan of 50 to 80 years (López Correa et al., 2005). The change of growth mode happens simultaneously with a sex change from male to female (Järnegren et al., 2007). *A. excavata* features a semi-continuous reproductive cycle with one spawning event in May/June and another one beginning in August and lasting the rest of the year (Järnegren et al., 2007). The annually formed increments make these species a good candidate for paleoenvironmental reconstructions using proxies such as Element/Ca ratios.

The majority of studies on bivalves conclude that possible temperature controls on elemental ratios such as Mg/Ca and Sr/Ca are strongly modulated by vital-effects (Takesue and van Geen, 2004; Schöne et al., 2010; Freitas et al., 2008; Elliot et al., 2009; Freitas et al., 2006; Wanamaker et al., 2008; Wanamaker and Gillikin, 2019; Poulain et al., 2015). Similarly for Na/Ca, controlling factors for Na incorporation into marine biogenic carbonates are not fully understood but possible mechanisms include salinity (Foraminifera (Bertlich et al., 2018; Mezger et al., 2016; Wit et al., 2013)), the Na/Ca ratio of the ambient water (Foraminifera (Hauzer et al., 2018; Evans et al., 2018)), temperature (CWC (Rollion-Bard and Blamart, 2015; Schleinkofer et al., 2019; Bertlich et al., 2018)) and growth rate related effects due to lattice defects and distortions (Mitsuguchi et al., 2010). Marine clams, such as the aragonitic bivalve *Arctica islandica,* show no reproducible Na/Ca time-series in specimens from the same location (Marali et al., 2017), which makes external forcing mechanisms unlikely. Whether this assumption holds true for other species has to be further investigated.

Here, we present, element to calcium ratios measured with laser-ablation mass spectrometry (LA-ICP-MS) from *A. excavata* compared to an *in-situ* instrumental record. Live specimens of *A. excavata* were collected from two Norwegian CWC reefs at 200 - 300 m to explore possible environmental and biological controls on Mg/Ca, Na/Ca, and Sr/Ca. Environmental data was gathered via two landers deployed in close proximity to the investigated reefs and provide one-year-long records of high-resolution data, which can be used for direct comparison. This data is a key part of this investigation, as *in-situ* environmental data from deep-waters is scarce and difficult to acquire. Resulting proxies from this study have the potential to improve our understanding of the physiological limits of CWC reef distribution in the past and could provide necessary information about the future of these important structures regarding the present-day climate change. This is especially important with regards to the location of our archive in intermediate water depths as there are not many archives from such depths. In addition, we test the effect of an oxidative cleaning step (using H_2O_2) on LA-ICP-MS trace element data.

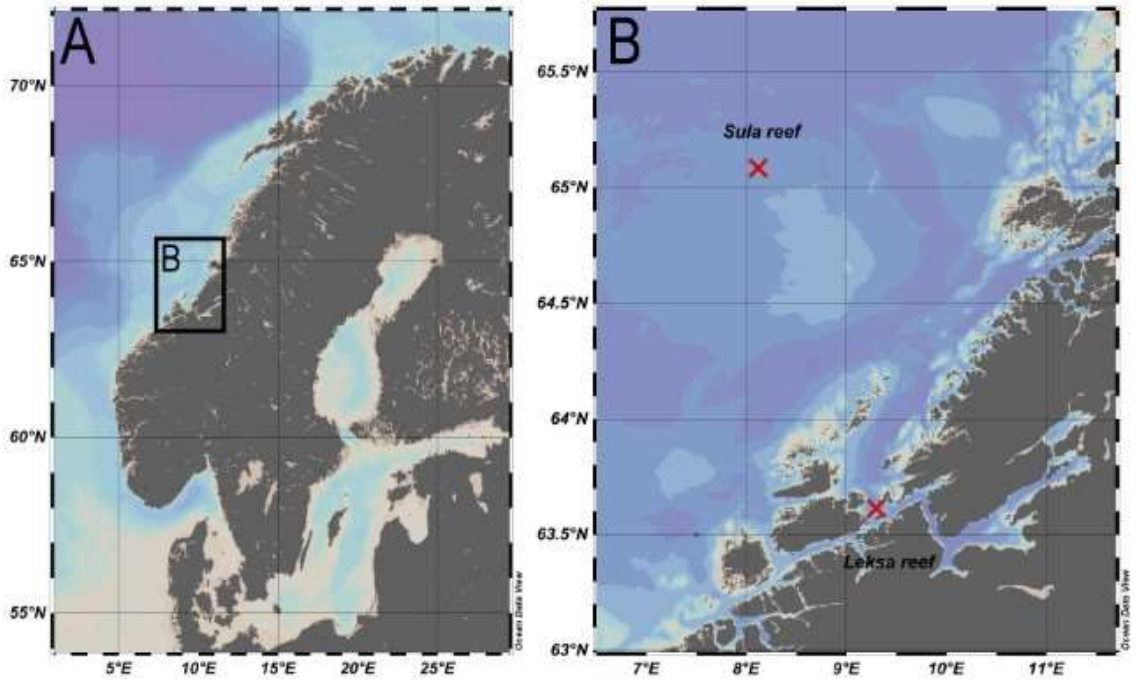

Figure 3-1 Map of the sampling locations. A. Overview of the Fennoscandian Peninsula. B. Enlarged section of the sampling locations

3.2.1 Sampling

Eight specimens of *A. excavata* from the Norwegian Atlantic region were investigated in this study. Four of them were collected in the Sula Reef (N 64°06.64'/E 08°07.11', depth ~ 300 m) and four were collected in a reef close to the island Nord-Leksa at the entrance of the Trondheimsfjord (N 63°36.47'/E 09°23.03', depth ~ 200 m) (Fig. 1). All specimens were collected live with the manned submersible JAGO from GEOMAR (Hissmann and Schauer, 2017) during RV POSEIDON (Lackschewitz and Heinitz, 2015) cruise 473 (Form et al., 2015). Permission for entering and sampling in Norwegian waters was granted by the Directorate of Fisheries and the Norwegian Armed Forces. Specific permissions to sample this particular species were not necessary as *A. excavata* does not appear in CITES lists and the Nagoya protocol was not yet established at the time of sampling. Directly after sampling the soft body was physically removed and the shells were dried in an oven at 40°C. Cleaning was conducted on board with knives as well as prior to further investigation in an ultrasonic bath (5 min).

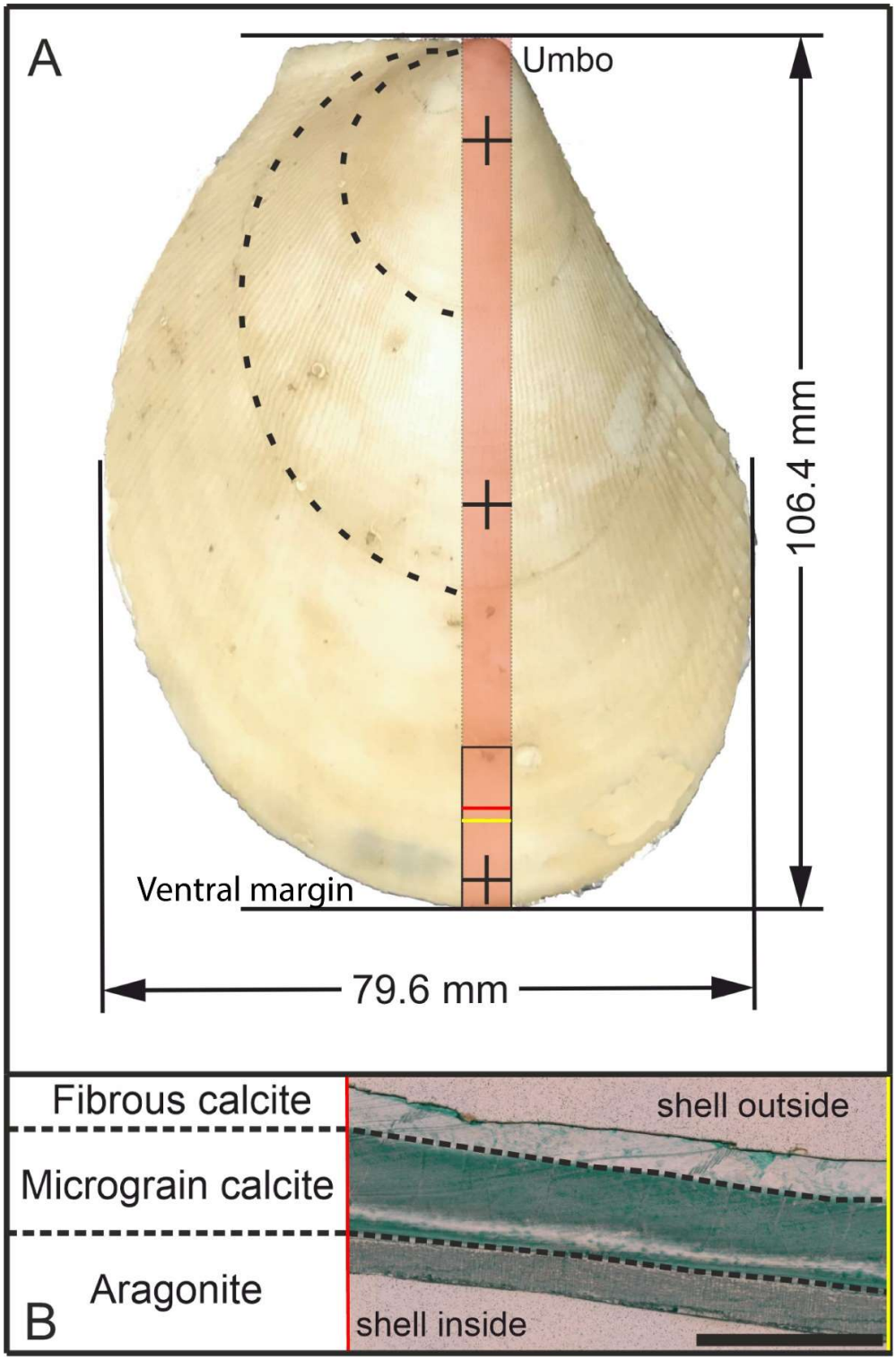

F**igure 3-2 Sample overview and crystalline phases in the shell of A. excavata.** A: Sample 17R from the Sula Reef. The red area marks the cut slab and the black rectangle shows the investigated area. Crosses mark the position of shell thickness measurements (15 mm from umbo, 50 mm from umbo and 5 mm from ventral margin). The shell length was measured perpendicular to the bivalve auricle and the width was measured parallel to the auricle of the bivalve along the maximum distance. Dashed lines show visible growth lines B: Cross-section of the shell (location marked in A with red and yellow lines), colored with Mutvei's solution (Schöne et al., 2005). Scalebar is 1 mm.

Slabs of 8 mm thickness were then cut along the major growth axis of each shell and 20 mm-long sub-samples were taken of the ontogenetic oldest part of the bivalve (ventral side; Fig. 2). These samples were mounted vertically into circular mounts and embedded in epoxy resin. Prior to the acquisition of trace element data using LA-ICP-MS, the slab surface was ground with 9 µm grid with silicon carbide sanding paper and then polished using 3 µm diamond-water based lapping paste.

Additional shell strips were prepared as thin sections and treated with Mutvei's solution (50 min, 45°C) to enhance growth increment visibility (Schöne et al., 2005). Pictures of the investigated specimens were taken with a Keyence VHX-6000 digital microscope with 200X magnification. Size measurements were conducted with the Keyence software, whereas size measurements of the shells were conducted with digital calipers (Mitutoyo).

3.2.2 Oceanographic data

Seawater properties (temperature, conductivity (Nord-Leksa Reef) and flow velocity (Sula Reef) were provided from a lander study conducted during research cruises (POS455 and POS473) with RV POSEIDON in the Norwegian Sea. The data used here is part of a separate study comprised of oceanographic data assimilation of multiple parameters over a full annual cycle, which is beyond the scope of the present study, but of which temperature in particular was used to correlate it to the shells from the same origin. Two Satellite Lander Modules (SLMs, GEOMAR) were deployed in the Leksa Reef. Each module was equipped with Seabird SBE16 PLUS CTD sensors (conductivity (±0.0005 S/m), temperature (±0.005°C), depth) as well as WETLabs ECO-FLNTU(RT)D turbidity & chlorophyll sensors and Seabird SBE43 oxygen sensors. The lander at Sula Reef was an Aanderaa Seaguard RCM mounted in a pyramid-shaped POM frame equipped with a current meter (linear flow velocity and absolute direction) as well as CTD sensors. The landers were deployed on July 2nd, 2013 (Trondheimsfjord) at a depth of 215m and July 4th, 2013 (Sula Reef) at a depth of 315 m. Data in the Sula Reef was recorded every 30 minutes, in the Nord-Leksa Reef every 15 minutes resulting in 20123 and 37603 data points, respectively. This translates to a total recorded time of 419 days in the Sula Reef and 391 days in the Nord-Leksa Reef (Form et al., 2015).

For the Sula Reef, temperature data from the ARGO project (Argo, 2000) were used for additional comparison. The data utilized here consists of composite temperature measurements from 5 – 9°E/63.5 – 64.5°N, as such temperatures from locations to the northeast of the CWC study sites are also included.

3.2.3 Elemental analysis by LA-ICP-MS

The polished mounts to be used for *in-situ* elemental analysis were cleaned in an ultrasonic bath with ethanol. Two samples (6R & 14R) were measured twice, prior to and after

submerging them for 1 hour in an alkaline 5% H_2O_2 solution (Boyle, 1983). Elemental compositions were measured in the outer calcitic shell portion (fibrous material) (Fig. 2B), 0.1 mm below the shell surface and in the microgranular calcite layer parallel to the fibrous section (López Correa et al., 2005). Laser ablation was performed using a Resolution M50 193 nm ArF Excimer Laser system (Resonetics), with a 72 µm beam diameter, a pulse rate of 10 Hz and 10 µm/s scan speed. Total sweep time was 0.65 s. Prior to the measurement a fast precleaning pass was conducted at 0.2 mm/s, 10Hz, and 104 µm laser spot size. Elemental ratio analysis was performed with a Thermo-Scientific ELEMENT XR sector field ICP-MS. NIST SRM 612 glass was used as the external standard and the MACS-3 nano-pellet standard was used to assess accuracy and precision. We used 62.4 µg/g for the NIST 612 Mg concentration (Evans and Müller, 2018), 78.4 µg/g for Sr and 101000 µg/g for Na (Jochum et al., 2011). Standards were ablated in an identical manner to the samples. The monitored isotopes (m/z) were ^{23}Na, ^{24}Mg, and ^{88}Sr. ^{43}Ca was used as the internal standard and for E/Ca calculation. Data processing was conducted in Excel without further specialized software. Accuracy and precision, assessed via repeat measurements of the MACS-3 standard (n = 5) resulted in a measured Mg/Ca ratio of 8.2 ± 0.3 mmol/mol (reference value = 7.8 ±0.4 mmol/mol (Jochum et al., 2012)), Na/Ca: 25.7 ± 1.3 mmol/mol (reference value = 27.3 ± 1.8 (Jochum et al., 2012)) and Sr/Ca: 8.5 ± 0.3 mmol/mol (reference value = 8.2 ± 0.4 mmol/mol (Jochum et al., 2012)). We additionally used NIST SRM 610 as an alternative external standard but the results show no significant differences in the Mg/Ca ratios compared to using NIST SRM 612 as the primary standard (when using 62.4 µg/g as the Mg concentration(Evans and Müller, 2018)).

3.2.4 Organic content and fluorescence microscopy

The organic content of the shell was measured by combustion analysis. Around 45 mg of powdered sample material was ground from the calcitic and the aragonitic shell section. The sample powder was heated in a furnace for 1 hour at 105°C to remove the water and was thereafter heated to 500°C for 20 hours to combust organic matter. The samples were weighed after every step to determine water and organic content. Marble and quartz powder standards were monitored to ensure reliable results.

In addition, we used fluorescence microscopy to investigate the distribution of the organic material in the shell. Fluorescent images were taken using a Leica DMRX-POL microscope with fluorescent front light and a 50W mercury lamp. The microscope is equipped with an H3 and D filter cube, which excites in the wavelength range of blue - violet (Bandpass filter: 420 – 490 nm) and violet - ultraviolet (Bandpass filter: 355 – 425 nm) (Wanamaker et al., 2009). The pictures were taken with a digital camera connected to the microscope with ¼ - 10 s exposure time.

3.2.5 Statistical analysis

All statistical calculations were conducted with OriginPro 2020. We used the T-test to compare means of different populations and a linear regression model to investigate the relationship between predictor and response variables. In addition, we used a multiple linear regression model to predict response variables from multiple predictor (temperature and salinity) variables.

$$y_i = \beta_0 + \beta_1 x_1 + \beta_2 x_2 + \ldots + \beta_n x_n + \varepsilon_n$$

Equation 3-9 Multiple linear regression modell

3.3 Results

3.3.1 Recorded temperature and salinity data

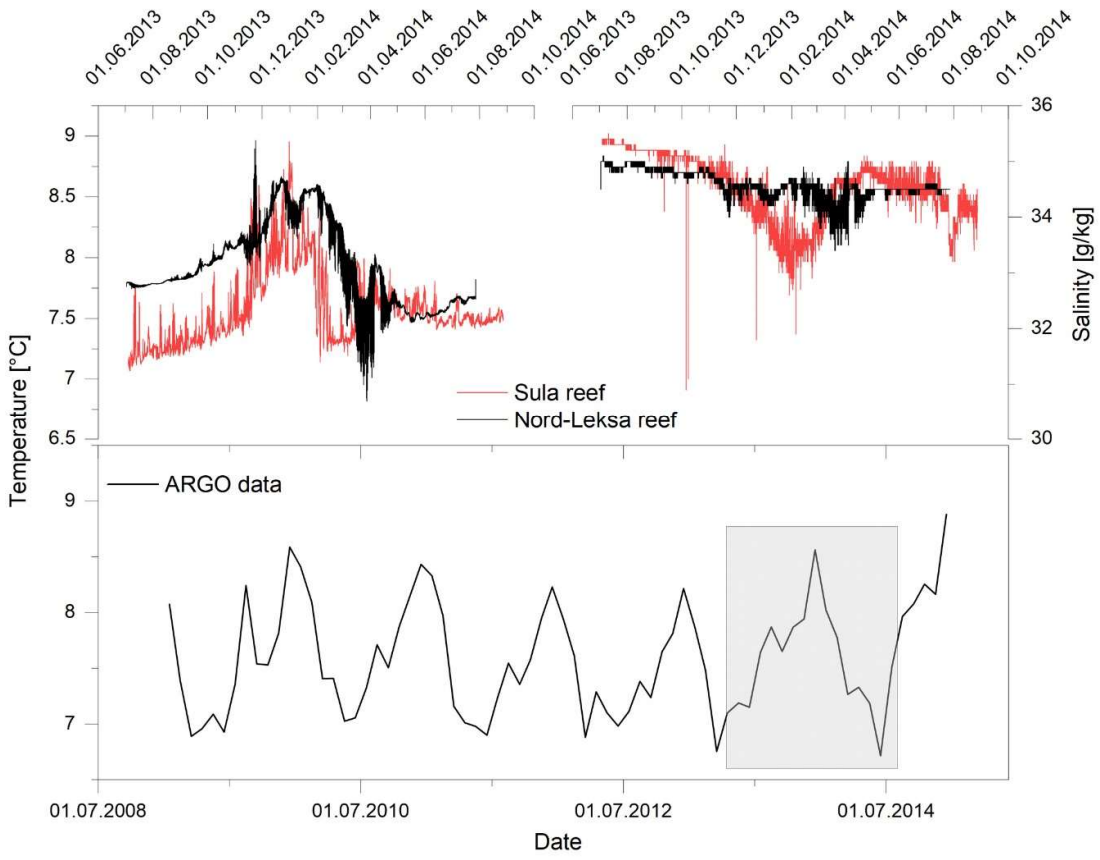

Figure 3-3 Environmental data gathered by two landers and ARGO data. A) Temperature. B) Salinity. C) ARGO Temperature data. The grey box gives the timeframe of the lander deployments.

The recorded environmental data shows a clear annual variability (Fig. 3). Temperature varies between 7.7°C in the summer months and 8.5°C in the winter months in the Leksa

Reef. High temperature and salinity in winter are caused by the replacement of the more brackish and colder Norwegian Coastal Current (NCC) by the warmer, saltier North Atlantic Current (Milzer et al., 2013; Sætre, 1999). This is an effect of increased meltwater supply and increasing northerly winds, which causes the depth of the NCC to decrease. The shallower NCC then allows the NAC water to replace the bottom water in the fjord. The temperature in the Sula Reef varies between 7°C and 8.8°C. Seawater salinity is highest during winter and low in summer, varying from 33.5 – 36 g/kg in the Sula Reef and 34 – 36 g/kg in the Leksa Reef.

3.3.2 Microscopic shell properties

The uppermost fibrous zone is similar to the underlying microgranular zone in its appearance. Following treatment with Mutvei's solution, the distinct identification is possible, since the fibrous zone is weakly stained compared to the microgranular zone (Fig. 2). The aragonitic zone shows a striped pattern consisting of gray and white bands. The relative thickness of the different shell portions is similar between investigated specimens, although variations within specimens are visible. Within the microgranular section a white band is visible that lies about 100 µm above the aragonitic zone. This white band appears to be related to the aragonitic zone as it runs parallel and is discontinued in the youngest shell portions where the aragonitic section disappears. Growth lines are faintly visible, however, a differentiation between yearly growth increments and microgrowth increments cannot be made as there is no difference in size, thickness or other morphological features. The growth lines span both the fibrous and the microgranular zone but are not present in the aragonitic zone. Some growth lines start from a dark colored area at the aragonite - calcite transition (López Correa et al., 2005) and end in a jagged edge on the shell surface (Fig. 4). These lines coincide with minima in Mg/Ca ratios and growth lines visible on the outer shell surface and are therefore regarded as annual growth lines (Halfar et al., 2000). The microgrowth increments are hard to count due to their poor visibility, but where counting was possible, samples show 20 to 30 micro growth increments between two major growth lines.

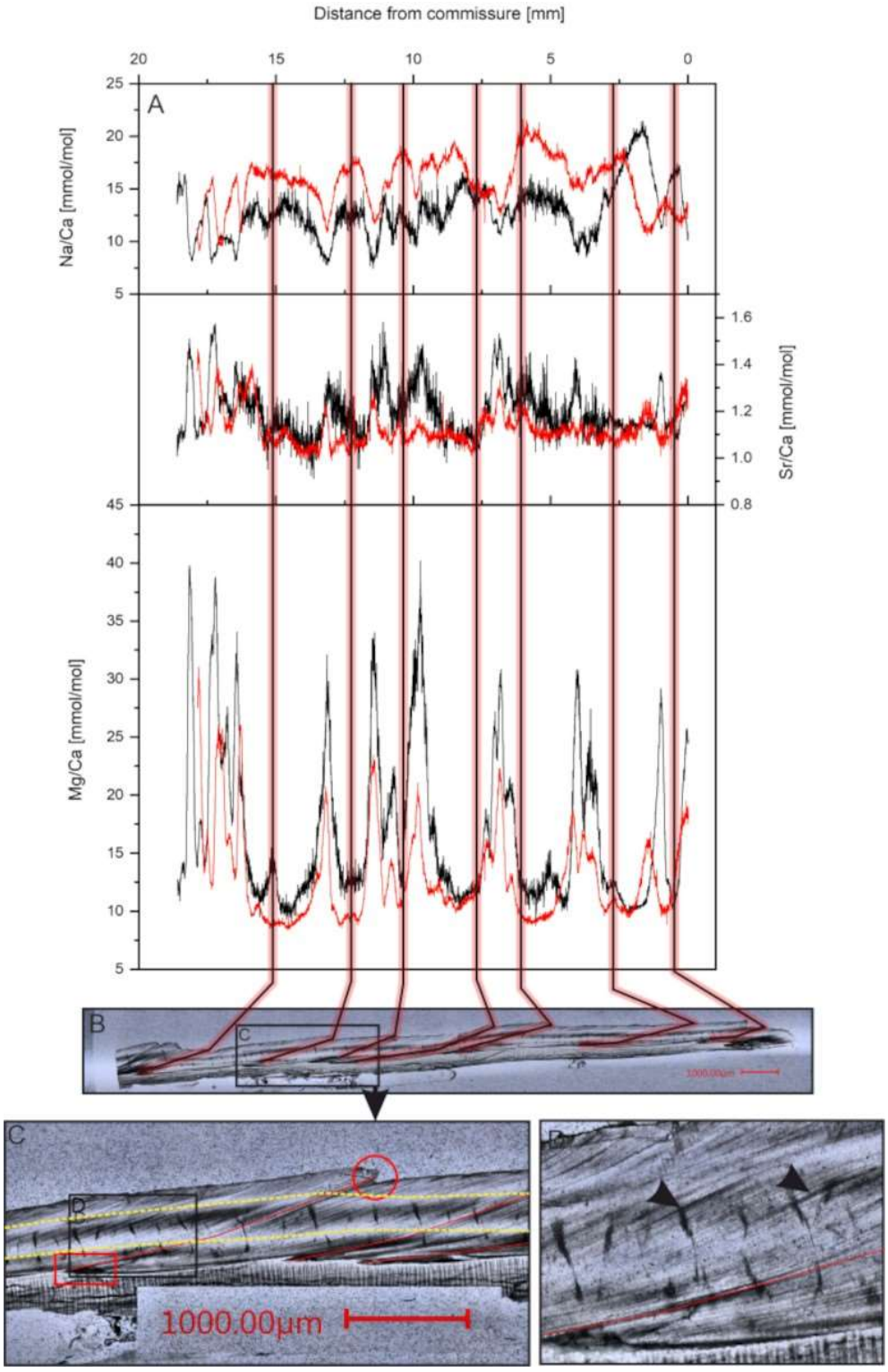

Figure 3-4 Microscopic shell images and elemental ratios of A. excavata. A) Mg/Ca, Sr/Ca and Na/Ca ratios of the fibrous (black line) and microgranular (red line) shell section of sample 14R plotted against distance from the ventral margin. B) Red lines indicate assumed yearly growth lines as seen from microscope pictures of the shell. C) Enlarged section of B) with the jagged edge on the shell surface (red circle) and dark areas (red square) from where the growth line emerges. Yellow dashed lines mark the laser track in the fibrous and microgranular shell layer. Black arrows in D mark microgrowth lines. Scale bars are 1 mm long. Width of the picture in panel D is 1mm. Additional figures are given in the supplementary material (S 7).

3.3.3 Organic content

Table 3-1 Results of combustion experiments A = 105°C for 1h, B = 500°C for 20h

	Weightloss after A (water content)	Weightloss after B (organic content)
Aragonite	0.44%	1.81%
Calcite	0.53%	1.50%
STD Marble	1.15%	0.40%
STD Quartz	0.40%	0.05%

The combustion experiments revealed low concentrations of organic material in the shell of *A. excavata* (Table 1). An excitation of autofluorescence in growth lines was not possible with either of the two filter cubes and wavelengths. The fluorescent microscope images show that the organic matter is not concentrated in specific areas (Fig. 5).

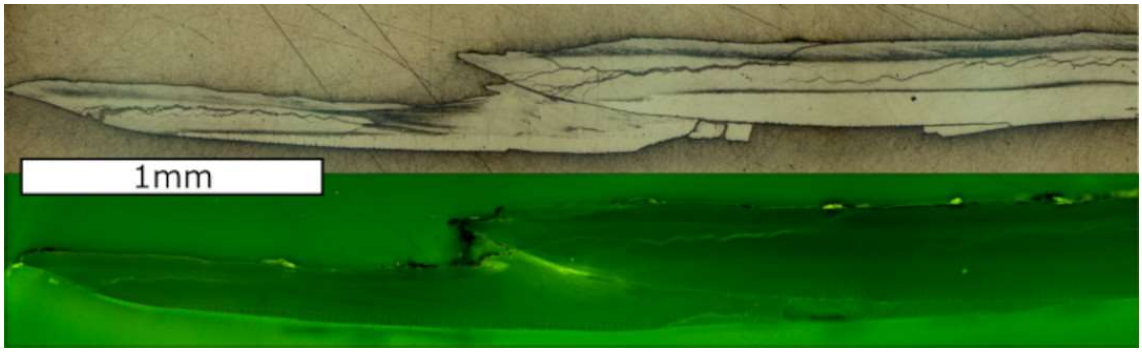

Figure 3-5 Light microscope and fluorescent microscope images of Sample 6R Magnification = 25X, H3 filtercube, ¼ s exposure time. Scale bar is 1 mm.

3.3.4 Elemental composition of different shell layers

3.3.4.1 Fibrous shell section

Measured Mg/Ca ratios of the eight investigated bivalves vary between 7.9 and 48.3 mmol/mol with a mean of 16.4 mmol/mol (median = 14.97 mmol/mol) and 1 standard deviation (SD) of 5.5 mmol/mol for all investigated specimens. Samples from the Trondheimsfjord show higher mean values of 17.8 mmol/mol (median = 16.35 mmol/mol, min=9.7 mmol/mol, max=48.3 mmol/mol) compared to 15.1 mmol/mol (median = 13.65 mmol/mol, min=7.9 mmol/mol, max= 40.2 mmol/mol) in the Sula Reef. Every investigated bivalve shows a well-developed pattern of minimum-maximum variations with relatively stable baseline values around 10 mmol/mol punctuated by repeating sharp peaks up to 48 mmol/mol (Fig. 4 and S7).

Sr/Ca ratios vary between 0.8 and 2.0 mmol/mol with a mean of 1.2 mmol/mol and 1SD of

0.1 mmol/mol. Sr/Ca ratios are only show slight variations of the measured distance.

Na/Ca ratios vary between 7.4 mmol/mol and 29.3 mmol/mol with a mean of 16.8 mmol/mol and 1SD of 3.8 mmol/mol. Similar to Mg/Ca, Na/Ca ratios show a distinct pattern of reoccurring minima and maxima.

Table 3-2 Mean E/Ca ratios (mmol/mol) and differences before and after H2O2 treatment. Differences between the two treatments were tested for significance with a T-test. E/Ca ratios are reported in mmol/mol. DF = Degrees of Freedom.

Sample	before H_2O_2			after H_2O_2			Difference		
	Mg/Ca	Na/Ca	Sr/Ca	Mg/Ca	Na/Ca	Sr/Ca	Mg/Ca	Na/Ca	Sr/Ca
6R	16.67	16.42	1.25	16.77	13.89	1.24	+0.1	-2.53	-0.01
14R	16.53	16.04	1.3	16.73	12.87	1.2	+0.2	-3.17	-0.1

T-test results									
Sample	DF	Mg/Ca			Na/Ca			Sr/Ca	
		t	*p*		t	*p*		t	*p*
6R	3875	-1.17	0.24		-32.08	1.6E-200		1.07	0.28
14R	3983	-0.5	0.62		38.95	1.8E-281		-25.9	3.9E-137

The effects of treating the samples with H_2O_2 were different for Mg/Ca, Na/Ca and Sr/Ca. Measured Mg/Ca ratios were not significantly different between treated and untreated specimens (Table 2) whereas Sr/Ca ratios displayed significant differences after the H_2O_2 treatment in the Sula Reef sample but not in the Nord-Leksa sample. Na/Ca ratios decreased significantly by 2.53 and 3.17 mmol/mol after the H_2O_2 treatment.

3.3.4.2 Microgranular shell section

Table 3-3 Mean E/Ca ratios (mmol/mol) and differences between the fibrous and microgranular shell layer. Differences between the t wo shell layers were tested for significance with a T-test**.** E/Ca ratios are reported in mmol/mol. DF = Degrees of Freedom.

Sample	Fibrous			Microgranular			Difference		
	Mg/Ca	Na/Ca	Sr/Ca	Mg/Ca	Na/Ca	Sr/Ca	Mg/Ca	Na/Ca	Sr/Ca
1R	17.47	17.87	1.2	12.72	21.18	1.12	+4.75	-3.31	+0.08
6R	16.73	13.89	1.24	13.56	16.38	1.28	+3.17	-2.49	-0.04
11R	16.64	20.47	1.07	11.69	20.21	1.02	+4.95	+0.26	+0.05
12R	20.18	13.56	1.23	12.2	17.27	1.3	+7.98	-0.71	-0.07
14R	16.77	12.87	1.2	12.86	15.67	1.13	+3.91	-2.8	+0.07
16R	16.54	18.26	1.18	14.6	19.71	1.23	+1.94	-1.45	-0.05
17R	12.45	17.56	1.14	10.33	23.64	1.18	+2.12	-6.08	-0.04
25R	14.59	19.85	1.11	9.9	23.12	1.16	+4.69	-3.27	-0.05

T-test results									
Sample	DF	Mg/Ca			Na/Ca			Sr/Ca	
		t	*p*		t	*p*		t	*p*
1R	4998	-38.4	2.3E-283		-35.9	5.1E-251		28	1.4E-160
6R	5040	24.3	3.3E-123		-36.5	3.6E-259		-11	2.8E-30
11R	5455	40	2.4E-286		3.8	1.6E-4		16.7	4.4E-61
12R	5434	37.6	2.0E-275		-59.7	2.4E-249		-33.1	1.1E-218
14R	5102	25.8	4.4E-138		-40.7	2.6E-234		27.1	3.1E-151
16R	5531	13.5	1.1E-40		-14.4	2.6E-46		-20.3	1.9E-88
17R	5192	29.0	1.1E-171		-86.4	3.5E-234		-23.3	1.3E-114
25R	5332	87.9	3.3E-253		-66.0	3.1E-263		-26.43	9.2E-145

Within the microgranular shell section the overall trend of the curves is similar to those from the fibrous sections (Fig. 4 and S7), although the absolute values are different. Significant mean differences are observable for every E/Ca ratio in all measured samples (Table 3). Mean Mg/Ca ratios decrease by 2 % to 39 % and Na/Ca ratios increase in the Microgranular shell layer by 5 % to 34 %. Mg/Ca ratios are more influenced in the peaks while baseline values remain unchanged. This is different for Na/Ca ratios, which show alterations in both minimum and maximum values. Unlike Mg/Ca and Na/Ca, Sr/Ca ratios display no systematic difference between the two investigated layers. Three samples show lower and five samples show higher mean Sr/Ca ratios in the microgranular shell layer compared to the fibrous shell layer.

3.3.5 Correlating element/Ca data to instrumental data

The temperature data from the deployed landers were compared to the measured Mg/Ca data to explore the relationship between the parameters. Based on previous studies (López Correa et al., 2005) and our own observations, we assume the growth lines were produced on an annual basis. We therefore identified the last minimum to minimum Mg/Ca cycle based on occurring growth lines, i.e. the cycle closest to the ventral margin of the shell, to which we then compared the recorded temperature. This reveals no overall correlation between Mg/Ca and seawater temperature (r^2=0.06, p<0.05) (Table 4). Four of the investigated samples (11R,12R,16R,17R) show high correlation coefficients (r^2=0.5-0.63) whereas other samples show poor or insignificant correlation. Similarly, Sr/Ca and Na/Ca ratios show no significant correlations with water temperature. Again, some samples show coefficients of determination of up to r^2 = 0.57.

Multiple linear regression with temperature and salinity as predictor variables and element/Ca as dependent variables show that temperature and salinity can account for a moderate to high amount of variability (33-79%) in Mg/Ca ratios (Table 5). This is also true for Sr/Ca and Na/Ca ratios. Sample 25R from the Sula reef distinguishes from the others by not displaying significant correlations for Mg/Ca and Sr/Ca ratios.

Table 3-4 Coefficients of determination r^2, slope and p-values of temperature and salinity with the investigated elemental ratios. Correlations between E/Ca and temperature-salinity are calculated with the same interval for each sample. The correlation for all samples is a combined regression with every sample using the same time interval. Sample 6R could not be tested as there is a particle embedded in the shell in the specific area. DF = Degrees of Freedom.

Sample		Mg/Ca	Na/Ca	Sr/Ca	Mg/Ca	Na/Ca	Sr/Ca
	DF	Water temperature			Salinity		
1R	596	r^2 = 0.01 Slope = 1.8 *p* = 0.001	0.14 -3.4 <0.001	0.1 -0.09 <0.001	0.05 -3.2 <0.001	<0.01 -0.09 0.8	0.24 -0.1 <0.001
11R	326	0.55 4.9 <0.001	0.04 -1.2 <0.001	0.39 -0.07 <0.001	0.13 2.1 <0.001	0.03 0.9 <0.001	0.15 -0.04 <0.001
12R	189	0.55 -10.2 <0.001	0.11 -1.2 <0.001	0.54 -0.28 <0.001	0.03 -2.4 0.01	0.54 -2.6 <0.001	0.34 -0.2 <0.001
14R	329	<0.001 -0.11 0.9	0.35 -5.7 <0.001	0.01 -0.03 0.03	0.59 -8.9 <0.001	0.29 3.25 <0.001	0.31 -0.07 <0.001
16R	259	0.63 10.66 <0.001	0.57 -6.2 <0.001	0.17 0.09 <0.001	0.01 -1.2 0.06	0.12 2.35 <0.001	<0.01 0.01 0.38
17R	503	0.50 11.2 <0.001	0.11 -2.0 <0.001	0.02 0.04 <0.001	0.15 -3.7 <0.001	0.01 -0.4 0.02	0.06 -0.04 <0.001
25R	295	0.05 1.4 <0.001	0.02 -0.9 0.02	<0.01 <0.01 0.85	0.01 -0.5 0.08	0.11 1.6 <0.001	<0.01 <0.01 0.4
All Samples	2509	0.06 3.8 <0.001	0.02 -1.1 <0.001	0.03 -0.05 <0.001	0.02 -1.6 <0.001	0.04 1.5 <0.001	0.06 -0.06 <0.001

Table 3-5 Coefficients of determination r^2 of multiple linear regressions with temperature and salinity as predictor variables and element/Ca as dependent variables. Slope = Sl and *p*-value of the regression are presented in column T = temperature and S = salinity. Sample 6R could not be tested as there is a particle embedded in the shell in the specific area. DF = Degrees of Freedom.

	DF	Mg/Ca	T	S	Na/Ca	T	S	Sr/Ca	T	S
1R	595	0.33	Sl = 16.9 *p* < 0.001	-15.7 <0.001	0.46	-11.4 <0.001	8.3 <0.001	0.28	0.1 <0.001	-0.2 <0.001
11R	325	0.79	9.97	-5.2	0.47	-7.3	6.3	0.45	-0.1	0.04

			<0.001	<0.001		<0.001	<0.001		<0.001	<0.001
12R	188	0.61	-12.37 <0.001	3.9 <0.001	0.54	0.3 0.15	-2.7 <0.001	0.59	-0.2 <0.001	-0.1 <0.001
14R	328	0.58	0.24 0.71	-8.9 <0.001	0.66	-5.9 <0.001	3.3 <0.001	0.32	-0.02 0.03	-0.07 <0.001
16R	258	0.64	10.8 <0.001	0.6 0.12	0.61	-5.8 <0.001	1.4 <0.001	0.19	0.1 <0.001	0.03 0.008
17R	502	0.59	10.5 <0.001	-2.9 <0.001	0.13	-2.2 <0.001	-0.6 <0.001	0.07	0.03 0.02	-0.04 <0.001
25R	294	0.04	1.6 <0.001	0.15 0.66	0.11	0.6 0.2	1.8 <0.001	0.002	0.005 0.74	0.009 0.38

3.3.6 Shell linear extension rate

Shell extension rates were calculated by measuring the distance between two maximum Mg/Ca peaks. Annual extension rates of the investigated shells are reported in Table 6. Except for two specimens, all investigated samples show similar annual extension rates between 1 mm/a and 4.8 mm/a. Only the samples 17R and 25R show higher annual rates between 6.9 mm/a and 7.9 mm/a. Both these samples were collected in the Sula Reef. We observe a significant inverse correlation between both Mg/Ca (DF = 12, r^2 = 0.63, p<0.001) and Sr/Ca (DF = 12, r^2 = 0.38, p = 0.02) with linear extension rate. No significant correlation is found between Na/Ca and linear extension rate (DF = 12, r^2 = 0.09, p = 0.57).

Table 3-6 Linear extension rates of the investigated samples. Extension rates for Sample 6R are missing for the years 2012 and 2013 due to embedded particles in the shell. Extension rate for the year 2104 cannot be reported since the samples were collected in summer 2014.

	Linear extension rate [mm/a]										
Sample	2004	2005	2006	2007	2008	2009	2010	2011	2012	2013	2014
1R			2.1	2.1	2.1	2.1	1.2	0.8	1.1	4.1	
6R					1.4	3.8	4.8	2.5			
11R					3.4	3.6	3.9	2.9	1.5	2.4	
12R	2.4	2.4	2.3	2.3	1.0	1.0	1.2	1.6	2.3	1.4	
14R				1.7	1.8	1.8	1.8	2.9	2.9	1.8	
16R			1.6	1.6	1.6	2.4	1.4	3.4	4.8	2.4	
17R									7.9	7.4	
25R								7.2	6.9	3.9	

3.4 Discussion

3.4.1 Sclerochronology

Sclerolomorphological features are difficult to interpret in *A. excavata* due to their poor visibility (weak contrast). The main growth lines described earlier, which emerge from dark areas and end in external shell features are interpreted as yearly growth increments (Fig. 4) due to the cyclic E/Ca variations within these growth increments and based on results of previous studies (López Correa et al., 2005). The dark areas could be caused by high amounts of organic matter (organic matrices) that are embedded in the shell during times of low calcification rates (Schöne et al., 2005a). However, the fluorescence microscopic pictures (Fig. 5) show no fluorescence in these areas, which makes high contents of organic

matter unlikely. Results from Wanamaker et al. (2009) suggest that organic matter in *Arctica islandica* is fluorescent under the excitation wavelengths used in our work (Wanamaker et al., 2009). Similar results are also reported by Mahé et al. (2010) who found clearly visible growth lines under fluorescent light in *Cerastoderma edule* (460 - 490nm excitation)(Mahé et al., 2010).

The Mg/Ca ratio of calcite is expected to increase with temperature as the substitution of Mg for Ca is an endothermic reaction ($\Delta H > 0$) (Mucci and Morse, 1983a), the correlation of growth lines with Mg/Ca minima would therefore indicate that they are formed during times of low temperature. There are 20 to 30 microgrowth lines within one yearly increment (Fig. 4). This results in a periodicity of 12 – 18 days, corresponding to a fortnightly growth rhythm. A REDFIT spectral analysis conducted on current velocity data from the Sula Reef revealed significant periodicities of 15d and 4.5-2d (Fig. 6). The 15d periodicity fits with the number of microgrowth increments and the lunisolar synodic fortnightly tide cycle. The recorded temperature and salinity data display a periodicity of 15 days in the Leksa Reef. While the temperature and salinity periodicity in the Sula Reef is four days longer than the tidal cycle, these periodicities are generally in acceptance with the growth line periodicity displayed by the bivalve shells (Fig. 6). Therefore, it is reasonable to assume that minor growth lines are caused by changes in the current velocity regime of the environment the bivalves live in, possibly coherent with internal neap/spring tide cycles (Surge and Schöne, 2015). Internal tides might regulate the food availability (Starr et al., 1990) or induce growth line formation by changing the ambient water mass of the organisms through changes of water temperature (Bonardelli et al., 1996; Minchin, 1992), salinity (Stephen, 1980) or other parameters (Ram et al., 1996; Pearson et al., 1998). Tide controlled growth line formation is also known from several other bivalve species including *Phacosoma japonicum* (Miyaji et al., 2007)*, Chione cortezi* (Goodwin et al., 2001) and *Clinocardium nuttalli* (Evans, 1972). *Phacosoma japonicum* and *Clinocardium nuttali* build the growth lines as a response to aerial exposure due to low tides. *Chione cortezi* builds these growth lines due to low tides and consequent increased temperatures, without aerial exposure (Miyaji et al., 2007; Evans, 1972; Goodwin et al., 2001).

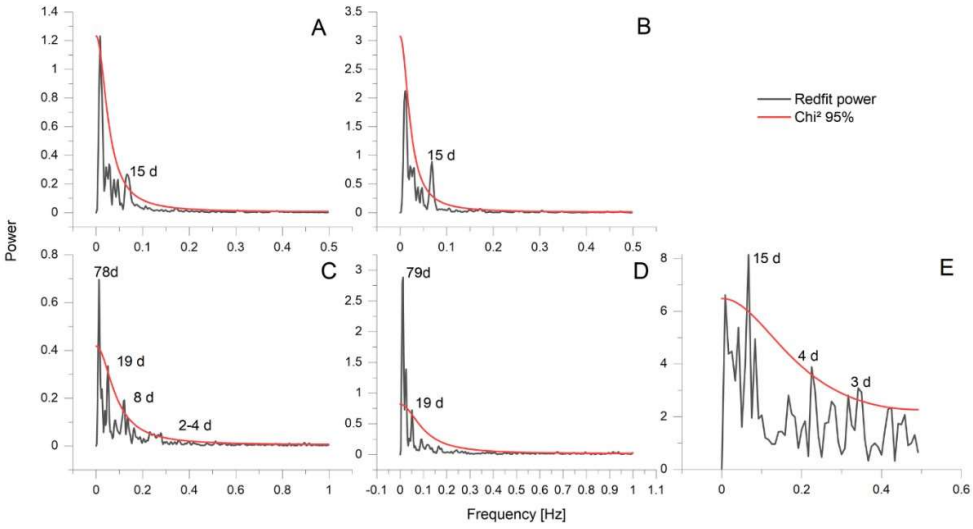

Figure 3-6 REDFIT spectral analysis of oceanographic data. Upper row: Temperature (A) and Salinity (B) at Nord-Leksa Reef. Lower row: Temperature (C), Salinity(D), and flow velocity (E) at Sula Reef.

3.4.2 Differences between shell layers

Differences between the two observed shell layers can be observed for Mg/Ca and Na/Ca, whereas Sr/Ca ratios show no reoccurring pattern (Fig. 4 & Table 3). Differences in the elemental composition between different shell layers are often accounted to differences in the crystal size and form (Schöne et al., 2013; Dalbeck et al., 2006). In *A. excavata* the outermost calcitic layer consists of 50 µm long and 5-10 µm wide prisms. The microgranular crystal in the inner calcitic layer are usually smaller than 1 µm (López Correa et al., 2005). It is suggested that a significant proportion of Na is absorbed to the crystal surface (Lorens and Bender, 1980). This would predict higher Na/Ca ratios in the microgranular layer than in the fibrous layer, as these crystals have a higher surface to volume ratio (Dalbeck et al., 2006). Indeed, we observe these higher Na/Ca ratios in the microgranular shell section. This is different for Mg as we observe higher ratios in the fibrous shell layer. Surface adsorption can therefore not explain the higher Mg/Ca ratios in the fibrous shell layer. Alternatively, sector zoning is proposed to explain compositional differences between shell layers consisting of different crystal forms (Reeder and Paquette, 1989). This effect results in a different incorporation potential for trace elements based on the crystallographic surface (Reeder and Paquette, 1989). In our case, the sector zoning model would predict a lower variability of Mg/Ca in the microgranular shell layers compared to the fibrous shell layers, due to the more uniform crystals. While we do observe such behavior, the effect is too weak to draw any finite conclusions. On the other hand, it is also possible, that the Mg/Ca ratio dictates the crystal form. It was proposed that Mg poisons the sideward growth of crystals, leading to a more elongated growth (Robert L. Folk, 1974), which is observable as the fibrous growth in the

outer shell layer.

3.4.3 Effect of H_2O_2 on bulk shell material

The purpose of H_2O_2 treatment on carbonates is to remove organic material that could potentially alter geochemical measurements (Blanco-Ameijeiras et al., 2012; Boyle, 1983). This process is claimed to influence Mg/Ca ratios as the organic matrices in bivalve shells are reported to be rich in magnesium (Schöne et al., 2010). However, we observe no such effects in the Acesta shells we studied for Mg/Ca. Only Na/Ca ratios are decreasing as an effect of the H_2O_2 treatment. While a sodium enrichment in organic rich zones is supported from other organism groups (corals and foraminifera (Rollion-Bard and Blamart, 2015; Branson et al., 2016; Amiel et al., 1973)) the limited amount of samples used here does not allow us to draw any strong conclusions. It is also proposed that distilled water leaches sodium which is not structurally bound in the lattice (Ragland et al., 1979). Based on the differences we observed between the fibrous and microgranular shell layer we expect a substantial amount of surface bound sodium in the fibrous shell layer. The decreasing Na/Ca ratios after H_2O_2 treatment can therefore also be caused by the leaching of this surface bound sodium. Since we conducted a cleaning ablation prior to the measurements it is also possible that the areas affected by the oxidative cleaning were already ablated during the cleaning ablation. In this case, however, no changes of E/Ca ratios should be visible.

3.4.4 Environmental control factors on element/Ca ratios

A. excavata shows a larger range in Mg/Ca ratios compared to other bivalves from the subclass of Pteriomorpha, such as *Pinna nobilis* (20.3 – 29.5 mmol/mol (ICP-AES) (Freitas et al., 2005)) and *Pecten maximus* (5.0 – 18.4 mmol/mol (ICP-AES) (Freitas et al., 2006)), although we note that these studies did not present highly spatially-resolved analyses such that any such heterogeneity may simply not be present in the data. The bivalve *Neopycnodonte zibrowii*, which lives in a similar setting as *A. excavata* shows similarly high mean Mg/Ca ratios (22.52 ± 17.61 mmol/mol) but higher maximum values of up to 90 mmol/mol, attributable to high concentrations of organic material (Wisshak et al., 2009). The factors that control Mg/Ca ratios in bivalves are not yet entirely resolved. In general, Mg/Ca ratios in bivalves appear to be partly controlled through the calcification temperature but strong (e.g.) kinetic effects inhibit the use of Mg/Ca ratios for environmental reconstructions (Poulain et al., 2015; Wanamaker and Gillikin, 2019; Freitas et al., 2006; Wanamaker et al., 2008; Elliot et al., 2009). Similarly, our results show that variations in Mg/Ca of *A. excavata* cannot be explained solely by changes in seawater temperature or salinity. Only 20 % of the variability in Mg/Ca can be explained by temperature in the Sula Reef species while it even less (6%) when accounting for all observed specimen from Sula and Leksa. As for many other bivalves, Mg/Ca ratios in *A. excavata* may therefore not be an ideal choice for temperature reconstructions Equally, salinity cannot explain a substantial amount of Mg/Ca

variability. On the contrary, multiple linear regression models with temperature and salinity as independent predictor variables together can explain up to 79 % of the Mg/Ca variability. This is also true for Na/Ca and Sr/Ca where temperature and salinity can account for 66 % of variability, respectively 59 %. The different slopes of the regression in the investigated samples, however, show that there is no mechanistic explanation for the correlation.

Kinetic effects are also evident for Mg/Ca and Sr/Ca as shown by the correlation with the linear extension rate. In conclusion these results indicate that Mg/Ca, Na/Ca and Sr/Ca are unlikely to be useful for environmental reconstructions. While environmental parameters such as temperature and salinity certainly have influence on the elemental composition of the shell, strong kinetic and/or biological effects mask these controls.

3.4.5 Further mechanisms potentially influencing Mg/Ca ratios

3.4.5.1 Linear extension rate

The strongest control on Mg/Ca and Sr/Ca is provided by the linear extension rate which is in accordance with results from other bivalve species (Takesue and van Geen, 2004; Lorrain et al., 2005). As this effect is not visible in inorganic precipitated calcite (Mucci and Morse, 1990; Lorens, 1981b), it must be caused by the bivalves' biological functions (Rosenberg and Hughes, 1991). Potentially, the control is not provided by the growth or calcification-rate of the organism, but instead by the metabolic activity and the amount of organic material in the shell (Rosenberg and Hughes, 1991). Calcification rate effects on Na/Ca are reported from inorganic precipitation experiments (Ishikawa and Ichikuni, 1984), whereas we do not observe such behavior in the bivalve calcite (Lorens and Bender, 1980). Again, opposing metabolic effects possibly mask these effects(Wang and Fisher, 1999). This will be discussed in greater detail in the following sections.

3.4.5.2 Organic material

High Mg/Ca ratios could possibly be caused by organic matrices, since these matrices may be characterized by high concentrations of magnesium (Schöne et al., 2010). Because parts of the organic matrices, that act as a framework during carbonate precipitation and mediate mineralization (Lowenstam, 1981; Veis, 2003), are embedded in the calcium carbonate skeleton (Schöne et al., 2010), geochemical measurements using laser ablation may be affected by organic matter due to different chemical compositions (Watanabe et al., 2001). Organic matter is strongly enriched in magnesium and manganese (Takesue et al., 2008; Schöne et al., 2010). Other elements, like barium, are less impacted by the presence of organic material (Takesue et al., 2008). However, these results are derived from the bivalve *Corbula amurensis,* which shows a much higher organic content than *A. excavata* (19% vs. 1.5%). With 1.5-1.8 wt% (Table 1) *A. excavata* shows organic concentrations, which are at the low end of Bivalvia (*C. virginica* 2.6 wt% (Kawaguchi and Watabe, 1993), *A. islandica*

10.33% (Schöne et al., 2010), *C. amurensis* 19.8 wt% (Takesue et al., 2008)). Given the low organic content in *A. excavata* in the investigated outer shell layer, we expect only minor alterations. While organic matter is usually enriched along major growth lines, our data shows that the high Mg/Ca ratios (>35 mmol/mol) of *A. excavata* cannot be accounted for by these organic-rich growth lines. We do note that in the vicinity of major growth lines Mg/Ca ratios irregularly show slight increases by up to 8 mmol/mol, which correlate with increases in Na/Ca and Sr/Ca ratios (Fig. 7). Schöne et al. (2010) demonstrated that strontium is enriched in the organic matrix of bivalves as well as magnesium. We are not aware of bivalve specific sodium enrichment in organic rich zones but Na/Ca ratios typically increase in organic rich regions in organisms such as foraminifera and CWC (Branson et al., 2016; Rollion-Bard and Blamart, 2015). Protein bound sodium and consequent enrichment of sodium in organic shell matrices is therefore possible, which is also supported by other studies (Amiel et al., 1973; Bilings and Ragland, 1968). Even if the amount of sodium bound to organic material might be small (10% in corals (Amiel et al., 1973)) organic compounds such as malate or citrate in the parent solution can increase the amount of sodium coprecipitated in calcite, which would lead to similar effects (White, 1977; Okumura and Kitano, 1986).

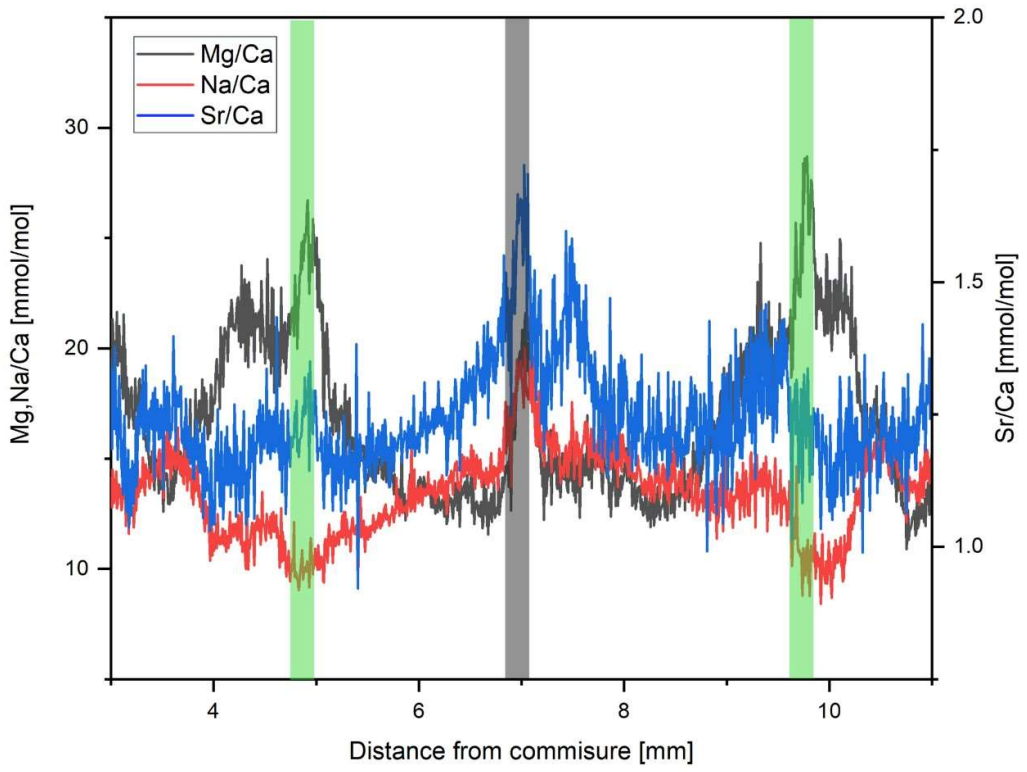

Figure 3-7 Mg/Ca Sr/Ca and Na/Ca ratios of sample 6R. The grey shaded area shows the location of a growth line, which demonstrates increases in all elemental ratios. Green shaded areas show high Mg/Ca winter values. Here increases of Mg/Ca and Sr/Ca are visible whereas Na/Ca is decreasing.

3.4.5.3 Stress and metabolic activity

High Mg/Ca variations not accountable to temperature variability are also reported for other bivalve species (Lorens and Bender, 1980; Wanamaker and Gillikin, 2019). M. edulis and A. islandica showed 14 times and 3 times increased Mg/Ca ratios in temperature-controlled aquarium experiments after handling them for size measurements, which was considered as a stress response by the authors (Lorens and Bender, 1980; Wanamaker and Gillikin, 2019). The underlying mechanisms for this process are yet to be studied, but could be related to a temporal breakdown of Mg-regulating mechanisms (Lorens and Bender, 1980) or changes in metabolic activity. In the natural environment stress related responses could be triggered by the influence of changing water masses that introduce large changes in the flow velocity regime. Recorded lander data from the Sula Reef shows flow velocity changes from a yearly mean of 7.8 cm/s up to 150 cm/s in the winter months when also the highest shell Mg/Ca ratios are measured (Fig. 3). The increased flow velocities can lead to decreased food concentrations in the water and consequently induce a nutrient deficit in the bivalve (Peterson et al., 2009). The effect of alterations in the current speed on physiological functions of bivalves was also shown by an increase in heart rate in *Mya arenaria*, which may be linked to an increase in metabolic activity (Akberali and Trueman, 1985). Mg/Ca and Sr/Ca ratios in the shells as well as in the extra pallial fluid (EPF) increase with higher metabolic activity (Rosenberg and Hughes, 1991; Wada, 1976). We observe strongly increasing current velocities in combination with increasing Mg/Ca ratios and Sr/Ca ratios. Thus, we assume that the observed, increasing Mg/Ca and Sr/Ca ratios in the precipitated shells are the result of a stress-related increase in metabolic activity due to high flow velocities (Gabbott and Bayne, 1973), which likely induced an increased influx of Mg and Sr into the EPF. Na/Ca ratios can be altered by changes in the metabolic activity (Ballesta-Artero et al., 2018) or Na^{+}/K^{*} exchange proteins, which are controlled by the metabolic activity could limit the influx of sodium into the EPF and consequently change the shell signature (Wang and Fisher, 1999). This is also supported by measurements of the chemical composition of the EPF. During resting periods (low metabolic activity) sodium concentrations in the EPF are higher than during periods of increased growth (high metabolic activity) (Wada and Fujinuki, 1974).

Thermal stress may be an additional factor for increasing Mg/Ca and Sr/Ca ratios in the warm winter months. Peak bottom temperatures of 8-9 °C in the study area in winter are presumably not problematic for this species. However, short-term variations from their usual adapted temperature may result in stress-induced increases in Mg/Ca and Sr/Ca, but no experimental studies have been conducted to test the thermal tolerance of *A. excavata* so far.

The usual mechanism of bivalves to survive and cope with stress situations is to close their

shells, thereby reducing the connection between the living organism and the surrounding medium to a minimum. Shell closure induces a series of consecutive effects on the bivalves such as changes in their heart rate (Taylor, 1976), accumulation of CO_2 and decrease of O_2 concentrations resulting in acidosis of the body fluids (Taylor, 1976; Thompson et al., 1980) and increases in metabolic waste products such as ammonia (Thompson et al., 1980). Acidosis could have effects on the geochemical signatures in the shell through the buffering process of the body fluids. An increased Ca concentration was measured in both, mantle cavity fluids and EPF in several bivalve species after shell closure (Crenshaw, 1972; Crenshaw and Neff, 1969; Dugal, 1939; Akberali and Trueman, 1985). Experiments with radioactive ^{45}C have shown that the calcium is provided by dissolution of the inner shell surfaces (Crenshaw and Neff, 1969). Dissolution should therefore lead to an increase of all elemental ratios. We do not observe such effects, nor does Wanamaker et al 2019 (Wanamaker and Gillikin, 2019). A significant contribution of this effect to shell E/Ca ratios can therefore likely be excluded.

3.4.6 Mineralogical influences on Sr/Ca ratios

Large ions such as strontium and barium are incompatible in calcite, because they cannot easily substitute for calcium due to the differences in ionic size (Astilleros et al., 2000; Tesoriero and Pankow, 1996). High concentrations of the small magnesium ion (0.72 Å (Shannon, 1976a)) that are incorporated can distort the crystal lattice, which increases the size of calcium lattice positions and allows for an increased incorporation of larger ions such as strontium (1.18 Å (Shannon, 1976b; Mucci and Morse, 1983b)) and barium (1.35 Å(Kitano et al., 1971; Shannon, 1976b)). Based on the relationship between [Mg] and distribution coefficient (Kd_{Sr}) given by Mucci and Morse, (1983) from inorganic precipitation experiments, we can calculate the variation of Sr/Ca that can be caused by the lattice deformation that may be induced by changes in shell Mg/Ca alone (Mucci and Morse, 1983a). The observed variation in [Mg] would result in a predicted Kd_{Sr} increase from 0.159 to 0.228. Accordingly, 0.6 mmol/mol of the Sr/Ca variation could be explicable through Mg-induced lattice distortion, which is in the range of the observed Sr/Ca variation of 1.0 mmol/mol. Individual samples show a good acceptance between [Mg]-predicted Sr/Ca ratios and observed Sr/Ca ratios, which shows that this mechanism can explain a large part (~50%) of the variance in the Sr/Ca data.

3.5 Conclusion

This study represents the first geochemical investigation of the deep-water bivalve *A. excavata.* Results of high-resolution LA-ICP-MS-derived Element/Ca profiles along the fibrous shell section indicate that elemental ratios in *A. excavata* are not well suited for paleo reconstructions due to weak correlations between proxy trace elements and the

environmental variables temperature and salinity, which is likely a result of biological vital effects. One of these vital effects might be the here observed correlation between Mg/Ca and linear shell extension rate, which suppresses the correlation with environmental variables.

The growth line periodicity suggests a control of the bivalve growth rhythm through internal tidal waves. These results provide an important indicator to investigate for the distribution of CWC reefs in the past as internal waves are an important distribution mechanism for nutrients in CWC reefs (Frederiksen et al., 1992).

We propose that the high Mg/Ca ratios in combination with high Sr/Ca ratios and low Na/Ca ratios that occur during winter are caused by combined effects of increasing temperature and salinity together with an increased metabolic activity due to stress. Mg/Ca peaks occurring during summer and in combination with increasing Sr/Ca and Na/a ratios are most likely an effect of a higher concentration of organic matrices. All investigated elemental ratios are known to increase in organic material and the location of these features is in acceptance with the distribution of growth lines, where organic material is concentrated.

The effect of oxidative cleaning with H_2O_2 on Na/Ca ratios can be ascribed to a leaching effect on surface bound sodium. The oxidative cleaning did not necessarily remove organic matter as there is no effect on Mg/Ca.

In conclusion it can be stated that Mg/Ca, Sr/Ca and Na/Ca ratios in *A. excavata* are unlikely to be good proxies for temperature and salinity reconstructions at this point, due to kinetic and biological effects on the composition of *A. excavata* calcite. Fully controlled cultivation studies are needed to gain a thorough understanding of the factors that influence element incorporation. In Combination with additional techniques such as clumped isotopes, vital effects might be accountable for and Acesta excavata might offer a high resolution archive for the reconstruction in deep-water coral reefs.

3.6 Acknowledgements

We are grateful to all cruise captains, crew members and cruise participants of research cruises POS455, POS473. We are also grateful for the comments of seven anonymous reviewers. This is FIERCE contribution No. 54

3.7 References

Adkins, J. F., Boyle, E. A., Curry, W. B., and Lutringer, A.: Stable isotopes in deep-sea corals and a new mechanism for “vital effects,” 67, 1129–1143, https://doi.org/10.1016/S0016-7037(02)01203-6, 2003.

Akberali, H. B. and Trueman, E. R.: Effects of Environmental Stress on Marine Bivalve Molluscs, 22, 101–198, https://doi.org/10.1016/S0065-2881(08)60051-6, 1985.

Amiel, A. J., Friedman, G. M., and Miller, D. S.: Distribution and nature of incorporation of trace elements in modern aragonitic corals, 20, 47–64, https://doi.org/10.1111/j.1365-3091.1973.tb01606.x, 1973.

Argo: Argo Float Data and Metadata, https://doi.org/10.17882/42182, 2000.

Astilleros, J. M., Pina, C. M., Fernández-Díaz, L., and Putnis, A.: The effect of barium on calcite {10$\bar{1}$4} surfaces during growth, 64, 2965–2972, https://doi.org/10.1016/S0016-7037(00)00405-1, 2000.

Austin, A., Austin, S., and Sale, P.: Community structure of the fauna associated with the coral Pocillopora damicornis (L.) on the Great Barrier Reef, 31, 163, https://doi.org/10.1071/MF9800163, 1980.

Babcock, R. C., Wills, B. L., and Simpson, C. J.: Mass spawning of corals on a high latitude coral reef, 13, 161–169, https://doi.org/10.1007/BF00301193, 1994.

Ballesta-Artero, I., Zhao, L., Milano, S., Mertz-Kraus, R., Schöne, B. R., van der Meer, J., and Witbaard, R.: Environmental and biological factors influencing trace elemental and microstructural properties of Arctica islandica shells, 645, 913–923, https://doi.org/10.1016/j.scitotenv.2018.07.116, 2018.

Bertlich, J., Nürnberg, D., Hathorne, E. C., de Nooijer, L. J., Mezger, E. M., Kienast, M., Nordhausen, S., Reichart, G. J., Schönfeld, J., and Bijma, J.: Salinity control on Na incorporation into calcite tests of the planktonic foraminifera Trilobatus sacculifer - Evidence from culture experiments and surface sediments, 15, 5991–6018, https://doi.org/10.5194/bg-15-5991-2018, 2018.

Bilings, G. K. and Ragland, P. C.: Geochemistry and mineralogy of the Recent reef and lagoonal sediments south of Belize (British Honduras), 3, 135–153, https://doi.org/10.1016/0009-2541(68)90006-5, 1968.

Blanco-Ameijeiras, S., Lebrato, M., Stoll, H. M., Iglesias-Rodriguez, M. D., Méndez-Vicente, A., Sett, S., Müller, M. N., Oschlies, A., and Schulz, K. G.: Removal of organic magnesium in coccolithophore calcite, 89, 226–239, https://doi.org/10.1016/j.gca.2012.04.043, 2012.

Bonardelli, J. C., Himmelman, J. H., and Drinkwater, K.: Relation of spawning of the giant scallop, Placopecten magellanicus, to temperature fluctuations during downwelling events, in: Marine Biology, 637–649, https://doi.org/10.1007/BF00351045, 1996.

Boyle, E. A.: Manganese carbonate overgrowths on foraminifera tests, 47, 1815–1819, https://doi.org/10.1016/0016-7037(83)90029-7, 1983.

Branson, O., Bonnin, E. A., Perea, D. E., Spero, H. J., Zhu, Z., Winters, M., Hönisch, B., Russell, A. D., Fehrenbacher, J. S., and Gagnon, A. C.: Nanometer-Scale Chemistry of a Calcite Biomineralization Template: Implications for Skeletal Composition and Nucleation, 113, 12934–12939, https://doi.org/10.1073/pnas.1522864113, 2016.

Brooke, S. and Järnegren, J.: Reproductive periodicity of the scleractinian coral Lophelia pertusa from the Trondheim Fjord, Norway, 160, 139–153, https://doi.org/10.1007/s00227-012-2071-x, 2013.

Büscher, J. V., Form, A. U., and Riebesell, U.: Interactive Effects of Ocean Acidification and Warming on Growth, Fitness and Survival of the Cold-Water Coral Lophelia pertusa under Different Food Availabilities, 4, 1–14, https://doi.org/10.3389/fmars.2017.00101, 2017.

Cohen, A. L., Gaetani, G. A., Lundälv, T., Corliss, B. H., and George, R. Y.: Compositional variability in a cold-water scleractinian, Lophelia pertusa: New insights into “vital effects,” 7, https://doi.org/10.1029/2006GC001354, 2006.

Crenshaw, M. A.: THE INORGANIC COMPOSITION OF MOLLUSCAN EXTRAPALLIAL FLUID, 143, 506–512, https://doi.org/10.2307/1540180, 1972.

Crenshaw, M. A. and Neff, J. M.: Decalcification at the mantle-shell interface in molluscs, 9, 881–885, https://doi.org/10.1093/icb/9.3.881, 1969.

Dalbeck, P., England, J., Cusack, M., Lee, M. R., and Fallick, A. E.: Crystallography and chemistry of the calcium carbonate polymorph switch in M. edulis shells, 18, 601–609, https://doi.org/10.1127/0935-1221/2006/0018-0601, 2006.

Dugal, L.-P.: The use of calcareous shell to buffer the product of anaerobic glycolysis in Venus mercenaria, 13, 235–251, https://doi.org/10.1002/jcp.1030130210, 1939.

Elliot, M., Welsh, K., Chilcott, C., McCulloch, M., Chappell, J., and Ayling, B.: Profiles of trace elements and stable isotopes derived from giant long-lived Tridacna gigas bivalves: Potential applications in paleoclimate studies, 280, 132–142, https://doi.org/10.1016/j.palaeo.2009.06.007, 2009.

Evans, D. and Müller, W.: Automated Extraction of a Five-Year LA-ICP-MS Trace Element Data Set of Ten Common Glass and Carbonate Reference Materials: Long-Term Data

Quality, Optimisation and Laser Cell Homogeneity, 42, 159–188, https://doi.org/10.1111/ggr.12204, 2018.

Evans, D., Müller, W., and Erez, J.: Assessing foraminifera biomineralisation models through trace element data of cultures under variable seawater chemistry, 236, 198–217, https://doi.org/10.1016/j.gca.2018.02.048, 2018.

Evans, J. W.: Tidal Growth Increments in the Cockle Clinocardium nuttalli, 176, 416–417, https://doi.org/10.1126/science.176.4033.416, 1972.

Form, A. U., Büscher, J., Hissmann, K., Flögel, S., Wisshak, M., Rüggenberg, A., Bannister, R., Kutti, T., Stapp, L., Bennecke, S., Küter, M., Nachtigall, K., Schauer, J., and Fenske, M.: RV POSEIDON Cruise Report POS473 LORELEI II LOphelia REef Lander Expedition and Investigation II, Tromsø-Bergen-Esbjerg, 15.08.-31.08.-04.09.2014, 25 pp. pp., https://doi.org/10.3289/CR_POS_473, 2015.

Frederiksen, R., Jensen, A., and Westerberg, H.: The distribution of the scleractinian coral lophelia pertu sa around the faroe Islands and the relation to internal tidal mixing, 77, 157–171, https://doi.org/10.1080/00364827.1992.10413502, 1992.

Freitas, P., Clarke, L. J., Kennedy, H., Richardson, C., and Abrantes, F.: Mg/Ca, Sr/Ca, and stable-isotope (δ18O and δ13C) ratio profiles from the fan mussel Pinna nobilis: Seasonal records and temperature relationships, 6, https://doi.org/10.1029/2004GC000872, 2005.

Freitas, P. S., Clarke, L. J., Kennedy, H., Richardson, C. A., and Abrantes, F.: Environmental and biological controls on elemental (Mg/Ca, Sr/Ca and Mn/Ca) ratios in shells of the king scallop Pecten maximus, 70, 5119–5133, https://doi.org/10.1016/j.gca.2006.07.029, 2006.

Freitas, P. S., Clarke, L. J., Kennedy, H. A., and Richardson, C. A.: Inter- and intra-specimen variability masks reliable temperature control on shell Mg/Ca ratios in laboratory- and field-cultured Mytilus edulis and Pecten maximus (bivalvia), 5, 1245–1258, https://doi.org/10.5194/bg-5-1245-2008, 2008.

Freiwald, A.: Reef-Forming Cold-Water Corals, in: Ocean Margin Systems, Springer Berlin Heidelberg, Berlin, Heidelberg, 365–385, https://doi.org/10.1007/978-3-662-05127-6_23, 2002.

Gabbott, P. A. and Bayne, B. L.: Biochemical Effects of Temperature and Nutritive Stress on Mytilus Edulis L., 53, 269–286, https://doi.org/10.1017/S0025315400022268, 1973.

Gass, S. E. and Roberts, J. M.: Growth and branching patterns of Lophelia pertusa (Scleractinia) from the North Sea, 91, 831–835, https://doi.org/10.1017/S002531541000055X, 2011.

Goodwin, D. H., Flessa, K. W., Schone, B. R., and Dettman, D. L.: Cross-Calibration of Daily Growth Increments, Stable Isotope Variation, and Temperature in the Gulf of California Bivalve Mollusk Chione cortezi: Implications for Paleoenvironmental Analysis, 16, 387, https://doi.org/10.2307/3515578, 2001.

Guinotte, J. M., Orr, J., Cairns, S., Freiwald, A., Morgan, L., and George, R.: Will human-induced changes in seawater chemistry alter the distribution of deep-sea scleractinian corals?, https://doi.org/10.1890/1540-9295(2006)004[0141:WHCISC]2.0.CO;2, April 2006.

Halfar, J., Zack, T., Kronz, A., and Zachos, J. C.: Growth and high-resolution paleoenvironmental signals of rhodoliths (coralline red algae): A new biogenic archive, 105, 22107–22116, https://doi.org/10.1029/1999JC000128, 2000.

Hauzer, H., Evans, D., Müller, W., Rosenthal, Y., and Erez, J.: Calibration of Na partitioning in the calcitic foraminifer Operculina ammonoides under variable Ca concentration: Toward reconstructing past seawater composition, 497, 80–91, https://doi.org/10.1016/j.epsl.2018.06.004, 2018.

Henry, L.-A. and Roberts, J. M.: Global Biodiversity in Cold-Water Coral Reef Ecosystems, in: Marine Animal Forests, Springer International Publishing, Cham, 235–256, https://doi.org/10.1007/978-3-319-21012-4_6, 2017.

Hill, T. M., Spero, H. J., Guilderson, T., Lavigne, M., Clague, D., MacAlello, S., and Jang, N.: Temperature and vital effect controls on bamboo coral (Isididae) isotope geochemistry: A test of the “lines method,” 12, 1–14, https://doi.org/10.1029/2010GC003443, 2011.

Hill, T. M., LaVigne, M., Spero, H. J., Guilderson, T., Gaylord, B., and Clague, D.: Variations in seawater Sr/Ca recorded in deep-sea bamboo corals, 27, 5–11, https://doi.org/10.1029/2011PA002260, 2012.

Hissmann, K. and Schauer, J.: Manned submersible „JAGO“, 3, https://doi.org/10.17815/jlsrf-3-157, 2017.

Ishikawa, M. and Ichikuni, M.: Uptake of sodium and potassium by calcite, 42, 137–146, https://doi.org/10.1016/0009-2541(84)90010-X, 1984.

Järnegren, J., Rapp, H. T., and Young, C. M.: Similar reproductive cycles and life-history traits in congeneric limid bivalves with different modes of nutrition, 28, 183–192, https://doi.org/10.1111/j.1439-0485.2006.00134.x, 2007.

Jensen, A. and Frederiksen, R.: The fauna associated with the bank-forming deepwater coral lophelia pertusa (scleractinaria) on the faroe shelf, 77, 53–69, https://doi.org/10.1080/00364827.1992.10413492, 1992.

Jochum, K. P., Weis, U., Stoll, B., Kuzmin, D., Yang, Q., Raczek, I., Jacob, D. E., Stracke, A., Birbaum, K., Frick, D. A., Günther, D., and Enzweiler, J.: Determination of reference values for NIST SRM 610-617 glasses following ISO guidelines, 35, 397–429, https://doi.org/10.1111/j.1751-908X.2011.00120.x, 2011.

Jochum, K. P., Scholz, D., Stoll, B., Weis, U., Wilson, S. A., Yang, Q., Schwalb, A., Börner, N., Jacob, D. E., and Andreae, M. O.: Accurate trace element analysis of speleothems and biogenic calcium carbonates by LA-ICP-MS, 318–319, 31–44, https://doi.org/10.1016/j.chemgeo.2012.05.009, 2012.

Kawaguchi, T. and Watabe, N.: The organic matrices of the shell of the American oyster Crassostrea virginica Gmelin, 170, 11–28, https://doi.org/10.1016/0022-0981(93)90126-9, 1993.

Kitano, Y., Kanamori, N., and Oomori, T.: Measurements of distribution coefficients of strontium and barium between carbonate precipitate and solution —Abnormally high values of distribution coefficients measured at early stages of carbonate formation, 4, 183–206, https://doi.org/10.2343/geochemj.4.183, 1971.

Lackschewitz, K. and Heinitz, M.: Research Vessel POSEIDON, 1, https://doi.org/10.17815/jlsrf-1-62, 2015.

Lartaud, F., Galli, G., Raza, A., Priori, C., Benedetti, M. C., Cau, A., Santangelo, G., Iannelli, M., Solidoro, C., and Bramanti, L.: Growth Patterns in Long-Lived Coral Species, in: Marine Animal Forests, Springer International Publishing, Cham, 1–32, https://doi.org/10.1007/978-3-319-17001-5_15-1, 2016.

LaVigne, M., Hill, T. M., Spero, H. J., and Guilderson, T. P.: Bamboo coral Ba/Ca: Calibration of a new deep ocean refractory nutrient proxy, 312, 506–515, https://doi.org/10.1016/j.epsl.2011.10.013, 2011.

Levin, L. A. and Bris, N. L.: The deep ocean under climate change, 350, 766–768, https://doi.org/10.1126/science.aad0126, 2015.

López Correa, M., Freiwald, A., Hall-Spencer, J., and Taviani, M.: Distribution and habitats of Acesta excavata (Bivalvia: Limidae) with new data on its shell ultrastructure, 173–205, https://doi.org/10.1007/3-540-27673-4_9, 2005.

Lorens, R. B.: Sr, Cd, Mn and Co distribution coefficients in calcite as a function of calcite precipitation rate, 45, 553–561, https://doi.org/10.1016/0016-7037(81)90188-5, 1981.

Lorens, R. B. and Bender, M. L.: The impact of solution chemistry on Mytilus edulis calcite and aragonite, 44, 1265–1278, https://doi.org/10.1016/0016-7037(80)90087-3, 1980.

Lorrain, A., Gillikin, D. P., Paulet, Y. M., Chauvaud, L., le Mercier, A., Navez, J., and André, L.: Strong kinetic effects on Sr/Ca ratios in the calcitic bivalve Pecten maximus, 33, 965–968, https://doi.org/10.1130/G22048.1, 2005.

Lowenstam, H.: Minerals formed by organisms, 211, 1126–1131, https://doi.org/10.1126/science.7008198, 1981.

Mahé, K., Bellamy, E., Lartaud, F., and De Rafélis, M.: Calcein and manganese experiments for marking the shell of the common cockle (Cerastoderma edule): Tidal rhythm validation of increments formation, 23, 239–245, https://doi.org/10.1051/alr/2010025, 2010.

Marali, S., Schöne, B. R., Mertz-Kraus, R., Griffin, S. M., Wanamaker, A. D., Butler, P. G., Holland, H. A., and Jochum, K. P.: Reproducibility of trace element time-series (Na/Ca, Mg/Ca, Mn/Ca, Sr/Ca, and Ba/Ca) within and between specimens of the bivalve Arctica islandica – A LA-ICP-MS line scan study, 484, 109–128, https://doi.org/10.1016/j.palaeo.2016.11.024, 2017.

McCulloch, M., Trotter, J., Montagna, P., Falter, J., Dunbar, R., Freiwald, A., Försterra, G., López Correa, M., Maier, C., Rüggeberg, A., and Taviani, M.: Resilience of cold-water scleractinian corals to ocean acidification: Boron isotopic systematics of pH and saturation state up-regulation, 87, 21–34, https://doi.org/10.1016/j.gca.2012.03.027, 2012.

Mezger, E. M., de Nooijer, L. J., Boer, W., Brummer, G. J. A., and Reichart, G. J.: Salinity controls on Na incorporation in Red Sea planktonic foraminifera, 31, 1562–1582, https://doi.org/10.1002/2016PA003052, 2016.

Milzer, G., Giraudeau, J., Faust, J., Knies, J., Eynaud, F., and Rühlemann, C.: Spatial distribution of benthic foraminiferal stable isotopes and dinocyst assemblages in surface sediments of the Trondheimsfjord, central Norway, 10, 4433–4448, https://doi.org/10.5194/bg-10-4433-2013, 2013.

Minchin, D.: Induced spawning of the scallop, Pecten maximus, in the sea, 101, 187–190, https://doi.org/10.1016/0044-8486(92)90242-D, 1992.

Mitsuguchi, T., Uchida, T., and Matsumoto, E.: Na/Ca variability in coral skeletons, 44, 261–273, https://doi.org/10.2343/geochemj.1.0067, 2010.

Miyaji, T., Tanabe, K., and Schöne, B. R.: Environmental controls on daily shell growth of Phacosoma japonicum (Bivalvia: Veneridae) from Japan, 336, 141–150, https://doi.org/10.3354/meps336141, 2007.

Mortensen, P. B., Hovland, T., Fosså, J. H., and Furevik, D. M.: Distribution, abundance and size of Lophelia pertusa coral reefs in mid-Norway in relation to seabed characteristics, 81, 581–597, https://doi.org/10.1017/S002531540100426X, 2001.

Mucci, A. and Morse, J.: Chemistry of low-temperature abiotic calcites: Experimental studies on coprecipitation, stability, and fractionation, 3, 217–254, 1990.

Mucci, A. and Morse, J. W.: The incorporation of Mg 2+ and Sr 2+ into calcite overgrowths: influences of growth rate and solution composition, 47, 217–233, 1983a.

Naumann, M. S., Orejas, C., Wild, C., and Ferrier-Pages, C.: First evidence for zooplankton feeding sustaining key physiological processes in a scleractinian cold-water coral, 214, 3570–3576, https://doi.org/10.1242/jeb.061390, 2011.

Okumura, M. and Kitano, Y.: Coprecipitation of alkali metal ions with calcium carbonate, 50, 49–58, https://doi.org/10.1016/0016-7037(86)90047-5, 1986.

Pearson, G. A., Serrao, E. A., and Brawley, S. H.: Control of Gamete Release in Fucoid Algae: Sensing Hydrodynamic Conditions via Carbon Acquisition, 79, 1725, https://doi.org/10.2307/176791, 1998.

Peterson, C. H., Summerson, H. C., and Duncan, P. B.: The influence of seagrass cover on population structure and individual growth rate of a suspension-feeding bivalve, Mercenaria mercenaria, 42, 123–138, https://doi.org/10.1357/002224084788506194, 2009.

Poulain, C., Gillikin, D. P., Thébault, J., Munaron, J. M., Bohn, M., Robert, R., Paulet, Y. M., and Lorrain, A.: An evaluation of Mg/Ca, Sr/Ca, and Ba/Ca ratios as environmental proxies in aragonite bivalve shells, 396, 42–50, https://doi.org/10.1016/j.chemgeo.2014.12.019, 2015.

Raddatz, J. and Rüggeberg, A.: Constraining past environmental changes of cold-water coral mounds with geochemical proxies in corals and foraminifera, https://doi.org/10.1002/dep2.98, 2019.

Raddatz, J., Liebetrau, V., Rüggeberg, A., Hathorne, E., Krabbenhöft, A., Eisenhauer, A., Böhm, F., Vollstaedt, H., Fietzke, J., López Correa, M., Freiwald, A., and Dullo, W. C.: Stable Sr-isotope, Sr/Ca, Mg/Ca, Li/Ca and Mg/Li ratios in the scleractinian cold-water coral Lophelia pertusa, 352, 143–152, https://doi.org/10.1016/j.chemgeo.2013.06.013, 2013.

Raddatz, J., Liebetrau, V., Trotter, J., Rüggeberg, A., Flögel, S., Dullo, W.-C., Eisenhauer, A., Voigt, S., and McCulloch, M.: Environmental constraints on Holocene cold-water coral reef growth off Norway: Insights from a multiproxy approach, 31, 1350–1367, https://doi.org/10.1002/2016PA002974, 2016.

Ragland, P. C., Pilkey, O. H., and Blackwelder, B. W.: Diagenetic changes in the elemental composition of unrecrystallized mollusk shells, 25, 123–134, https://doi.org/10.1016/0009-2541(79)90088-3, 1979.

Ram, J. L., Fong, P. P., and Kyozuka, K.: Serotonergic mechanisms mediating spawning and oocyte maturation in the zebra mussel, Dreissena polymorpha, 30, 29–37, https://doi.org/10.1080/07924259.1996.9672529, 1996.

Reeder, R. J. and Paquette, J.: Sector zoning in natural and synthetic calcites, 65, 239–247, https://doi.org/10.1016/0037-0738(89)90026-2, 1989.

Robert L. Folk: The Natural History Of Crystalline Calcium Carbonate: Effect of Magnesium Content And Salinity, Vol. 44, 40–53, https://doi.org/10.1306/74d72973-2b21-11d7-8648000102c1865d, 1974.

Roberts, J. M., Wheeler, A., Freiwald, A., and Cairns, S.: Cold-Water Corals, Cambridge University Press, Cambridge, 1–350 pp., https://doi.org/10.1017/CBO9780511581588, 2009.

Rogers, A. D.: The Biology of Lophelia pertusa (Linnaeus 1758) and Other Deep-Water Reef-Forming Corals and Impacts from Human Activities., 84, 315–406, https://doi.org/10.1002/iroh.199900032, 1999.

Rollion-Bard, C. and Blamart, D.: Possible controls on Li, Na, and Mg incorporation into aragonite coral skeletons, 396, 98–111, https://doi.org/10.1016/j.chemgeo.2014.12.011, 2015.

Rosenberg, G. D. and Hughes, W. W.: A metabolic model for the determination of shell composition in the bivalve mollusc, Mytilus edulis, 24, 83–96, https://doi.org/10.1111/j.1502-3931.1991.tb01182.x, 1991.

Sætre, R.: Features of the central Norwegian shelf circulation, https://doi.org/10.1016/S0278-4343(99)00041-2, 1999.

Schleinkofer, N., Raddatz, J., Freiwald, A., Evans, D., Beuck, L., Rüggeberg, A., and Liebetrau, V.: Environmental and biological controls on Na/Ca ratios in scleractinian cold-water corals, 16, 3565–3582, https://doi.org/10.5194/bg-16-3565-2019, 2019.

Schöne, B. R., Houk, S. D., Freyre Castro, A. D., Fiebig, J., Oschmann, W., Kröncke, I., Dreyer, W., and Gosselck, F.: Daily growth rates in shells of Arctica islandica: Assessing sub-seasonal environmental controls on a long-lived bivalve mollusk, 20, 78–92, https://doi.org/10.2110/palo.2003.p03-101, 2005a.

Schöne, B. R., Dunca, E., Fiebig, J., and Pfeiffer, M.: Mutvei's solution: An ideal agent for resolving microgrowth structures of biogenic carbonates, 228, 149–166, https://doi.org/10.1016/j.palaeo.2005.03.054, 2005b.

Schöne, B. R., Zhang, Z., Jacob, D., Gillikin, D. P., Tütken, T., Garbe-Schönberg, D., McConnaughey, T., and Soldati, A.: Effect of organic matrices on the determination of the trace element chemistry (Mg, Sr, Mg/Ca, Sr/Ca) of aragonitic bivalve shells (Arctica islandica) - Comparison of ICP-OES and LA-ICP-MS data, 44, 23–37, https://doi.org/10.2343/geochemj.1.0045, 2010.

Schöne, B. R., Radermacher, P., Zhang, Z., and Jacob, D. E.: Crystal fabrics and element impurities (Sr/Ca, Mg/Ca, and Ba/Ca) in shells of Arctica islandica-Implications for paleoclimate reconstructions, 373, 50–59, https://doi.org/10.1016/j.palaeo.2011.05.013, 2013.

Shannon, R. D.: Revised effective ionic radii and systematic studies of interatomic distances in halides and chalcogenides, 32, 751–767, https://doi.org/10.1107/S0567739476001551, 1976a.

Shannon, R. D.: Revised effective ionic radii and systematic studies of interatomic distances in halides and chalcogenides, 32, 751–767, https://doi.org/10.1107/S0567739476001551, 1976b.

Sinclair, D. J., Williams, B., Allard, G., Ghaleb, B., Fallon, S., Ross, S. W., and Risk, M.: Reproducibility of trace element profiles in a specimen of the deep-water bamboo coral Keratoisis sp., 75, 5101–5121, https://doi.org/10.1016/j.gca.2011.05.012, 2011.

Spellerberg, I. F. and Fedor, P. J.: A tribute to Claude Shannon (1916-2001) and a plea for more rigorous use of species richness, species diversity and the 'Shannon-Wiener' Index, 12, 177–179, https://doi.org/10.1046/j.1466-822X.2003.00015.x, 2003.

Starr, M., Himmelman, J. H., and Therriault, J. C.: Direct coupling of marine invertebrate spawning with phytoplankton blooms, 247, 1071–1074, https://doi.org/10.1126/science.247.4946.1071, 1990.

Stephen, D.: The reproductive biology of the Indian oyster Crassostrea madrasensis (Preston), 21, 139–146, https://doi.org/10.1016/0044-8486(80)90022-8, 1980.

Surge, D. M. and Schöne, B. R.: Bivalve Sclerochronology, in: Encyclopedia of Scientific Dating Methods, edited by: Rink, W. J. and Thompson, J., Springer Netherlands, Dordrecht, 108–115, https://doi.org/10.1007/978-94-007-6304-3_165, 2015.

Takesue, R. K. and van Geen, A.: Mg/Ca, Sr/Ca, and stable isotopes in modern and Holocene Protothaca staminea shells from a northern California coastal upwelling region, 68, 3845–3861, https://doi.org/10.1016/j.gca.2004.03.021, 2004.

Takesue, R. K., Bacon, C. R., and Thompson, J. K.: Influences of organic matter and calcification rate on trace elements in aragonitic estuarine bivalve shells, 72, 5431–5445, https://doi.org/10.1016/j.gca.2008.09.003, 2008.

Taylor, A. C.: The cardiac responses to shell opening and closure in the bivalve Arctica islandica (L.)., 64, 751–759, 1976.

Tesoriero, A. J. and Pankow, J. F.: Solid solution partitioning of Sr2+, Ba2+, and Cd2+ to calcite, 60, 1053–1063, https://doi.org/10.1016/0016-7037(95)00449-1, 1996.

Thompson, R. J., Livingstone, D. R., and de Zwaan, A.: Physiological and biochemical aspects of the valve snap and valve closure responses in the giant scallop Placopecten magellanicus, 137, 97–104, https://doi.org/10.1007/BF00689207, 1980.

Veis, A.: Mineralization in Organic Matrix Frameworks, 54, 249–289, https://doi.org/10.2113/0540249, 2003.

Wada, K.: Biomineralization in bivalve molluscs with emphasis on the chemical composition of the extrapallial fluid, 1976.

Wada, K. and Fujinuki, T.: Physiological regulation of shell formation in molluscs, I. Chemical composition of extrapallial fluid, 18, 2085–2110, 1974.

Wanamaker, A. D. and Gillikin, D. P.: Strontium, magnesium, and barium incorporation in aragonitic shells of juvenile Arctica islandica: Insights from temperature controlled experiments, 526, 117–129, https://doi.org/10.1016/j.chemgeo.2018.02.012, 2019.

Wanamaker, A. D., Kreutz, K. J., Wilson, T., Borns, H. W., Introne, D. S., and Feindel, S.: Experimentally determined Mg/Ca and Sr/Ca ratios in juvenile bivalve calcite for Mytilus edulis: Implications for paleotemperature reconstructions, 28, 359–368, https://doi.org/10.1007/s00367-008-0112-8, 2008.

Wanamaker, A. D., Baker, A., Butler, P. G., Richardson, C. A., Scourse, J. D., Ridgway, I., and Reynolds, D. J.: A novel method for imaging internal growth patterns in marine mollusks: A fluorescence case study on the aragonitic shell of the marine bivalve Arctica islandica (Linnaeus), 7, 673–681, https://doi.org/10.4319/lom.2009.7.673, 2009.

Wang, W. X. and Fisher, N. S.: Effects of calcium and metabolic inhibitors on trace element uptake in two marine bivalves, 236, 149–164, https://doi.org/10.1016/S0022-0981(98)00195-6, 1999.

Watanabe, T., Minagawa, M., Oba, T., and Winter, A.: Pretreatment of coral aragonite for Mg and Sr analysis: Implications for coral thermometers, 35, 265–269, https://doi.org/10.2343/geochemj.35.265, 2001.

White, A. F.: Sodium and potassium coprecipitation in aragonite, 41, 613–625, https://doi.org/10.1016/0016-7037(77)90301-5, 1977.

Wisshak, M., López Correa, M., Gofas, S., Salas, C., Taviani, M., Jakobsen, J., and Freiwald, A.: Shell architecture, element composition, and stable isotope signature of the giant deep-sea oyster Neopycnodonte zibrowii sp. n. from the NE Atlantic, 56, 374–407, https://doi.org/10.1016/j.dsr.2008.10.002, 2009.

Wit, J. C., De Nooijer, L. J., Wolthers, M., and Reichart, G. J.: A novel salinity proxy based on na incorporation into foraminiferal calcite, 10, 6375–6387, https://doi.org/10.5194/bg-10-6375-2013, 2013.

4 Host influenced geochemical signature in the parasitic foraminifer *Hyrrokkin sarcophaga*

Nicolai Schleinkofer[1,2], David Evans[1,2], Max Wisshak[3]; Janina Vanessa Büscher[4,5], Jens Fiebig[1,2], André Freiwald[3], Sven Härter[1], Horst R. Marschall[1,2], Silke Voigt[1,2], Jacek Raddatz[1,2]

[1]Goethe Universität Frankfurt, Institut für Geowissenschaften, Frankfurt am Main, Germany

[2]Goethe Universität Frankfurt, Frankfurt Isotope and Element Research Center (FIERCE), Frankfurt am Main, Germany

[3]Senckenberg am Meer, Marine Research Department, Wilhelmshaven, Germany

[4]National University of Ireland Galway, Department of Earth and Ocean Sciences, Galway, Ireland

[5]GEOMAR Helmholtz Centre for Ocean Research Kiel, Department of Biological Oceanography, Kiel, Germany

Published in Biogeosciences on 20.08.2021 under the DOI 10.5194/bg-18-4733-202

(https://bg.copernicus.org/articles/18/4733/2021/)

4.1 Abstract

Hyrrokkin sarcophaga is a parasitic foraminifera that is commonly found in cold-water coral reefs where it infests the file clam *Acesta excavata* and the scleractinian coral *Desmophyllum pertusum* (formerly known as *Lophelia pertusa)*. Here, we present measurements of the trace-element and isotopic composition of these parasitic foraminifera, analyzed by inductively coupled optical emission spectrometry (ICP-OES), electron probe micro analysis (EPMA) and mass spectrometry (Gas-source-MS and Inductively-coupled-plasma-MS).

Our results reveal that the geochemical signature of *H. sarcophaga* depends on the host organism it infests. Sr/Ca ratios are 1.1 mmol mol^{-1} higher in *H. sarcophaga* that infest *D. pertusum*, which could be an indication that dissolved host carbonate material is utilised in shell calcification, given that the aragonite of *D. pertusum* has a naturally higher Sr concentration compared to the calcite of *A. excavata*. Similarly, we measure 3.1 ‰ lower $\delta^{13}C$ and 0.25 ‰ lower $\delta^{18}O$ values in *H. sarcophaga* that lived on *D. pertusum*, which might be caused by the direct uptake of the host's carbonate material with a more negative isotopic composition or different pH regimes in these foraminifera (pH can exert a control on the extent of CO_2 hydration/hydroxylation) due to the uptake of body fluids of the host. We also observe higher Mn/Ca ratios in foraminifera that lived on *A. excavata* but did not penetrate the host shell compared to specimen that penetrated the shell, which could be interpreted as a change in food source, changes in the calcification rate, Rayleigh fractionation or changing oxygen conditions.

While our measurements provide an interesting insight into the calcification process of this unusual foraminifera, these data also indicate that the geochemistry of this parasitic foraminifera is unlikely to be a reliable indicator of paleoenvironmental conditions using Sr/Ca, Mn/Ca, $\delta^{18}O$ or $\delta^{13}C$ unless the host organism is known and its geochemical composition can be accounted for.

4.2 Introduction

The foraminifera are a very diverse group of marine shelly organisms that are commonly used for paleoenvironmental reconstructions using the isotopic or elemental composition of their carbonate shell (Petersen et al., 2018; Hönisch et al., 2011; Gray and Evans, 2019; Lear and Rosenthal, 2006; Raddatz et al., 2017). They first appeared in the Cambrian (Culver, 1991) and, over the course of the Phanerozoic, occupied oceanic settings from coastal waters to the open ocean, as well as deep sea benthic habitats (Goldstein, 1999). Multiple feeding methods are known from foraminifera, including suspension feeding,

grazing, predation and parasitic feeding (Hancock et al., 2015). The latter is probably the least common feeding mechanism among the foraminifera with only nine species that are known to be parasitic and a further 13 that are suspected to be (Walker et al., 2017). One of the known parasitic species is *Hyrrokkin sarcophaga* (Cedhagen, 1994), a common foraminifera in cold-water coral reefs in the NE-Atlantic (Beuck et al., 2008). *H. sarcophaga* preferentially colonises the file clam *Acesta excavata*, but also other organisms such as the bivalve *Delectopecten vitreus*, sponges of the family Geodiidae and Ancorinidae, cold-water corals such as *Desmophyllum pertusum* (formerly known as *Lophelia pertusa* (Addamo et al., 2016)*), Madrepora occulata* and *Flabellum japonicum,* as well as other foraminifera (Beuck et al., 2008; Cheng and Dai, 2016; Cedhagen, 1994). Besides biogenic hard substrates, *H. sarcophaga* can also be found settling on rocks which shows that it can at least survive short periods without a host (Cedhagen, 1994). *H. sarcophaga* forms an attachment etching, i.e. mirroring its spiral outline on the host. From this depression the foraminifera etch a canal into the shell of the host (Cedhagen, 1994) (Fig. 1). This allows the foraminifera to feed on the bivalve host's tissue (Cedhagen, 1994) and possibly assimilate amino acids from its extrapallial calcifying fluid (Schweizer et al., 2012; Alexander and Delaca, 1987).

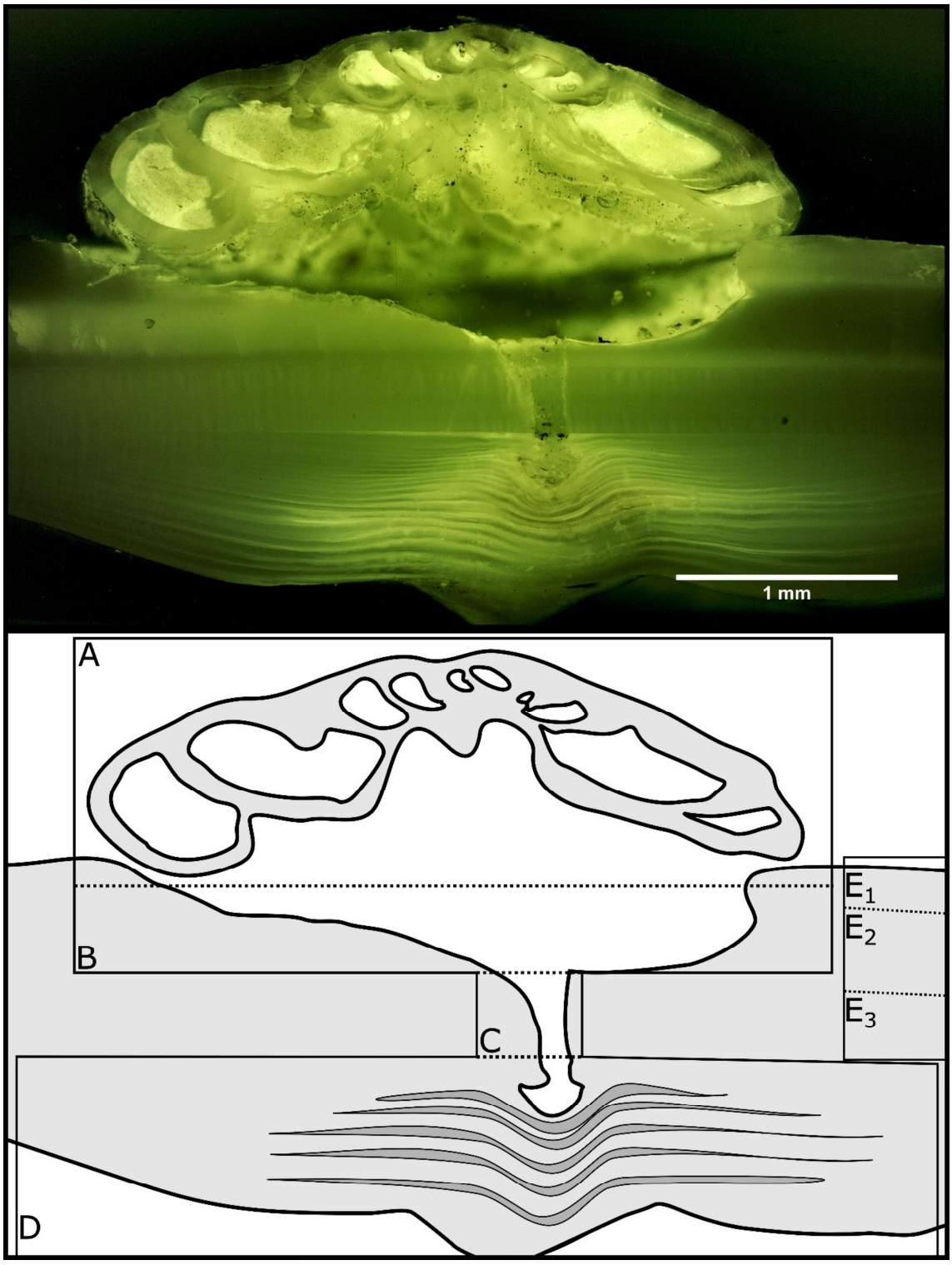

Figure 4-1 Fluorescence microscopic image (excitation 420 – 490 nm) and schematic figure of *H. sarcophaga* on *A. excavata*. A: *H. sarcophaga*, B: Attachment depression corroded by *H. sarcophaga*, C: Bored canal, D: Callus built by *A. excavata* (SRZ = shell repair zone), E: Undisturbed shell, E_1: Calcitic shell layer (fibrous), E_2: Calcitic shell layer (microgranular), E_3: Aragonitic shell layer

The bivalve reacts by building a callus (layered aragonite rich in organics) to seal this boring (Fig 1D) and defend the organism from the parasite's attack (Beuck et al., 2008). In *D. pertusum*, borings into the inner calyx area were not observed (Beuck et al., 2008). Instead, multiple "whip"-shaped tunnels protrude into the coral's skeleton, which possibly serve an anchoring function (Beuck et al., 2008). The pit is possibly formed either as a way to protect itself from cleaning attempts of the host and increase attachment strength or to serve the foraminifera's need for calcium and/or DIC (Beuck et al., 2008; Cedhagen, 1994).

As the parasitic foraminifera ingests material from its host, the question arises whether this process exerts an influence on the shell geochemistry of the parasite. Should this be the case, this factor may need to be accounted for, especially as some parasitic foraminifera, such as *Cibicides refulgens,* are also used in geochemical studies for paleoenvironmental reconstructions (García-Gallardo et al., 2017; Mackensen and Nam, 2014; Rathburn and de Deckker, 1997; Raddatz et al., 2011; Alexander and Delaca, 1987).

Here, we present element to Ca ratios (Mg/Ca, Sr/Ca, Na/Ca and Mn/Ca) and stable isotope data (oxygen and carbon) analyzed in *H. sarcophaga* collected from different host organisms (*A. excavata* and *D. pertusum*) from the Trondheimsfjord (Norway) to explore if and how the different hosts influence the geochemical composition of the test of foraminifera. In addition, we present element maps analyzed by electron microprobe analysis (EPMA) of the callus region of *A. excavata* in order to explore geochemical differences between the callus region and undisturbed shell areas.

4.3 Material and methods

4.3.1 Sampling

All investigated samples were collected in the Leksa Reef, located at the entrance to the Trondheimsfjord in Norway (N 63.613056/E 9.384167, depth ~ 200 m) by means of the manned submersible JAGO (GEOMAR Helmholtz-Zentrum für Ozeanforschung, 2017) during the scientific cruises POS473 and POS525 with RV *Poseidon* (Form et al., 2015; Büscher, 2018; GEOMAR Helmholtz-Zentrum für Ozeanforschung, 2015). In total we analyzed 30 specimens of *H. sarcophaga*, which were divided into three groups: 1. *H. sarcophaga* that infested *A. excavata* with callus formation (henceforth called HAW), 2. *H. sarcophaga* that infested *A. excavata* without callus formation (henceforth called HAO; HAW + HAO = HA), 3. *H. sarcophaga* that infested *D. pertusum* (henceforth called HL). Samples of *A. excavata* and *D. pertusum* were alive when sampled. We cannot be entirely certain that *H. sarcophaga* were still alive when sampled, but upon death they easily become detached from the shell whereas in our samples the foraminifera were still firmly attached. For ICP-OES,

ICP-MS and GS-MS, the samples were ultrasonically rinsed in deionized water for five minutes and allowed to dry before crushing in an agate mortar

4.3.2 Shell carbonate polymorph

The polymorph of the foraminiferal shell was determined using cobalt nitrate solution (Meigen solution). The foraminifera samples were crushed in an agate mortar and transferred to Eppendorf containers. The samples were mixed with 10 wt% $Co(NO_3)_2$ aqueous solution and allowed to react at 95°C for 20 minutes. Afterwards the samples were washed four times with deionized-water and inspected under a KEYENCE VHX-S660E microscope. Aragonite stains purple/pink in cobalt nitrate solution, whereas calcite remains unaffected (Kato et al., 2003)

4.3.3 Fluorescence microscopy

We used fluorescence microscopy to investigate the distribution of the organic material in the foraminifera and the underlying bivalve shell. The sample was cut, ultrasonically cleaned in deionized-water, embedded in epoxy resin (Araldite 2020) and polished with 3 µm diamond-lapping paste Fluorescent images were taken using a Leica DMRX-POL microscope with fluorescent front light and a 50 W mercury lamp. The microscope was equipped with an H3 filter cube, which excites in the wavelength range of blue to violet (Bandpass filter: 420 – 490 nm) The pictures were taken with a digital camera connected to the microscope with 0.25 s exposure time.

4.3.4 EPMA

Two samples of *A. excavata* with attached *H. sarcophaga* were analysed by electron probe micro analysis (EPMA). The area of interest was cut from the shell with a handheld drilling tool, ultrasonically cleaned in deionized-water for five minutes, mounted vertically into circular mounts and embedded in epoxy resin (Araldite 2020). The sample surface was ground with 9 µm grid with silicon carbide sanding paper and then polished using 3 µm diamond-water based lapping paste. After polishing the samples were coated with carbon.

The EPMA analyses were conducted at Goethe University Frankfurt on a JEOL JXA-8530F Plus Field Emission Gun Electron Probe Micro Analyzer (FEG-EPMA). Analysis conditions were: 15 kV acceleration voltage, 20 nA current with a beam diameter of 3 µm. We used a TAP crystal for Mg, TAPL for Na and Sr and PETH for S. Detection limits are calculated with the equation given in Goldstein et al., 2017 and amount to: Mg = 178 µg g^{-1} (Mg/Ca = 0.7 mmol mol^{-1}), Na = 170 µg g^{-1} (Na/Ca = 0.7 mmol mol^{-1}), Sr = 129 µg g^{-1} (Sr/Ca = 0.1 mmol mol^{-1}), S = 152 µg g^{-1} (S/Ca = 0.4 mmol mol^{-1}) and Ca = 195 µg g^{-1}.Molar ratios were calculated from the weight fractions of the specific oxides (CaO, MgO, Na_2O, SrO, SO_3) by calculating the concentration of the observed elements (in µg/g) and normalization to Ca accounting for their relative atomic mass. The chemical maps were recorded with a beam diameter of 2 µm, 15 kV acceleration voltage and 20 nA current.

4.3.5 ICP-OES

For ICP-OES measurements we used ten HAW, ten HAO and ten HL samples. About 120 µg of sample powder was transferred to Eppendorf tubes (acid cleaned with 5 % HNO_3) and sealed. Each sample was analyzed three times.

Elemental ratios Mg/Ca, Sr/Ca, Na/Ca and Mn/Ca (only for foraminifera and bivalves) were analyzed by inductively coupled plasma-optical emission spectrometry (ICP-OES). ICP-OES analysis was carried out using a Thermoscientific iCap 6300 Duo at the Institute of Geosciences, Goethe University Frankfurt. The sample powder (≈ 140 µg) was dissolved in 500 µL HNO_3 (2%) and 300µL aliquots were separated. Subsequently 1500 µL of 1.2 mg L^{-1} yttrium solution was added to each aliquot as an internal standard resulting in a concentration of Y= 1mg L^{-1} and Ca = 25mg L^{-1}. The intensity data were background corrected, standardized internally to Y and normalized to Ca. Accuracy is reported in %-deviation from values of standard reference material JCP1 and USGS MACS-3 (n = 5) (Jochum et al., 2005) and is better than 1% for Mg/Ca and Sr/Ca, 5% for Na/Ca and 3% for Mn/Ca. Precision is reported in relative standard deviation; % RSD of the USGS MACS-3 and JCP1 carbonate reference material (n = 5)(Jochum et al., 2005) and is better than 3% for all analyzed elements.

Bivalve (n = 3) and coral (n = 3) samples were treated similarly to foraminifera samples. We took 15 - 20 samples per shell from the outermost shell section along the main growth axis, starting at the ventral margin resulting in a total of 49 samples. The corals were sampled randomly over the whole calyx area resulting in 44 samples.

4.3.6 ICP-MS

The manganese concentration of *D. pertusum* had to be determined by ICP-MS because it was below the limit of detection by ICP-OES. We used three specimens (two from the Leksa Reef, one from the Sula Reef) of which we sampled 150 µg from the fibrous shell section. Each sample was measured twice.

For solution based ICP-MS measurements we used 150 µg of sample powder and dissolved it in 500 µL 2% HNO_3. The dissolved sample (300 µL) was mixed with 1500 µL 1.2 mg L^{-1} yttrium solution which was used as the internal standard. The reference material ECRM 752-1 (Greaves et al., 2008) was used to monitor measurement precision and accuracy, reported in %-deviation from the reported values of the standard reference material ECRM 752-1 (n = 3) (Greaves et al., 2005) and equals 7% for this analytical session. Precision is reported in relative standard deviation; % RSD of the ECRM 752 carbonate reference material (n= 3) is better than 1% for Mn/Ca

4.3.7 Stable oxygen and carbon isotopes

We used nine HAW, nine HAO and ten HL for stable isotope measurements. About 100 µg of sample powder was transferred to borosilicate glass tubes and sealed with plastic caps. Each sample was measured three times.

Stable isotopes were measured at Goethe University Frankfurt on a Thermo MAT 253 Mass Spectrometer interfaced with a Thermo Fisher Scientific GasBench II. The sample material (100 µg) was reacted with 99% H_3PO_4 at 72°C in continuous flow mode. Analytical procedures followed Spötl and Vennemann (2003). $\delta^{13}C$ and $\delta^{18}O$ values are reported in δ-notation, i.e. ‰-deviation relative to Vienna Pee Dee Belemnite (VPDB) and Vienna Standard Mean Ocean (VSMOW), respectively. Internal precision is better than 0.06‰ ($\delta^{13}C$) and 0.08‰ ($\delta^{18}O$).

Samples of the ambient water were collected during scientific cruise POS525 with R/V *Poseidon* in July 2018 (Büscher, 2018; GEOMAR Helmholtz-Zentrum für Ozeanforschung, 2015). A Rosette Sampler equipped with conductivity, temperature and depth sensors (CTD, Sea-Bird Scientific. SBE 911 Plus) was used to sample water from the investigated reefs. The water samples were transferred from 12 L Niskin bottles to 250 mL borosilicate bottles and sealed after adding 100 µL $HgCl_2$ to prevent biological activity of microorganisms that may alter the isotopic composition. The samples were stored in a fridge at 4°C until measurement.

Water samples were analyzed for their isotopic composition at Friedrich-Alexander University Erlangen-Nürnberg by an automated equilibration unit (Gasbench II; Thermo Fisher Scientific) coupled in continuous flow mode to a Delta *plus* XP isotope ratio mass spectrometer (Thermo Fisher Scientific, Bremen, Germany).

Water for $\delta^{13}C$ analyses was extracted from the sample bottles by a 1-mL disposable syringe through the septa without opening the bottle to avoid loss of CO_2 during sample transfer. During water extraction, the removed volume was simultaneously replaced by inert gas through a second needle connected to an argon-filled gas sampling bag (Grace, Deerfield, IL, USA). The samples were injected into 12 mL Labco Exetainers™ (Labco Ltd. Lampeter, U.K) that were prepared with phosphoric acid and pre-flushed with helium (purity 99.999%). For seawater the injection volume was 0.85 mL per vial. Samples were analyzed in duplicates and the reported values are arithmetic means. All values are reported in the standard δ-notation in per mille (‰) vs. VPDB.

Sample bottles for $\delta^{18}O$ were de-capped and 0.5 mL water were extracted with a pipette for CO_2 equilibration. The samples were transferred into 12 mL Labco Exetainers™ (Labco Ltd. Lampeter, U.K) and subsequently flushed with 0.3% CO_2 in helium. Equilibration time was 24

hours at 25 °C. All samples were measured in duplicates and the reported values are arithmetic means. All values are reported in the standard δ-notation in per mille (‰) vs. VSMOW. External reproducibility based on repeated analysis of control samples was better than 0.1‰ and 0.05‰ for $\delta^{13}C$ and $\delta^{18}O$, respectively.

4.3.8 Statistical computation

We used one-way ANOVA to test the effect of the host species on the elemental and isotopic composition in *H. sarcophaga*. Shapiro-Wilk test and Levene's test were used to ensure normal distribution and equal variance of the target variables. Most groups and target variables are normally distributed except for Na/Ca in the HAO group and $\delta^{18}O$ in the HL group. All target variables except for Mn/Ca and Sr/Ca show equal variance based on the Levene's test. Normal distribution and equal variance are considered a prerequisite for ANOVA. As these prerequisites are not met in some sample groups, we additionally tested the data with a Kruskal-Wallis test which is a non-parametric alternative to ANOVA (Lantz, 2013). Pairwise comparison of the different groups was accomplished with Bonferroni adjusted Tuckey-HSD test. To test the relationship between different variables we used a linear regression model fitted with ordinary least squares (OLS). All reported *p*-values are Bonferroni adjusted. Some measurements could be considered outliers, based on the interquartile range (IQR); Q1 – 1.5*IQR and Q3 + 1.5*IQR. However, we have not truncated these measurements because most of them are just slightly outside the range mentioned above. Only one measurement shows a high deviation, but keeping it in the dataset does not change the outcome of the analysis.

4.4 Results

4.4.1 Carbonate polymorph

The investigated *H. sarcophaga* samples show no staining (Supplement S1) under the influence of cobalt nitrate solution. Consequently, the shells are calcitic as is the case for other species of the order Rotaliida (Horton et al., 2021).

4.4.2 Fluorescence microscopy

The fluorescence microscopic image of *H. sarcophaga* attached to *A. excavata* (Fig. 1) shows distinct fluorescent and non-fluorescent layers in the shell repair zone (SRZ) of the bivalve. Highly fluorescent material is also observable on *H. sarcophaga*, especially in the test apertures.

The SRZ has a maximum thickness of 900 µm, decreasing in all directions. The fluorescent layers in the SRZ are 20 – 40 µm thick. These layers taper off distally from the bore canal and disappear. Non-fluorescent layers are generally smaller ranging from 9- 20 µm. The asymmetric pit that is produced by the foraminifera is observable, one side of the pit is rising

steeply whereas the other side has a shallower angle. The bore canal, which starts at the bottom of the attachment etching, is 400 µm long in the undisturbed bivalve shell, but continues in the callus by another 240 µm. At the start of the bore the canal is 340 µm in diameter and continuously narrows to 140 µm. The canal ends in the SRZ with a “mushroom-like” shape.

4.4.3 Element composition of point measurements (EPMA)

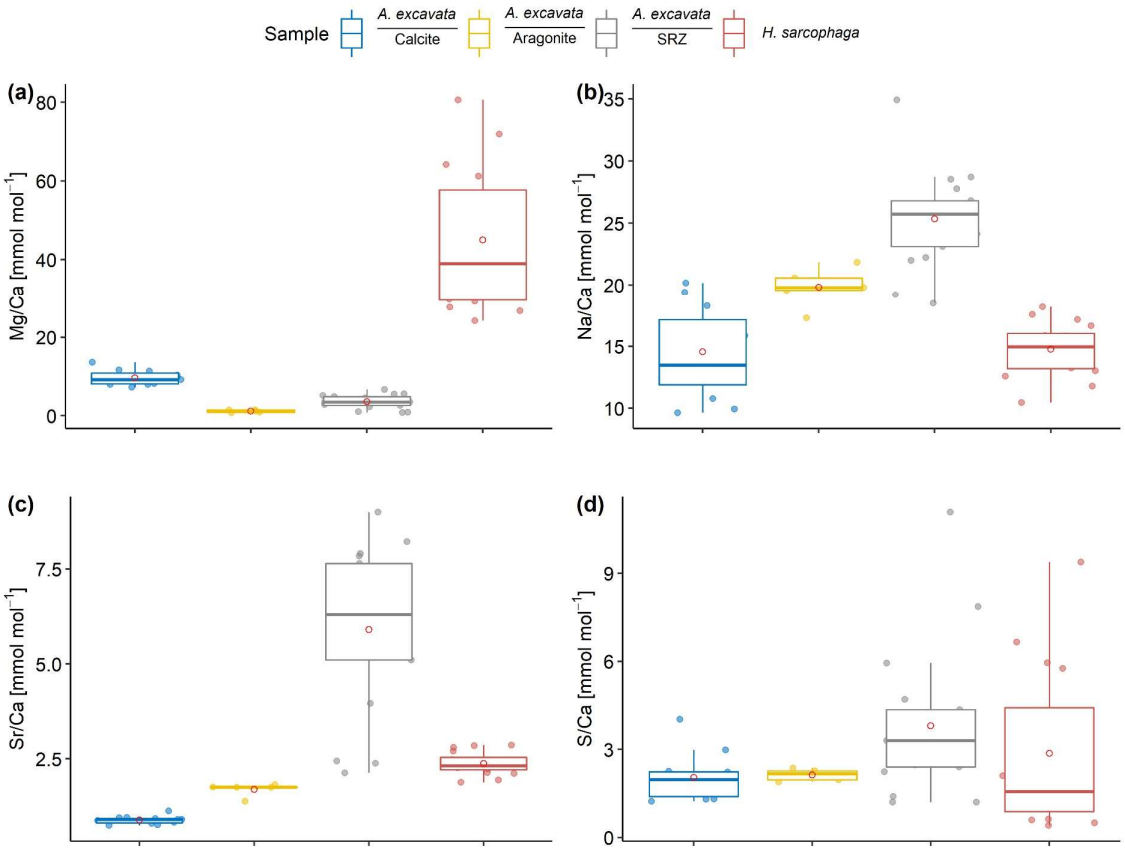

Figure 4-2 Results of point measurements by EPMA in different sections of *A. excavata* and *H. sarcophaga* (two specimens each). A: Mg/Ca, B: Na/Ca, C: Sr/Ca, D: S/Ca. Boxes display the interquartile range (IQR) and lines the median values. The whiskers show min and max values that are within the range of Q1-1.5*IQR - Q3 + 1.5*IQR. Red circles show the mean values. Sample size = 11, 5, 17, 16 (Calcite, Aragonite, SRZ, *H. Sarcophaga*). Text below the horizontal lines in the legend is the sampled area.

Table 4-1 Wilcoxon-Mann-Whitney test results of E/Ca comparison between the observed shell sections. Bold fields show significant differences between the two groups. *p*-values are Bonferroni adjusted.

Wilcoxon-Mann-Whitney Test			
	Group 1	**Group 2**	***p***
Mg/Ca	**Calcite**	**Aragonite**	**0.003**
	Calcite	**SRZ**	**<0.001**
	Calcite	***H. sarcophaga***	**<0.001**
	Aragonite	SRZ	0.051

	Aragonite	***H. sarcophaga***	**<0.001**
	SRZ	***H. sarcophaga***	**<0.001**
Na/Ca	Calcite	Aragonite	0.052
	Calcite	**SRZ**	**<0.001**
	Calcite	*H. sarcophaga*	1
	Aragonite	**SRZ**	**0.027**
	Aragonite	***H. sarcophaga***	**0.002**
	SRZ	***H. sarcophaga***	**<0.001**
Sr/Ca	**Calcite**	**Aragonite**	**0.003**
	Calcite	**SRZ**	**<0.001**
	Calcite	***H. sarcophaga***	**<0.001**
	Aragonite	**SRZ**	**<0.001**
	Aragonite	***H. sarcophaga***	**<0.001**
	SRZ	***H. sarcophaga***	**<0.001**
S/Ca	Calcite	Aragonite	1
	Calcite	SRZ	0.116
	Calcite	*H. sarcophaga*	1
	Aragonite	SRZ	0.286
	Aragonite	*H. sarcophaga*	1
	SRZ	*H. sarcophaga*	0.66

Within the bivalve shell Mg/Ca varies between 0.2 and 13.7 mmol mol^{-1} (Fig. 2). Lowest values were found in the aragonitic shell layer (Fig 1/E_3) and highest values are measured in the microgranular calcitic shell layer (Fig 1/E_2). The highest Mg/Ca ratios are measured in the foraminiferal calcite (mean = 45.0 ± 17.9 mmol mol^{-1}, max = 80.6 mmol mol^{-1}).

Na/Ca ratio are characterized by similar values in the different sections when considering the carbonate polymorph, that they are built of. The aragonitic sections (Fig 1/E_3), bivalve aragonite and SRZ, have mean Na/Ca ratios of 22.0 ± 2.3 mmol mol^{-1} (mean ± sd) and 25.3 ± 3.8 mmol mol^{-1} respectively. The SRZ displays a higher variability than the undisturbed aragonite. The microgranular calcite is characterised by a mean Na/Ca of 14.8 ± SD = 3.7 mmol mol^{-1} (Fig 1/E_2).

The SRZ is enriched in Sr/Ca compared to the undisturbed shell sections. Mean ratios are nearly four times higher than in the undisturbed aragonitic shell parts (5.9 ± 2.1 mmol mol^{-1} compared to 1.5 ± 0.2 mmol mol^{-1}). Lowest values are measured in the bivalve's microgranular calcite (mean = 0.9 ± 0.1 mmol mol^{-1}).

S/Ca ratios are comparable in the undisturbed bivalve aragonite and microgranular calcite, with 1.9 ± 0.3 mmol mol^{-1} and 2.1 mmol mol^{-1} ± 0.8 mmol mol^{-1}, respectively. Similar to Sr/Ca,

the highest mean and maximum S/Ca ratios are measured in the SRZ (mean = 3.8 ± 2.5 mmol mol^{-1}, max = 11.1 mmol mol^{-1}. However, all these differences are insignificant (Table 1).

4.4.4 Elemental composition of the SRZ

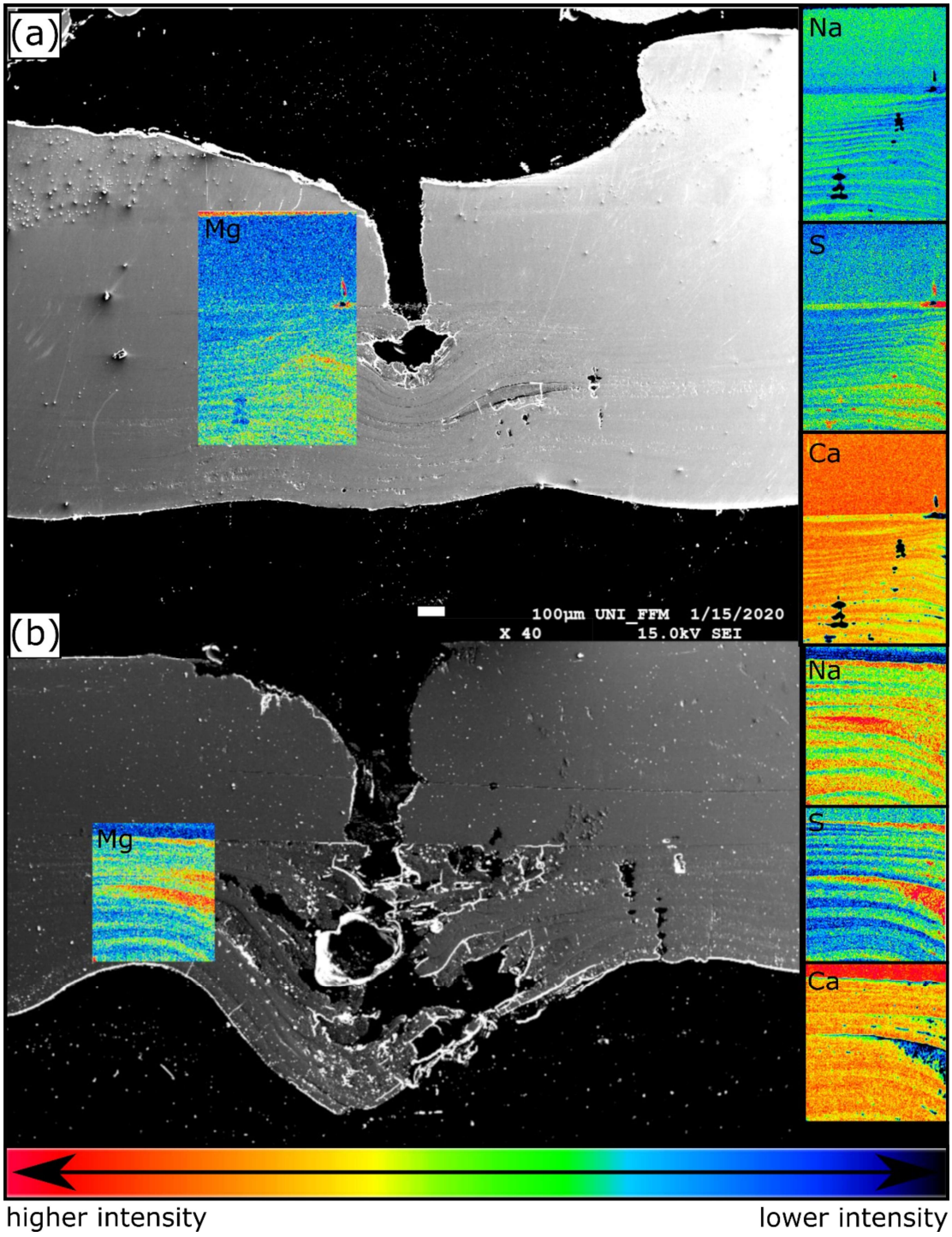

Figure 4-3 EPMA element maps and secondary-electron image from an SEM of the callus area of two specimen (A & B) of *A. excavata*. Intensity scale in counts per second (cps). Min-Max counts amount to: Mg (10-24 cps), Na (76-132 cps) Ca (7600-8650 cps), S (8.5-33)

As also visible in the fluorescence image (Fig. 1), the EPMA chemical maps show a layering pattern (Fig. 3). Highly fluorescent layers, that coincide with Mg and S maxima and Ca minima are variable in size ranging from 15 to 80 µm in thickness. Non-fluorescent layers that coincide with Mg and S minima and Ca maxima are more uniform in size, ranging from 12.5 to 30 µm in thickness. Mean composition of the fluorescent (fl) and non-fluorescent (nfl) layers, based on EPMA point measurements amount to: fl: Mg/Ca = 3.8 mmol mol^{-1} ± 1.7 mmol mol^{-1}, Sr/Ca = 7.4 mmol mol^{-1} ± 1.2 mmol mol^{-1}, Na/Ca = 24.4 mmol mol^{-1} ± 5.4 mmol mol^{-1}, S/Ca = 5.5 mmol mol^{-1} ± 2.7 mmol mol^{-1}; nfl: Mg/Ca = 3.2 mmol mol^{-1} ± 1.8 mmol mol^{-1}, Sr/Ca = 4.6 mmol mol^{-1} ± 1.9 mmol mol^{-1}, Na/Ca = 26.6 mmol mol^{-1} ± 1.3 mmol mol^{-1}, S/Ca = 2.3 mmol mol^{-1} ± 0.9 mmol mol^{-1}. Significant mean differences between fluorescent and non-fluorescent layers, based on Wilcoxon-Mann-Whitney test, are evident with regards to the S/Ca (p<0.001) and Sr/Ca ratios (p=0.006).

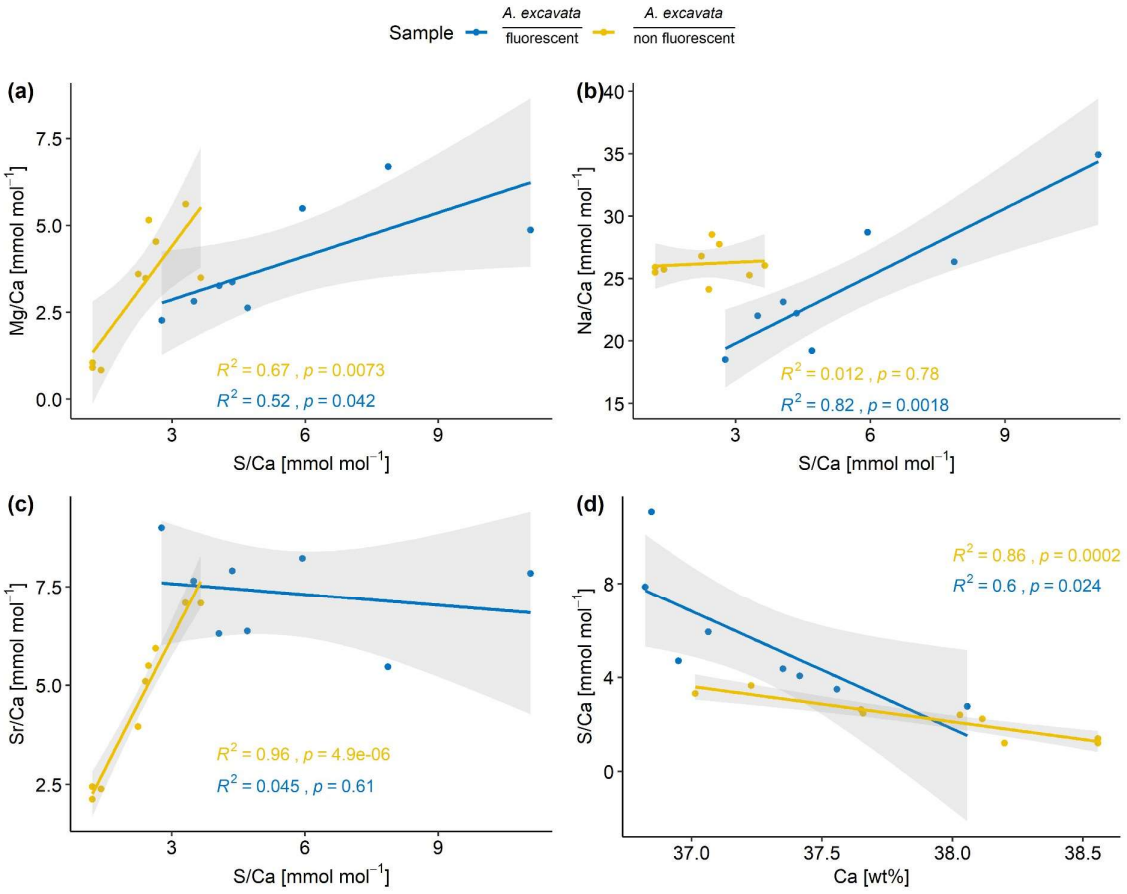

Figure 4-4 Elemental composition of the SRZ divided according to their fluorescence. Linear correlations are shown for both layers with 95% confidence intervals in gray. Correlations are calculated with a linear regression model with OLS.

Mg/Ca and S/Ca as well as Na/Ca and S/Ca display significant correlations in the fluorescent layers (Fig. 4). In the non-fluorescent shell layers, Mg/Ca and S/Ca, Sr/Ca and S/Ca are significantly correlated. In both layers, S/Ca ratios are inverse correlated with Ca wt% (Fig. 4).

4.4.5 Stable carbon and oxygen isotope

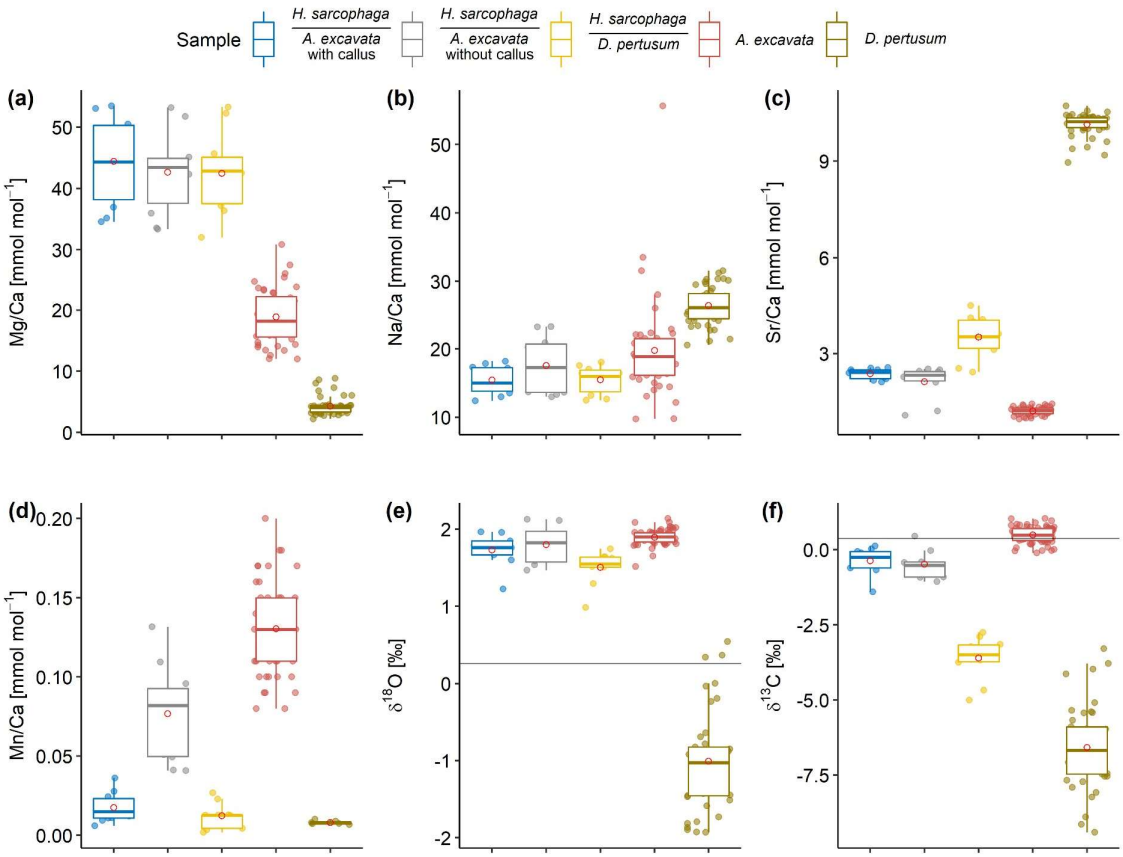

Figure 4-5 Box- and whisker plots displaying the E/Ca (ICP-OES and ICP-MS) and stable isotope analysis (MS) of the investigated specimens. Boxes display the interquartile range and lines the median values. The whiskers show min and max values that are within the range of Q1- 1.5*IQR - Q3 + 1.5*IQR. Red circles show mean values. Lines in E and F show the isotopic composition of the ambient seawater. Text below the horizontal lines in the legend is the host organism that *H. sarcophaga* grew on.

The different *H. sarcophaga* shells exhibit differences in their isotopic composition based on their host organism (Fig. 4 E/F). In particular, $\delta^{18}O$ values are similar in HL and HA with +1.51 ± 0.22 ‰ and +1.80 ± 0.25 ‰, respectively. These values are in accordance with $\delta^{18}O$ values from the host organism *A. excavata*, which range from +1.52 ‰ to +2.1 ‰. *D. pertusum* displays more depleted $\delta^{18}O$ and $\delta^{13C}C$ values, ranging from -1.93 ‰ to +0.54 ‰ and -9.41 ‰ to -3.30 ‰.

Larger differences between the different *H. sarcophaga* samples are observable in the carbon isotopic signature of specimens taken from different host organisms. HA display $\delta^{13}C$ values of -0.43 ± 0.47 ‰ which is close to the ratios of their host organism, being +0.49 ± 0.28 ‰. HL are more depleted in heavy carbon isotopes with a measured value of -3.61 ± 0.71 ‰. For reference, the isotopic composition of the ambient seawater is $\delta^{18}O$ = +0.26 ‰ and $\delta^{13}C$ = +0.38 ‰.

The isotopic composition of HAW and HAO can be described by linear functions whereas the isotopic composition in HL cannot:

$\delta^{13}C_{HAW} = 1.8\pm0.4 * \delta^{18}O - 3.4\pm0.8$ ($r^2 = 0.7$, p=0.004, df = 7)

Equation 4-10 Oxygen and carbon isotopic composition of HAW samples described as linear function

$\delta^{13}C_{HAO} = 1.1\pm0.3 * \delta^{18}O - 2.6\pm0.6$ ($r^2 = 0.6$, p=0.02, df = 6)

Equation 4-11 Oxygen and carbon isotopic composition of HAO samples described as linear function

$\delta^{13}C_{HL} = 1.7\pm1.0 * \delta^{18}O - 6.2\pm1.5$ ($r^2 = 0.18$, p=0.12, df = 8)

Equation 4-12 Oxygen and carbon isotopic composition of HL samples described as linear function

4.4.6 ICP-OES results from *H. sarcophaga* grown on different host organisms

H. sarcophaga samples from different host organisms are similar in their chemical composition with regard to Mg/Ca and Na/Ca (Fig. 5 A/B). Mean Mg/Ca ratios range from 42.7 ± 6.8 to 44.4 ± 7.2 mmol mol^{-1}. Both host organisms have lower mean Mg/Ca ratios of 4.3 ± 1.5 mmol $mol^{-1}$and 18.9 ± 4.5 mmol mol^{-1} in *D. pertusum* and *A. excavata*, respectively.

Mean Na/Ca ratios range between 15.4 ± 2.1 to 17.6 ± 4.3 mmol mol^{-1} for *H. sarcophaga*. The highest Na/Ca ratios and variations are measured in HAO. *D. pertusum* displays overall higher Na/Ca ratios than *H. sarcophaga* (26.3 ± 2.8 mmol mol^{-1}). The highest variation is measured in *A. excavata* ranging from 9.8 to 55.6 mmol $mol^{-1}$with a mean of 19.8 ± 7.3 mmol mol^{-1}.

A clear difference in Sr/Ca of 1.1 ± 0.16 mmol mol^{-1} is evident between *H. sarcophaga* from the different host organisms (Fig. 5 C). HAW and HAO show mean Sr/Ca ratios of 2.4 ± 0.2 and 2.1 ± 0.5 mmol mol^{-1}, respectively. The host organism *A. excavata* has lower Sr/Ca ratios (1.2 ± 0.1 mmol mol^{-1}). On the contrary, HL and *D. pertusum*, display higher mean Sr/Ca ratios of 3.5 ± 0.7 and 10.13 ± 0.3 mmol mol^{-1} respectively.

Prominent differences between *H. sarcophaga* groups are also evident in their Mn/Ca ratios (Fig. 5 D). HAW, HL and *D. pertusum* display Mn/Ca ratios of 0.017 ± 0.01 mmol mol^{-1}, 0.012

± 0.008 mmol mol^{-1} and 0.008 ± 0.001 mmol mol^{-1}, whereas HAO and *A. excavata* show higher Mn/Ca ratios of 0.077 ± 0.03 mmol mol^{-1} and 0.13 ± 0.03 mmol mol^{-1}, respectively.

4.4.7 Compositional differences in *H. sarcophaga* related to their host organism

Table 4-2 Results of the one-way ANOVA and Kruskal-Wallis analysis with the host organism as predictor variable. Bold fields show elemental and isotopic ratios in *H. sarcophaga* that may be significantly influenced by the chemistry of the host organism. *p*-values are Bonferroni adjusted.

ANOVA						
	Mg/Ca	Na/Ca	**Sr/Ca**	**Mn/Ca**	**$\delta^{18}O$**	**$\delta^{13}C$**
DFn	2					
DFd	25					
F	0.2	0.22	23	32	4.1	97
p	0.82	0.8	**<0.001**	**<0.001**	**0.029**	**<0.001**
Generalized eta squared	0.015	0.018	0.65	0.74	0.26	0.89
Kruskal-Wallis test						
n	28					
df	2					
p	0.83	0.92	**<0.001**	**<0.001**	**0.03**	**<0.001**

We conducted a one-way ANOVA and Kruskal-Wallis test (Table 2) in order to explore if the investigated *H. sarcophaga* groups (HAW, HAO, HL) show significant differences in their geochemical composition related to their host organism. We used the measured elemental and isotopic composition as target variables and the host organisms (*A. excavata* with callus, *A. excavata* without callus, *D. pertusum*) as the factor variable. Tukey-HSD (Table 3) was used as post-hoc test to investigate group specific mean differences.

Table 4-3 Tukey-HSD test results. Bold fields show significant differences between the two groups. HAW = *H. sarcophaga* that infested *A. excavata* with callus formation, HAO 0 *H. sarcophaga* that infested *A. excavata* without callus formation, HL = *H. sarcophaga* that infested *D. pertusum*. *p*-values are Bonferroni adjusted.

Tukey-HSD test				
	Group 1	**Group 2**	**Difference**	***p***
Mg/Ca	HAW	HAO	-1.22	0.93
	HAW	HL	-1.95	0.81
	HAO	HL	-0.73	0.97
Na/Ca	HAW	HAO	0.74	0.81
	HAW	HL	0.05	0.99
	HAO	HL	-0.68	0.84
Sr/Ca	HAW	HAO	-0.004	1
	HAW	**HL**	**1.14**	**<0.001**
	HAO	**HL**	**1.14**	**<0.001**
Mn/Ca	**HAW**	**HAO**	**0.05**	**<0.001**
	HAW	HL	-0.005	0.75
	HAO	**HL**	**-0.05**	**<0.001**

	HAW	HAO	0.07	0.81
$\delta^{18}O$	HAW	HL	-0.23	0.11
	HAO	**HL**	**-0.30**	**0.032**
	HAW	HAO	-0.11	0.91
$\delta^{13}C$	**HAW**	**HL**	**-3.24**	**<0.001**
	HAO	**HL**	**-3.12**	**<0.001**

The one-way ANOVA reveals no significant difference in the Mg/Ca and Na/Ca ratios of the foraminifera that were collected from the different host organisms (Table 2). In contrast, the ANOVA suggests a significant difference between Sr/Ca and Mn/Ca ratios between these two groups. In the case of Sr/Ca, significant differences based on the Tukey-HSD post-hoc test are observable between HL and HA, whereas we find no significant differences between HAW and HAO. In addition, we observe no significant differences between HAW and HL in their Mn/Ca composition, but significant differences are present between both these groups and HAO.

In the case of the stable oxygen isotope composition, we observe significant differences between *H. sarcophaga* specimens from different host organisms. The $\delta^{18}O$ measured in HL is significantly lower than in HAO. Significant differences are also observable for $\delta^{13}C$ ratios. Here, differences in the isotopic composition are detectable between HL and HA, with the latter showing higher $\delta^{13}C$ ratio.

The Kruskal-Wallis test, which was used as a non-parametric cross validation for the ANOVA test, shows the same results as the ANOVA test

4.5 Discussion

4.5.1 Mechanisms of etching and boring

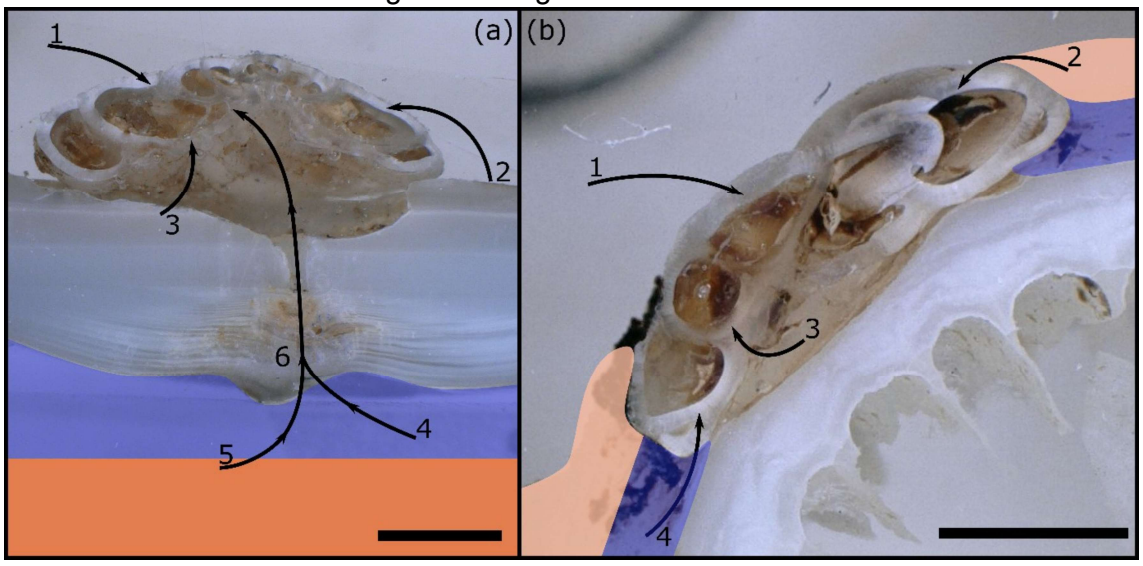

Figure 4-6 Possible pathways of E/Ca and isotopic signals into the foraminiferal calcite. A: *H. sarcophaga* on *A. excavata*, B: *H. sarcophaga* on *D. pertusum.* Blue areas represent the calcifying space, orange areas represent mantle tissue in *A. excavata* (A) and organic layer (coenosarc/mucus) in *D. pertusum* (B). Uptake of seawater and free-floating particles (1), Ingestion of host organic material (periostracum, coral tissue/mucus) (2), Ingestion of dissolved carbonate material (3), Ingestion of extracellular calcifying fluid (ECF)

(4), Ingestion of Mantle tissue (5), ingestion of carbonate and organic material from the deposited callus (6). Scalebar is 100 µm. Please note that the calcifying space and organic layers are displayed enlarged for improved visibility. Actual size of the calcifying space amounts to 1-100 nm (Nakahara, 1991; Tambutté et al., 2007b). The organic layer (coenosarc) is ~ 25 µm in thickness (Tambutté et al., 2007b).

The boring and etching of *H. sarcophaga* in *A. excavata* and *D. pertusum* can serve multiple purposes. The attachment etchings of foraminifera have been proposed to serve as an anchoring function and increase protection from predators and the hydrodynamic regime. Possibly, the foraminifera also dissolve the host's carbonate material to satisfy the calcium and/or DIC requirements of *H. sarcophaga* for the calcification of its shell (Cedhagen, 1994; Vénec-Peyré, 1996; Todd, 1965), rather than expending further energy to source Ca/DIC from the surrounding seawater (Fig 6A).

The boring in *A. excavata* is presumably produced to access the softbody of the bivalve, indicated by the mantle damage in the vicinity of the boring (Cedhagen, 1994). Additionally, the foraminifera may benefit from ingesting the ECF of the bivalve, containing carbohaydrates, proteins, glycoproteins and amino acids therefore constituting a valuable nutrient source (Yin et al., 2005). The ECF is also enriched in Ca and CO_2 compared to the ambient seawater, maybe providing additional ions for the calcification of *H. sarcophaga* (Crenshaw, 1972). Feeding on mantle fluids of bivalves by parasitic foraminifera is also supported by tracer experiments on C*. refulgens* (Alexander and Delaca, 1987). With *D. pertusum* as host, the foraminifera can access the coenosarc and underlying calcifying space of the coral without having to bore through the carbonate skeleton (Fig. 6B).

H. sarcophaga probably uses chemical etching, as indicated by the xenoglyph surface texture of the trace that changes in correlation with the host's microstructure (Beuck et al., 2008; Todd, 1965) A possible mechanism was investigated in the non-symbiotic benthic foraminifera *Ammonia* sp., which uses H^+-ATPase to actively pump H^+-ions out of their protoplasm to facilitate calcification (Toyofuku et al., 2017). This proton-flux causes a pH decrease by up to 1.1 in a 100 µm wide zone around the foraminifera (Toyofuku et al., 2017). Similar effects are reported from excavating sponges. *Cliona varians* displays pH values as low as 5 in their filopodia during carbonate dissolution (Webb et al., 2019).

4.5.2 Sr/Ca differences in *H. sarcophaga* related to the host organism

We observe significant differences in the Sr/Ca and Mn/Ca composition between *H. sarcophaga* from different host organisms.

HL show significantly higher Sr/Ca ratios than HA. Given that this result is based on measurements from multiple individuals distributed across more than one host organism, we suggest that this is most likely a signal of the high Sr/Ca aragonite precipitated from *D. pertusum* that is imprinted into the test of *H. sarcophaga*. By chemically corroding the

attachment etching as well as by the penetrating boring and by taking up the resulting solutions, the foraminifera gains access to a pre-concentrated calcium carbonate solution from which it can precipitate its shell (Fig. 6). Naturally, the foraminifera would also reflect other characteristics of the host, such as the high Sr/Ca ratio from the aragonite of *D. pertusum* (Raddatz et al., 2013; Schleinkofer et al., 2019b). In agreement with the much lower Sr/Ca ratios in calcite and aragonite in *A. excavata* (Schleinkofer et al., 2021a) compared to the coralline aragonite, we do not observe such high Sr/Ca ratios in HA. Still, the observed Sr/Ca ratios in HA are higher by a factor of two than in the host organism. Since we do not observe differences between HAW and HAO, the Sr/Ca surplus cannot be derived from the ingestion of organic material from within the shell cavity. We hypothesis that a possible further control is likely provided through the mixture of dissolved host $CaCO_3$ material and ambient seawater from which the foraminifera calcify, which is explored in more detail in the next section.

4.5.3 Mixing model

In order to further investigate the observed results, we created a simple two-component model to explore how the trace-element chemistry of *H. sarcophaga* could change by delivery of ions to the calcification site that were derived from dissolution of the host organism. In this model we calculate changes of the foraminifera composition in dependence from an assumed calcification from a variable mixture of seawater and dissolved host carbonate material. We excluded the addition of the hosts calcifying fluid in the model because there is no data available for the chemical composition of the calcifying fluid of *D. pertusum* nor *A. excavata*, and because the model is intended only as an initial exploration of whether the geochemistry of *H. sarcophaga* can be explained by calcification from a mixture of seawater and dissolved host material. Furthermore, measurements of the chemical composition of the calcifying fluid of other bivalve species indicate that the composition is close to the composition of seawater (Wada and Fujinuki, 1976; Crenshaw, 1972).

The model calculates element/Ca ratios based on calcite precipitation from a fluid that is derived from a mix of seawater (transported to the calcification site, see e.g., (Erez, 2003)), and $CaCO_3$ dissolved from the host organism:

$$\frac{E}{Ca}_{Hyrrokkin} = \frac{E_{SW} + \frac{\frac{10^R}{M_{Carb}} * \frac{E}{Ca}_{Host}}{1000}}{Ca_{SW} + \frac{10^R}{M_{Carb}}} * D_E * 1000$$

Equation 4-13 Model to predict E/Ca ratios in *H. sarcophaga* based on a potential mixture between dissolved host material and seawater

Where E_{SW} = element concentration in seawater, E/Ca_{Host} = element/Ca in host carbonate [mmol mol^{-1}], Ca_{SW} = Calcium concentration in seawater (0.010 mol L^{-1}), D_E = Calcite-Water distribution coefficient, M_{Carb} = atomic mass of $CaCO_3$ (100.08 g mol^{-1}) and R = log mixing ratio between carbonate and seawater [g L^{-1}].

Table 4 Parameters used in the proposed model to explore the effects of carbonate and water uptake of *H. sarcophaga* on the shell chemistry. Host element/Ca ratios are derived from this study. D_E^1 & D_E^2 = Distribution coefficient

	Model parameters				
	E_{SW} [mol L^{-1}]	E/Ca_{Acesta} [mmol mol^{-1}]	$E/Ca_{Desmophyllum}$ [mmol mol^{-1}]	D_E^1	D_E^2
Mg	0.053	19	4.2	0.015 (Segev and Erez, 2006)	0.009 (Oomori et al., 1987)
Na	0.450	20	26	0.00028 (Evans et al., 2015)	0.0001 (Füger et al., 2019)
Sr	0.0001	1.2	10.1	0.16 (Raitzsch et al., 2010)	0.2 (Mucci and Morse, 1983; Evans et al., 2015)
Mn	$5*10^{-9}$	0.131	0.008	0.5 (van Dijk et al., 2020)	10 (Mucci, 1988)

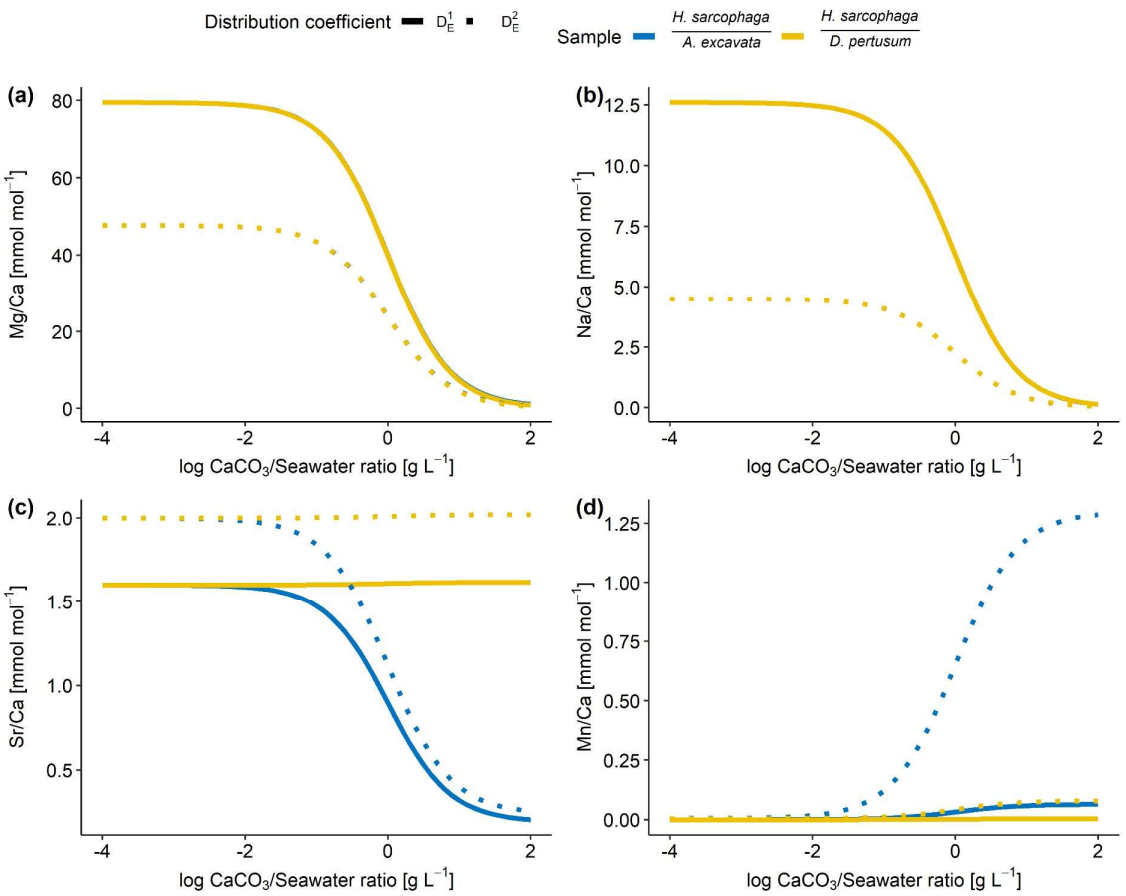

Figure 4-7 Results of model calculations with the parameters listed in Tab. 4 for the measured E/Ca ratios. Text below the horizontal lines in the legend is the host organism that *H. sarcophaga* grew on. Independently of the mixing ratio of dissolved host $CaCO_3$ and ambient water, no differences of the geochemical signature is predictable in Mg/Ca and Na/Ca. On the contrary, Sr/Ca and Mn/Ca ratios are predicted to diverge at mixing ratios > 0.01 g $CaCO_3$ L^{-1} seawater. Solid lines are produced with D_E^1 for the calculation and dotted lines are produced with D_E^2 for the calculation (see Tab. 4). In panel a and b, the different samples overlap each other.

As we have no information about the amount of dissolved material and water that is taken up by *H. sarcophaga*, we modelled it over six orders of magnitude (log dissolved $CaCO_3$/seawater ratios of -4 to +2). The parameters used are reported in Table 4.

Based on the model shown in Fig. 7, the Mg/Ca and Na/Ca ratios in *H. sarcophaga* are independent of the geochemical signature of the host it lived on, which is in agreement with our measurements. This is caused by the high concentration of these elements in the ambient seawater in comparison to the host's carbonate. The composition of the mixture is largely controlled by the addition of Ca, which is equal for both host organisms.

In contrast, the model predicts that, at high ratios of $CaCO_3$ derived from the host compared to the surrounding seawater, different Sr/Ca and Mn/Ca ratios should be observed between foraminifera living on different host organisms. The modelled Sr/Ca ratios for HL are constant at 2.0 mmol mol^{-1} independent from the mixing ratio (Fig. 7C). When the foraminifera dissolves aragonitic material of *D. pertusum* and this material is mixed with seawater, the resulting Sr/Ca ratios in this solution do not change due to the aragonitic D_{Sr} being close to 1. Consequently, if the shell Sr/Ca ratio in *H. sarcophaga* depends on calcite D_{Sr} and the Sr/Ca ratio in the calcifying fluid of *H. sarcophaga*, the resulting Sr/Ca ratio in HL is equivalent to a specimen that calcifies solely from seawater (specimen without a host). As the calcitic D_{Sr} is below 1 (Raitzsch et al., 2010; Mucci and Morse, 1983a; Evans et al., 2015), the addition of dissolved material from *A. excavata* in the calcifying space results in decreasing Sr/Ca ratios in the calcifying fluid and lower Sr/Ca ratios in the precipitated calcite of the foraminifera. Similar results are obtained in the case of Mn/Ca ratios. The addition of dissolved host material to the calcifying space of *H. sarcophaga* results in an increase of the Mn/Ca ratio in the calcifying fluid, which leads to increasing Mn/Ca ratios in the foraminiferal calcite.

The proposed model can help us understand why we do not see changes in the Mg/Ca and Na/Ca composition of H. sarcophaga from different host organisms and why Sr/Ca and Mn/Ca ratios differ between these groups (Fig. 2). Nonetheless, other processes are clearly required to explain the details of trace element uptake in *H. sarcophaga*. Sr/Ca ratios in HL, for instance, can only be modelled up to 2 mmol mol^{-1}, whereas we measure a mean of 3.5 mmol mol^{-1}. The results of this model are largely driven by the distribution coefficients used, however, the distribution coefficients used in this model are not empirically determined on *H. sarcophaga* but derive from other foraminifera species (D_E^1) or inorganic precipitation experiments (D_E^2). The model does also not account for growth-rate driven differences in

trace element portioning, while this is especially relevant in the case of Na and Mn (Mucci, 1988; Füger et al., 2019). In addition, we have to consider lattice strain-effects that increase the distribution coefficient for other elements such as Sr and Na, as *H. sarcophaga* has relatively high concentrations of Mg (Evans et al., 2015; Mucci and Morse, 1983a).

As discussed above, this is a simplified model that uses seawater and dissolved carbonate as endmembers. An additional possibility is that the foraminifera pumps or channels ions into and out of the calcifying fluid. In particular, it has been suggested foraminifera are able to transport Mg out of the calcifying space (Nehrke et al., 2013; Toyofuku et al., 2017; Bentov and Erez, 2006), but intermediate and high-Mg foraminifera such as *A. lessonii* appear to exert a lower degree of control over the composition of their calcifying fluid compared to low-Mg species (Evans et al., 2018b; Geerken et al., 2018). Assuming the calcifying fluid is depleted in Mg in comparison to seawater, the model would predict lower Mg/Ca ratios, although importantly, it would still not predict a difference in the Mg/Ca ratios of *H. sarcophaga* influenced by the host organism.

Another factor that should be considered is the transport pathway of the dissolved material into the foraminifera's calcifying fluid. The dissolution process of the host organism could modify the chemistry of the ambient seawater in a limited area around the foraminifera (Toyofuku et al., 2017), although this process is hard to imagine in an environment (cold-water coral reef) that relies on constant water movement to provide nutrients to the main inhabitants (Mienis et al., 2007). As such, we suggest it is more likely, that the dissolved material is transported through the cytoplasm to the calcification site (Spero, 1988; Erez, 2003), although further work is required to confirm this.

4.5.4 Mn/Ca differences in *H. sarcophaga* related to the host organism

Based on the ANOVA analysis (Table 2), significant differences are also observable in the Mn/Ca ratios. HAO display four times higher Mn/Ca ratios then in the other two observed groups. HL show similar Mn/Ca ratios as their host organism, both HAW and HAO show lower Mn/Ca ratios. Based on the differences we observe between the samples that were picked from *A. excavata*, it is unlikely that the Mn/Ca signal in *H. sarcophaga* derives from the host shell material (Fig. 6/A3 & B3). In this case we would expect to see differences between HA and HL as Mn/Ca in *A. excavata* is approximately one order of magnitude higher than in *D. pertusum*. Influences of the surrounding water cannot explain the observed differences either. Manganese, as a redox-sensitive element, is controlled by the oxygen concentration of the ambient water. Under well oxygenated conditions, the main species Mn^{2+} is oxidized to Mn-oxyhydroxides and precipitated (Calvert and Pedersen, 1996, 1993). Low-oxygen conditions lead to a reduction of Mn-oxyhydroxides to the bioavailable Mn^{2+} and a consequent increase of Mn/Ca ratios in biogenic carbonates (Tribovillard et al., 2006;

Groeneveld and Filipsson, 2013; Koho et al., 2015b). The Leksa Reef, however, is well oxygenated (Milzer et al., 2013; Jacobson, 1983).

An influence of the precipitation rate on Mn/Ca ratio was shown in inorganically precipitated calcite overgrowths and the planktic foraminifera *Orbulina universa* (Mucci, 1988; Lorens, 1981; Holland et al., 2017). Generally speaking, increased calcification rates cause Mn/Ca ratios in the precipitates to decrease (Mucci, 1988; Holland et al., 2017). In our investigated samples, this effect would imply lower calcification rates in HAO compared to HAW and HL. The possibility of HAO having low calcification rates is likely, as it is missing a valuable nutrient source (Fig. 6). Due to the high distribution coefficient of manganese, Rayleigh fractionation might add an additional control on Mn/Ca ratios in the foraminifera shell (Holland et al., 2017). The model of Rayleigh fractionation relies on a number of assumptions about the internal reservoir of the foraminifera regarding the size, initial composition, refreshment rate and calcification rate (Elderfield, 1996). As these parameters are not fully understood, both for *H. sarcophaga* and foraminifera in general, we cannot provide further information about the possible influence.

A significant influence of the potentially Mn-enriched bodily fluids of bivalves (Wada and Fujinuki, 1976) also cannot explain the differences in the chemical composition as the samples that discern from the others are picked from HAO. These foraminifera did not have access to the internal organic material of the bivalve (Fig. 6/A4). Instead, the high Mn signal in HAO must derive from a source that is located on the outside of the bivalve host (Fig. 6/A2). When the foraminifera initially infests the bivalve and starts boring into the shell, nutrient sources other than the internal organic parts of the bivalve have to be utilised by *H. sarcophaga.* The organic periostracum of the bivalve could depict this nutrient source as it is a highly nutritional source for organic material on the outside of the bivalve's shell (Secor et al., 1993). High concentrations of Mn and Fe were measured in the periostracum of freshwater and marine bivalves (Swinehart and Smith, 1979; Allen, 1960). The mechanistic explanation for this enrichment of Mn and Fe is reported to be the high amount of the amino acids containing glycine and tyrosin in the periostracum of bivalves (Piez, 1961; Whitney et al., 2019), which act as complexing sites for metal ions (Swinehart and Smith, 1979). The existence of living *H. sarcophaga* attached to rocks demonstrates that they do not necessarily rely on a living host but can also supply themselves through other feeding strategies (Cedhagen, 1994). Since algae take up Mn and concentrate it internally (Sunda and Huntsman, 1985), the increased Mn/Ca in HAO could also be caused by a facultative suspension feeding mode of *H. sarcophaga* during its juvenile stage.

At this point we can only speculate about the mechanistic explanation for the enrichment of Mn/Ca in HAO. Future research on *H. sarcophaga* should involve spatially resolved Mn and

Fe measurements, to explore if there is an ontogenetic decrease of Mn/Ca ratios in the test of *H. sarcophaga* picked from *A. excavata*. This decrease would mark the time of the first penetration of the bivalve shell.

4.5.5 Carbonate isotopic composition in *H. sarcophaga* based on the host organism

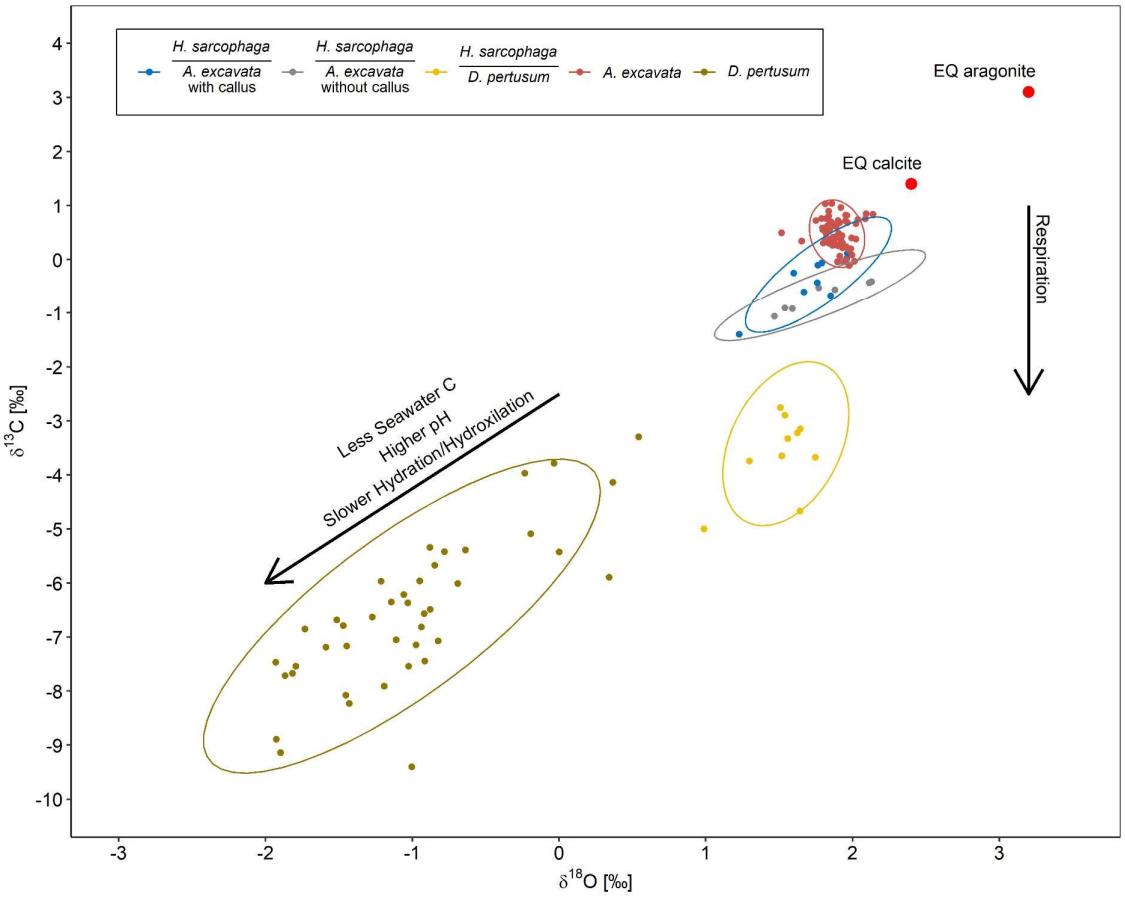

Figure 4-8 $\delta^{18}O$ plotted against $\delta^{13}C$ for *H. sarcophaga* from different host organisms and the host organisms *A. excavata* and *D. pertusum* with 95 % confidence ellipse. Arrows show compositional changes induced by kinetic effects and respiration. Text below the horizontal lines in the legend is the host organism that *H. sarcophaga* grew on. Red points show the equilibrium composition for calcite and aragonite as calculated from the isotopic composition of the ambient seawater.

The oxygen and carbon isotopic composition of the different organisms are characterised by large differences. *A. excavata* does not show signs of kinetic effects which would be indicated by a correlation of $\delta^{13}C$ and $\delta^{18}O$ values (McConnaughey, 2003; Adkins et al., 2003; Bajnai et al., 2018b). Bivalves are largely considered to calcify in equilibrium with the surrounding water (Immenhauser et al., 2016), which appears to be valid for *A. excavata* as it displays an isotopic composition close to the expected equilibrium (Fig. 8). The host organism *D. pertusum* displays higher departures from the expected aragonite equilibrium, which is mainly caused by additional incorporation of isotopically lighter, metabolic CO_2 and by kinetic isotope effects associated with hydration/hydroxylation reactions given that this

coral raises the calcification site pH to values significantly exceeding seawater pH (Chen et al., 2018; McCulloch et al., 2012a).

Interestingly, the *HA* samples display an isotopic composition very similar to the composition of its host organism (Fig. 8). The 95 % confidence ellipsoids of HAW, HAO and *A. excavata* all overlap at highest $\delta^{18}O$ values. However, in contrast to *A. excavata,* HAW and HAO display positive correlations between $\delta^{18}O$ and $\delta^{13}C$. This may indicate that all three organisms closely mineralize their carbon from the same source, but hydration/hydroxylation kinetics occur more pronounced in HAW and HAO relative to *A. excavata.*

The observable differences in the carbon isotopic composition between HA and HL can also be caused by different proportions of the carbon sources. HL presumably have constant access to the host's carbon pool, whereas the access of HA to the host's carbon pool is limited due to the defence mechanism of *A. excavata* (Fig. 3). When the bivalve has successfully closed the boring of the foraminifera, the foraminifera must use seawater DIC as a carbon source until it penetrates the shell again. This mixing of different carbon sources in HA in contrast to the stable carbon source of HL can explain the lower $\delta^{13}C$ values in HL due to an increased influence of host derived carbon.

HL is characterized by significantly more positive $\delta^{18}O$ values than its host, and is also characterized by a slightly steeper positive correlation between $\delta^{13}C$ and $\delta^{18}O$. Both circumstances point to faster hydration/hydroxylation kinetics to be effective during the mineralization of HL compared to its host (Chen et al., 2018). If the pH at which HA precipitates carbonate is lower than the pH of the calcifying fluid in *D. pertusum*, the hydration kinetics would be accelerated as a result (Raddatz et al., 2014b; Cohen, 2003; Crenshaw, 1972). Both organisms may derive their carbon from the same source which likely occurs depleted in ^{13}C relative to seawater, possibly due to significant admixture from metabolic CO_2. This assertion is supported by the fact that HL has constant access to the host's carbon pool.

Another mechanism potentially altering the $\delta^{13}C$ from equilibrium might be the etching mechanism that pumps H^+-ions in the ambient water around the foraminifera (Toyofuku et al., 2017). The decreasing pH around the foraminifera shifts the carbon speciation towards CO_2. As CO_2 is depleted in ^{13}C compared to the total inorganic carbon pool, the utilization of CO_2 for calcification would also explain the deviations of the foraminifera's shell $\delta^{13}C$ from isotopic equilibrium (Toyofuku et al., 2017; McCorkle et al., 1997).

4.5.6 Implications for paleoceanographic reconstructions

The results presented here have implications for paleoreconstructions in two ways. When using bivalves for paleo reconstructions or geochemical investigations in general, the shells

must be carefully examined for potential traces of bioerosion. In case of callus formation, the carbonate formed can have a significantly different composition than the original carbonate mineralogy.

Even more critical are the implications for paleoceanographic reconstructions using foraminifera which are regularly analyzed for this purpose. Several foraminifera species are known to live on different host organisms and act as parasites and/or bioeroders (Walker et al., 2017; Dupuy et al., 2010; Freiwald and Schönfeld, 1996). Some of these are also used for isotope and element based paleoenvironmental reconstructions or geochemical investigations in general, such as *Cibicides refulgens* (Mackensen and Nam, 2014; Rathburn and de Deckker, 1997; García-Gallardo et al., 2017), *Hanzawaia concentrica* (Smith and Emiliani, 1968) and *Discanomalia coronata* (Baranwal et al., 2014).

As an example, we use a $\delta^{18}O$-temperature conversion formula for benthic foraminifera (Marchitto et al., 2014) and our measured $\delta^{18}O$ ratios to reconstruct a temperature for the Leksa Reef of 7.5 °C using HAO and 7.8 °C using HAW with $\delta^{18}O_{SW}$ derived from seawater measurements. *In-situ* measurements of the water temperature in the Leksa Reef by CTD show a mean temperature of 7.8°C (min= 7.1°C, max=8.8°C) (Büscher, 2018). If we however use $\delta^{18}O$ ratios from HL we would reconstruct a water temperature of 8.8°C and consequently overestimate the water temperature by 1.0 °C

If the aforementioned species show similar host specific alterations of their isotopic and elemental composition, paleotemperature reconstructions on the basis of these species could be biased. Given that our results indicate that host specific isotopic and elemental composition changes can be present in the parasitic foraminifera *H. sarcophaga* we draw attention to other parasitic foraminifera that should be investigated for similar host-parasite relations, especially if they are used for geochemical investigations.

4.5.7 Chemical composition of *H. sarcophaga* compared to other benthic foraminifera

H. sarcophaga displays significantly higher Mg/Ca ratios than most other benthic foraminifera species with comparable ecology, that show Mg/Ca ratios between 0.5 and 10 mmol/mol (Lear et al., 2002). Foraminifera that have comparable Mg/Ca ratios to *H. sarcophaga* include *Amphistegina* (23- 77 mmol mol^{-1} (van Dijk et al., 2019; Raja et al., 2005; Geerken et al., 2018)), *Quinqueloculina* (50 – 135 mmol mol^{-1} (Gussone et al., 2016; Toyofuku et al., 2000)) and *Pyrgo* (4 – 85 mmol mol^{-1} (Gussone et al., 2016)) but these species are biologically and mineralogically distinct from *H. sarcophaga. Quinqueloculina* and *Pyrgo* are porcelaneous, whereas *H. sarcophaga* is hyaline. Furthermore, *H. sarcophaga* is not inhabited by photosymbionts in contrast to *Amphistegina*.

The exact processes involved in ion transportation, seawater vacuolization and pH-regulation utilized by *H. sarcophaga* remain to be discovered. High Mg/Ca ratios in *H. sarcophaga* that are similar to inorganic precipitated calcite (Oomori et al., 1987; Mucci and Morse, 1983a) may indicate a calcification mechanism without ways of discriminating against elements such as magnesium. These species rely on an increase of the calcification site pH (Erez, 2003; de Nooijer et al., 2009; Toyofuku et al., 2017) to facilitate calcification. The main control on calcite Mg/Ca ratios is then provided by the composition of the calcifying fluid (Raitzsch et al., 2010). The high Mg content would therefore indicate a calcifying space that is more similar to ambient seawater i.e. with no or minor modification via ion channels or pumps (de Nooijer et al., 2014; Bentov and Erez, 2006). Additionally, high Mg/Ca ratios in the calcifying space might be necessary for the stabilization of ACC, a suggested metastable calcite precursor phase in foraminifera and other calcifying organisms (Addadi et al., 2003; Jacob et al., 2011, 2017). High amounts of Mg in the calcite can also cause lattice strain effects, due to the size difference of Mg and Ca ions that causes lattice distortion(Evans et al., 2015; Mucci and Morse, 1983a). The lattice distortion can cause an increased incorporation of elements such as Sr and Na (Mucci and Morse, 1983a; Evans et al., 2015), a feature that we observe in our samples compared to the species *A. lessonii,* that has slightly lower Mg/Ca ratios than *H. sarcophaga* (35 vs. 45 mmol mol^{-1}) and consequently lower Na/Ca and Sr/Ca ratios (Geerken et al., 2018)

4.5.8 Biomineralization in the callus region

In order to protect itself from the parasitizing foraminifera, *A. excavata* seals the canal etched through the shell. This is accomplished by rapidly calcifying over the foraminifera boring (Beuck et al., 2008; Cedhagen, 1994). The calcification process produces a callus on the inside of the bivalve shell that is 3-5 mm in diameter and 1-2 mm in height. In the SRZ, evidence can be found for the biomineralization model for bivalves proposed by (Addadi et al., 2006; Checa et al., 2005; Wada and Fujinuki, 1976), i.e. that this process starts with the formation of an organic sheet indicated by the high fluorescence, high S concentration and low Ca concentration of this region, which then acts as a framework during calcification The following layer is depleted in S and enriched in Ca and therefore represents a higher Ca concentration (Fig. 3 & 4). This sequence is repeated multiple times leading to the formation of the visible callus. As long as the foraminifera does not stop the boring process, the bivalve needs to continually counter the boring process by calcifying in the region of infestation.

The callus displays high concentrations of organic material that are not observable in the undisturbed regions. The layers that are characterised by high organic contents appear to be preferentially dissolved (Fig. 3B) In cross sections, organic rich areas make up 50 % of the callus (Fig 1D). It appears unlikely that the high amounts of organic material in the SRZ are solely deposited as a calcification framework, considering the differences between

undisturbed shell areas and the SRZ. Therefore, the high amount of deposited organic material probably serves some other purpose, such as an increase of the overall material deposition rate and the provision of an initial sealant from the surrounding water.

The Boring organisms pose a threat to the bivalve in multiple ways. It has been shown that *H. sarcophaga* penetrated the mantle of *A. excavata* which led to a destruction of the mantle epithelium of the bivalve due to ingestion by *H. sarcophaga* (Cedhagen, 1994). Infested sections showed larger numbers of cell nuclei, indicating higher cell division rates and higher metabolic rates (Cedhagen, 1994). The pathway through the bivalve shell furthermore allows pathogens to reach and attack the bivalve and could allow surrounding water to permeate into the extra pallial fluid (EPF) of the bivalve. Even though the EPF in several bivalve species shows trace element concentrations close to seawater (Wada and Fujinuki, 1976; Crenshaw, 1972), the bivalve still has to actively concentrate Ca in the calcifying space to reach concentrations that exceed the solubility product (Wilbur and Saleuddin, 1983; Wheeler, 2020). This concentration of Ca is accomplished through active pumping by means of enzymes such as Ca-ATPase (Klein et al., 1996) or through ion channels (Carré et al., 2006). In case of an unsealed calcifying space, the dilution with seawater makes high concentrations of Ca-ions to levels needed for calcification in the extra EPF less likely. A fast-sealing method, by means of organic deposition, is therefore necessary to ensure that the bivalve's calcification capability is not compromised.

Geochemically, the SRZ shows the largest differences to the undisturbed aragonite in Mg/Ca and Sr/Ca ratios (Fig 2 & 3). Mg/Ca ratios are five times higher in the SRZ than in undisturbed aragonite. Magnesium is thought to be enriched in organic matrices secreted by the bivalve compared to the shell $CaCO_3$ (Schöne et al., 2010). The distribution of magnesium in the SRZ, especially its enrichment in fluorescent layers rich in sulfur (Fig. 1,3 and 4), makes an enrichment of Mg due to high organic concentrations likely. Beside an enrichment of Mg in the secreted organic matter, peptides similar to that found at the site of calcification in bivalves (Moradian-Oldak et al., 1990) can increase the Mg concentration in precipitated calcite by reducing the dehydration enthalpy (Stephenson et al., 2008). These peptides are also regularly found in molluscs (Marin et al., 2007; Falini et al., 1996; Halloran and Donachy, 1995; Zhang and Zhang, 2006). As these peptides do furthermore increase the growth rate by 25 % to 50 % (Stephenson et al., 2008), due to the need of fast calcification (Beuck et al., 2008), it may suggest that a high concentration of peptides in the SRZ is likely. Higher growth rates can additionally lead to an increase of crystal impurities which could alter other elements besides Mg (Lorens, 1981c).

In contrast to Mg, Sr was not found to be enriched in organic matter compared to shell $CaCO_3$ (Takesue et al., 2008), and therefore the presence of organics cannot explain the

observed high Sr/Ca of the aragonite in the SRZ. Yet, there is evidence for the influence of peptides on the incorporation of other elements such as Sr (Stephenson et al., 2008). Sr incorporation in the aragonitic bivalves is considered to be controlled in-part by growth rate effects (Lorrain et al., 2005; Füllenbach et al., 2017; Takesue et al., 2008; Carré et al., 2006). A calcification rate control on Sr incorporation is also supported from abiogenic calcite (Gabitov et al., 2014) but not from abiogenic aragonite (Gabitov et al., 2006). Accordingly, this growth rate effect is probably of biologic nature in aragonite precipitates.

Sr likely arrives into the calcifying space via similar pathways as Ca, as was shown by the effects of calcium channel blockers in corals (Ferrier-Pagès et al., 2002). However, Ca-ATPase has a higher affinity for Ca than Sr (Yu and Inesi, 1995). Therefore, a higher Ca-ATPase activity, as a result of increased growth rates, should lead to decreasing Sr/Ca ratios in the precipitates, which was shown in corals (Ferrier-Pagès et al., 2002; de Villiers et al., 1995). As we expect high growth rates in the SRZ, Ca channels that also transport Sr cannot explain the observed Sr distribution in this zone. Alternatively, the organism's metabolic rate has been suggested to control Sr/Ca in bivalves through metabolic pumping (Klein et al., 1996). High metabolic activity was observed in *A. excavata* infested by *H. sarcophaga,* indicated by a high concentration of cell-nuclei (Cedhagen, 1994). The model of Klein et al. (1996) would predict lower Sr/Ca ratios in these areas, thus a mechanism other than metabolic pumping must control the high Sr/Ca ratios in the SRZ.

Füllenbach et al. (2015) proposed that in slow growing areas of bivalves, the organisms exert less biological control over element incorporation, leading to elevated Sr/Ca ratios. While this hypothesis does not fit to our observation of elevated Sr/Ca ratios in a potentially fast-growing shell area, a similar hypothesis was suggested concerning Mg/Ca in *Mytilus edulis* (Lorens and Bender, 1980). The authors found strongly elevated Mg/Ca ratios in shells sections that were precipitated after handling the specimens for size measurements and attributed this effect to stress (Lorens and Bender, 1980). The boring of *H. sarcophaga* is very likely to be a stress factor on *A. excavata*. An influence of such stress related effects on Mg/Ca and potentially Sr/Ca (Fig. 4) are, therefore, possible. The high Mg- concentrations in the EPF due to a potential breakdown of Mg-regulating mechanisms however, would inhibit the organism from calcification due to the inhibiting effects of Mg on crystal nucleation and growth (Pytkowicz, 1965; Lorens and Bender, 1980). *A. excavata* might circumvent this by releasing additional sulphate bearing organic molecules that provide additional nucleation sites and higher Ca- concentrations at the nucleation sites (Lorens and Bender, 1980), which might potentially be the cause of the observed increased S/Ca ratios in the SRZ (Fig. 4).

4.6 Conclusion

Our results demonstrate that the elemental and isotopic composition of the parasitic foraminifera *H. sarcophaga* varies depending on the host organisms that the foraminifera settle on. *H. sarcophaga* that lived on the coral *D. pertusum* shows significantly higher Sr/Ca ratios than those that lived on the bivalve *A. excavata*. Combining these data with a simple mixing model, we propose that this could point towards a biomineralization pathway that is influenced by uptake of carbonate material derived from the host. The dissolution of the host shell could serve to satisfy the foraminifera's demand for calcium and DIC.

We also observe significant differences between *H. sarcophaga* specimens that grew on *A. excavata* that can be correlated to the success of the penetration progress. Foraminifera that fully penetrated the bivalve's shell, recognizable by the hosts callus formation, display significantly lower Mn/Ca ratios than foraminifera that did not completely penetrate the shell. This could be an effect of a suspension feeding period of the foraminifera or grazing of Mn-rich material of the periostracum until it penetrated the bivalve's shell when switching to a parasitic mode of feeding. Other possibilities include differences in the growth rate caused by changes of the nutrient availability or Rayleigh fractionation.

The oxygen and carbon isotopic composition of *H. sarcophaga* also appears to be influenced by the type of host organism that it infests. Again, this might be an effect of a direct uptake of the host's organic material and/or $CaCO_3$. Other effects such as different pH regimes in the host organisms and varying equilibration may also play a role. Different extents of the calcification site carbonate system equilibration between *H. sarcophaga* that infested *D. pertusum* (HL) and *H. sarcophaga* that infested *A. excavata* (HA) could also explain the missing signs of kinetic fractionation in HL compared to HA.

As the elemental and isotopic composition of some parasitic foraminifera is used for paleoceanographic reconstructions, our results indicate that such studies should only be performed when the host organism is known.

4.7 Author contribution

NS: Investigation**,** Conceptualization, Data curation, formal analysis, Investigation, Visualization, Writing (Original Draft)

DE: Methodology, Formal Analysis, Writing (Review & Editing)

MW: Resources**,** Writing (Review & Editing)

JVB: Resources, Writing (Review & Editing)

JF: Investigation, Resources, Writing (Review & Editing)

AF: Resources, Writing (Review & Editing)

SH: Investigation, Writing (Review & Editing)

HM: Investigation, Resources, Writing (Review & Editing)

SV: Supervision, Resources, Writing (Review & Editing)

JR: Funding Acquisition, Investigation, Project administration, Supervision, Resources, Writing (Review & Editing)

4.8 Acknowledgments

We are grateful to all cruise captains, crew members and cruise participants of research cruises POS473 and POS525. We are also grateful for the help of Celestine Beyer and Luciano Zolezzi, who aided with the EPMA measurements. We also want to thank Lennart de Nooijer and Inge van Dijk, whose detailed comments substantially improved our manuscript. This work was funded by the Deutsche Forschungsgemeinschaft, RA 2156-5/1 to JR. This is FIERCE contribution No. 75

4.9 Supplements

[1] Pictures of Meigen test

[2] Measurement data

[3] RAW and TIFF pictures of Fig.1

[4] R code for statistical investigation

4.10 Competing Interests

The authors declare that they have no conflict of interest.

4.11 References

Addadi, L., Raz, S., and Weiner, S.: Taking Advantage of Disorder: Amorphous Calcium Carbonate and Its Roles in Biomineralization, Advanced Materials, 15, 959–970, https://doi.org/10.1002/adma.200300381, 2003.

Addadi, L., Joester, D., Nudelman, F., and Weiner, S.: Mollusk Shell Formation: A Source of New Concepts for Understanding Biomineralization Processes, Chemistry - A European Journal, 12, 980–987, https://doi.org/10.1002/chem.200500980, 2006.

Addamo, A. M., Vertino, A., Stolarski, J., García-Jiménez, R., Taviani, M., and Machordom, A.: Merging scleractinian genera: The overwhelming genetic similarity between solitary Desmophyllum and colonial Lophelia, BMC Evolutionary Biology, 16, https://doi.org/10.1186/s12862-016-0654-8, 2016.

Adkins, J. F., Boyle, E. A., Curry, W. B., and Lutringer, A.: Stable isotopes in deep-sea corals and a new mechanism for “vital effects,” Geochimica et Cosmochimica Acta, 67, 1129–1143, https://doi.org/10.1016/S0016-7037(02)01203-6, 2003.

Alexander, S. P. and Delaca, T. E.: Feeding adaptations of the foraminiferan Cibicides refulgens living epizoically and parasitically on the Antarctic scallop Adamussium colbecki, Biological Bulletin, 173, 136–159, https://doi.org/10.2307/1541868, 1987.

Allen, J. A.: Manganese deposition on the shells of living molluscs, Nature, 185, 336–337, https://doi.org/10.1038/185336b0, 1960.

Bajnai, D., Fiebig, J., Tomašových, A., Milner Garcia, S., Rollion-Bard, C., Raddatz, J., Löffler, N., Primo-Ramos, C., and Brand, U.: Assessing kinetic fractionation in brachiopod calcite using clumped isotopes, Scientific Reports, 8, 533, https://doi.org/10.1038/s41598-017-17353-7, 2018.

Baranwal, S., Sauer, S., Knies, J., Chand, S., Jensen, H., and Klug, M.: Benthic foraminifera as tools in interpretation of subsurface hydrocarbon fluid flow at Veslemøy High and Hola-Vesterålen areas of the Barents Sea, Geophysical Research Abstracts, 2014-1843 pp., 2014.

Bentov, S. and Erez, J.: Impact of biomineralization processes on the Mg content of foraminiferal shells: A biological perspective, Geochemistry, Geophysics, Geosystems, 7, https://doi.org/10.1029/2005GC001015, 2006.

Beuck, L., López Correa, M., and Freiwald, A.: Biogeographical distribution of Hyrrokkin (Rosalinidae, Foraminifera) and its host-specific morphological and textural trace variability, Current Developments in Bioerosion, 329–360, https://doi.org/10.1007/978-3-540-77598-0-17, 2008.

Bonucci, E. and Wheeler, A. P.: Mechanisms of Molluscan Shell Formation, in: Calcification in Biological Systems, Plenum Press, 179–216, https://doi.org/10.1201/9781003068396-10, 2020.

Büscher, J.: Cold-water coral habitat characterisation and in situ physiological state analyses of four spatially distinct reefs in North- and mid-Norway-Cruise Report RV POSEIDON 525 [POS525], GEOMAR, Kiel, Germany, https://doi.org/10.3289/CR_POS525, 2018.

Calvert, S. E. and Pedersen, T. F.: Geochemistry of Recent oxic and anoxic marine sediments: Implications for the geological record, Marine Geology, https://doi.org/10.1016/0025-3227(93)90150-T, 1993.

Calvert, S. E. and Pedersen, T. F.: Sedimentary geochemistry of manganese: Implications for the environment of formation of manganiferous black shales, Economic Geology, https://doi.org/10.2113/gsecongeo.91.1.36, 1996.

Carré, M., Bentaleb, I., Bruguier, O., Ordinola, E., Barrett, N. T., and Fontugne, M.: Calcification rate influence on trace element concentrations in aragonitic bivalve shells: Evidences and mechanisms, Geochimica et Cosmochimica Acta, 70, 4906–4920, https://doi.org/10.1016/j.gca.2006.07.019, 2006.

Cedhagen, T.: Taxonomy and biology of hyrrokkin sarcophaga gen. Et Sp. N., a parasitic foraminiferan (rosalinidae), Sarsia, 79, 65–82, https://doi.org/10.1080/00364827.1994.10413549, 1994.

Checa, A. G., Rodríguez-Navarro, A. B., and Esteban-Delgado, F. J.: The nature and formation of calcitic columnar prismatic shell layers in pteriomorphian bivalves, Biomaterials, 26, 6404–6414, https://doi.org/10.1016/j.biomaterials.2005.04.016, 2005.

Chen, S., Gagnon, A. C., and Adkins, J. F.: Carbonic anhydrase, coral calcification and a new model of stable isotope vital effects, Geochimica et Cosmochimica Acta, 236, 179–197, https://doi.org/10.1016/j.gca.2018.02.032, 2018.

Cheng, Y. R. and Dai, C. F.: A bioeroding foraminifer, Hyrrokkin sarcophaga, on deepwater corals from the South China Sea, Coral Reefs, 35, 901, https://doi.org/10.1007/s00338-016-1447-7, 2016.

Cohen, A. L.: Geochemical Perspectives on Coral Mineralization, Reviews in Mineralogy and Geochemistry, 54, 151–187, https://doi.org/10.2113/0540151, 2003.

Crenshaw, M. A.: The inorganic composition of molluscan extrapallial fluid, The Biological Bulletin, 143, 506–512, https://doi.org/10.2307/1540180, 1972.

Culver, S. J.: Early Cambrian foraminifera from West Africa, Science, 254, 689–691, https://doi.org/10.1126/science.254.5032.689, 1991.

van Dijk, I., Mouret, A., Cotte, M., le Houedec, S., Oron, S., Reichart, G. J., Reyes-Herrera, J., Filipsson, H. L., and Barras, C.: Chemical Heterogeneity of Mg, Mn, Na, S, and Sr in Benthic Foraminiferal Calcite, Frontiers in Earth Science, 7, 281, https://doi.org/10.3389/feart.2019.00281, 2019.

van Dijk, I., de Nooijer, L. J., Barras, C., and Reichart, G. J.: Mn Incorporation in Large Benthic Foraminifera: Differences Between Species and the Impact of pCO2, Frontiers in Earth Science, https://doi.org/10.3389/feart.2020.567701, 2020.

Dupuy, C., Rossignol, L., Geslin, E., and Pascal, P. Y.: Predation of mudflat meio-macrofaunal metazoans by a calcareous foraminifer, Ammonia tepida (Cushman, 1926), Journal of Foraminiferal Research, 40, 305–312, https://doi.org/10.2113/gsjfr.40.4.305, 2010.

Elderfield, H.: A biomineralization model for the incorporation of trace elements into foraminiferal calcium carbonate, Earth and Planetary Science Letters, 142, 409–423, https://doi.org/10.1016/0012-821X(96)00105-7, 1996.

Erez, J.: The Source of Ions for Biomineralization in Foraminifera and Their Implications for Paleoceanographic Proxies, Reviews in Mineralogy and Geochemistry, 54, 115–149, https://doi.org/10.2113/0540115, 2003.

Evans, D., Erez, J., Oron, S., and Müller, W.: Mg/Ca-temperature and seawater-test chemistry relationships in the shallow-dwelling large benthic foraminifera Operculina ammonoides, Geochimica et Cosmochimica Acta, 148, 325–342, https://doi.org/10.1016/j.gca.2014.09.039, 2015.

Evans, D., Müller, W., and Erez, J.: Assessing foraminifera biomineralisation models through trace element data of cultures under variable seawater chemistry, Geochimica et Cosmochimica Acta, 236, 198–217, https://doi.org/10.1016/j.gca.2018.02.048, 2018.

Falini, G., Albeck, S., Weiner, S., and Addadi, L.: Control of Aragonite or Calcite Polymorphism by Mollusk Shell Macromolecules, Science, 271, 67–69, https://doi.org/10.1126/science.271.5245.67, 1996.

Ferrier-Pagès, C., Boisson, F., Allemand, D., and Tambutté, E.: Kinetics of strontium uptake in the scleractinian coral Stylophora pistillata, Marine Ecology Progress Series, 245, 93–100, https://doi.org/10.3354/meps245093, 2002.

Form, A. U., Büscher, J. v., Hissmann, K., Flögel, S., Wisshak, M., Rüggeberg, A., Bannister, R., Kutti, T., Stapp, L., Bennecke, S., Küter, M., Nachtigall, K., Schauer, J., and Fenske, M.: RV POSEIDON Cruise Report POS473 LORELEI II: LOphelia REef Lander Expedition and Investigation II, Tromsø – Bergen – Esbjerg, 15.08. – 31.08. – 04.09.2014., 25 pp., https://doi.org/10.3289/CR_POS_473, 2015.

Freiwald, A. and Schönfeld, J.: Substrate pitting and boring pattern of Hyrrokkin sarcophaga Cedhagen, 1994 (Foraminifera) in a modern deep-water coral reef mound, Marine Micropaleontology, 28, 199–207, 1996.

Füger, A., Konrad, F., Leis, A., Dietzel, M., and Mavromatis, V.: Effect of growth rate and pH on lithium incorporation in calcite, Geochimica et Cosmochimica Acta, 248, 14–24, https://doi.org/10.1016/j.gca.2018.12.040, 2019.

Füllenbach, C. S., Schöne, B. R., Shirai, K., Takahata, N., Ishida, A., and Sano, Y.: Minute co-variations of Sr/Ca ratios and microstructures in the aragonitic shell of Cerastoderma edule (Bivalvia) – Are geochemical variations at the ultra-scale masking potential environmental signals?, Geochimica et Cosmochimica Acta, 205, 256–271, https://doi.org/10.1016/j.gca.2017.02.019, 2017.

Gabitov, R. I., Cohen, A. L., Gaetani, G. A., Holcomb, M., and Watson, E. B.: The impact of crystal growth rate on element ratios in aragonite: An experimental approach to understanding vital effects, Geochimica et Cosmochimica Acta, 70, A187, https://doi.org/10.1016/j.gca.2006.06.377, 2006.

Gabitov, R. I., Sadekov, A., and Leinweber, A.: Crystal growth rate effect on Mg/Ca and Sr/Ca partitioning between calcite and fluid: An in situ approach, Chemical Geology, 367, 70–82, https://doi.org/10.1016/j.chemgeo.2013.12.019, 2014.

García-Gallardo, Á., Grunert, P., Voelker, A. H. L., Mendes, I., and Piller, W. E.: Re-evaluation of the “elevated epifauna” as indicator of Mediterranean Outflow Water in the Gulf of Cadiz using stable isotopes (δ13C, δ18O), Global and Planetary Change, 155, 78–97, https://doi.org/10.1016/j.gloplacha.2017.06.005, 2017.

Geerken, E., Jan De Nooijer, L., van DIjk, I., and Reichart, G. J.: Impact of salinity on element incorporation in two benthic foraminiferal species with contrasting magnesium contents, Biogeosciences, 15, 2205–2218, https://doi.org/10.5194/bg-15-2205-2018, 2018.

GEOMAR Helmholtz-Zentrum für Ozeanforschung: Research Vessel POSEIDON, Journal of large-scale research facilities JLSRF, 1, 60–63, https://doi.org/10.17815/jlsrf-1-62, 2015.

GEOMAR Helmholtz-Zentrum für Ozeanforschung: Manned submersible „JAGO“, Journal of large-scale research facilities JLSRF, 3, 1–12, https://doi.org/10.17815/jlsrf-3-157, 2017.

Goldstein, J. I., Newbury, D. E., Michael, J. R., Ritchie, N. W. M., Scott, J. H. J., and Joy, D. C.: Scanning Electron Microscopy and X-Ray Microanalysis, Springer New York, New York, NY, https://doi.org/10.1007/978-1-4939-6676-9, 2018.

Goldstein, S. T.: Foraminifera: A biological overview, in: Modern Foraminifera, https://doi.org/10.1007/0-306-48104-9_3, 1999.

Gray, W. R. and Evans, D.: Nonthermal Influences on Mg/Ca in Planktonic Foraminifera: A Review of Culture Studies and Application to the Last Glacial Maximum, Paleoceanography and Paleoclimatology, 34, 306–315, https://doi.org/10.1029/2018PA003517, 2019.

Greaves, M., Barker, S., Daunt, C., and Elderfield, H.: Accuracy, standardization, and interlaboratory calibration standards for foraminiferal Mg/Ca thermometry, Geochemistry, Geophysics, Geosystems, 6, 2–13, https://doi.org/10.1029/2004GC000790, 2005.

Greaves, M., Caillon, N., Rebaubier, H., Bartoli, G., Bohaty, S., Cacho, I., Clarke, L., Cooper, M., Daunt, C., Delaney, M., DeMenocal, P., Dutton, A., Eggins, S., Elderfield, H., Garbe-Schoenberg, D., Goddard, E., Green, D., Groeneveld, J., Hastings, D., Hathorne, E., Kimoto, K., Klinkhammer, G., Labeyrie, L., Lea, D. W., Marchitto, T., Martínez-Botí, M. A., Mortyn, P. G., Ni, Y., Nuernberg, D., Paradis, G., Quinn, T., Rosenthal, Y., Russel, A., Sagawa, T., Sosdian, S., Stott, L., Tachikawa, K., Tappa, E., Thunell, R., and Wilson, P. A.: Interlaboratory comparison study of calibration standards for foraminiferal Mg/Ca thermometry, Geochemistry, Geophysics, Geosystems, 9, 1–27, https://doi.org/10.1029/2008GC001974, 2008.

Groeneveld, J. and Filipsson, H. L.: Mg/Ca and Mn/Ca ratios in benthic foraminifera: the potential to reconstruct past variations in temperature and hypoxia in shelf regions, Biogeosciences, 10, 5125–5138, https://doi.org/10.5194/bg-10-5125-2013, 2013.

Gussone, N., Filipsson, H. L., and Kuhnert, H.: Mg/Ca, Sr/Ca and Ca isotope ratios in benthonic foraminifers related to test structure, mineralogy and environmental controls, Geochimica et Cosmochimica Acta, 173, 142–159, https://doi.org/10.1016/j.gca.2015.10.018, 2016.

Halloran, B. A. and Donachy, J. E.: Characterization of organic matrix macromolecules from the shells of the antarctic scallop, Adamussium colbecki, Comparative Biochemistry and Physiology -- Part B: Biochemistry and, 111, 221–231, https://doi.org/10.1016/0305-0491(94)00245-P, 1995.

Hancock, L. G., Walker, S. E., Pérez-Huerta, A., and Bowser, S. S.: Population Dynamics and Parasite Load of a Foraminifer on Its Antarctic Scallop Host with Their Carbonate Biomass Contributions, PLOS ONE, 10, e0132534, https://doi.org/10.1371/journal.pone.0132534, 2015.

Holland, K., Eggins, S. M., Hönisch, B., Haynes, L. L., and Branson, O.: Calcification rate and shell chemistry response of the planktic foraminifer Orbulina universa to changes in microenvironment seawater carbonate chemistry, Earth and Planetary Science Letters, 464, 124–134, https://doi.org/10.1016/j.epsl.2017.02.018, 2017.

Hönisch, B., Allen, K. A., Russell, A. D., Eggins, S. M., Bijma, J., Spero, H. J., Lea, D. W., and Yu, J.: Planktic foraminifers as recorders of seawater Ba/Ca, Marine Micropaleontology, 79, 52–57, https://doi.org/10.1016/j.marmicro.2011.01.003, 2011.

Horton, T., Kroh, A., Ahyong, S., Bailly, N., Boyko, C. B., Brandão, S. N., Gofas, S., Hooper, J. N. A., Hernandez, F., Holovachov, O., Mees, J., Molodtsova, T. N., Paulay, G., Decock, W., Dekeyzer, S., Poffyn, G., Vandepitte, L., Vanhoorne, B., Adlard, R., Agatha, S., Ahn, K. J., Akkari, N., Alvarez, B., Anderberg, A., Anderson, G., Angel, M. v, Antic, D., Arango, C., Artois, T., Atkinson, S., Auffenberg, K., Baldwin, B. G., Bank, R., Barber, A., Barbosa, J. P., Bartsch, I., Bellan-Santini, D., Bergh, N., Bernot, J., Berta, A., Bezerra, T. N., Bieler, R., Blanco, S., Blasco-Costa, I., Blazewicz, M., Bock, P., Bonifacino de León, M., Böttger-Schnack, R., Bouchet, P., Boury-Esnault, N., Boxshall, G., Bray, R., Bruce, N. L., Cairns, S., Calvo Casas, J., Carballo, J. L., Cárdenas, P., Carstens, E., Chan, B. K., Chan, T. Y., Cheng, L., Christenhusz, M., Churchill, M., Coleman, C. O., Collins, A. G., Collins, G. E., Corbari, L., Cordeiro, R., Cornils, A., Coste, M., Costello, M. J., Crandall, K. A., Cremonte, F., Cribb, T., Cutmore, S., Dahdouh-Guebas, F., Daly, M., Daneliya, M., Dauvin, J. C., Davie, P., de Broyer, C., de Grave, S., de Mazancourt, V., de Voogd, N. J., Decker, P., Defaye, D., d'Hondt, J. L., Dippenaar, S., Dohrmann, M., Dolan, J., Domning, D., Downey, R., Ector, L., Eisendle-Flöckner, U., Eitel, M., Encarnação, S. C. d., Enghoff, H., Epler, J., Ewers-Saucedo, C., et al.: World Register of Marine Species (WoRMS), http://www.marinespecies.org, 2021.

Immenhauser, A., Schöne, B. R., Hoffmann, R., and Niedermayr, A.: Mollusc and brachiopod skeletal hard parts: Intricate archives of their marine environment, Sedimentology, 63, 1–59, https://doi.org/10.1111/sed.12231, 2016.

Jacob, D. E., Wirth, R., Soldati, A. L., Wehrmeister, U., and Schreiber, A.: Amorphous calcium carbonate in the shells of adult Unionoida, Journal of Structural Biology, 173, 241–249, https://doi.org/10.1016/j.jsb.2010.09.011, 2011.

Jacob, D. E., Wirth, R., Agbaje, O. B. A., Branson, O., and Eggins, S. M.: Planktic foraminifera form their shells via metastable carbonate phases, Nature Communications, 8, 1–8, https://doi.org/10.1038/s41467-017-00955-0, 2017.

Jacobson, P.: Physical Oceanography of the Trondheimsfjord, Geophysical & Astrophysical Fluid Dynamics, 26, 3–26, https://doi.org/10.1080/03091928308221761, 1983.

Jochum, K. P., Nohl, U., Herwig, K., Lammel, E., Stoll, B., and Hofmann, A. W.: GeoReM: A New Geochemical Database for Reference Materials and Isotopic Standards, Geostandards and Geoanalytical Research, 29, 333–338, https://doi.org/10.1111/j.1751-908X.2005.tb00904.x, 2005.

Kato, K., Wada, H., and Fujioka, K.: The application of chemical staining to separate calcite and aragonite minerals for micro-scale isotopic analyses, Geochemical Journal, 37, 291–297, https://doi.org/10.2343/geochemj.37.291, 2003.

Klein, R. T., Lohmann, K. C., and Thayer, C. W.: Sr/Ca and 13C/12C ratios in skeletal calcite of Mytilus trossulus: Covariation with metabolic rate, salinity, and carbon isotopic composition of seawater, Geochimica et Cosmochimica Acta, https://doi.org/10.1016/S0016-7037(96)00232-3, 1996.

Koho, K. A., de Nooijer, L. J., and Reichart, G. J.: Combining benthic foraminiferal ecology and shell Mn/Ca to deconvolve past bottom water oxygenation and paleoproductivity, Geochimica et Cosmochimica Acta, 165, 294–306, https://doi.org/10.1016/j.gca.2015.06.003, 2015.

Lantz, B.: The impact of sample non-normality on ANOVA and alternative methods, British Journal of Mathematical and Statistical Psychology, 66, 224–244, https://doi.org/10.1111/j.2044-8317.2012.02047.x, 2013.

Lear, C. H. and Rosenthal, Y.: Benthic foraminiferal Li/Ca: Insights into Cenozoic seawater carbonate saturation state, Geology, 34, 985, https://doi.org/10.1130/G22792A.1, 2006.

Lear, C. H., Rosenthal, Y., and Slowey, N.: Benthic foraminiferal Mg/Ca-paleothermometry: A revised core-top calibration, Geochimica et Cosmochimica Acta, 66, 3375–3387, https://doi.org/10.1016/S0016-7037(02)00941-9, 2002.

Lorens, R. B.: Sr, Cd, Mn and Co distribution coefficients in calcite as a function of calcite precipitation rate, Geochimica et Cosmochimica Acta, 45, 553–561, https://doi.org/10.1016/0016-7037(81)90188-5, 1981.

Lorens, R. B. and Bender, M. L.: The impact of solution chemistry on *Mytilus edulis* calcite and aragonite, Geochimica et Cosmochimica Acta, 44, 1265–1278, https://doi.org/10.1016/0016-7037(80)90087-3, 1980.

Lorrain, A., Gillikin, D. P., Paulet, Y. M., Chauvaud, L., le Mercier, A., Navez, J., and André, L.: Strong kinetic effects on Sr/Ca ratios in the calcitic bivalve Pecten maximus, Geology, 33, 965–968, https://doi.org/10.1130/G22048.1, 2005.

Mackensen, A. and Nam, S. il: Taxon-specific epibenthic foraminiferal δ18O in the Arctic Ocean: Relationship to water masses, deep circulation, and brine release, Marine Micropaleontology, 113, 34–43, https://doi.org/10.1016/j.marmicro.2014.09.002, 2014.

Marchitto, T. M., Curry, W. B., Lynch-Stieglitz, J., Bryan, S. P., Cobb, K. M., and Lund, D. C.: Improved oxygen isotope temperature calibrations for cosmopolitan benthic foraminifera, Geochimica et Cosmochimica Acta, 130, 1–11, https://doi.org/10.1016/j.gca.2013.12.034, 2014.

Marin, F., Luquet, G., Marie, B., and Medakovic, D.: Molluscan Shell Proteins: Primary Structure, Origin, and Evolution, Current Topics in Developmental Biology, 80, 209–276, https://doi.org/10.1016/S0070-2153(07)80006-8, 2007.

McConnaughey, T. A.: Sub-equilibrium oxygen-18 and carbon-13 levels in biological carbonates: Carbonate and kinetic models, Coral Reefs, 22, 316–327, https://doi.org/10.1007/s00338-003-0325-2, 2003.

McCorkle, D. C., Corliss, B. H., and Farnham, C. A.: Vertical distributions and stable isotopic compositions of live (stained) benthic foraminifera from the North Carolina and California continental margins, Deep-Sea Research Part I: Oceanographic Research Papers, 44, 983–1024, https://doi.org/10.1016/S0967-0637(97)00004-6, 1997.

McCulloch, M., Falter, J., Trotter, J., and Montagna, P.: Coral resilience to ocean acidification and global warming through pH up-regulation, Nature Climate Change, 2, 623–627, https://doi.org/10.1038/nclimate1473, 2012.

Mienis, F., de Stigter, H. C., White, M., Duineveld, G., de Haas, H., and van Weering, T. C. E.: Hydrodynamic controls on cold-water coral growth and carbonate-mound development at the SW and SE Rockall Trough Margin, NE Atlantic Ocean, Deep-Sea Research Part I: Oceanographic Research Papers, 54, 1655–1674, https://doi.org/10.1016/j.dsr.2007.05.013, 2007.

Milzer, G., Giraudeau, J., Faust, J., Knies, J., Eynaud, F., and Rühlemann, C.: Spatial distribution of benthic foraminiferal stable isotopes and dinocyst assemblages in surface sediments of the Trondheimsfjord, central Norway, Biogeosciences, 10, 4433–4448, https://doi.org/10.5194/bg-10-4433-2013, 2013.

Moradian-Oldak, J., Addadi, L., Weiner, S., and Berman, A.: Tuning of Crystal Nucleation and Growth by Proteins: Molecular Interactions at Solid-Liquid Interfaces in Biomineralization, Croatica Chemica Acta, 63, 539–544, 1990.

Mucci, A.: Manganese uptake during calcite precipitation from seawater: Conditions leading to the formation of a pseudokutnahorite, Geochimica et Cosmochimica Acta, 52, 1859–1868, https://doi.org/10.1016/0016-7037(88)90009-9, 1988.

Mucci, A. and Morse, J. W.: The incorporation of Mg 2+ and Sr 2+ into calcite overgrowths: influences of growth rate and solution composition, Geochimica et Cosmochimica Acta, 47, 217–233, 1983.

Nakahara, H.: Nacre Formation in Bivalve and Gastropod Molluscs, in: Mechanisms and Phylogeny of Mineralization in Biological Systems, Springer Japan, Tokyo, 343–350, https://doi.org/10.1007/978-4-431-68132-8_55, 1991.

Nehrke, G., Keul, N., Langer, G., de Nooijer, L. J., Bijma, J., and Meibom, A.: A new model for biomineralization and trace-element signatures of Foraminifera tests, Biogeosciences, https://doi.org/10.5194/bg-10-6759-2013, 2013.

de Nooijer, L. J., Toyofuku, T., and Kitazato, H.: Foraminifera promote calcification by elevating their intracellular pH, Proceedings of the National Academy of Sciences of the United States of America, 106, 15374–15378, https://doi.org/10.1073/pnas.0904306106, 2009.

de Nooijer, L. J., Spero, H. J., Erez, J., Bijma, J., and Reichart, G. J.: Biomineralization in perforate foraminifera, Earth-Science Reviews, 135, 48–58, https://doi.org/10.1016/j.earscirev.2014.03.013, 2014.

Oomori, T., Kaneshima, H., Maezato, Y., and Kitano, Y.: Distribution Coefficient of Mg2+ ions between calcite and solution at 10-50°C, Marine Chemistry, 20, 327–336, https://doi.org/10.1016/B978-044452228-3/50006-6, 1987.

Petersen, J., Barras, C., Bézos, A., La, C., de Nooijer, L. J., Meysman, F. J. R., Mouret, A., Slomp, C. P., and Jorissen, F. J.: Mn/Ca intra- and inter-test variability in the benthic foraminifer Ammonia tepida, Biogeosciences, 15, 331–348, https://doi.org/10.5194/bg-15-331-2018, 2018.

Piez, K. A.: Amino Acid Composition of Some Calcified Proteins, Science, 134, 841–842, https://doi.org/10.1126/science.134.3482.841, 1961.

Pytkowicz, R. M.: Rates of Inorganic Calcium Carbonate Nucleation, The Journal of Geology, 73, 196–199, https://doi.org/10.1086/627056, 1965.

Raddatz, J., Rüggeberg, A., Margreth, S., and Dullo, W. C.: Paleoenvironmental reconstruction of Challenger Mound initiation in the Porcupine Seabight, NE Atlantic, Marine Geology, 282, 79–90, https://doi.org/10.1016/j.margeo.2010.10.019, 2011.

Raddatz, J., Liebetrau, V., Rüggeberg, A., Hathorne, E., Krabbenhöft, A., Eisenhauer, A., Böhm, F., Vollstaedt, H., Fietzke, J., López Correa, M., Freiwald, A., and Dullo, W. C.: Stable Sr-isotope, Sr/Ca, Mg/Ca, Li/Ca and Mg/Li ratios in the scleractinian cold-water coral *Lophelia pertusa*, Chemical Geology, 352, 143–152, https://doi.org/10.1016/j.chemgeo.2013.06.013, 2013.

Raddatz, J., Rüggeberg, A., Flögel, S., Hathorne, E. C., Liebetrau, V., Eisenhauer, A., and Dullo, W. C.: The influence of seawater pH on U/Ca ratios in the scleractinian cold-water coral Lophelia pertusa, Biogeosciences, 11, 1863–1871, https://doi.org/10.5194/bg-11-1863-2014, 2014.

Raddatz, J., Nürnberg, D., Tiedemann, R., and Rippert, N.: Southeastern marginal West Pacific Warm Pool sea-surface and thermocline dynamics during the Pleistocene (2.5–0.5 Ma), Palaeogeography, Palaeoclimatology, Palaeoecology, 471, 144–156, https://doi.org/10.1016/j.palaeo.2017.01.024, 2017.

Raitzsch, M., Duenas-Bohórquez, A., Reichart, G. J., de Nooijer, L. J., and Bickert, T. T.: Incorporation of Mg and Sr in calcite of cultured benthic foraminifera: Impact of calcium concentration and associated calcite saturation state, Biogeosciences, 7, 869–881, https://doi.org/10.5194/bg-7-869-2010, 2010.

Raja, R., Saraswati, P. K., Rogers, K., and Iwao, K.: Magnesium and strontium compositions of recent symbiont-bearing benthic foraminifera, Marine Micropaleontology, 58, 31–44, https://doi.org/10.1016/j.marmicro.2005.08.001, 2005.

Rathburn, A. E. and de Deckker, P.: Magnesium and strontium compositions of Recent benthic foraminifera from the Coral Sea, Australia and Prydz Bay, Antarctica, Marine Micropaleontology, 32, 231–248, https://doi.org/10.1016/S0377-8398(97)00028-5, 1997.

Schleinkofer, N., Raddatz, J., Freiwald, A., Evans, D., Beuck, L., Rüggeberg, A., and Liebetrau, V.: Environmental and biological controls on Na/Ca ratios in scleractinian cold-water corals, Biogeosciences, 16, 3565–3582, https://doi.org/10.5194/bg-16-3565-2019, 2019.

Schleinkofer, N., Raddatz, J., Evans, D., Gerdes, A., Flögel, S., Voigt, S., Büscher, J. V., and Wisshak, M.: Compositional variability of Mg/Ca, Sr/Ca, and Na/Ca in the deep-sea bivalve Acesta excavata (Fabricius, 1779), PLOS ONE, 16, e0245605, https://doi.org/10.1371/journal.pone.0245605, 2021.

Schöne, B. R., Zhang, Z., Jacob, D., Gillikin, D. P., Tütken, T., Garbe-Schönberg, D., McConnaughey, T., and Soldati, A.: Effect of organic matrices on the determination of the trace element chemistry (Mg, Sr, Mg/Ca, Sr/Ca) of aragonitic bivalve shells (*Arctica islandica*) - Comparison of ICP-OES and LA-ICP-MS data, Geochemical Journal, 44, 23–37, https://doi.org/10.2343/geochemj.1.0045, 2010.

Schweizer, M., Bowser, S. S., Korsun, S., and Pawlowski, J.: Emendation of Cibicides antarcticus (Saidova, 1975) based on molecular, morphological, and ecological data, Journal of Foraminiferal Research, https://doi.org/10.2113/gsjfr.42.4.340, 2012.

Secor, C. L., Mills, E. L., Harshbarger, J., Kuntz, H. T., Gutenmann, W. H., and Lisk, D. J.: Bioaccumulation of toxicants, element and nutrient composition, and soft tissue histology of zebra mussels (Dreissena polymorpha) from New York State waters, Chemosphere, https://doi.org/10.1016/0045-6535(93)90224-S, 1993.

Segev, E. and Erez, J.: Effect of Mg/Ca ratio in seawater on shell composition in shallow benthic foraminifera, Geochemistry, Geophysics, Geosystems, 7, 1–8, https://doi.org/10.1029/2005GC000969, 2006.

Smith, P. B. and Emiliani, C.: Oxygen-isotope analysis of recent tropical pacific benthonic foraminifera, Science, https://doi.org/10.1126/science.160.3834.1335, 1968.

Spero, H. J.: Ultrastructural examination of chamber morphogenesis and biomineralization in the planktonic foraminifer Orbulina universa, Marine Biology, 99, 9–20, https://doi.org/10.1007/BF00644972, 1988.

Spötl, C. and Vennemann, T. W.: Continuous-flow isotope ratio mass spectrometric analysis of carbonate minerals, Rapid Communications in Mass Spectrometry, 17, 1004–1006, https://doi.org/10.1002/rcm.1010, 2003.

Stephenson, A. E., Deyoreo, J. J., Wu, L., Wu, K. J., Hoyer, J., and Dove, P. M.: Peptides enhance magnesium signature in calcite: Insights into origins of vital effects, Science, 322, 724–727, https://doi.org/10.1126/science.1159417, 2008.

Sunda, W. G. and Huntsman, S. A.: Regulation of cellular manganese and manganese transport rates in the unicellular alga Chlamydomonas, Limnology and Oceanography, 30, 71–80, https://doi.org/10.4319/lo.1985.30.1.0071, 1985.

Swinehart, J. H. and Smith, K. W.: Iron And Manganese Deposition In The Periostraca Of Several Bivalve Molluscs, The Biological Bulletin, 156, 369–381, https://doi.org/10.2307/1540924, 1979.

Takesue, R. K., Bacon, C. R., and Thompson, J. K.: Influences of organic matter and calcification rate on trace elements in aragonitic estuarine bivalve shells, Geochimica et Cosmochimica Acta, 72, 5431–5445, https://doi.org/10.1016/j.gca.2008.09.003, 2008.

Tambutté, E., Allemand, D., Zoccola, D., Meibom, A., Lotto, S., Caminiti, N., and Tambutté, S.: Observations of the tissue-skeleton interface in the scleractinian coral Stylophora pistillata, Coral Reefs, 26, 517–529, https://doi.org/10.1007/s00338-007-0263-5, 2007.

Todd, R.: A new Rosalina (foraminifera) parasitic on a bivalve, Deep-Sea Research and Oceanographic Abstracts, 12, 831–837, https://doi.org/10.1016/0011-7471(65)90806-5, 1965.

Toyofuku, T., Kitazato, H., Kawahata, H., Tsuchiya, M., and Nohara, M.: Evaluation of Mg/Ca thermometry in foraminifera: Comparison of experimental results and measurements in nature, Paleoceanography, 15, 456–464, https://doi.org/10.1029/1999PA000460, 2000.

Toyofuku, T., Matsuo, M. Y., de Nooijer, L. J., Nagai, Y., Kawada, S., Fujita, K., Reichart, G. J., Nomaki, H., Tsuchiya, M., Sakaguchi, H., and Kitazato, H.: Proton pumping accompanies calcification in foraminifera, Nature Communications, 8, 1–6, https://doi.org/10.1038/ncomms14145, 2017.

Tribovillard, N., Algeo, T. J., Lyons, T., and Riboulleau, A.: Trace metals as paleoredox and paleoproductivity proxies: An update, Chemical Geology, 232, 12–32, https://doi.org/10.1016/j.chemgeo.2006.02.012, 2006.

Vénec-Peyré, M. T.: Bioeroding foraminifera: A review, Marine Micropaleontology, 28, 19–30, https://doi.org/10.1016/0377-8398(95)00037-2, 1996.

de Villiers, S., Nelson, B. K., and Chivas, A.: Biological Control on Coral Sr/Ca and d18O Reconstructions of Sea Surface Temperatures, Science, 269, 1247–1249, 1995.

Wada, K. and Fujinuki, T.: Biomineralization in bivalve molluscs with emphasis on the chemical composition of the extrapallial flui, Book chapter, 1976.

Walker, S. E., Hancock, L. G., and Bowser, S. S.: Diversity, biogeography, body size and fossil record of parasitic and suspected parasitic foraminifera: A review, Journal of Foraminiferal Research, 47, 34–55, https://doi.org/10.2113/gsjfr.47.1.34, 2017.

Webb, A. E., Pomponi, S. A., van Duyl, F. C., Reichart, G. J., and de Nooijer, L. J.: pH Regulation and Tissue Coordination Pathways Promote Calcium Carbonate Bioerosion by Excavating Sponges, Scientific Reports, 9, 1–10, https://doi.org/10.1038/s41598-018-36702-8, 2019.

Whitney, N. M., Johnson, B. J., Dostie, P. T., Luzier, K., and Wanamaker, A. D.: Paired bulk organic and individual amino acid δ15N analyses of bivalve shell periostracum: A paleoceanographic proxy for water source variability and nitrogen cycling processes, Geochimica et Cosmochimica Acta, 254, 67–85, https://doi.org/10.1016/j.gca.2019.03.019, 2019.

Wilbur, K. M. and Saleuddin, A. S. M.: Shell Formation, in: The Mollusca, Elsevier, 235–287, https://doi.org/10.1016/B978-0-12-751404-8.50014-1, 1983.

Yin, Y., Huang, J., Paine, M. L., Reinhold, V. N., and Chasteen, N. D.: Structural Characterization of the Major Extrapallial Fluid Protein of the Mollusc Mytilus edulis : Implications for Function, Biochemistry, 44, 10720–10731, https://doi.org/10.1021/bi0505565, 2005.

Yu, X. and Inesi, G.: Variable stoichiometric efficiency of Ca2+ and Sr2+ transport by the sarcoplasmic reticulum ATPase, Journal of Biological Chemistry, 270, 4361–4367, https://doi.org/10.1074/jbc.270.9.4361, 1995.

Zhang, C. and Zhang, R.: Matrix proteins in the outer shells of molluscs, Marine Biotechnology, 8, 572–586, https://doi.org/10.1007/s10126-005-6029-6, 2006.

5 Effects of ethanol preservation on the geochemical signature of marine biogenic carbonates

Nicolai Schleinkofer[1,2], Jacek Raddatz[1,2], Max Wisshak[3]

[1]Goethe University Frankfurt, Institute of Geosciences, Frankfurt am Main, Germany

[2]Goethe University Frankfurt, Frankfurt Isotope and Element Research Center (FIERCE), Frankfurt am Main, Germany

[3]Senkenberg am Meer, Marine Research Department, Wilhelmshaven, Germany

Submitted to Limonology and Oceanography: Methods on 27.09.2021

5.1 Abstract

We investigated different marine biogenic carbonates by inductively coupled plasma optical emission spectroscopy to assess the effects of post-sampling preservation in ethanol on the geochemical signature. Samples were measured every 1.5 months for a total preservation time of 3 to 6 months. We detect significant decreases in Mg/Ca and Na/Ca ratios by up to 70 % after the treatment in ethanol. The amount of decrease of Mg/Ca ratios is significantly different between calcitic and aragonitic samples, most likely due to higher amounts of weakly bound magnesium in aragonite. On the contrary, significant effects on Sr/Ca ratios were not observed. The results indicate that samples preserved in ethanol are not suitable for paleoenvironmental reconstructions using Mg/Ca or Na/Ca ratios due to the leaching effects of the ethanol.

5.2 Introduction

Marine biogenic carbonates are important proxy carriers to reconstruct past environmental conditions. Especially deep-water carbonates from cold-water coral reefs can help to understand important questions on past climatic and oceanic changes. In order to acquire reliable results a thorough understanding of the alteration history of the samples is needed. Foraminifera from drill cores have shown decreasing Na/Ca ratios with increasing depth,

suggesting that structurally-substituted Na is leached by pore water (Yoshimura et al., 2017). Similar results are reported from freshwater gastropods which showed significant decreases of Na/Ca and Mg/Ca by 10 % and 15 % respectively after leaching in distilled water for three weeks (Rosenthal and Katz, 1989). Sr/Ca on the other hand appears to be undisturbed. Corals show similar results in leaching experiments with water where lattice bound Mg and Na leached through the influence of water (Amiel et al., 1973).

Besides natural alteration through the influence of water, similar effects can also through the preservation of samples in ethanol. Fish otoliths have been shown to be significantly altered by ethanol in several elements (Na, K, S, Cl), whereas others elements are not affected (Sr, Mg) (Milton and Chenery, 1998; Proctor and Thresher, 1998). Results from calcitic bamboo corals similarly indicate no alteration of Mg/Ca and Sr/Ca after a 13-month preservation period in ethanol (Strzepek et al., 2014). Other marine carbonate materials have not yet been studied for the specific effects of ethanol preservation, but existing studies indicate potential effects.

Likewise, bivalves also show decreasing Mg/Ca and Sr/Ca ratios through the influence of ammonium acetate (Walls et al., 1977). In general, the leaching effect is explained through the preferential dissolution of domains that are rich in Na, Mg and/or Sr (Walls et al., 1977; Amiel et al., 1973; Yoshimura et al., 2017) which is also possible under the influence of ethanol. Due to difficulties and costs associated with the collection of marine carbonate material it is not unusual to investigate samples from different origins including museum samples with different preservation protocols (Strzepek et al., 2014). The effects of post-collection preservation methods on the geochemical signal in marine carbonates, however, is poorly understood.

Here we present geochemical measurements by inductively coupled plasma optical emission spectrometry (ICP-OES) on different biogenic carbonate materials. We collected sample material from eight different species and stored the samples in denatured ethanol for different time periods (1.5, 3, 4.5 and 6 months). Following storage, the samples were

analyzed for their chemical composition and compared with untreated samples.

5.3 Material and methods

5.3.1 Sample material

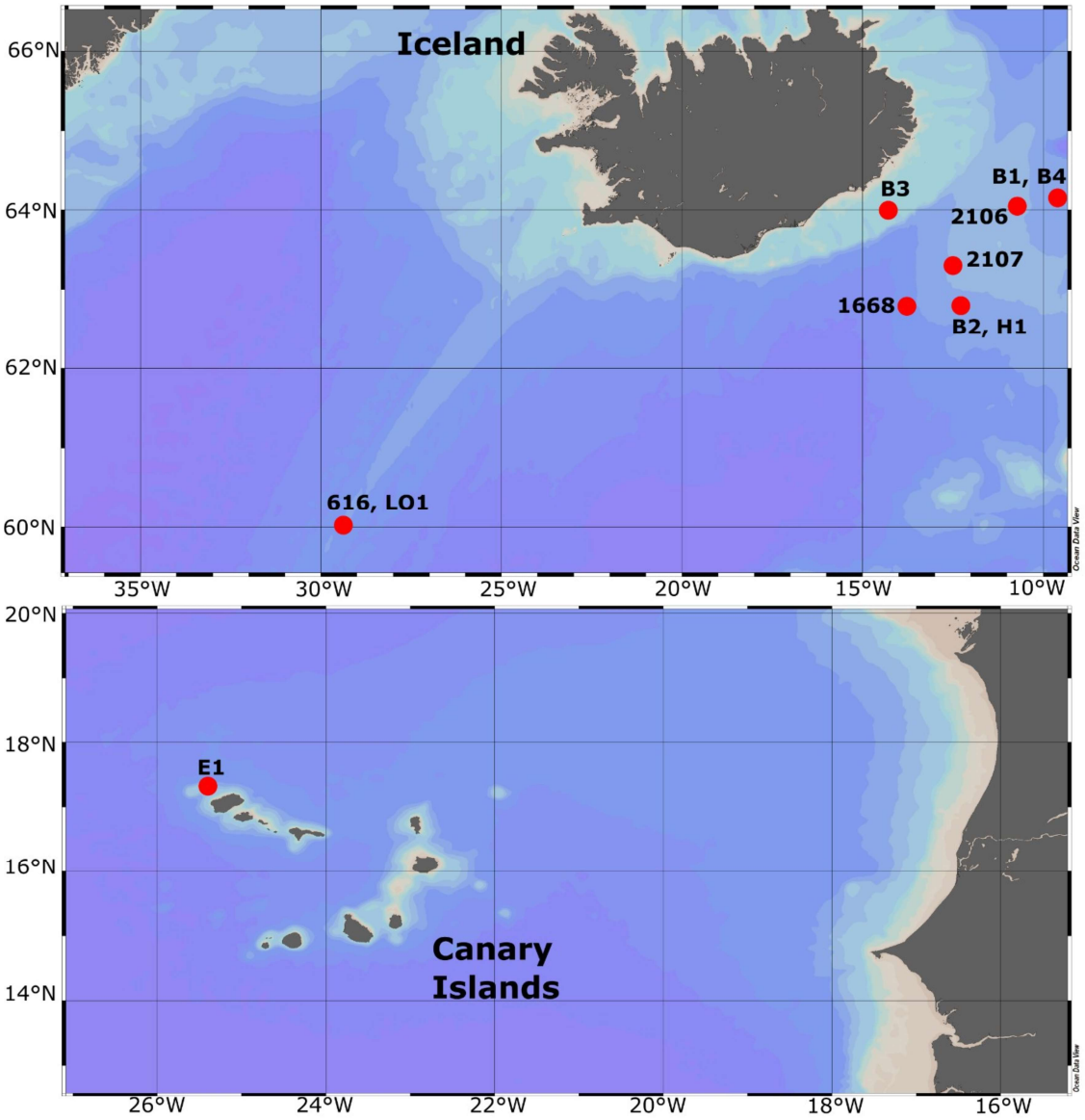

Figure 5-1 Map of the sampling locations around Iceland and the Canary Islands.

All samples except E1 were collected during cruise SO275 (Brix et al., 2020) on RV SONNE in the North-Atlantic. Sample E1 was collected during cruise M80/3 (Hansteen et al., 2014) on RV Meteor around the Canary Islands (Fig. 1). In total we tested eight different biogenic carbonates from eleven samples bivalves, corals and foraminifera (Fig 2 & Table 1)

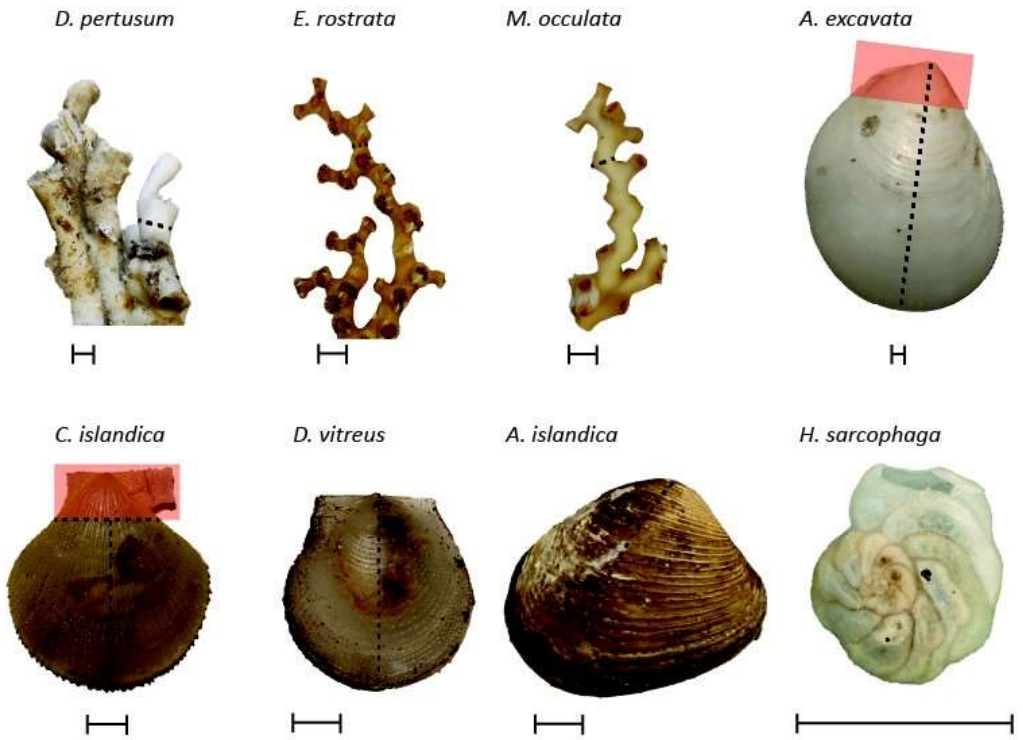

Figure 5-2 Sample pictures of the different studied species. Dashed line show the cut samples. Red areas are disregarded during sampling. Scalebars are 1 mm.

Table 5-1 Species, source, sample technique, sampling location, polymorph and experiment time of the investigated samples. ROV = Remotely operated vehicle, BC = Boxcorer

Sample	Species	Source	Sampling equipment	Station/Cast	Coordinates	Depth [m]	Polymorph	Experiment time [months]
616	*Madrepora oculata*	SO276	ROV	103/14	60° 13.996' N 029° 08.587' W	660	A	3
1668	*Acesta excavata*	SO276	ROV	97/12	63° 52.396' N 014° 00.193' W	295	C	6
2106	*Arctica islandica*	SO276	BC	74/1	64° 26.189' N 011° 37.458' W	415	A	3
2107	*Chlamys islandica*	SO276	ROV	97/8	63° 52.821' N 013° 58.964' W	315	C	6
B1	*Delectopecten vitreus*	SO276	BC	56/1	64° 53.511' N 009° 38.049' W	680	C	3
B2	*Acesta*	SO276	ROV	92/10	63° 51.500' N	413	A	3

	excavata				013° 46.677' W			
B3	*Chlamys islandica*	SO276	ROV	66/8	64° 04.978' N 014° 27.263' W	238	C	3
B4	*Delectopecten vitreus*	SO276	BC	56/1	64° 53.511' N 009° 38.049' W	680	C	6
H1	*Hyrrokkin sarcophaga*	SO276	ROV	92/10	63° 51.500' N 013° 46.677' W	413	C	3
E1	*Enallopsammia rostrata*	M80/3	ROV	84	17° 14.03’ N 025° 23.02 W	700	A	3
LO1	*Desmophyllum pertusum*	SO276	ROV	106/3	60° 13.926' N 029° 08.946' W	661	A	3

The bivalves were divided in left and right valve. One valve was stored in ethanol for the duration of the experiment, the other valve was stored dry in a sealed container. The coral samples were prepared as longitudinal slices through the corals calice. Similar to the bivalve samples, these slices were equally divided in test and control sample. *Hyrrokkin sarcophaga* is a parasitic foraminifera that lives on different host species such as *A. excavata* and *D. pertusum* (Cedhagen, 1994). The foraminifera were picked from *A. excavata* shells and treated with ethanol without further cutting. However, all foraminifera derive from one *A. excavata* shell to ensure that the foraminifera experienced similar environmental settings.

5.3.2 Experimental setup

After preparation the samples were submerged in denatured ethanol (96 %). The ethanol was changed twice during the first week. Total exposure time to alcohol is different for the different samples (Table 2) and amounts to 3 months or 6 months. During this time the samples were kept refrigerated at 4° C. Geochemical measurements by ICP-OES were carried out every 1.5 months. After the exposure time the samples were ultrasonically rinsed, dried and ground in an agate mortar for geochemical measurements. In case of inequilateral shells (i.e. *Chlamys islandica & Acesta excavata* auricle) the affected parts were disregarded during sampling (Fig. 2).

5.3.3 ICP-OES measurements

Elemental ratios of carbonate and ethanol samples were measured by inductively coupled plasma-optical emission spectrometry (ICP-OES) on a Thermoscientific ICAP 6300 dual viewing at Goethe University, Frankfurt. The sample powder (~ 120 µg) was dissolved in 500 µl 2% HNO_3 to reach a calcium concentration of 25 mg/L. 300 µl aliquots were separated and diluted with yttrium-solution to reach an yttrium concentration of 1 mg/L. The yttrium is used as an internal standard element to correct for matrix effects during measurements. Each sample was measured three times and the reported results are the arithmetic means of these three measurements. The intensity data was background corrected, standardized to Y and normalized to Ca. The carbonate standard JCp-1 was measured after every tenth sample to correct for machine drift and monitor precision and accuracy. Accuracy, as reported as the deviation of our JCp-1 measurements from reported values (Jochum et al., 2005), is better than 5 % for Mg/Ca, Na/Ca and Sr/Ca. Precision, as reported as the relative standard deviation of our JCp-1 measurements (n=10), is better than 3.5 % for Mg/Ca, Na/Ca and Sr/Ca.

Ethanol samples (100 µl) were mixed with 200 µl of 2 % HNO3 and added to 1.5 ml of 1.2 mg/L yttrium-solution, similar to the protocol described in Chaves et al. (2011). Each sample was measured three times and the reported results are the arithmetic means of these three measurements. The measured intensity data was background corrected and standardized to Y. The JCp-1 carbonate standard was measured every tenth sample to monitor accuracy and precision. Equally to the ethanol samples, the JCp-1-standards were also prepared with 100 µl ethanol, to avoid matrix effects due to different matrix composition. Accuracy is better than 5 %, precision is better than 3 %.

5.3.4 Data processing

The data was processed and statistically investigated using R. We used an ANOVA test for differences between different test groups (ethanol preservation vs. no ethanol preservation, calcite vs. aragonite). The prerequisites for ANOVA analysis were tested with Levene's test and Shapiro-Wilk test (equal variance and normal distribution). A paired T-test with

Bonferroni correction was used to do pairwise comparisons between the different treatment groups (duration of ethanol preservation).

5.4 Results

5.4.1 E/Ca differences in ethanol treatment

Table 5-2 Mean E/Ca ratios for each treatment group. Each value is reported as the mean of three independent measurements. Values in brackets are the standard deviation.

Sample	Experiment time [month]														
	No alcohol			1.5			3			4.5			6		
	Mg/Ca	Na/Ca	Sr/Ca	Mg/Ca	Na/Ca	Sr/Ca	Mg/Ca	Na/Ca	Sr/Ca	Mg/Ca	Na/Ca	Sr/Ca	Mg/Ca	Na/Ca	Sr/Ca
616 ***Madrepora oculata***	4.7 (0.3)	23.9 (0.2)	10.5 (0.2)	3.6 (0.1)	23.0 (0.4)	10.5 (0.2)	2.8 (0.1)	22.6 (0.7)	10.6 (0.1)						
1668 ***Acesta excavata*** **(C)**	11.4 (0.6)	21.3 (0.8)	1.1 (0.01)				10.7 (0.2)	17.4 (0.3)	1.1 (0.02)	10.0 (0.8)	16.8 (0.6)	1.2 (0.04)	9.1 (0.5)	15.7 (0.9)	1.1 (0.03)
2107 ***Chlamys islandica***	10.4 (0.9)	14.9 (0.4)	1.3 (0.04)				10.2 (0.4)	12.8 (0.3)	1.2 (0.02)	10.1 (0.4)	11.6 (0.2)	1.30 (0.04)	9.2 (0.4)	11.4 (0.2)	1.3 (0.03)
2106 ***Arctica islandica***	1.4 (0.3)	19.8 (0.3)	2.5 (0.1)	1.1 (0.1)	19.0 (0.3)	2.5 (0.1)	0.5 (0.1)	18.3 (0.4)	2.6 (0.04)						
B1 ***Delectopecten vitreus***	9.6 (0.8)	14.7 (0.6)	1.1 (0.03)	9.0 (0.3)	14.1 (0.2)	1.1 (0.03)	8.7 (0.7)	12.6 (0.5)	1.1 (0.02)						

B2 ***Acesta excavata*** **(A)**	3.0 (0.2)	21.0 (0.6)	2.3 (0.2)	2.7 (0.2)	18.6 (0.3)	2.9 (0.2)	1.3 (0.2)	17.3 (0.5)	2.5 (0.04)						
B3 ***Chlamys islandica***	11.4 (0.2)	18.2 (0.9)	1.3 (0.01)	11.3 (0.5)	10.7 (0.3)	1.3 (0.01)	10.5 (0.5)	10.2 (0.2)	1.2 (0.01)						
B4 ***Delectopecten vitreus***	14.9 (1.4)	34.2 (3.6)	1.3 (0.1)				10.0 (0.2)	12.0 (0.2)	1.2 (0.02)	6.9 (0.4)	14.3 (0.1)	1.0 (0.01)	7.9 (0.1)	12.3 (0.2)	1.1 (0.02)
H1 ***Hyrrokkin sarcophaga***	49.3 (5.6)	35.2 (2.1)	2.2 (0.04)	51.0 (0.8)	29.4 (3.0)	2.6 (0.2)	48.9 (1.6)	21.8 (1.5)	2.3 (0.06)						
E1 **Enallopsammia rostrata**	6.7 (0.4)	38.8 (2.6)	10.6 (0.4)	4.3 (0.5)	22.1 (0.9)	11.0 (0.2)	2.0 (0.1)	22.0 (0.3)	10.7 (0.2)						
LO1 ***Desmophyllum pertusum***	5.0 (0.1)	26.6 (1.5)	10.4 (0.4)	4.2 (0.3)	23.0 (0.3)	10.3 (0.1)	3.2 (0.1)	22.3 (1.4)	10.5 (0.1)						

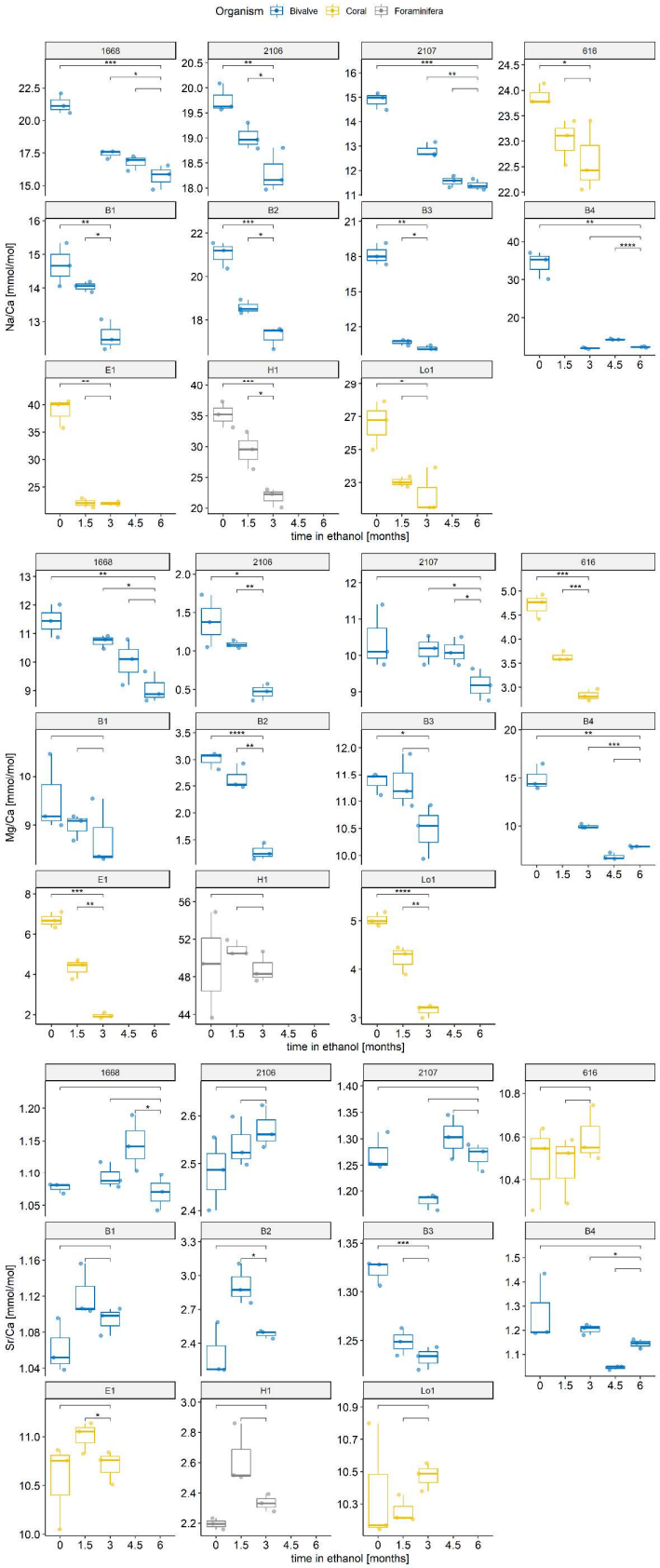
Organism Bivalve Coral Foraminifera
1668
2106
2107
616
B1
B2
B3
B4
E1
H1
Lo1
Na/Ca [mmol/mol]
Mg/Ca [mmol/mol]
Sr/Ca [mmol/mol]
time in ethanol [months]

Figure 5-3 Boxplots of the results of the ICP-OES measurements over the course of the experiment. Boxes show the IQR (25 % quartile to 75 % quartile). Lines in the boxes display the median. The whiskers show minimum and maximum values. Brackets above the boxes display the results of a paired t-test. Asterisk's indicate significant differences between treatment groups

The investigated samples display a large variability in their chemical composition (Table 2). Mg/Ca ratios range from 1.4 (± 0.3) mmol/mol in the aragonitic bivalve *A. islandica* to 49.4 (± 5.6) mmol/mol in the calcitic foraminifera *H. sarcophaga.* The compositional variability is smaller in Na/Ca ratios, ranging from 14.7 (± 0.6) mmol/mol in *D. vitreus* to 38.8 (± 2.6) mmol/mol in *E. rostrata.* Sr/Ca ratios are co-varying with both, material and organism group of the investigated samples. Calcitic samples display low Sr/Ca ratios < 2 mmol/mol. Aragonitic samples have naturally higher Sr/Ca ratios between 2.3 and 10.6 mmol/mol. Aragonitic bivalves are characterized by Sr/Ca ratios of about 2.5 mmol/mol whereas aragonitic corals are characterized by Sr/Ca ratios around 10 mmol/mmol. *H. sarcophaga*, a parasitic, calcitic foraminifera, is an exception and displays Sr/Ca ratios of 2.2 mmol/mol (± 0.04).

Sr/Ca ratios are not systematically influenced by the preservation process in ethanol. Measurements throughout the experiment time reveal changes in the Sr/Ca ratios of the investigated samples between - 0.15 and + 0.09 mmol/mol over the 6 months exposure, corresponding to a variability of ± 10 %. The natural variance of Sr/Ca ratios (reported as RSD) amounts to a maximum of 11 % in sample B4 with a mean of 3.9 %.

Contrary to Sr/Ca ratios, Mg/Ca and Na/Ca ratios display a systematic decrease with ongoing ethanol treatment. We detect a decrease of 0.8 to 70 % in Mg/Ca over the experiment time of six months. Similarly, we detect a decrease of Na/Ca ratios of 5.3 to 64 %

The ANOVA and t-test indicate that every sample shows a significant (p<0.05) decrease of mean Na/Ca ratios throughout the preservation time in ethanol (Fig. 3). Considering Mg/Ca ratios we detect significant decreases in nine samples and insignificant decreases in two samples (B1, H1). The percental decrease in Mg/Ca ratios throughout the experiment time is significantly different (p=0.003) between calcitic and aragonitic samples based on ANOVA,

with aragonitic samples displaying a higher decrease. No significant differences are observed for Na/Ca and Sr/Ca ratios between aragonitic and calcitic samples. Significant differences between the decrease of E/Ca ratios, based on the organism group, are not observed for any of the investigated elemental ratios.

5.4.2 Element concentration in preservation ethanol

Table 5-3 Elemental concentrations of Mg, Na and Sr in ethanol used for sample preparation. Reported values are arithmetic means of three measurements.

	Mg [mg/l]	**Na [mg/l]**	**Sr [mg/l]**
1668	5543	49832	21
2106	462	1223	260
2107	931	15055	0
616	6889	35271	1700
B1	801	7065	0
B2	0	0	0
B3	1093	15085	0
B4	186	1396	0
E1	12251	264056	0
H1	1785	33978	90
Lo1	4917	40048	277
Ethanol (ultrapure)	0	0	0

The ultrapure ethanol used for sample preservation shows no measurable concentration of Mg, Na and Sr (Table 3). On the contrary, we measure high concentrations of Mg and Na in the ethanol, after the samples were submerged in it. Ten of eleven samples display elemental concentrations above the detection limits (90 mg/l Mg, 420 mg/l Na, 8 mg/l Sr) in Na and Mg. Sample B2 does not display concentrations above the detection limit but the raw intensities are higher than in the ultrapure ethanol. Five samples (1668, 2106, 616, H1, LO1) do also show measurable concentrations of Sr. In contrast to Mg and Na concentrations, samples that are characterized by Sr concentrations below the detection limits do not display

raw intensities that are higher than the measured ultrapure ethanol. Aragonitic samples display a significant correlation between the measured Na concentration in the preservation ethanol and the absolute decrease of Na in the submerged sample ($r^2 = 0.97$, $p = 0.013$, $\alpha = 0.05$), whereas no significant correlation can be observed in calcitic samples (Fig. 4). This is similar for magnesium; however, the correlation is not significant on a 5% significance level

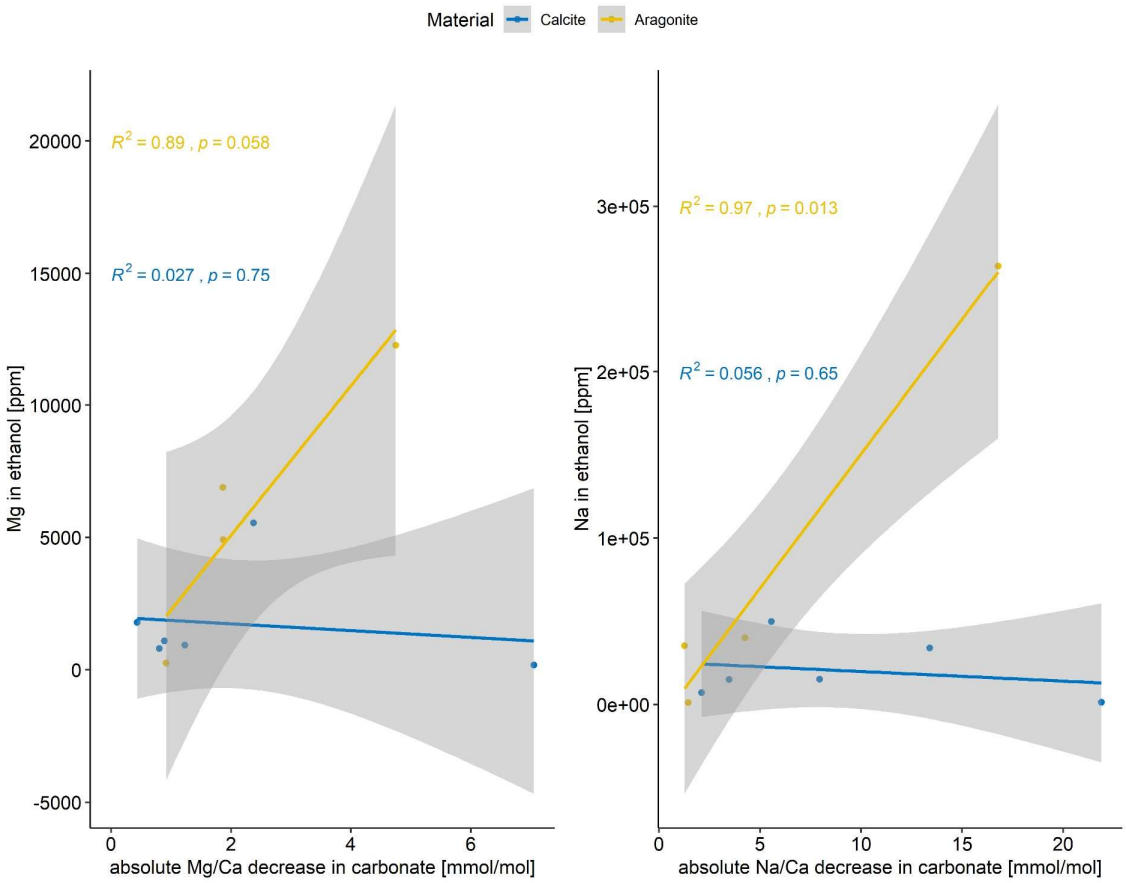

($r^2 = 0.89$, $p = 0.058$). No significant correlations are observable between Sr concentration in the ethanol and absolute decrease of the Sr concentration in the biogenic carbonate independent of the shell material.

Figure 5-4 Measured elemental concentrations of Mg and Na in ethanol compared to the decrease of these E/Ca ratios in the carbonate samples over the course of the experiment time. Aragonitic samples display a significant correlation with regards to Na and a barely insignificant correlation with regards to Mg.

5.5 Discussion

5.5.1 Dissolution effects of ethanol preservation

Preservation of biogenic samples in ethanol is a common technique to allow extended storage of biogenic samples without alteration to the DNA material (Kilpatrick, 2002), however our results indicate that this method of storage in ethanol does significantly modify the geochemical composition of the biogenic carbonate material. With regards to Mg/Ca and Na/Ca we detect decreasing ratios of up to 70 % after a preservation period of six months. These results are in accordance with similar studies on fish otoliths (Proctor and Thresher, 1998; Milton and Chenery, 1998). However, we detect stronger decreases in the respective E/Ca ratios, probably owing to the extended preservation time in our experiment (3 weeks and 1 month vs. 6 months (Milton and Chenery, 1998; Proctor and Thresher, 1998). Similarly, we detect no systematic, significant differences in Sr/Ca ratios after the ethanol preservation(Hedges et al., 2004; Strzepek et al., 2014). It was suggested that the mode of incorporation of specific elements predicts the effect that the ethanol treatment has on these specific elements. Tightly bound elements, such as Sr show no alteration whereas loosely bound elements such as Mg and Na show alteration as an effect of the ethanol treatment (Milton and Chenery, 1998; Proctor and Thresher, 1998; Hedges et al., 2004). Studies show that the majority of Na (90%) in both, biogenic aragonite and calcite is substituted with Ca and structurally bound to the carbonate lattice(Yoshimura et al., 2017; Amiel et al., 1973). Similarly, in calcite Mg-ions are incorporated into the lattice in exchange for Ca-ions (Raz et al., 2000), whereas in aragonite Mg-ions are more likely hosted by organic material or a highly disordered phase such as amorphous calcium carbonate (ACC) or hydroxides (Finch and Allison, 2008; Foster et al., 2008). If the mode of incorporation of the specific elements predicts the effect, there should be differences of the amount of Mg/Ca decrease controlled by the shell polymorph. Indeed, we can observe a significant difference of the percental

decrease of Mg/Ca between calcitic and aragonitic samples, with aragonitic samples showing stronger decreases. This is most likely caused by the higher solubility of aragonite compared to calcite (higher by about 16%) (Curl, 1962). Similar effects are expected from high-Mg calcite, but only with Mg contents above 8.5 mole%. Calcite with less than 8.5 mol% of Mg, such as our investigated samples, are less soluble than aragonite (Berner, 1975). Still there must be further reasons for the removal of elements from the carbonate lattice, other than solely the mode of incorporation into the crystal lattice. A possible explanation could be the dissolution of carbonate material by the ethanol. With respect to the Brønsted-Lowry acid-base theory (Lowry, 1923; Brönsted, 1923), ethanol must be considered amphoteric, meaning that it can act both as an acid and a base. However, water itself is a stronger acid than ethanol (pK_{a_water} = 14, $pK_{a\_ethanol}$ = 15.9 (Haynes, 2014)), therefore this effect is negligible in aqueous solution. Instead, ethanol acts as a proton acceptor in aqueous solutions and represents a weak base.

Preferential dissolution of areas rich in sodium and magnesium can potentially cause the geochemical alterations we observe. Such effects, especially considering Mg/Ca, are known, for instance, from aragonitic corals and calcitic foraminifera(Yu et al., 2007; Hendy et al., 2007). Decreasing Mg/Ca ratios were found in aragonitic *Porites* corals caused by preferential dissolution of magnesium-rich areas under the influence of seawater(Hendy et al., 2007). Similarly, cleaning methods with solutions containing citrate, such as used for the preparation of foraminifera, caused a substantial decrease of Mg/Ca, Mn/Ca, Zn/Ca, Cd/Ca, and U/Ca ratios but not in Sr/Ca ratios (Yu et al., 2007). Magnesium incorporation in calcite has been shown to increase the mineral solubility in comparison to magnesium-free calcite (Berner, 1975; Davis, 2000). Similar effects in aragonite are not to be expected as the magnesium is mostly not structurally bound to the aragonite (Berner, 1975; Finch and Allison, 2008; Foster et al., 2008). The decrease of Mg/Ca ratios in calcitic samples is therefore potentially caused by the increased solubility of magnesium-bearing calcite in comparison to magnesium-free calcite. Similarly, ACC which is discussed as one of the main Mg-bearing phases in aragonite, has a higher solubility than crystalline

aragonite(Mergelsberg et al., 2020). Consequently, the effects of the preservation in ethanol on magnesium in aragonite and calcite can be explained with the increased solubility of ACC and magnesium-bearing calcite, respectively (Mergelsberg et al., 2020; Berner, 1975; Davis, 2000). Observable differences in the Mg/Ca reduction between aragonitic and calcitic samples are probably an effect of the generally lower binding strength of magnesium in ACC and organic material of aragonite compared to the structurally bound magnesium in calcite. Similar results were also obtained from ammonium acetate leaching experiments on calcitic and aragonitic bivalves. These experiments revealed that in the calcitic *Crassostrea virginica* only 6 % of the magnesium is readily exchangeable, whereas in the aragonitic *Mercenaria mercenaria* 26 % is (Walls et al., 1977).

A study on abiogenic and biogenic calcite and aragonite suggests that sodium substitutes with calcium (Yoshimura et al., 2019). Consequently, we did not expect to observe significant differences of the ethanol preservation effect between calcite and aragonite, which is in accordance to our results. Several researchers presented results of leaching experiments with water on carbonates. All these studies find that about 10 % of sodium is readily exchangeable and bound to organic material (Amiel et al., 1973; Walls et al., 1977; Rosenthal and Katz, 1989). Our results, display stronger decreasing Na/Ca ratios up to 64 %, which is not explainable if only the organically bound sodium is released. As in the aforementioned studies, leaching was acquired with water, we assume that ethanol is more effective as a leaching agent than water is and therefore also leaches structurally bound Na to some extent.

5.5.2 Elements in preservation ethanol

The analysis of the preservation ethanol yields results that are largely in accordance to the results of the carbonate measurements, however some results appear to too high and need further discussion. For example, we measured no magnesium and sodium in ethanol sample B2, despite observing a significant decrease in both these elements in the carbonate fraction. Also, sample B2 displays similar levels of Mg/Ca and Na/Ca decrease as other samples but no measurable concentrations of these elements in the solvent. The underlying reason for

this is probably the amount of ethanol used for submerging the samples. Sample B2 (*A. excavata*) was the biggest sample, leading to an increased amount of ethanol needed to fully submerge the sample and consequently a decrease in elemental concentrations below the detection limit.

Additionally, we detect Sr in five of the ethanol samples (1668, 2106, 616, H1, LO1), despite measuring no significant decrease in the sample carbonate. The most likely explanation for this, is a contamination with seawater. This could be either caused by insufficient cleaning after sampling or by fluid inclusions in the carbonate material (Vonhof et al., 2015; Gaffey, 1988). Fluid inclusions are known from many marine species including scleractinians, molluscs and foraminifera with water contents from a few tenths of percent to three percent by weight (Gaffey, 1988). Partial carbonate dissolution could open these microscopic reservoirs leading to measurable Sr concentrations in the ethanol despite of not having a significant effect on the measured carbonate material. This effect would also explain the very high Mg and Na concentrations in some samples (616, LO1).

5.5.3 Usability of ethanol preserved samples

Our results indicate no alteration of the Sr/Ca ratios as an effect of the preservation in ethanol, at least for a duration of up to 6 months. Therefore, ethanol preserved samples are likely still usable for reconstructions using Sr/Ca, a temperature reconstruction technique often used on coral samples(Cohen et al., 2001; Hathorne et al., 2013; DeLong et al., 2013; Swart et al., 2002; Raddatz et al., 2013). However, one should keep in mind that samples from museums potentially experienced longer preservation periods, potentially decades. On the contrary, our results show that paleoenvironmental reconstructions using Mg/Ca and Na/Ca (Nürnberg et al., 1996; Bertlich et al., 2018; Schleinkofer et al., 2019; Zhou et al., 2021; Lear et al., 2002; Bryan and Marchitto, 2008; Evans et al., 2015; Raddatz and Rüggeberg, 2019) cannot be conducted on samples that were preserved in ethanol, even if that preservation lasted for a few months only. As the amount of decrease in these elements is not regular, but a function of different variables such as the carbonate polymorph, porosity, preservation time and element distribution, the decrease cannot be reasonably corrected for.

A study on otoliths furthermore suggests significant alterations of oxygen isotope ratios (Storm-Suke et al., 2007), therefore the most commonly used proxy techniques Mg/Ca and $\delta^{18}O$ cannot be used on ethanol preserved samples. Consequently, biogenic carbonate sample material should be stored separately from organic tissue material if at all possible.

5.6 Conclusion

We have tested the effects of ethanol preservation on the elemental composition of different biogenic carbonate materials. The results suggest a significant decrease of Mg/Ca and Na/Ca ratios even after only 1.5-month preservation time. The decrease is likely caused by preferential dissolution of sodium and magnesium-rich areas and leaching of loosely bound sodium and magnesium in organic material and ACC. In the contrary, no systematic effects are evident for Sr/Ca ratios and paleotemperature reconstructions using Sr/Ca ratios on corals are therefore still possible with samples that were preserved in ethanol. Commonly used proxies such as Mg/Ca as well as the emerging Na/Ca proxy are not feasible on ethanol preserved samples. The results of this study showcase the importance of sample specific preservation techniques to utilize samples to their full potential. In general, it is best to dissect biological samples such as bivalves prior to the ethanol preservation and air-dry the carbonate material to retain its geochemical information. A correction for the effects of ethanol storage does not seem possible, as the degree of decrease of the elemental ratios is not solely a systematic function of the controlled by the preservation time.

5.7 Supplements

S1 ICP-OES results

5.8 Acknowledgments

We want to thank Saskia Brix and all crew and cruise participants of the research cruise SO276 (DFG funded under “MerMet17-06”) and M80/3. This work was funded by the Deutsche Forschungsgemeinschaft, RA 2156-5/1 to JR. This is FIERCE contribution No. XXX

5.9 References

Amiel, A. J., Friedman, G. M., and Miller, D. S.: Distribution and nature of incorporation of trace elements in modern aragonitic corals, 20, 47–64, https://doi.org/10.1111/j.1365-3091.1973.tb01606.x, 1973.

Berner, R. A.: The role of magnesium in the crystal growth of calcite and aragonite from sea water, 39, 489–504, https://doi.org/10.1016/0016-7037(75)90102-7, 1975.

Bertlich, J., Nürnberg, D., Hathorne, E. C., de Nooijer, L. J., Mezger, E. M., Kienast, M., Nordhausen, S., Reichart, G. J., Schönfeld, J., and Bijma, J.: Salinity control on Na incorporation into calcite tests of the planktonic foraminifera Trilobatus sacculifer - Evidence from culture experiments and surface sediments, 15, 5991–6018, https://doi.org/10.5194/bg-15-5991-2018, 2018.

Brönsted, J. N.: Einige Bemerkungen über den Begriff der Säuren und Basen, 42, 718–728, https://doi.org/10.1002/recl.19230420815, 1923.

Bryan, S. P. and Marchitto, T. M.: Mg/Ca-temperature proxy in benthic foraminifera: New calibrations from the Florida Straits and a hypothesis regarding Mg/Li, 23, 1–17, https://doi.org/10.1029/2007PA001553, 2008.

Cedhagen, T.: Taxonomy and biology of hyrrokkin sarcophaga gen. Et Sp. N., a parasitic foraminiferan (rosalinidae), 79, 65–82, https://doi.org/10.1080/00364827.1994.10413549, 1994.

Cohen, A. L., Layne, G. D., Hart, S. R., and Lobel, P. S.: Implications for the paleotemperature proxy a, 16, 20–26, 2001.

Curl, R. I.: The Aragonite-Calcite Problem, 1962.

Davis, K. J.: The Role of Mg2+ as an Impurity in Calcite Growth, 290, 1134–1137, https://doi.org/10.1126/science.290.5494.1134, 2000.

DeLong, K. L., Quinn, T. M., Taylor, F. W., Shen, C. C., and Lin, K.: Improving coral-base paleoclimate reconstructions by replicating 350years of coral Sr/Ca variations, 373, 6–24, https://doi.org/10.1016/j.palaeo.2012.08.019, 2013.

Evans, D., Erez, J., Oron, S., and Müller, W.: Mg/Ca-temperature and seawater-test chemistry relationships in the shallow-dwelling large benthic foraminifera Operculina ammonoides, 148, 325–342, https://doi.org/10.1016/j.gca.2014.09.039, 2015.

Finch, A. A. and Allison, N.: Mg structural state in coral aragonite and implications for the paleoenvironmental proxy, 35, 1–5, https://doi.org/10.1029/2008GL033543, 2008.

Foster, L. C., Finch, A. A., Allison, N., Andersson, C., and Clarke, L. J.: Mg in aragonitic bivalve shells: Seasonal variations and mode of incorporation in Arctica islandica, 254, 113–119, https://doi.org/10.1016/j.chemgeo.2008.06.007, 2008.

Gaffey, S. J.: Water in skeletal carbonates, 58, 397–414, https://doi.org/10.1306/212F8DA5-2B24-11D7-8648000102C1865D, 1988.

Hathorne, E. C., Gagnon, A., Felis, T., Adkins, J., Asami, R., Boer, W., Caillon, N., Case, D., Cobb, K. M., Douville, E., Demenocal, P., Eisenhauer, A., Garbe-Schönberg, D., Geibert, W., Goldstein, S., Hughen, K., Inoue, M., Kawahata, H., Kölling, M., Cornec, F. L., Linsley, B. K., McGregor, H. v., Montagna, P., Nurhati, I. S., Quinn, T. M., Raddatz, J., Rebaubier, H., Robinson, L., Sadekov, A., Sherrell, R., Sinclair, D., Tudhope, A. W., Wei, G., Wong, H., Wu, H. C., and You, C. F.: Interlaboratory study for coral Sr/Ca and other element/Ca ratio measurements, 14, 3730–3750, https://doi.org/10.1002/ggge.20230, 2013.

Haynes, W. M.: CRC handbook of chemistry and physics, CRC press, 2014.

Hedges, K. J., Ludsin, S. A., and Fryer, B. J.: Effects of ethanol preservation on otolith microchemistry, 64, 923–937, https://doi.org/10.1111/j.1095-8649.2004.00353.x, 2004.

Hendy, E. J., Gagan, M. K., Lough, J. M., McCulloch, M., and deMenocal, P. B.: Impact of skeletal dissolution and secondary aragonite on trace element and isotopic climate proxies in Porites corals, 22, https://doi.org/10.1029/2007PA001462, 2007.

Kilpatrick, C. W.: Noncryogenic preservation of mammalian tissues for DNA extraction: An assessment of storage methods, 40, 53–62, https://doi.org/10.1023/A:1014541222816, 2002.

Lear, C. H., Rosenthal, Y., and Slowey, N.: Benthic foraminiferal Mg/Ca-paleothermometry: A revised core-top calibration, 66, 3375–3387, https://doi.org/10.1016/S0016-7037(02)00941-9, 2002.

Lowry, T. M.: The uniqueness of hydrogen, 42, 43–47, https://doi.org/10.1002/jctb.5000420302, 1923.

Mergelsberg, S. T., de Yoreo, J. J., Miller, Q. R. S., Marc Michel, F., Ulrich, R. N., and Dove, P. M.: Metastable solubility and local structure of amorphous calcium carbonate (ACC), 289, 196–206, https://doi.org/10.1016/j.gca.2020.06.030, 2020.

Michaud, C. L. and Foran, D. R.: Simplified Field Preservation of Tissues for Subsequent DNA Analyses*, 56, 846–852, https://doi.org/10.1111/J.1556-4029.2011.01771.X, 2011.

Milton, D. A. and Chenery, S. R.: The effect of otolith storage methods on the concentrations of elements detected by laser-ablation ICPMS, 53, 785–794, https://doi.org/10.1006/jfbi.1998.0745, 1998.

Nürnberg, D., Bijma, J., and Hemleben, C.: Assessing the reliability of magnesium in foraminiferal calcite as a proxy for water mass temperatures, 60, 803–814, https://doi.org/10.1016/0016-7037(95)00446-7, 1996.

Proctor, C. H. and Thresher, R. E.: Effects of specimen handling and otolith preparation on concentration of elements in fish otoliths, 131, 681–694, https://doi.org/10.1007/s002270050360, 1998.

Raddatz, J. and Rüggeberg, A.: Constraining past environmental changes of cold-water coral mounds with geochemical proxies in corals and foraminifera, https://doi.org/10.1002/dep2.98, 2019.

Raddatz, J., Liebetrau, V., Rüggeberg, A., Hathorne, E., Krabbenhöft, A., Eisenhauer, A., Böhm, F., Vollstaedt, H., Fietzke, J., Correa, M. L., Freiwald, A., and Dullo, W.: Stable Sr-isotope , Sr / Ca , Mg / Ca , Li / Ca and Mg / Li ratios in the scleractinian cold-water coral Lophelia pertusa, 352, 143–152, https://doi.org/10.1016/j.chemgeo.2013.06.013, 2013.

Raz, S., Weiner, S., and Addadi, L.: Formation of high-magnesian calcites via an amorphous precursor phase: Possible biological implications, 12, 38–42, https://doi.org/10.1002/(SICI)1521-4095(200001)12:1<38::AID-ADMA38>3.0.CO;2-I, 2000.

Rosenthal, Y. and Katz, A.: The applicability of trace elements in freshwater shells for paleogeochemical studies, 78, 65–76, https://doi.org/10.1016/0009-2541(89)90052-1, 1989.

Schleinkofer, N., Raddatz, J., Freiwald, A., Evans, D., Beuck, L., Rüggeberg, A., and Liebetrau, V.: Environmental and biological controls on Na/Ca ratios in scleractinian cold-water corals, 16, 3565–3582, https://doi.org/10.5194/bg-16-3565-2019, 2019.

Storm-Suke, A., Dempson, J. B., Caron, F., and Power, M.: Effects of formalin and ethanol preservation on otolith δ18O stable isotope signatures, 21, 503–508, https://doi.org/10.1002/rcm.2850, 2007.

Strzepek, K. M., Thresher, R. E., Revill, A. T., Smith, C. I., Komugabe, A. F., and Fallon, S. F.: Preservation effects on the isotopic and elemental composition of skeletal structures in the deep-sea bamboo coral Lepidisis spp. (Isididae), 99, 199–206, https://doi.org/10.1016/j.dsr2.2013.07.010, 2014.

Swart, P. K., Elderfield, H., and Greaves, M. J.: A high-resolution calibration of Sr/Ca thermometry using the Caribbean coral Montastraea annularis , 3, 1–11, https://doi.org/10.1029/2002gc000306, 2002.

Vonhof, H., Reijmer, J., Feenstra, E., and Mienis, F.: Isotope analysis of water trapped in fluid inclusions in deep sea corals, 17, 8294, 2015.

Walls, R. A., Ragland, P. C., and Crisp, E. L.: Experimental and natural early diagenetic mobility of Sr and Mg in biogenic carbonates, 41, 1731–1737, https://doi.org/10.1016/0016-7037(77)90204-6, 1977.

Yoshimura, T., Tamenori, Y., Suzuki, A., Kawahata, H., Iwasaki, N., Hasegawa, H., Nguyen, L. T., Kuroyanagi, A., Yamazaki, T., Kuroda, J., and Ohkouchi, N.: Altervalent substitution of sodium for calcium in biogenic calcite and aragonite, 202, 21–38, https://doi.org/10.1016/j.gca.2016.12.003, 2017.

Yoshimura, T., Maeda, A., Tamenori, Y., Suzuki, A., Fujita, K., and Kawahata, H.: Partitioning and chemical environments of minor elements in individual large benthic foraminifera cultured in temperature-controlled tanks, 7, 1–9, https://doi.org/10.3389/feart.2019.00124, 2019.

Yu, J., Elderfield, H., Greaves, M., and Day, J.: Preferential dissolution of benthic foraminiferal calcite during laboratory reductive cleaning, 8, https://doi.org/10.1029/2006GC001571, 2007.

Zhou, X., Rosenthal, Y., Haynes, L., Si, W., Evans, D., Huang, K.-F., Hönisch, B., and Erez, J.: Planktic foraminiferal Na/Ca: A potential proxy for seawater calcium concentration, 305, 306–322, https://doi.org/10.1016/j.gca.2021.04.012, 2021.

6 Ba/Ca, P/Ca and Mn/Ca ratios in *Acesta excavata* (Bivalvia): Valuable tools to reconstruct plankton dynamics in the deep sea?

N. Schleinkofer[1,2], J. Raddatz[1,2], D. Evans[1,2], A. Gerdes[1,2], S. Voigt[1,2]; M. Wisshak[3]

[1]Goethe University Frankfurt, Institute of Geosciences, Altenhöferallee 1, 60438 Frankfurt am Main, Germany

[2]Frankfurt Isotope and Element Research Center (FIERCE), Goethe University Frankfurt, Altenhöferallee 1, 60438 Frankfurt am Main, Germany

[3]Senckenberg am Meer, Marine Research Department, Südstrand 40, 26382 Wilhelmshaven, Germany

7.1. Introduction

Plancton dynamics are an important parameter in oceanic sciences as the amount and composition greatly influences the food web. Cold-water corals and other filtrating organisms that inhabit the same locations such as the bivalve *Acesta excavata* are greatly dependent on supply of POM (particulate organic matter) from the surface waters (White et al., 2005; Duineveld et al., 2004). Generally, surface waters above cold-water coral reefs are characterized by a higher mean surface productivity (Davies et al., 2008). While today's surface productivity can be easily determined (e.g. satellite measurement of chlorophyll (Eppley et al., 1985)), proxies for paleoenvironmental reconstructions are scarce.

Barium in the ocean behaves similary to cadmium and $\delta^{13}C$, meaning they are removed from the surface water and incorporated into sinking particles eventually dissolving deeper in the water column. Due to the covariance with Phosphor, Barium might be useful to reconstruct labile nutrient concentrations as was shown in foraminifera (Lea and Boyle, 1989). Ba/Ca ratios in bivalves are rather well researched and show potential to reconstruct phytoplankton dynamics and oceanic Ba/Ca concentrations. However, the different internal and external forcing mechanisms are not fully understood. In general Ba/Ca ratios in bivalves are characterized by stable background levels (Putten et al., 2000; Lazareth et al., 2003; Gillikin et al., 2008; Chauvaud et al., 2009; Barats et al., 2009; Gillikin et al., 2006) ,that are controlled by the aqueous Ba/Ca ratio (Gillikin et al., 2006), with sharp, intense maxima. These maxima appear to be correlated to phytoplankton blooms (Stecher et al., 1996; Lazareth et al., 2003; Putten et al., 2000) but further research revealed that they cannot be used as a direct proxy for seawater Ba/Ca or phytoplankton activity (Gillikin et al., 2006, 2008). The Ba/Ca signal in the bivalve calcite/aragonite does not appear to derive from ingested phytoplankton, but instead are a product of processes that happen during the phytoplankton decay (Gillikin et al., 2006). However, even if Ba/Ca ratios are more controlled by decay processes, valuable information about plankton dynamics are still possible to gather. Besides phytoplankton dynamics as an external forcing mechanism, biological factors that control Ba/Ca ratios in bivalves are evident. Interestingly bivalves show similar Ba/Ca ratios regardless if the shell is built from aragonite or calcite indicating that the D_{Ba} is predominantly controlled by biological or chemical effects within the extrapallial fluid (Elliot et al., 2009). Additionally, in other organisms such as the zooxanthelate coral *Porites lutea*, stress is discussed as a factor controlling Ba/Ca ratios (Chen et al., 2011). Similar effects are also known from bivalves regarding Mg/Ca ratios (Lorens and Bender, 1980; Wanamaker and Gillikin, 2019).

Only a few studies have measured Mn/Ca ratios in bivalves in order to relate them to environmental or biological mechanisms. Manganese is a redox-sensitive element, which is mainly present as Mn^{2+} in seawater. Under oxygenated conditions, Mn^{2+} is easily oxidized to Mn-oxyhydroxides causing it to precipitate. Under low-oxygen conditions Mn is reduced which causes the concentration of Mn^{2+} to increase, which also increases its bioavailability (Tribovillard et al., 2006). Therefore, Mn/Ca ratios hold potential to be used as a redox/oxygen concentration proxy Mn/Ca ratio in *Isognomon ehippium*, from a mangrove setting, where suggested to be related to phytoplankton blooms caused by increased riverine discharge (Lazareth et al., 2003). Shell Mn/Ca in *Mytilus edulis* from the Netherlands showed a seasonal cyclicity with high values in late spring that were also considered to be related to primary productivity (Putten et al., 2000). Phytoplankton blooms in the Menai Street (Great Britain) however preceded the Mn/Ca maxima and therefore cannot constitute the major control. Instead, it is proposed that shell Mn/Ca ratios reflect the seawater Mn concentration (Freitas et al., 2006). A correlation with phytoplankton activity however, is still very plausible since the amount of dissolved Mn in the ocean is controlled by the redox conditions (Landing and Bruland, 1987) and decaying organic matter from phytoplankton could consume oxygen and therefore change the redox potential. Additional influences could derive from riverine input, diffusion from shelf sediments and atmospheric particles as these processes constitute the main input flux for Mn into the ocean (Bender et al., 1977)

P/Ca ratios are barely researched, despite the importance of Phosphor in every biological process. In corals the usability of P/Ca as a nutrient proxy and potential use to reconstruct water mass dynamics is discussed (Anagnostou et al., 2011; LaVigne et al., 2010; Montagna et al., 2006). In bivalves, this has not been researched but P/Ca ratios might also be useful to locate organic rich growth lines (Cusack et al., 2008). This is also possible using Mutvei solution (Schöne et al., 2005b) but some bivalves such as *Acesta excavata* do not show good visible growth lines after Mutvei treatment. Additionally, the Mutvei solution possibly destroys the sample for further geochemical investigations due to the influence of Alcian blue and glutaraldehyde. Therefore, P/Ca ratios might constitute a way to locate growth lines in bivalves with bad growth line visibility and without potentially destroying the sample. This might also hold true for Mn/Ca ratios which show high concentrations in organic rich layers (Takesue et al., 2008).

Here we present Ba/Ca, Mn/Ca and P/Ca ratios from *Acesta excavata* measured by LA-ICP-MS on samples from two cold-water coral reefs inshore and offshore the Norwegian margin. Environmental data derives from two landers that were deployed in near proximity to the reefs as well as satellite-based chlorophyll data from MODIS AQUA (NASA Goddard Space Flight Center, 2018)

7.2. Methods

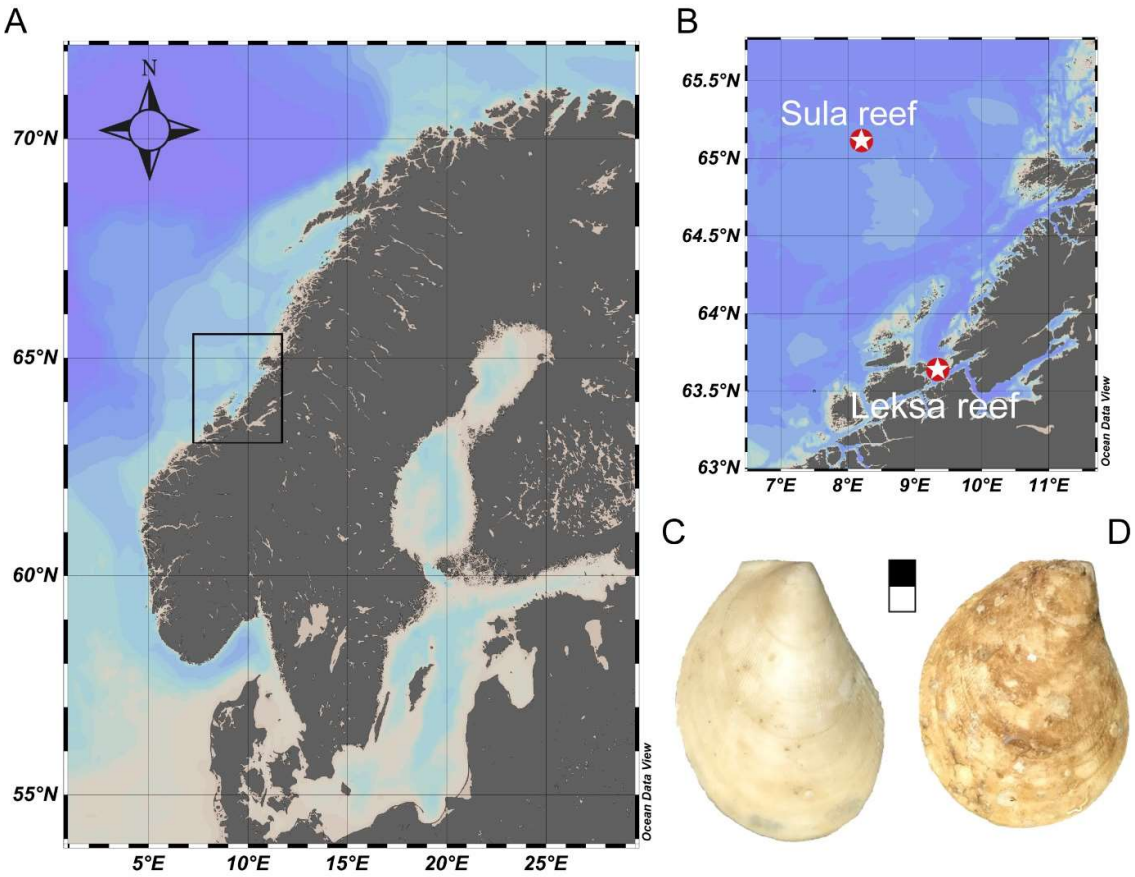

Figure 6-1 Map of sampling location and examples of two specimen. B shows an enlarged section marked by the square in A. C and D show two collected specimens from the Sula reef and Leksa reef, respectively. The scalebar is 2 cm long.

7.2.1. Sampling location & samples

The samples were collected in two distinct reefs in the northeast Atlantic along the Norwegian coast (Fig. 1). In total four samples were measured for their chemical composition, four were collected in north of the island Leksa at the entrance of the Trondheimfjord and four were collected in the Sula reef on the Norwegian margin. The shells were collected in august 2014 with the submersible JAGO during cruise POS473. After collection the shells were physically cleaned from organic material and dried in an oven.

The samples for laser ablation were cut with a handheld Dremel tool. Strips of 8mm width and 20 mm length were cut from the youngest shell section (ventral shell section). These strips were ultrasonically cleaned for 5 minutes and allowed to dry. Samples strips were placed sideways in plastic rings, moulded with epoxy resin. The surface to be ablated was ground and polished.

7.2.2. LA-ICP-MS

The measurement configuration consists of a Thermo-Scientific ELEMENT II sector field ICP-MS coupled to a Resolution M50 193 nm ArF Excimer Laser system (Resonetics). Ablation was conducted with 72 µm spot size, 10 µm/s scan speed and 10 Hz repetition rate. Before ablation the samples were ultrasonically cleaned in ethanol. Additionally, a fast cleaning pass was executed before each track measurements to further clean the material to be ablated.

Tracks were measured in the uppermost calcitic fibrous shell section (0.1 mm below the surface). Measured tracks are around 20 mm long which results in ablation times of roughly 30 minutes per track. All elements were measured in medium resolution in order to resolve molecular interferences ion (e.g. $N\text{-}O^+$ and $N\text{-}O\text{-}H^+$) which is especially important for the P/Ca measurements. We used the NIST SRM 612 glass as an external standard and NIST SRM 610 glass was used to measure instrumental accuracy. These non-matrix matched standards are suboptimal because of matrix dependant fractionation. However, these are minimized when using 193 nm lasers (Longerich et al., 1996; Guillong et al., 2003; Hathorne et al., 2008). We used a spreadsheet-based software for data reduction, including blank subtraction, normalization to Ca^{43} and finally standardization. Accuracy is calculated through repeated measurements of the NIST SRM 610 glass (n=3) and amounts to: Ba/Ca = 1.61 ± 0.05 mmol/mol (1.62 mmol/mol (Jochum et al., 2011)), Mn/Ca = 4.04 ± 0.09 mmol/mol (3.98 mmol/mol (Jochum et al., 2011)) and P/Ca = 6.14 ± 0.16 mmol/mol (6.56 (Jochum et al., 2011)). Accordingly, the accuracy for Ba/Ca and Mn/Ca is within 5% and for P/Ca within 10%. Precision (1SD) is better than ± 3% for all measured elements. Measurements were conducted in one consecutive session that took 5h to complete

7.3. Results

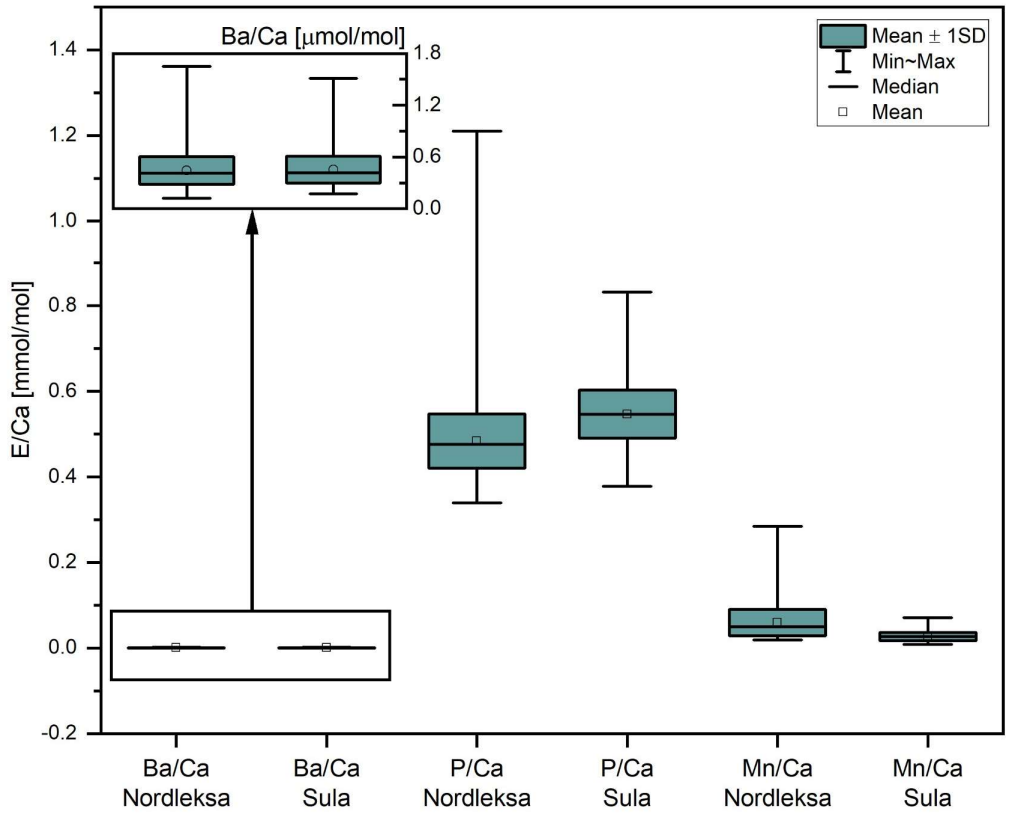

Figure 6-2 Ba/Ca, P/Ca and Mn/Ca ratios in Bivalve shells from the two investigated reefs. Ba/Ca ratios show no differences between the two reefs. P/Ca ratios are higher in the Sula reef but show a higher variability in the Leksa reef. Mn/Ca ratios from the Leksa reef also show higher variability as well as higher values in general.

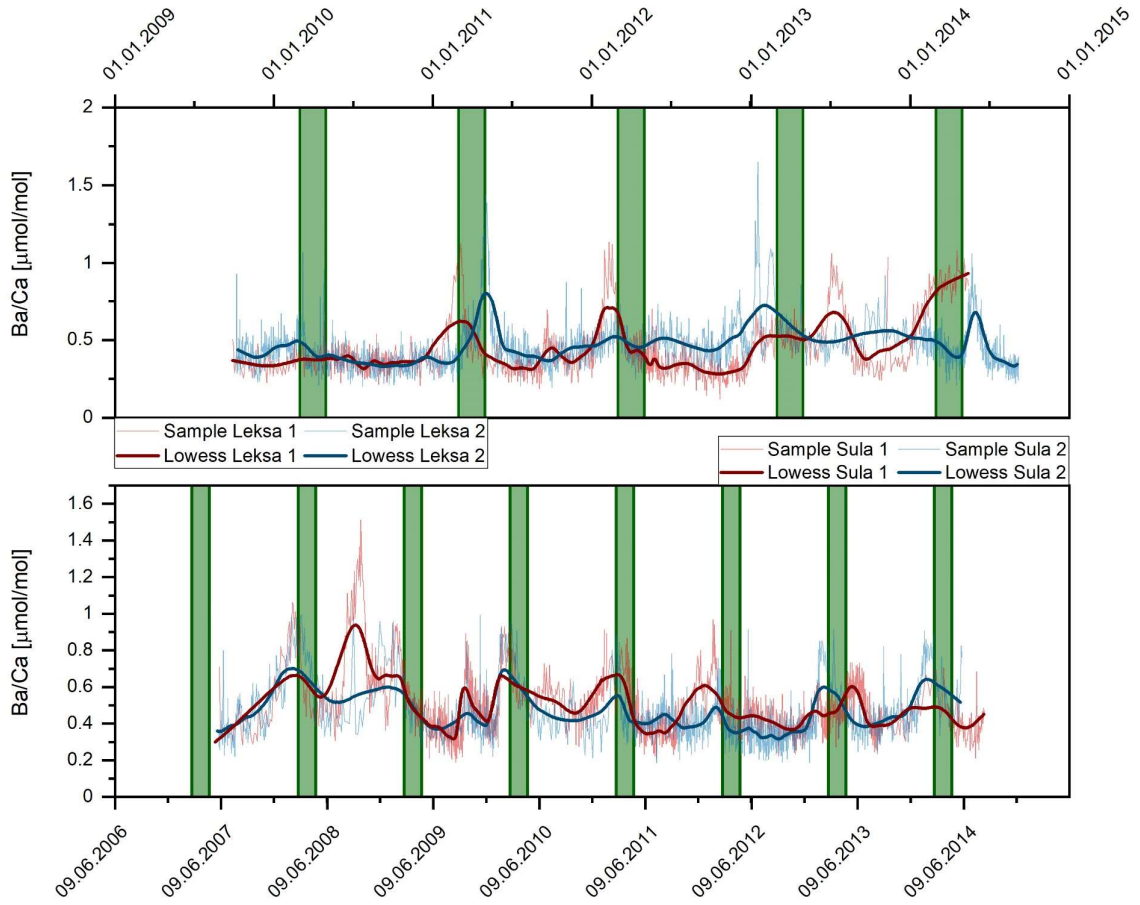

Figure 6-3 Ba/Ca ratios in Bivalve shells from the two investigated reefs. Inter-individual synchronicity is clearly visible in the samples. Green lines show major plankton blooms (Wassmann et al., 1996). Ba/Ca peaks are usually found in times of these blooms

Ba/Ca ratios in the investigated samples vary between 0.12 and 2 µmol/mol with a mean of 0.45 µmol/mol. These ratios are in acceptance with other studies which report ratios of 0.24-4.5 µmol/mol (Barats et al., 2009; Chauvaud et al., 2009). The overall trend however is greatly different from other studies where Ba/Ca ratios are characterized by stable baselevels with irregularly occurring sharp peaks (e.g. (Barats et al., 2009; Gillikin et al., 2008; Putten et al., 2000). While the sharp peaks are observable in every sample, the baselevels in these studies samples are much less stable and show a more cyclic trend. Differences in the baselevels or absolute increases are absent between the two locations.

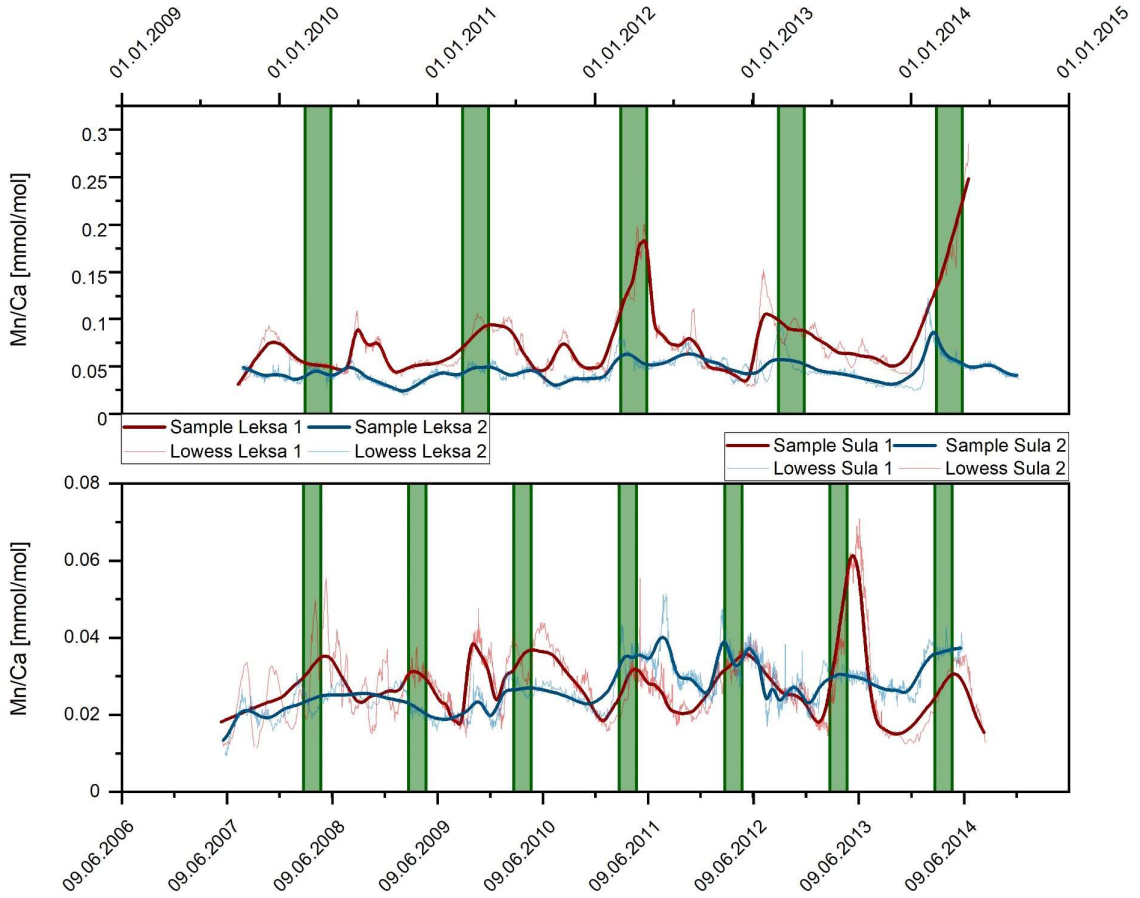

Figure 6-4 Mn/Ca ratios in Bivalve shells from the two investigated reefs. Inter-individual synchronicity is clearly visible in the samples. Green lines show major plankton blooms (Wassmann et al., 1996).

Mn/Ca ratios in all samples show seasonal cycles with great variability from 0.008 – 0.285 mmol/mol which is in acceptance with other published values (0.014 – 0.11 mmol/mol (Freitas et al., 2006)). Mn/Ca ratios in samples from the Trondheimsfjord are higher than in samples from the Sula reef and show higher variability (mean 0.059 vs. 0.027 mmol/mol; STD 0.03 vs. 0.01 mmol/mol). Mn/Ca peaks are often accompanied by Ba/Ca peaks but Mn/Ca peaks are slightly phase shifted and occur after the corresponding Ba/Ca peaks. Despite this correlation, the relative increase of corresponding Mn/Ca and Ba/Ca is independent from each other.

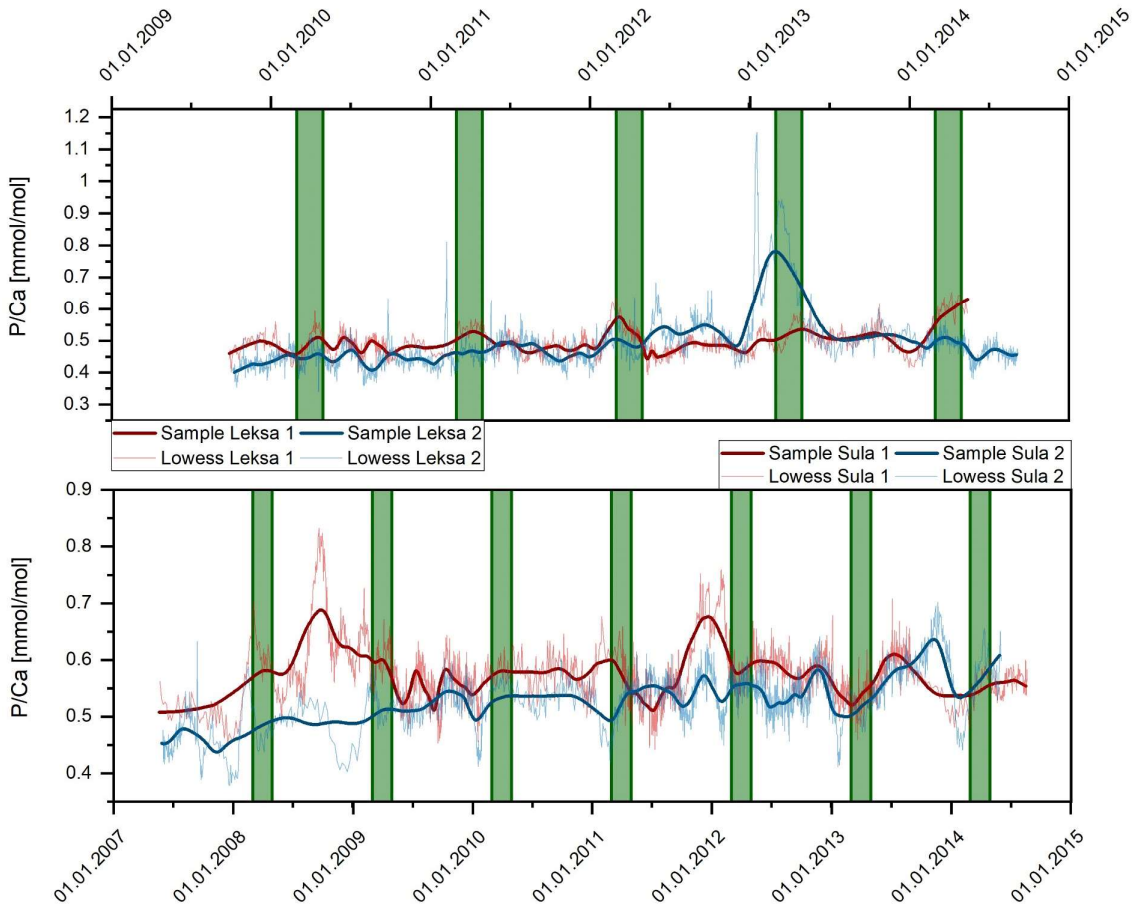

Figure 6-5 P/Ca ratios in Bivalve shells from the two investigated reefs. Inter-individual synchronicity is clearly visible in the samples. Green lines show major plankton blooms (Wassmann et al., 1996)

P/Ca ratios in the investigated shells vary between 0.34 – 1.2 mmol/mol. *Mytilus galloprovincialis* is reported to have much higher phosphorus concentrations of 1510 to 4680 ppm (5 – 15 mmol/mol (Hahn et al., 2011)). Sample 16R (Sula 2 in Fig. 5) shows a trend to higher P/Ca ratios with ongoing ontogeny but the other samples do not follow this trend. In general, there is no reoccurring pattern perceptible that is common for all the samples. Sample 14 R shows low frequency variability whereas samples 1R and 11R are characterized by higher frequency variability. Sample 11R additionally shows a very high and sharp peak, a feature only visible in this sample.

Correlations between the observed E/Ca ratios are mostly absent. Only the samples from the Sula reef show weak linear correlations between P/Ca and Mn/Ca (R = 0.3), Ba/Ca and Mn/Ca (R = 0.22). Additionally, Ba/Ca and P/Ca from all samples show a weak linear correlation (R = 0.27)

7.4. Discussion

7.4.1. Detecting growth structures with P/Ca ratios

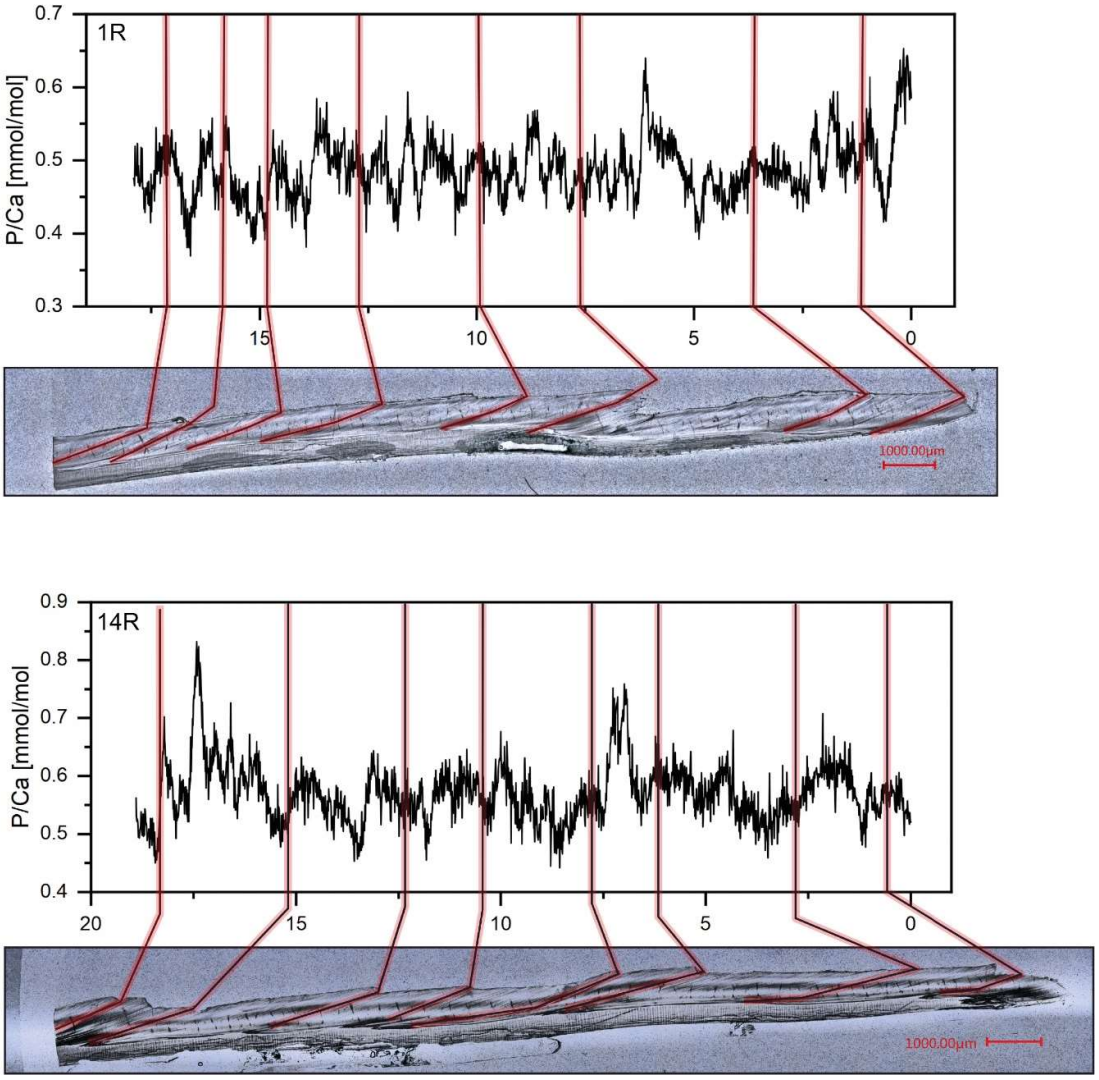

Figure 6-6 Light microscopic images of Samples 1R (Leksa) and 14R (Sula) and P/Ca ratios. Red lines show visible growth lines. Significant increases in P/Ca ratios are not visible in the vicinity of these growth lines.

As growth structures such as yearly built growth lines are usually characterized by increased concentration of organic matter, which is embedded in the skeleton during phases of low calcification (Schöne et al., 2010, 2005a), P/Ca ratios might be a convenient tool to locate these areas. However, the P/Ca records show no distinct, characteristic maxima in the vicinity of growth lines (Fig. 2) as would be expected. Instead, we recognize that the growth lines on the shell are often located shortly after a P/Ca minimum. Consequently, the organic matrices that are concentrated in the area of growth lines is not strongly phosphorylated

and/or external mechanisms overlay this increasing effect of phosphorylated regions. While we cannot give information about proteins that are utilized specifically by *A. excavata* for calcification purposes, studies show that phosphorylated proteins are common in different bivalves and that the phosphor groups fulfil an important role in controlling the calcification process (Halloran and Donachy, 1995; Rusenko et al., 1991; Samata et al., 2008). Therefore, P/Ca ratios must be controlled to a higher degree by external factors or biological/mineralogical factors other than shell organic matrix concentration. Further control mechanisms are discussed in the coming sections.

7.4.2. Factors controlling elemental incorporation

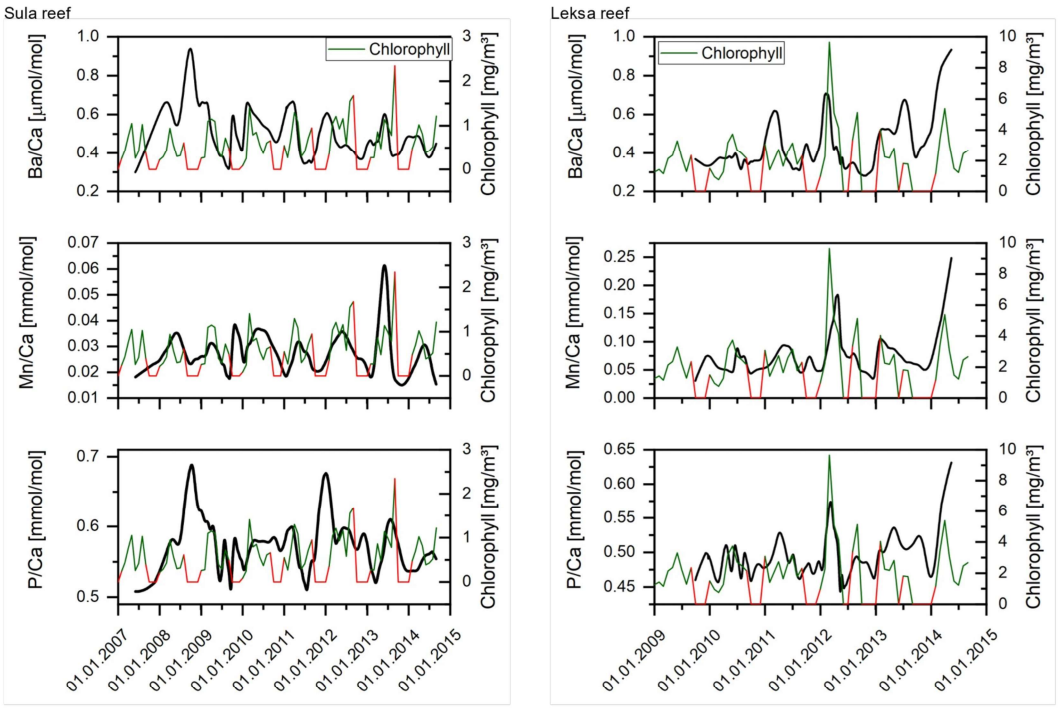

Figure 6-7 E/Ca ratios of Samples 1R (Leksa) and 14R (Sula) and chlorophyll concentrations from MODIS AQUA. Red lines show immeasurable chlorophyll concentrations due to cloud overcast. Each E/Ca ratio shows synchronous peaks with the chlorophyll concentration.

7.4.2.1. Ba/Ca

Ba/Ca ratios show no significant differences between the two observed reefs. Samples from the Sula reef show a good correlation (R^2=0.61) which indicates an external forcing mechanism. The correlation between the samples from the Nordleksa reef is generally weak (R^2=0.24) but still contemporous peaks are obvious. While Ba/Ca background levels are considered to record the concentration of Ba in the surrounding water (Gillikin et al., 2006;

Tabouret et al., 2012; Barats et al., 2009), Ba/Ca peaks are argued to be linked to primary productivity (Stecher et al., 1996; Putten et al., 2000; Lazareth et al., 2003).

Norwegian fjords usually experience phytoplankton blooms in March-April (Wassmann et al., 1996). A second bloom happens in autumn but it is not as regular as the spring bloom, due to light limitations and dependency on high riverine discharge (Sakshaug and Myklestad, 1973). Our results reveal that maximum Ba/Ca ratios in every investigated bivalve are reached during February-March. This in acceptance with the occurring phytoplankton blooms. Barium is probably quickly released at the end of the bloom due to decay of the planktonic organisms (Stecher and Kogut, 1999). Especially organic rich, siliceous microenvironments formed by decaying assemblies of diatoms have the potential to form barite which is then transported to the sediment surface (Stecher et al., 1996). The bivalves can take up these barite crystals by ingestion if they are covered by organic matter, as bivalves have the ability to distinguish between organic and inorganic matter(Bricelj and Malouf, 1984). This behaviour could also explain why not every phytoplankton bloom results in an adjacent Ba/Ca peak. If the barite crystals are not surrounded by organic material (possible consumption through microorganisms in the water column) the bivalve will probably reject the ingestion.

As the bivalves do not directly react to the plankton bloom but instead to decay products, the Ba/Ca response in the shell cannot be correlated to the bloom dimension (Gillikin et al., 2006; Stecher et al., 1996; Barats et al., 2009). Additionally, besides phytoplankton activity, other processes can induce changes to the Barium concentration in the water. One example is terrestrial input through rivers, as river and groundwaters are enriched in barium compared to ocean water (Hanor, 2019). As ocean water are usually rich in sulphate, increased terrestrial input could trigger barite formation which is then recorded in the bivalve shell. If the barite particles are not ingested, they accumulate at the sediment surface where oxygen depletion could lead to remineralization of the barite and consequent increase of solved barium. Shells from the Leksa reef show a lesser degree of correlation than shells from the Sula reef. This could be an effect of rivers draining into the Trondheimsfjord. The formed barite through riverine input can be remobilized through oxygen depletion which would increase the bioavailability and could lead to increased Ba/Ca ratios in the shell without a contemporous plankton bloom.

Problematic with the explanation of shell Ba/Ca control through diatom activity is that we do not observe differences in Ba/Ca ratios between the two observed reefs despite seeing significant differences in the chlorophyll concentration. This holds also true for the mentioned riverine input of Ba. Due to the rivers that drain into the Trondheimsfjord we would expect higher barium input and consequent higher shell ratios which is not the case. The rivers

Orkla and Nidelva which drain into the Trondheimsfjord reach their maximum discharge in May-June, two to three months after the maximum Ba/Ca peaks. Riverine barium input seems therefore negligible as a control mechanism. Additionally, sometimes the Ba/Ca maxima occur before the measured chlorophyll maxima. This is also true for the reported blooms by Wassman et al., 1996, who report maximum blooms in March-April whereas chlorophyll maxima occur in April-May. One explanation for this is that our constructed time-series is not perfect. As we interpolate the months between each growth line, there are possibly errors, as growth rates in between those growth lines are not constant. In addition, the measured chlorophyll values only relate to chlorophyll-a, whereas diatoms possess more chlorophyll-c than chlorophyll-a (Alberte et al., 1981). The maximum chlorophyll values are therefore probably more controlled by subsequent blooms of *Phaenocystis sp.* and other plankton species that only utilize chlorophyll-a. Weak chlorophyll increases probably caused by diatom blooms are visible in February.

7.4.2.2. Mn/Ca

Manganese is a redox-sensitive element, which is mainly present as Mn^{2+} in seawater. Under oxygenated conditions, Mn^{2+} is easily oxidized to Mn-oxyhydroxides causing it to precipitate. Under low-oxygen conditions Mn is reduced which causes the concentration of Mn^{2+} to increase, which also increases its bioavailability (Tribovillard et al., 2006). Therefore, Mn/Ca ratios hold potential to be used as a redox/oxygen concentration proxy. A striking feature of the Mn/Ca measurements is the difference between the two observed locations. Mean Mn/Ca ratios in the Nordleksa Reef are roughly twice as high as in the Sula Reef and maximum values are nearly four times higher. CTD measurements from both locations conducted in Summer 2018 show that both reefs are well oxygenated with 6.0 ml/l and 6.14 ml/l in Nordleksa and Sula, respectively. While the Sula reef is probably well oxygenated and stable throughout the year, the Nordleksa reef may experiences a higher variability in the oxygen concentration. This could be caused by a sill that elevates up to -90m water depth and restricts the exchange of water with the open ocean. An exchange of deep-water is therefore restricted to spring and autumn (Jacobson, 1983; Strømgren, 1974). Since our oxygen measurements, that were conducted between the water renewal, show that the bottom water is well oxygenated, we would decline oxygen concentration as a suitable explanation for the variability in Mn/Ca ratios. However, the degradation of organic material consumes oxygen and can therefore cause a local decrease of the oxygen concentration and therefore might contribute to variations in Mn/Ca ratios. It was also suggested that weak current speed and increased nutrient supply from surface waters due to plankton blooms could both decrease the oxygen replenishment in a CWC-reef while simultaneously increasing the oxygen demand of the corals (Guihen et al., 2018). This caused daily oxygen

anomalies of -0.5 mg/l ion the Tisler reef (Guihen et al., 2018) and could therefore also influence the reduction of Mn and increase incorporation in the bivalve shell.

A control of Mn/Ca ratios through plankton blooms is suggested by (Putten et al., 2000; Carroll et al., 2009). Increases in suspended particulate Mn can be caused by two processes. On one hand algae efficiently take up Mn and concentrate it intracellularly due to its role in the oxidization of water during photosynthesis (Sunda and Huntsman, 1985). On the other hand, Photosynthesis can also generate high pH microenvironments in dense algal populations, especially in colonies of *Phaenocystis*, which causes the formation of insoluble Mn oxides (Richardson and Stolzenbach, 1995; Richardson et al., 1988; Lubbers et al., 1990). As we do observe contemporous peaks in shells from the same location which occur during spring, in times of the major plankton blooms, these peaks are possibly caused by the ingestion of Mn-enriched algal particles. A control through plankton activity does also explain the generally lower Mn/Ca ratios in shells from the Sula reef. Chlorophyll concentrations from the Sula reef are much lower than measured in the Trondheimsfjord, indicating a reduced plankton activity. However, it is not completely clear if bivalves take up Mn in form of particulate matter (Lazareth et al., 2003; Putten et al., 2000) or through the dissolved form (Freitas et al., 2006).

Mn/Ca ratios in bivalves can also be altered by changing the flux of Manganese into the water. The most important influx sources for manganese into the ocean are aeolian dust and riverine input (van Hulten et al., 2016). Since several large rivers drain into the Trondheimsfjord (Orkla, Gaula, Nidelva, Stjørdalselva, Verdal-selva and Steinkjerelva) the influx of manganese can vary based on precipitation in the source areas. As the influx of freshwater into the Trondheimsfjord is greater than in the Sula reef we would expect higher Mn/Ca ratio in Nordleksa. A feature that is clearly visible in our dataset. An influence of the Mn concentration in seawater on the Mn/Ca ratios in *A. excavata* is therefore evident.

In addition to exogenic effects, biological effects are discussed to control the incorporation of Mn into the shell of bivalves. Mn/Ca ratios in the EPF of four different bivalve species (not including *A. excavata*) were higher during periods of increased growth compared to periods of reduced growth (Wada, 1976). If we accept a simple linear relationship between Mn/Ca ratios in the EPF and Mn/Ca ratios of the shell, Mn/Ca ratios in the shell must ultimately increases during periods of high growth. This can be explained based on the model for trace metal incorporation as suggested by Carre et al. (2006). They suggest that trace metal ions are transported into the EPF through Ca-channels. As the selectivity for Ca-ions of these channels decreases with an increased ion flux, Mn transport into the EPF would increase at higher growth rates (Carré et al., 2006).

7.4.2.3. P/Ca

Similar to Mn/Ca ratios, P/Ca ratios do show significant differences between the two investigated reefs. In the Sula Reef mean P/Ca ratios are higher than in the Nordleksa Reef but the overall variability is higher in the Nordleksa reef. We are not aware of other studies that researched P/Ca ratios in bivalves, but experiments with radioactive labelled phosphorous and its accumulation in the different body parts of bivalves indicate that phosphorous is mainly ingested by filtration and only to 0.5% through dissolved Phosphorous in the water (Allen, 1970; Kuenzler, 1961). However, the amount taken up from solution is not negligible in times of short food supply (Allen, 1970). As we do observe higher mean P/Ca ratios in shells from the Sula reef despite showing lower chlorophyll concentrations, P/Ca ratios cannot be controlled through phytoplankton activity.

The main uptake mechanism through particles indicates a potential control through plankton activity. As we observe lower mean P/Ca ratios in the Trondheimsfjord despite the higher chlorophyll values compared to the Leksa reef, a strong control through phytoplankton activity seems improbable. However, other planktonic species could contribute to P/Ca signals in bivalve shells. This species should occur after the main spring diatom bloom. One possibility would be the already mentioned *Phaeocystis* as it is proposed that they only start to bloom after the main diatom bloom (Larsen et al., 2004), when Si is leached from the ambient water through the growth of the diatoms (Egge and Aksnes, 1992). However, like diatoms, this species is photoautotroph (Weisse et al., 1994) and can therefore not explain the P/Ca differences between the reefs given the differences in chlorophyll concentration. Another possibility would be zooplankton that feeds on diatoms and other photoautotrophic organisms and therefor reaches its maximum quantity after the diatom bloom (Weisse et al., 1994). While it is difficult to imagine that zooplankton abundance should be higher in the Sula reef compared to the Leksa reef, it was observed in the Beaufort Sea that some species increase in abundance with higher distance to the coast line (Darnis et al., 2008). This was attributed to differences in the feeding strategy (herbivore, omnivore, carnivore) and concerns species such as *Cyclopina* sp., *Oncaea borealis* and *Microcalanus pygmaeus* (Darnis et al., 2008), all of which are also present in Norwegian marine waters (Wiborg, 1954). We cannot give a definitive answer on this question but we would assume that like Ba/Ca ratios, P/Ca ratios might be controlled partly through the abundance of Zooplankton.

In addition to possible external effects, little is known about the incorporation of phosphor into biogenic calcite and possible controlling factors. The amount of incorporated phosphor in inorganic calcite was shown to be reliant on the phosphor concentration in the parent solution (Ishikawa and Ichikuni, 1981; Kitano et al., 1978). Since bivalves do not directly calcify from the seawater but instead the internal EPF an easy linear relationship between seawater and shell phosphor concentration is questionable. Temperature had no significant

effects on phosphor incorporation in inorganic calcite, but a pH and calcification rate had (House and Donaldson, 1986). As phosphor is incorporated in exchange for carbonate ions (3 CO^{2-}_3 ↔ 2 PO^{3-}_4) a control through carbonate vacancies as observable for Na-incorporation is excludable (Kitano et al., 1975; Yoshimura et al., 2017, 2019).

7.4.2.4. Sequence of E/Ca peaks

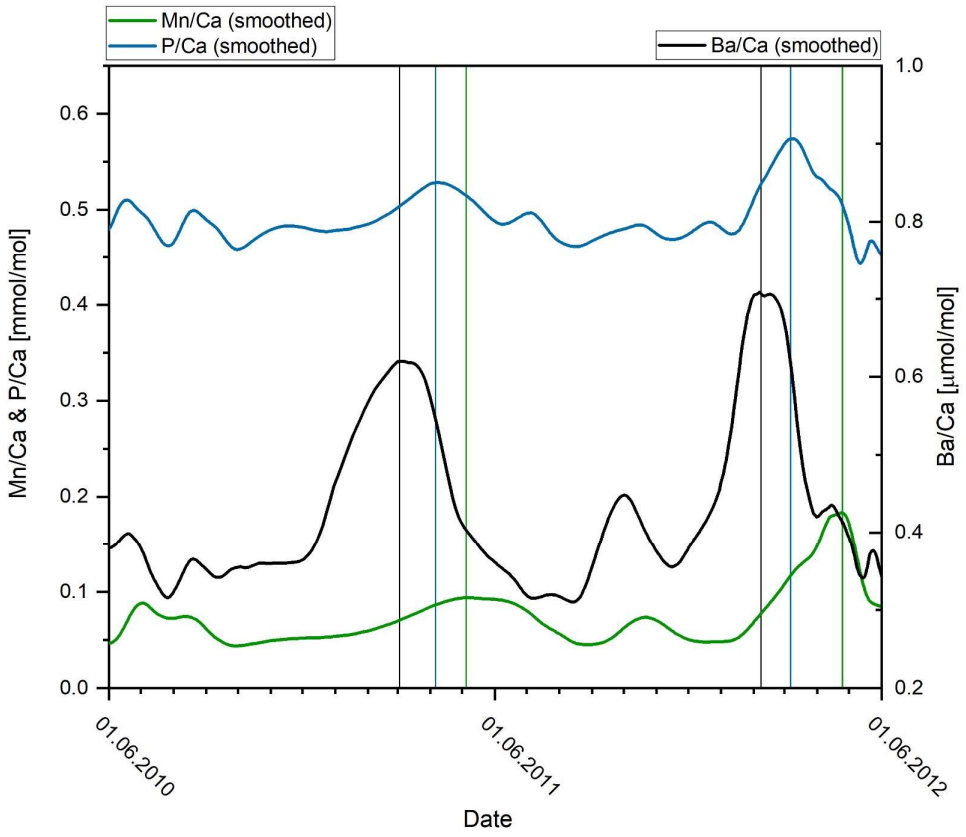

Figure 6-8 Common sequence of E/Ca peaks. The Sequence starts with a peak in Ba/Ca followed by a peak in P/Ca and Mn/Ca

Even though we do not observe general correlation between different elemental ratios, we can clearly observe similar trends. Quasi-contemporous peaks between all E/Ca ratios are observable however, they are always slightly phase shifted from each other. The sequence generally starts with a peak in Ba/Ca, followed by a peak in P/Ca. These peaks are variable in their respective timing. Often a smaller P/Ca peak is also visible prior to the Ba/Ca peak. Lastly the Mn/Ca peak develops. This peak is mostly less pronounced and sometimes completely missing.

We propose that Ba/Ca and P/Ca are mostly controlled through plankton dynamics, but by different planktonic species that show a sequential occurrence during blooms. As presented, we propose that Ba/Ca peaks are controlled by decay-products of diatom blooms. Diatom

blooms in Norwegian coastal water are accompanied by blooms of other planktonic organisms. Prior and after the diatom blooms, autotrophic picoeukaryotes, *Phaeocystis* sp. and the cyanobacterium *Synechococcus sp.* increase in abundance and contribute a large part to the local primary productivity (Larsen et al., 2004; Erga et al., 2005). Additionally, Zooplankton blooms occur after the main phytoplankton spring blooms (Weisse et al., 1994). Sinking and ingestion of these particles as nutrition from the bivalve could then lead to increased P/Ca ratios in the bivalve's shell. A response could also be triggered when the plankton accumulates on the ocean floor. Decay processes could mobilize phosphor and lead to locally increased phosphor concentrations and to consequent increases in the bivalve's shell. Even though Mn/Ca maxima occur after P/Ca maxima, the onset of the increase is simultaneous. We propose that Mn/Ca maxima are caused by Mn-rich aggregates that are formed in high-pH microenvironments produced by dense *Phaeocystis* colonies (Lubbers et al., 1990; Richardson and Stolzenbach, 1995; Richardson et al., 1988), a plankton group that is also common in Norwegian coastal waters (Passow and Wassmann, 1994). As this plankton groups appears to be reliant on soil extracts to grow (Kornmann, 1955) we would expect lower abundances away from the coastline (Sula reef) which would explain the lower observable Mn/Ca ratios in the shells from this location.

7.5. Conclusion

Based on the results of this study we propose that Ba/Ca, Mn/Ca and P/Ca ratios in the calcitic shell section of *Acesta excavata* are to a large degree controlled by plankton dynamics. High Ba/Ca maxima are possibly caused by Ba-rich particles that are formed by decaying diatoms during spring phytoplankton blooms. The amount of Ba/Ca increase is not consistent with chlorophyll concentrations; therefore Ba/Ca ratios cannot be used to reconstruct absolute phytoplankton concentrations but might be used to reconstruct the timing of occurring blooms.

P/Ca ratios that increase shortly after the Ba/Ca maxima are potentially caused by similar effects as Ba/Ca ratios but triggered by the growth of plankton groups other than diatoms such as *Phaeocystis* sp. or zooplankton species. While we expected that P/Ca ratios might be usable to locate growth lines in the shells, we have to refute this hypothesis.

As *Phaeocystis* colonies are known to create microenvironments suitable for the formation of Mn-aggregates, simultaneous increases in P/Ca and Mn/Ca might be an effect of increased abundances of this plankton group. Additionally, Mn/Ca ratios can also be altered through variations of the oxygen concentration caused by the decay of these organisms or through oxygen consumption of adjacent cold-water corals. Increased nutrient availability in combination with slow water replacement, could increases oxygen consumption of the corals

while also decreasing oxygen replenishment. This would increase Mn mobilization and increase the bioavailability

7.6. References

Alberte, R. S., Friedman, A. L., Gustafson, D. L., Rudnick, M. S., and Lyman, H.: Light-harvesting systems of brown algae and diatoms. Isolation and characterization of chlorophyll a c and chlorophyll a fucoxanthin pigment-protein complexes, 635, 304–316, https://doi.org/10.1016/0005-2728(81)90029-3, 1981.

Allen, J. A. A.: Experiments on the uptake of radioactive phosphorous by bivalves and its subsequent distribution within the body, 36, 131–141, https://doi.org/10.1016/0010-406X(70)90659-6, 1970.

Anagnostou, E., Sherrell, R. M., Gagnon, A., LaVigne, M., Field, M. P., and McDonough, W. F.: Seawater nutrient and carbonate ion concentrations recorded as P/Ca, Ba/Ca, and U/Ca in the deep-sea coral Desmophyllum dianthus, 75, 2529–2543, https://doi.org/10.1016/j.gca.2011.02.019, 2011.

Barats, A., Amouroux, D., Chauvaud, L., Pécheyran, C., Lorrain, A., Thébault, J., Church, T. M., and Donard, O. F. X.: High frequency Barium profiles in shells of the Great Scallop Pecten maximus: A methodical long-term and multi-site survey in Western Europe, 6, 157–170, https://doi.org/10.5194/bg-6-157-2009, 2009.

Bender, M. L., Klinkhammer, G. P., and Spencer, D. W.: Manganese in seawater and the marine manganese balance, 24, 799–812, https://doi.org/10.1016/0146-6291(77)90473-8, 1977.

Bricelj, V. M. and Malouf, R. E.: Influence of algal and suspended sediment concentrations on the feeding physiology of the hard clam Mercenaria mercenaria, 84, 155–165, https://doi.org/10.1007/BF00393000, 1984.

Carré, M., Bentaleb, I., Bruguier, O., Ordinola, E., Barrett, N. T., and Fontugne, M.: Calcification rate influence on trace element concentrations in aragonitic bivalve shells: Evidences and mechanisms, 70, 4906–4920, https://doi.org/10.1016/j.gca.2006.07.019, 2006.

Carroll, M. L., Johnson, B. J., Henkes, G. A., McMahon, K. W., Voronkov, A., Ambrose, W. G., and Denisenko, S. G.: Bivalves as indicators of environmental variation and potential

anthropogenic impacts in the southern Barents Sea, 59, 193–206, https://doi.org/10.1016/j.marpolbul.2009.02.022, 2009.

Chauvaud, L., Helguen, L., Clavier, J., Pe, C., Thébault, J., L'Helguen, S., Barats, A., Jacquet, S., Pécheyran, C., and Amouroux, D.: Barium and molybdenum records in bivalve shells: Geochemical proxies for phytoplankton dynamics in coastal environments?, 54, 1002–1014, 2009.

Chen, T., Yu, K., Li, S., Chen, T., and Shi, Q.: Anomalous Ba/Ca signals associated with low temperature stresses in Porites corals from Daya Bay, northern South China Sea, 23, 1452–1459, https://doi.org/10.1016/S1001-0742(10)60606-7, 2011.

Cusack, M., Dauphin, Y., Cuif, J. P., Salomé, M., Freer, A., and Yin, H.: Micro-XANES mapping of sulphur and its association with magnesium and phosphorus in the shell of the brachiopod, Terebratulina retusa, 253, 172–179, https://doi.org/10.1016/j.chemgeo.2008.05.007, 2008.

Darnis, G., Barber, D. G., and Fortier, L.: Sea ice and the onshore-offshore gradient in pre-winter zooplankton assemblages in southeastern Beaufort Sea, 74, 994–1011, https://doi.org/10.1016/j.jmarsys.2007.09.003, 2008.

Egge, J. K. and Aksnes, D. L.: Silicate as regulating nutrient in phytoplankton competition, 83, 281–289, https://doi.org/10.3354/meps083281, 1992.

Elliot, M., Welsh, K., Chilcott, C., McCulloch, M., Chappell, J., and Ayling, B.: Profiles of trace elements and stable isotopes derived from giant long-lived Tridacna gigas bivalves: Potential applications in paleoclimate studies, 280, 132–142, https://doi.org/10.1016/j.palaeo.2009.06.007, 2009.

Erga, S. R., Aursland, K., Frette, Ø., Hamre, B., Lotsberg, J. K., Stamnes, J. J., Aure, J., Rey, F., and Stamnes, K.: UV transmission in Norwegian marine waters: Controlling factors and possible effects on primary production and vertical distribution of phytoplankton, 305, 79–100, https://doi.org/10.3354/meps305079, 2005.

Freitas, P. S., Clarke, L. J., Kennedy, H., Richardson, C. A., and Abrantes, F.: Environmental and biological controls on elemental (Mg/Ca, Sr/Ca and Mn/Ca) ratios in shells of the king scallop Pecten maximus, 70, 5119–5133, https://doi.org/10.1016/j.gca.2006.07.029, 2006.

Gillikin, D. P., Dehairs, F., Lorrain, A., Steenmans, D., Baeyens, W., and André, L.: Barium uptake into the shells of the common mussel (Mytilus edulis) and the potential for estuarine paleo-chemistry reconstruction, 70, 395–407, https://doi.org/10.1016/j.gca.2005.09.015, 2006.

Gillikin, D. P., Lorrain, A., Paulet, Y. M., André, L., and Dehairs, F.: Synchronous barium peaks in high-resolution profiles of calcite and aragonite marine bivalve shells, 28, 351–358, https://doi.org/10.1007/s00367-008-0111-9, 2008.

Guihen, D., White, M., and Lundälv, T.: Zooplankton drive diurnal changes in oxygen concentration at Tisler cold-water coral reef, 37, 1013–1025, https://doi.org/10.1007/s00338-018-1711-0, 2018.

Guillong, M., Horn, I., and Günther, D.: A comparison of 266 nm, 213 nm and 193 nm produced from a single solid state Nd:YAG laser for laser ablation ICP-MS, 18, 1224–1230, https://doi.org/10.1039/b305434a, 2003.

Hahn, S., Rodolfo-Metalpa, R., Griesshaber, E., Schmahl, W. W., Buhl, D., Hall-Spencer, J. M., Baggini, C., Fehr, K. T., and Immenhauser, A.: Marine bivalve geochemistry and shell ultrastructure from modern low pH environments, 8, 10351–10388, https://doi.org/10.5194/bgd-8-10351-2011, 2011.

Halloran, B. A. and Donachy, J. E.: Characterization of organic matrix macromolecules from the shells of the antarctic scallop, Adamussium colbecki, 111, 221–231, https://doi.org/10.1016/0305-0491(94)00245-P, 1995.

Hanor, J. S.: Barite-celestine geochemistry and environments of formation, in: Sulfate Minerals: Crystallography, Geochemistry, and Environmental Significance, vol. 40, 193–275, https://doi.org/10.2138/rmg.2000.40.4, 2019.

Hathorne, E. C., James, R. H., Savage, P., and Alard, O.: Physical and chemical characteristics of particles produced by laser ablation of biogenic calcium carbonate, 23, 240–243, https://doi.org/10.1039/b706727e, 2008.

House, W. A. and Donaldson, L.: Adsorption and coprecipitation of phosphate on calcite, 112, 309–324, https://doi.org/10.1016/0021-9797(86)90101-3, 1986.

van Hulten, M., Dutay, J.-C., Middag, R., de Baar, H., Roy-Barman, M., Gehlen, M., Tagliabue, A., and Sterl, A.: Manganese in the world ocean: a first global model, 1–38, https://doi.org/10.5194/bg-2016-282, 2016.

Ishikawa, M. I. and Ichikuni, M.: Coprecipitation of phosphate with calcite the calcite lattice , where 3 CO3 ions are replaced by 2 P04 ions in aqueous solution , as described by the 3 (C03) L + 2 (PO4) S diluted with distilled water to 180m1 , and stirred with a magnetic stirrer at , 15, 283–288, 1981.

Jacobson, P.: Physical Oceanography of the Trondheimsfjord, 26, 3–26, https://doi.org/10.1080/03091928308221761, 1983.

Jochum, K. P., Weis, U., Stoll, B., Kuzmin, D., Yang, Q., Raczek, I., Jacob, D. E., Stracke, A., Birbaum, K., Frick, D. A., Günther, D., and Enzweiler, J.: Determination of reference values for NIST SRM 610-617 glasses following ISO guidelines, 35, 397–429, https://doi.org/10.1111/j.1751-908X.2011.00120.x, 2011.

Kitano, Y., Okumura, M., and Idogaki, M.: Incorporation of sodium, chloride and sulfate with calcium carbonate., 9, 75–84, https://doi.org/10.2343/geochemj.9.75, 1975.

Kitano, Y., Okumura, M., and Idogaki, M.: Uptake of phosphate ions by calcium carbonate., 12, 29–37, https://doi.org/10.2343/geochemj.12.29, 1978.

Kornmann, P.: Beobachtungen an Phaeocystis-Kulturen, 5, 218–233, https://doi.org/10.1007/BF01610509, 1955.

Kuenzler, E. J.: Phosphorus Budget of a Mussel Population, 6, 400–415, https://doi.org/10.4319/lo.1961.6.4.0400, 1961.

Landing, W. M. and Bruland, K. W.: The contrasting biogeochemistry of manganese and iron in the Pacific ocean., 51, 29–43, https://doi.org/10.1016/0016-7037(87)90004-4, 1987.

Larsen, A., Fonnes Flaten, G. A., Sandaa, R. A., Castberg, T., Thyrhaug, R., Erga, S. R., Jacquet, S., and Bratbak, G.: Spring phytoplankton bloom dynamics in Norwegian coastal waters: Microbial community succession and diversity, 49, 180–190, https://doi.org/10.4319/lo.2004.49.1.0180, 2004.

LaVigne, M., Matthews, K. A., Grottoli, A. G., Cobb, K. M., Anagnostou, E., Cabioch, G., and Sherrell, R. M.: Coral skeleton P/Ca proxy for seawater phosphate: Multi-colony calibration with a contemporaneous seawater phosphate record, 74, 1282–1293, https://doi.org/10.1016/j.gca.2009.11.002, 2010.

Lazareth, C. E., Vander Putten, E., André, L., and Dehairs, F.: High-resolution trace element profiles in shells of the mangrove bivalve Isognomon ephippium: A record of environmental spatio-temporal variations?, 57, 1103–1114, https://doi.org/10.1016/S0272-7714(03)00013-1, 2003.

Lea, D. and Boyle, E.: Barium content of benthic foraminifera controlled by bottom-water composition, 338, 751–753, https://doi.org/10.1038/338751a0, 1989.

Longerich, H. P., G??nther, D., and Jackson, S. E.: Elemental fractionation in laser ablation inductively coupled plasma mass spectrometry, 355, 538–542, 1996.

Lorens, R. B. and Bender, M. L.: The impact of solution chemistry on Mytilus edulis calcite and aragonite, 44, 1265–1278, https://doi.org/10.1016/0016-7037(80)90087-3, 1980.

Lubbers, G., Gieskes, W., Castilho, P., del Salomons, W., and Bril, J.: Manganese accumulation in the high pH microenvironment of Phaeocystis sp. (Haptophyceae) colonies from the North Sea, 59, 285–293, https://doi.org/10.3354/meps059285, 1990.

Montagna, P., McCulloch, M., Taviani, M., Mazzoli, C., and Vendrell, B.: Phosphorus in cold-water corals as a proxy for seawater nutrient chemistry, 312, 1788–1791, https://doi.org/10.1126/science.1125781, 2006.

Passow, U. and Wassmann, P.: On the trophic fate of Phaeocystis pouchetii (Hariot): IV. The formation of marine snow by P. pouchetii, 104, 153–161, 1994.

Putten, E. Vander, Dehairs, F., Keppens, E., and Baeyens, W.: High resolution distribution of trace elements in the calcite shell layer of modern Mytilus edulis: Environmental and biological controls, 64, 997–1011, https://doi.org/10.1016/S0016-7037(99)00380-4, 2000.

Richardson, L. L. and Stolzenbach, K. D.: Phytoplankton cell size and the development of microenvironments, 16, 185–191, https://doi.org/10.1016/0168-6496(94)00082-8, 1995.

Richardson, L. L., Aguilar, C., and Nealson, K. H.: Manganese oxidation in pH and O2 microenvironments produced by phytoplankton, 33, 352–363, https://doi.org/10.4319/lo.1988.33.3.0352, 1988.

Rusenko, K. W., Donachy, J. E., and Wheeler, A. P.: Purification and Characterization of a Shell Matrix Phosphoprotein from the American Oyster, 107–124, https://doi.org/10.1021/bk-1991-0444.ch008, 1991.

Sakshaug, E. and Myklestad, S.: Studies on the phytoplankton ecology of the trondheimsfjord. III. Dynamics of phytoplankton blooms in relation to environmental factors, bioassay experiments and parameters for the physiological state of the populations, 11, 157–188, https://doi.org/10.1016/0022-0981(73)90053-1, 1973.

Samata, T., Ikeda, D., Kajikawa, A., Sato, H., Nogawa, C., Yamada, D., Yamazaki, R., and Akiyama, T.: A novel phosphorylated glycoprotein in the shell matrix of the oyster Crassostrea nippona, 275, 2977–2989, https://doi.org/10.1111/j.1742-4658.2008.06453.x, 2008.

Schöne, B. R., Houk, S. D., Freyre Castro, A. D., Fiebig, J., Oschmann, W., Kröncke, I., Dreyer, W., and Gosselck, F.: Daily growth rates in shells of Arctica islandica: Assessing sub-seasonal environmental controls on a long-lived bivalve mollusk, 20, 78–92, https://doi.org/10.2110/palo.2003.p03-101, 2005a.

Schöne, B. R., Dunca, E., Fiebig, J., and Pfeiffer, M.: Mutvei's solution: An ideal agent for resolving microgrowth structures of biogenic carbonates, 228, 149–166, https://doi.org/10.1016/j.palaeo.2005.03.054, 2005b.

Schöne, B. R., Zhang, Z., Jacob, D., Gillikin, D. P., Tütken, T., Garbe-Schönberg, D., Mcconnaughey, T., and Soldati, A.: Effect of organic matrices on the determination of the trace element chemistry (Mg, Sr, Mg/Ca, Sr/Ca) of aragonitic bivalve shells (Arctica islandica) - Comparison of ICP-OES and LA-ICP-MS data, 44, 23–37, https://doi.org/10.2343/geochemj.1.0045, 2010.

Stecher, H. A. and Kogut, M. B.: Rapid barium removal in the Delaware estuary, 63, 1003–1012, https://doi.org/10.1016/S0016-7037(98)00310-X, 1999.

Stecher, H. A., Krantz, D. E., Lord, C. J., Luther, G. W., and Bock, K. W.: Profiles of strontium and barium in Mercenaria mercenaria and Spisula solidissima shells, 60, 3445–3456, https://doi.org/10.1016/0016-7037(96)00179-2, 1996.

Strømgren, Tor.: Zooplankton and Hydrography in Trondheimsfjorden on the west coast of Norway, 51–60, 1–38, https://doi.org/10.1016/0024-3841(84)90026-3, 1974.

Sunda, W. G. and Huntsman, S. A.: Regulation of cellular manganese and manganese transport rates in the unicellular alga Chlamydomonas, 30, 71–80, https://doi.org/10.4319/lo.1985.30.1.0071, 1985.

Tabouret, H., Pomerleau, S., Jolivet, A., Pécheyran, C., Riso, R., Thébault, J., Chauvaud, L., and Amouroux, D.: Specific pathways for the incorporation of dissolved barium and molybdenum into the bivalve shell: An isotopic tracer approach in the juvenile Great Scallop (Pecten maximus), 78, 15–25, https://doi.org/10.1016/j.marenvres.2012.03.006, 2012.

Takesue, R. K., Bacon, C. R., and Thompson, J. K.: Influences of organic matter and calcification rate on trace elements in aragonitic estuarine bivalve shells, 72, 5431–5445, https://doi.org/10.1016/j.gca.2008.09.003, 2008.

Tribovillard, N., Algeo, T. J., Lyons, T., and Riboulleau, A.: Trace metals as paleoredox and paleoproductivity proxies: An update, 232, 12–32, https://doi.org/10.1016/j.chemgeo.2006.02.012, 2006.

Wada, K.: Biomineralization in bivalve molluscs with emphasis on the chemical composition of the extrapallial fluid, 1976.

Wanamaker, A. D. and Gillikin, D. P.: Strontium, magnesium, and barium incorporation in aragonitic shells of juvenile Arctica islandica: Insights from temperature controlled experiments, 526, 117–129, https://doi.org/10.1016/j.chemgeo.2018.02.012, 2019.

Wassmann, P., Svendsen, H., Keck, A., and Reigstad, M.: Selected aspects of the physical oceanography and particle fluxes in fjords of northern Norway, 8, 53–71, https://doi.org/10.1016/0924-7963(95)00037-2, 1996.

Weisse, T., Tande, K., Verity, P., Hansen, F., and Gieskes, W.: The trophic significance of Phaeocystis blooms, 5, 67–79, https://doi.org/10.1016/0924-7963(94)90017-5, 1994.

Wiborg, K. F.: Investigations on zooplankton in coastal and offshore waters of western and northwestern Norway with special reference to the copepods, 11, 1–246, 1954.

Yoshimura, T., Tamenori, Y., Suzuki, A., Kawahata, H., Iwasaki, N., Hasegawa, H., Nguyen, L. T., Kuroyanagi, A., Yamazaki, T., Kuroda, J., and Ohkouchi, N.: Altervalent substitution of sodium for calcium in biogenic calcite and aragonite, 202, 21–38, https://doi.org/10.1016/j.gca.2016.12.003, 2017.

Yoshimura, T., Maeda, A., Tamenori, Y., Suzuki, A., Fujita, K., and Kawahata, H.: Partitioning and chemical environments of minor elements in individual large benthic foraminifera cultured in temperature-controlled tanks, 7, 1–9, https://doi.org/10.3389/feart.2019.00124, 2019.

7 Boron isotopes and B/Ca ratios in the parasitic foraminifera *Hyrrokkin sarcophaga.* Controlled through internal pH-regulation of the host?

Nicolai Schleinkofer[1,2], Jacek Raddatz[1,2], David Evans[1,2], Narimane Dorey[3], Max Wisshak[4]

[1]Goethe Universität Frankfurt, Institut für Geowissenschaften, Frankfurt am Main, Germany

[2]Goethe Universität Frankfurt, Frankfurt Isotope and Element Research Center (FIERCE), Frankfurt am Main, Germany

[3]ENS Paris, École Normale Supérieure, Paris, France

[4]Senckenberg am Meer, Marine Research Department, Wilhelmshaven, Germany

7.1 Introduction

Foraminifera use multiple different feeding strategies which include suspension feeding, grazing, predation and parasitic feeding (Hancock et al., 2015; Walker et al., 2017). The least common strategy is parasitism with only nine species that are known to facilitate this feeding strategy (Walker et al., 2017). One of these parasitic species is *Hyrrokkin sarcophaga* (Cedhagen, 1994), a common inhabitant of cold-water coral reefs in the NE-Atlantic (Beuck et al., 2008). This foraminifer is found parasitizing on the bivalve *Acesta excavata* and the coral *Desmophyllum pertusum* among other species (Beuck et al., 2008; Cheng and Dai, 2016; Cedhagen, 1994). In a previous study we showed that the elemental and isotopic composition of *H. sarcophaga* is significantly dependent on the host species it lived on. Specimen that lived on *A. excavata* display lower Sr/Ca ratios and higher $\delta^{18}O$ and $\delta^{13}C$ values than specimen that lived on *D. pertusum*. Specimen that lived on *A. excavata* without complete penetration of the host shell furthermore display significantly increased Mn/Ca ratios (Schleinkofer et al., 2021b). Considering the elemental ratios, we suggest that these differences are a sign of uptake of material that is derived from the host. This material can be either dissolved host carbonate material or body fluids such as the internal calcifying fluid. Similar reasons can also explain the differences in the isotopic composition but a further possible explanation is rooted in the different internal pH-regimes of the host species. Corals usually increase their internal pH to facilitate calcification, most likely by pumping H^+-ions out of the calcifying space (McCulloch et al., 2012a). Bivalves on the other hand usually display decreased internal pH values (Crenshaw, 1972; Hammer et al., 2011). Uptake of these fluids could also alter the pH regime in the foraminifera and alter the isotopic composition by controlling the rate of hydration/hydroxylation reactions (Chen et al., 2018).

Here we present boron isotope and B/Ca data measured on *H. sarcophaga* and its host species *A. excavata* and *D. pertusum* to test if the transfer of body fluids with different pH values from host to parasite causes significant differences of the boron isotopic composition. In addition, we present boron isotopic data from *A. excavata* that were kept in acidified conditions ($\Delta pH = -0.4$) for a period of five months.

7.2 Samples & Methods

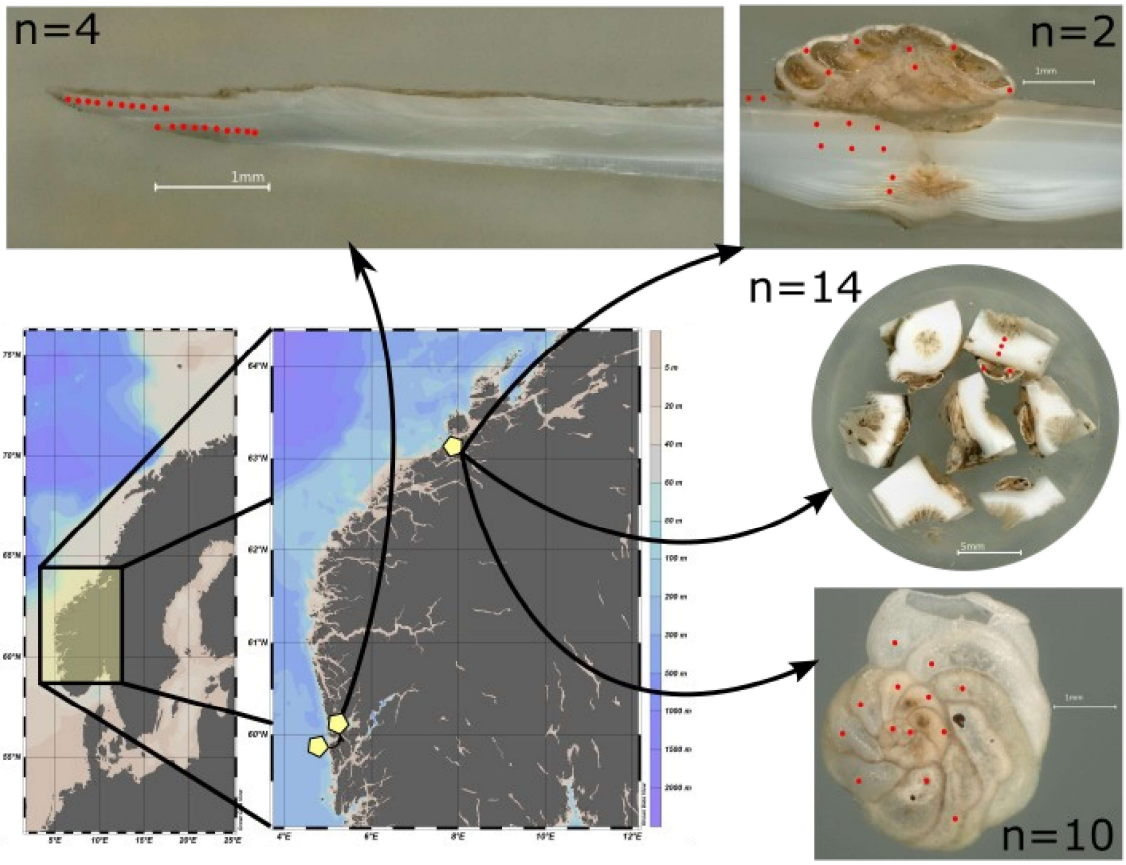

Figure 7-1 Sampling locations and sample preparation. Red dots show the measurement strategy for the different used samples. n = number of samples of the specific sample group

The samples used in this study were collected in the Leksa reef and Nakken reef (Norway) (Fig.1). All samples of *D. pertusum, H. sarcophaga* and two samples of *A. excavata* were collected in the Leksa reef (N 63°36.47'/E 09°23.03', depth ~ 200 m). All samples were collected alive during RV POSEIDON cruise 473. After sampling the bivalves were physically cleaned from soft tissue and dried in an oven alongside the samples of *D. pertusum.* All samples of *H. sarcophaga* derive from the Trondheimsfjord.

More samples of *A. excavata* were collected from Nakken reef ((N 59°49.81', E 05°33.31' , depth = 210 m). After sampling the bivalves from Nakken reef were transferred to Austevoll Research station, where they were kept for 5 months in natural deep seawater from the Hardangerfjord. Half of the bivalves were kept in acidified (-0.4 pH) seawater for the five-month period. The bivalves were not kept in tanks for this specific study and consequently no shell marking with dye (e.g. calcein) was conducted, however a pH decrease by 0.4 should be well visible in the measured samples even without knowledge of the growth in captivity.

After the five-month period in the tanks, the bivalves were physically cleaned from soft tissue and dried.

In total we measured six specimen of *A. excavata.* Four samples (Nakken reef + pH cultivation) were measured along the main growth axis in both the microgranular and fibrous calcitic shell section to detect the effects of acidification. Two additional samples (Trondheimsfjord) with adjacent foraminifera were measured in all shell section including the aragonitic section and the callus region. The samples were cut from the youngest shell section (ventral side) with a length of ≈ 15mm and embedded in epoxy resin in circular mounts. After embedding the samples were ground and polished up to 3 µm with silicon-carbide sandpaper and diamond-water based lapping paste. 14 samples of *L. pertusa* were measured alongside 14 samples of *H. sarcophaga* that were connected to the corals (henceforth called HL). The samples were prepared as transversal cuts through the coral's calyx and through the adjacent foraminifera and treated equally to the aforementioned bivalve samples. Ten additional samples of *H. sarcophaga* were picked from A. excavata shells sampled in the Trondheimsfjord and were measured in different chambers along their ontogenetic growth (henceforth called HA). The samples were mounted in in plasticine. All samples were cleaned with NaOCl or NaOH, sonicated and rinsed multiple times with 18.2 Ω water prior to the measurements.

7.2.1 LA-MC-ICPMS

Boron isotopes were measured using a multicollector-inductively coupled plasma-mass spectrometer (Neptune Plus) coupled to a RESOlution LR (S-155 cell) laser ablation system (LA-MC-ICPMS) at the Frankfurt Isotope & Element Research Center (FIERCE) located in Goethe Universität Frankfurt. A detailed description of the method and used parameters can be found in Evans et al., (2021). In short, we used sample-standard bracketing using NIST SRM612 as a primary standard after every 15 samples. All analyses are gas-blank corrected and corrected for mass bias using the temporally closest NIST SRM612 measurements. Measurements of MACS-3, JCp-1 and JCt-1 allow for an empirical correction of Ca interferences and are therefore measured at least six times during a three-hour session with identical ablation conditions as the samples (Beam diameter = 90 µm, repetition rate = 6 Hz, fluence ≈ 6 J cm^{-2}). Mean 2 SE precision amounts to 0.6 ‰.

pH values are calculated from boron isotope data using the standard equation:

$$pH = pK_B - \log\left[\frac{\delta^{11}B_{SW} - \delta^{11}B_{borate}}{\delta^{11}B_{SW} - \left(K_B * \delta^{11}B_{Borate}\right) - 10^3\left(K_B - 1\right)}\right]$$

Equation 7-14 Equation to calculate pH from $\delta^{11}B$ values

with $\delta^{11}B_{SW}$ being the isotopic composition of seawater (39.61‰ (Foster et al., 2010)), K_B the isotope fractionation factor between borate ion and boric acid (1.0272 (Klochko et al., 2006)) and pK_B the dissociation constant at *in-situ* temperature, salinity and pressure (8.8). To calculate pH, we have to assume that only borate is incorporated into the carbonate.

7.2.2 Statistical computation

All statistical computations were conducted with R (Version 4.1.1). We identified outliers per measurement group (*A. excavata*, *D. pertusum*, HA, HL) and measured variable (B/Ca, $\delta^{11}B$). We consider measurements as outliers if the absolute difference between the measurement and the median of the group is larger than 1.5 times the standard deviation of the group. This procedure removes 67 of the 475 measurements. 26 are removed based on $\delta^{11}B$ measurements and 41 based on B/Ca measurements.

7.3 Results

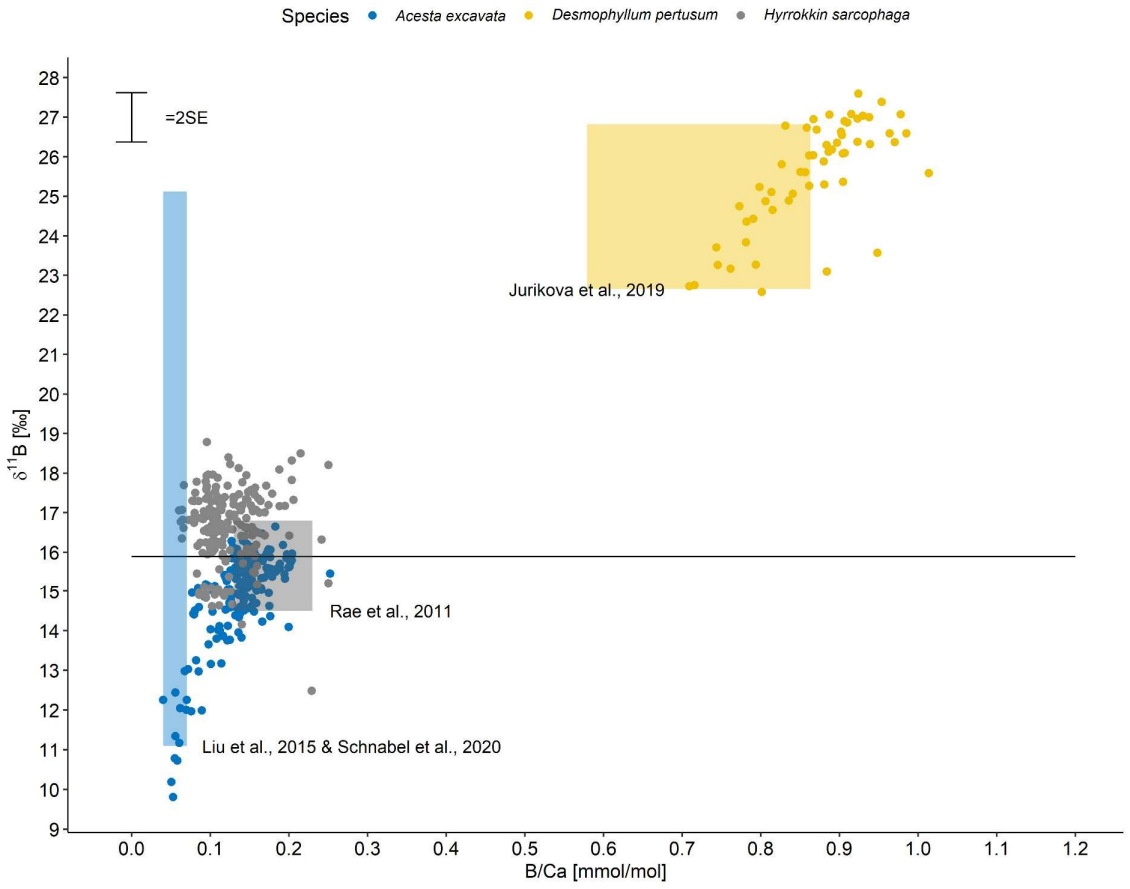

Figure 7-2 Results of B/Ca and $\delta^{11}B$ measurements by means of LA-MC-ICPMS. Coloured squares show measurement results of other studies. Grey rectangle = *D. pertusum* from Jurikova et al. (2019), yellow rectangle = compilation of benthic foraminifera from Rae et al., 2011, blue rectangle = *Arctica islandica*, B/Ca from Schnabel et al., 2020 and $\delta^{11}B$ from Liu et al., 2015. The black line indicates the borate isotopic composition at pH of 8.02.

In total the presented data consists of 408 single measurement points (Fig. 2). Generally, the data points plot in two distinct areas. Samples from *A. excavata* and *H. sarcophaga* display low $\delta^{11}B$ and B/Ca ratios between 9- 20 ‰ and 0.05 – 0.25 mmol/mol, respectively. Samples of *D. pertusum* display higher $\delta^{11}B$ and B/Ca ratios of 22-28 ‰ and 0.7 – 1.0 mmol/mol. *Hyrrokkin sarcophaga* from the two different hosts show no signifcant differences in $\delta^{11}B$. Mean B/Ca ratios in HL are 0.045 mmol/mol higher then in HA (Fig. 3) (ANOVA: F=77.3, p<0.001). In both subgroups mean $\delta^{11}B$ values amount to 16.7. and 16.9 ‰, respectively. Differences in maximum or minimum values are not evident. The two host species, *A. excavata* and *D. pertusum* display B/Ca ratios and $\delta^{11}B$ values of 0.14 and 0.87 mmol/mol and 14.9 and 25.6 ‰, respectively.

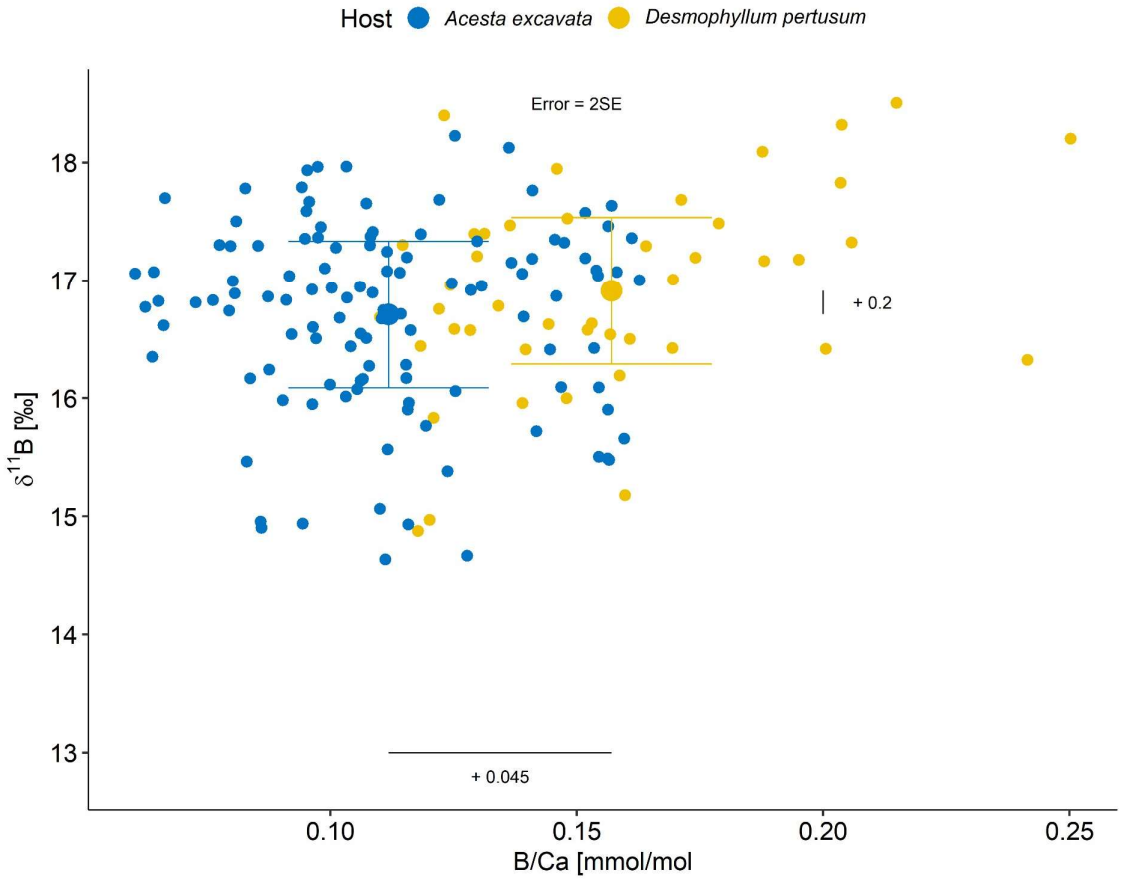

Figure 7-3 Measurement results of *H. sarcophaga* divided by their specific host. No significant difference in $\delta^{11}B$ is observable based on the different hosts, however B/Ca ratios are significantly higher in *H. sarcophaga* picked from *D. pertusum*

Reconstructed pH values for *H. sarcophaga* amount to 8.13 and 8.14 for HA and HL ,respectively and are therfore 0.11 and 0.12 points above the ambient water pH (8.02). Samples of *D. pertusum* diverge more strongly from the ambient water pH with a mean

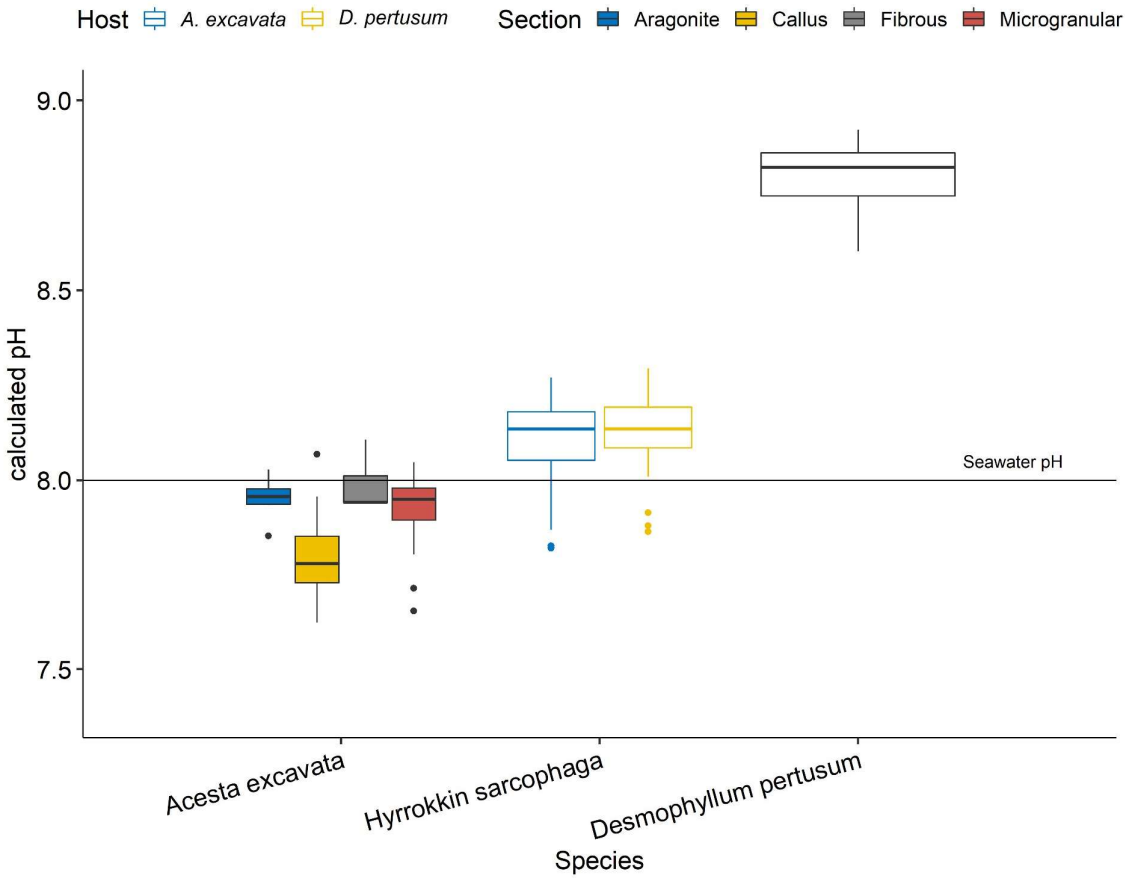

calculate pH of 8.79. Results of *A. excavata* show differences based on the measured shell section. The aragonitic and fibrous calcitic shell section display pH values of 7.95, close to the ambient water. Calculated pH values of the calcitic microgranular and aragonitic callus section are lower with 7.88 and 7.81, respectively.

Figure 7-4 Reconstructed pH of the measured specimens. Results for *A. excavata* are divided according to the shell section, results for *H. sarcophaga* according to their specific host.

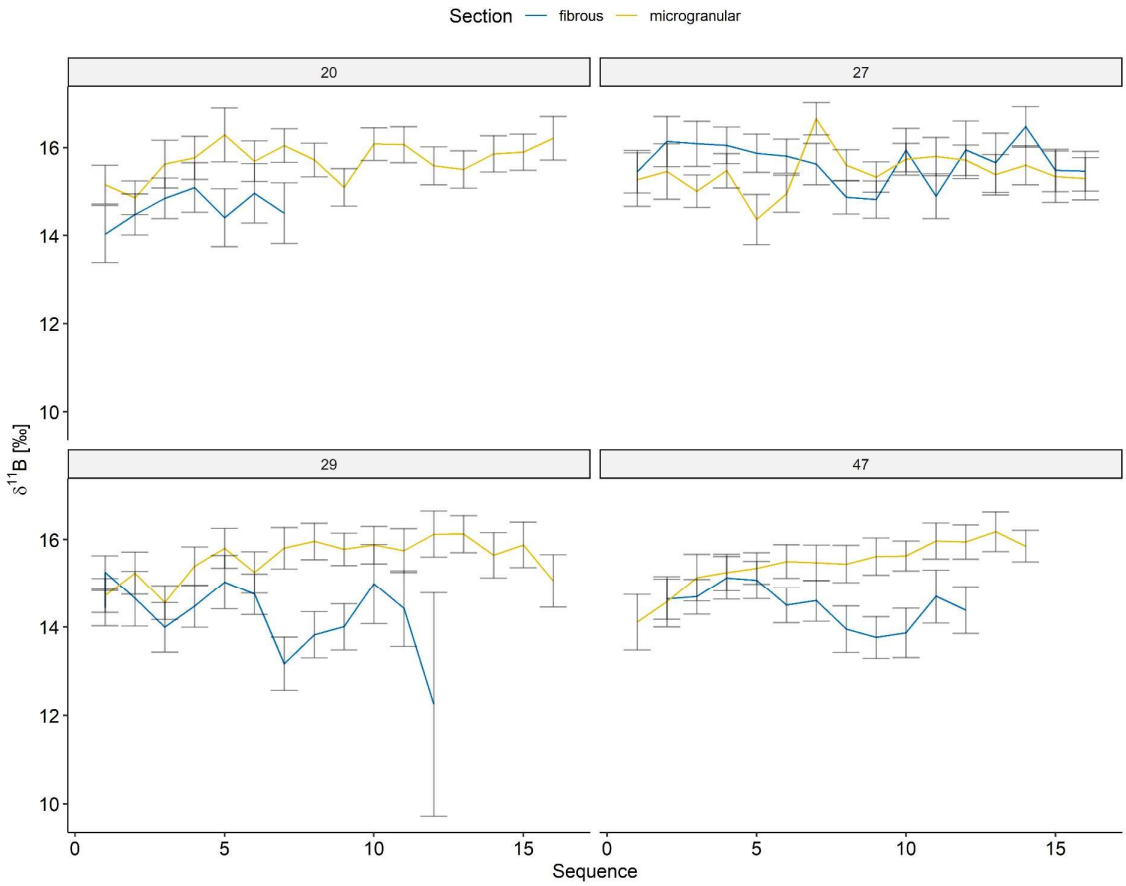

Figure 7-5 Measurement sequence along the ontogenetic growth of the laboratory cultivated *A. excavata* specimen. Little variability is observable in the microgranular shell sections.

Laboratory cultivated samples show stable $\delta^{11}B$ values in the fibrous shell section with a mean of 14.8 ‰ and a standard deviation of 0.5 ‰. $\delta^{11}B$ values in the microgranular shell section are generally higher with a mean of 15.5 ‰ and a standard deviation of 0.5 ‰. A significant drop of $\delta^{11}B$ values as a result of the cultivation in acidified seawater is not observable. The measured transects are largely independent from each other when comparing fibrous and microgranular shell section as are the different samples despite originating from the same location.

Measurements along the ontogenetic growth of HA show little variability outside the measurement error (Fig. 4). A systematic decrease of $\delta^{11}B$ as an effect of shell penetration is not observable. Ontogenetic trends are not evident.

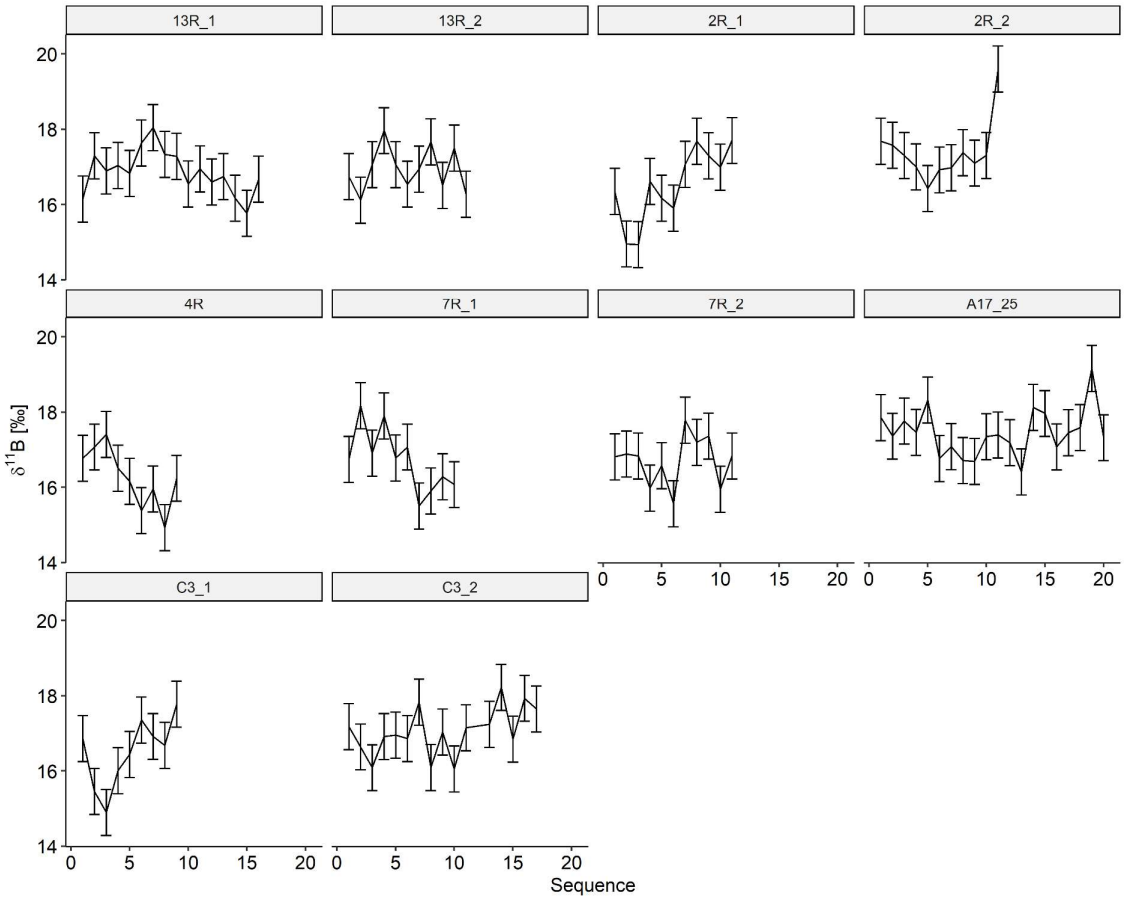

Figure 7-6 $\delta^{11}B$ measurements along the ontogenetic growth of *H. sarcophaga* grown on *A. excavata*. A systematic decrease of δ11B values as an effect of shell penetration is not observable. The sequence goes from the youngest (0) to the oldest (20) chambers.

7.4 Discussion

7.4.1 Parasitism related changes of the calcifying fluid in *H. sarcophaga*

In a recent study, results from the geochemical composition of *H. sarcophaga* were presented and shown to be significantly influenced by the host species (Schleinkofer et al., 2021b). We observe similar results with respect to B/Ca ratios, which are significantly different based on the host species *H. sarcophaga* was living on. Generally, the B/Ca ratios in *H. sarcophaga* evolve towards the B/Ca ratio of the host species. Consequently, HL display higher B/Ca ratios compared to HA. Contrary to B/Ca ratios we do not observe significant differences in the $\delta^{11}B$ composition between HA and HL despite observing large differences in the host species. Consequently, there is either no transfer of body fluids from

the host to the parasite, the pH-upregulation mechanisms of the parasite or boric acid diffusion masks the pH alteration.

We cannot definitively rule out the possibility that a transfer of body fluids from host to parasite is absent. However, feeding on the bivalve's soft body without simultaneous ingestion of the surrounding body fluids does not seem likely, with respect to the nutritional value of these fluids (Cedhagen, 1994; Schweizer et al., 2012; Alexander and Delaca, 1987).

Reconstructed pH values in HA and HL amount to 8.11 and 8.13, respectively, and therefore 0.1 above the ambient seawater pH of 8.02. This pH increases, reconstructed with boron isotopes, is uncommon for foraminifera, as several investigated epifaunal benthic foraminifera show no offset from seawater borate $\delta^{11}B$ values (Rae et al., 2011)(Fig.7) despite their pH-regulation mechanisms.

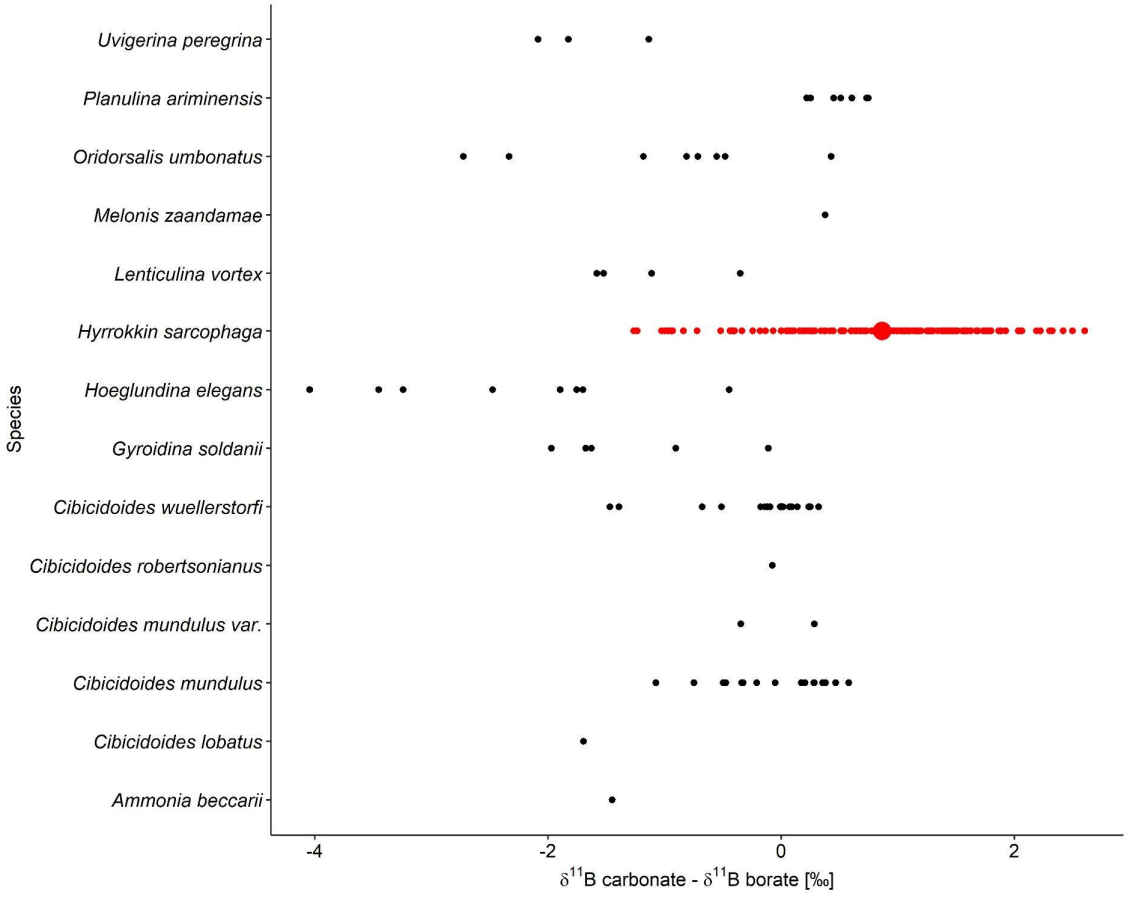

Figure 7-7 Offset of $\delta^{11}B$ values measured in the foraminiferal carbonate to $\delta^{11}B$ values in seawater borate. Red points indicate data from this study, the bigger data point shows the mean. Data from all other species is from Rae et al., 2011.

The reason for the missing sensitivity of $\delta^{11}B$ on the pH-regulation mechanism is not yet resolved. A possibly mechanisms to explain this observation is the diffusion of boric acid into

the calcifying space (Gagnon et al., 2021). Boric acid can potentially diffuse through biological membranes into the calcifying space consequently equalizing the $\delta^{11}B$ of boric acid in the calcifying fluid and the surrounding seawater. Equilibrium isotope fractionation is then rapidly established between borate and boric acid (Zeebe and Wolf-Gladrow, 2001) leading to a further equalization between borate in the calcifying fluid and borate in the seawater (Gagnon et al., 2021). This model also assumes two separate endmembers: one endmember with rapid boric acid diffusion and resulting $\delta^{11}B$ values close to seawater borate despite any occurring pH-regulation mechanisms (i.e., foraminifera) and one endmember with slow boric acid diffusion resulting in $\delta^{11}B$ carbonate values that are different from seawater borate (i.e., corals) (Gagnon et al., 2021). In the case of *H. sarcophaga*, the endmember with very limited boric acid diffusion does not fit with our data as the measured pH increase of 0.1 is far below other foraminifera where pH increases of 0.5 are measured (Bentov et al., 2009; De Nooijer et al., 2009). However, we can still see a pH increase in comparison to the ambient seawater in our $\delta^{11}B$ data, therefore a very rapid diffusion is unlikely. Instead, we have to assume that boric acid diffusion is possible in this species, however with a slightly lower rate and/or speed than in other foraminifera species.

Similar to $\delta^{11}B$, B/Ca ratios are expected to be controlled by carbonate system parameters (Rae et al., 2011). However, a simple relationship between B/Ca and [Borate] or pH was not found (Foster, 2008; Yu et al., 2007; Rae et al., 2011). A good correlation was found between B/Ca and the carbonate ion saturation (Yu and Elderfield, 2007). Unfortunately, this relation requires a species-specific calibration and is therefore not easily transferable to the investigated *H. sarcophaga* specimen.

7.4.2 Ontogenetic variation in *H. sarcophaga*

As to be expected from the general $\delta^{11}B$ measurements, we observe no systematic trend in the ontogenetic $\delta^{11}B$ profiles of HA that would indicate an uptake of more acidic bivalve calcifying fluid. The underlying reasons are discussed in more detail in the previous section. Similarly, we detect no systematic trend in B/Ca profiles. Based on the research of (Yu and Elderfield, 2007a) this would indicate no change in the carbonate ion saturation as an effect of boring progress and access to the calcifying fluid of the bivalve. Generally, the ionic composition of the calcifying fluid in bivalves is mostly equivalent to the ambient water (Crenshaw, 1972; Wada, 1976), therefore significant change of B/Ca in HA is not necessarily expected. On the other hand, this could also indicate that host specific alterations of the geochemical composition in H. sarcophaga are not controlled through uptake of the hosts calcifying fluid but instead the uptake of dissolved shell material. This material likely is available right after the settlement of *H. sarcophaga* on the host.

7.4.3 Effects of acidification on $\delta^{11}B$ in A. excavata

We detect no effect of the decreased pH in samples that were cultivated for 5 months in acidified seawater (ΔpH = -0.4). Furthermore, we observe no correlation between parallel profiles from the fibrous and microgranular shell section. As stated previously, we have no information on the shell growth during the cultivation period and can therefore not guarantee that we actually measured in the sections that grew during the cultivation period. However, we would expect a growth of 0.5- 3 mm during the cultivation period (Schleinkofer et al., 2021a) which is easily resolvable by LA-ICP-MS. It is still possible though, that the specimens ceased or reduced growing due to the reduced pH. While this theory is not supported by results gathered from *M. edulis* (Berge et al., 2006), *A. excavata* might show different responses to acidification, as *M. edulis* is potentially more adapted to high pH-variations due to its natural environment. *M. edulis* can experience regular tide induced air exposure which leads to hypercapnic acidosis and consequently to a higher resilience to pH changes (Walsh et al., 1984).

7.5 Preliminary Conclusion

Our preliminary results show no significant difference in the boron isotopic composition between HA and HL. The missing response could indicate that no transfer of fluids and consequently no pH change in *H. sarcophaga* is accomplished or the transferred amount is too small to cause significant pH changes in the foraminifera. Alternatively, the missing response is explainable with boric acid diffusion (Gagnon et al., 2021). In this case we must assume a reduced rate of boric acid transfer, since the foraminifera records pH values above the ambient seawater indicating an insufficient equilibration between boric acid and the borate ion. B/Ca ratios show significant differences between HA and HL. Based on the results of Yu and Elderfield, 2007b this would indicate differences in the carbonate ion saturation, which is in acceptance with our hypothesis. However, species specific calibration is necessary to transfer this relationship to H. sarcophaga. Additionally, it is possible that the B/Ca differences are caused by transferred material from host to parasite as explained in Schleinkofer et al., 2021b.

Specimen of *A. excavata* display that were kept in acidified conditions for five months show no alterations in the boron isotopic composition. Due to missing growth information, we cannot guarantee that the bivalves grew sufficiently. Therefore, the missing reaction to the acidified conditions could be caused by insufficient growth of the specimens or due to the pH regulation of the bivalve. However, bivalve samples from the Trondheimsfjord do appear to record the ambient seawater pH despite their pH regulation (boric acid diffusion). Therefore, I suggest that it is more likely that the bivalves ceased growing in the acidified conditions.

7.6 References

Akberali, H. B. and Trueman, E. R.: Effects of Environmental Stress on Marine Bivalve Molluscs, Advances in Marine Biology, 22, 101–198, https://doi.org/10.1016/S0065-2881(08)60051-6, 1985.

Alexander, S. P. and Delaca, T. E.: Feeding adaptations of the foraminiferan Cibicides refulgens living epizoically and parasitically on the Antarctic scallop Adamussium colbecki, Biological Bulletin, 173, 136–159, https://doi.org/10.2307/1541868, 1987.

Bentov, S., Brownlee, C., and Erez, J.: The role of seawater endocytosis in the biomineralization process in calcareous foraminifera, Proceedings of the National Academy of Sciences of the United States of America, 106, 21500–21504, https://doi.org/10.1073/pnas.0906636106, 2009.

Berge, J. A., Bjerkeng, B., Pettersen, O., Schaanning, M. T., and Øxnevad, S.: Effects of increased sea water concentrations of CO2 on growth of the bivalve Mytilus edulis L., Chemosphere, 62, 681–687, https://doi.org/10.1016/J.CHEMOSPHERE.2005.04.111, 2006.

Beuck, L., Correa, M. L., and Freiwald, A.: Biogeographical distribution of Hyrrokkin (Rosalinidae, Foraminifera) and its host-specific morphological and textural trace variability, in: Current Developments in Bioerosion, Springer Berlin Heidelberg, Berlin, Heidelberg, 329–360, https://doi.org/10.1007/978-3-540-77598-0_17, 2008.

Cedhagen, T.: Taxonomy and biology of hyrrokkin sarcophaga gen. Et Sp. N., a parasitic foraminiferan (rosalinidae), Sarsia, 79, 65–82, https://doi.org/10.1080/00364827.1994.10413549, 1994.

Cheng, Y. R. and Dai, C. F.: A bioeroding foraminifer, Hyrrokkin sarcophaga, on deepwater corals from the South China Sea, Coral Reefs, 35, 901, https://doi.org/10.1007/s00338-016-1447-7, 2016.

Chen, S., Gagnon, A. C., and Adkins, J. F.: Carbonic anhydrase, coral calcification and a new model of stable isotope vital effects, Geochimica et Cosmochimica Acta, 236, 179–197, https://doi.org/10.1016/j.gca.2018.02.032, 2018.

Crenshaw, M. A.: The inorganic composition of molluscan extrapallial fluid, The Biological Bulletin, 143, 506–512, https://doi.org/10.2307/1540180, 1972.

Crenshaw, M. A. and Neff, J. M.: Decalcification at the mantle-shell interface in molluscs, Integrative and Comparative Biology, 9, 881–885, https://doi.org/10.1093/icb/9.3.881, 1969.

Evans, D., Gerdes, A., Coenen, D., Marschall, H. R., and Müller, W.: Accurate correction for the matrix interference on laser ablation MC-ICPMS boron isotope measurements in CaCO 3

and silicate matrices , Journal of Analytical Atomic Spectrometry, https://doi.org/10.1039/d1ja00073j, 2021.

Foster, G. L.: Seawater pH, pCO2 and [CO2-3] variations in the Caribbean Sea over the last 130 kyr: A boron isotope and B/Ca study of planktic foraminifera, Earth and Planetary Science Letters, 271, 254–266, https://doi.org/10.1016/j.epsl.2008.04.015, 2008.

Foster, G. L., Strandmann, P. A. E. P. von, and Rae, J. W. B.: Boron and magnesium isotopic composition of seawater, Geochemistry, Geophysics, Geosystems, 11, 8015, https://doi.org/10.1029/2010GC003201, 2010.

Gagnon, A. C., Gothmann, A. M., Branson, O., Rae, J. W. B., and Stewart, J. A.: Controls on boron isotopes in a cold-water coral and the cost of resilience to ocean acidification, Earth and Planetary Science Letters, 554, https://doi.org/10.1016/j.epsl.2020.116662, 2021.

Hammer, K. M., Kristiansen, E., and Zachariassen, K. E.: Physiological effects of hypercapnia in the deep-sea bivalve Acesta excavata (Fabricius, 1779) (Bivalvia; Limidae), Marine Environmental Research, 72, 135–142, https://doi.org/10.1016/j.marenvres.2011.07.002, 2011.

Hancock, L. G., Walker, S. E., Pérez-Huerta, A., and Bowser, S. S.: Population Dynamics and Parasite Load of a Foraminifer on Its Antarctic Scallop Host with Their Carbonate Biomass Contributions, PLOS ONE, 10, e0132534, https://doi.org/10.1371/journal.pone.0132534, 2015.

Klochko, K., Kaufman, A. J., Yao, W., Byrne, R. H., and Tossell, J. A.: Experimental measurement of boron isotope fractionation in seawater, Earth and Planetary Science Letters, 248, 276–285, https://doi.org/10.1016/J.EPSL.2006.05.034, 2006.

McCulloch, M., Falter, J., Trotter, J., and Montagna, P.: Coral resilience to ocean acidification and global warming through pH up-regulation, Nature Climate Change, 2, 623–627, https://doi.org/10.1038/nclimate1473, 2012a.

McCulloch, M., Trotter, J., Montagna, P., Falter, J., Dunbar, R., Freiwald, A., Försterra, G., López Correa, M., Maier, C., Rüggeberg, A., and Taviani, M.: Resilience of cold-water scleractinian corals to ocean acidification: Boron isotopic systematics of pH and saturation state up-regulation, Geochimica et Cosmochimica Acta, 87, 21–34, https://doi.org/10.1016/j.gca.2012.03.027, 2012b.

de Nooijer, L. J., Toyofuku, T., and Kitazato, H.: Foraminifera promote calcification by elevating their intracellular pH, Proceedings of the National Academy of Sciences of the United States of America, 106, 15374–15378, https://doi.org/10.1073/pnas.0904306106, 2009.

Rae, J. W. B., Foster, G. L., Schmidt, D. N., and Elliott, T.: Boron isotopes and B/Ca in benthic foraminifera: Proxies for the deep ocean carbonate system, Earth and Planetary Science Letters, 302, 403–413, https://doi.org/10.1016/j.epsl.2010.12.034, 2011.

Schleinkofer, N., Raddatz, J., Evans, D., Gerdes, A., Flögel, S., Voigt, S., Büscher, J. V., and Wisshak, M.: Compositional variability of Mg/Ca, Sr/Ca, and Na/Ca in the deep-sea bivalve Acesta excavata (Fabricius, 1779), PLOS ONE, 16, e0245605, https://doi.org/10.1371/journal.pone.0245605, 2021a.

Schleinkofer, N., Evans, D., Wisshak, M., Büscher, J. v, Fiebig, J., Freiwald, A., Härter, S., Marschall, H. R., Voigt, S., and Raddatz, J.: Host influenced geochemical signature in the parasitic foraminifer Hyrrokkin sarcophaga, Biogeosciences Discussions, 2021, 1–35, https://doi.org/10.5194/bg-2021-74, 2021b.

Schweizer, M., Bowser, S. S., Korsun, S., and Pawlowski, J.: Emendation of Cibicides Antarcticus (Saidova, 1975) Based on Molecular, Morphological, and ecological Data, The Journal of Foraminiferal Research, 42, 340–344, https://doi.org/10.2113/gsjfr.42.4.340, 2012.

Wada, K.: Biomineralization in bivalve molluscs with emphasis on the chemical composition of the extrapallial fluid, The mechanism of mineralization in the invertebrates and plants, 1976.

Walker, S. E., Hancock, L. G., and Bowser, S. S.: Diversity, biogeography, body size and fossil record of parasitic and suspected parasitic foraminifera: A review, Journal of Foraminiferal Research, 47, 34–55, https://doi.org/10.2113/gsjfr.47.1.34, 2017.

Walsh, P. J., McDonald, D. G., and Booth, C. E.: Acid-base-balance in the sea mussel, Mytilus edulis. II. Effects of hypoxia and air-exposure on intracellular acid-base status, Marine Biology Letters, 5, 359–369, 1984.

Yu, J. and Elderfield, H.: Benthic foraminiferal B/Ca ratios reflect deep water carbonate saturation state, Earth and Planetary Science Letters, 258, 73–86, https://doi.org/10.1016/J.EPSL.2007.03.025, 2007a.

Yu, J., Elderfield, H., Greaves, M., and Day, J.: Preferential dissolution of benthic foraminiferal calcite during laboratory reductive cleaning, Geochemistry, Geophysics, Geosystems, 8, https://doi.org/10.1029/2006GC001571, 2007.

Zeebe, R. E. and Wolf-Gladrow, D. A.: CO2 in seawater : equilibrium, kinetics, isotopes, 346 pp., 2001.

8 Conclusions

8.1 English

This study aims to extend our knowledge about geochemical proxies in different species inhabiting cold-water coral reefs. With regards to our research on *A. excavata,* the presented results are largely in acceptance with studies on other bivalves. Elemental ratios are just not feasible for paleoenvironmental reconstructions on bivalves due to the strong vital effects. While temperature and salinity certainly contribute to the variability of Mg/Ca, Sr/Ca and Na/Ca ratios, strong vital effects heavily complicate their use as proxies. An important finding is the possible contribution of stress to vital effects, which was already suggested by other studies (Lorens and Bender, 1980; Wanamaker and Gillikin, 2019). Future studies should aim to quantify these effects (even though a quantification of stress is probably not easy). The growth increments in *A. excavata* appear to be controlled by tidal cycles and therefore can be useful for the investigation of the influence of internal tides on the distribution pattern of different co-occurring species such as cold-water corals. Internal waves contribute an important factor for their distribution by controlling the food availibity (Kiriakoulakis et al., 2007; Mienis et al., 2007). Reconstruction of plankton blooms and consequently the nutrient availability might be possible with Ba/Ca, Mn/Ca and P/Ca ratios measured in *A. excavata.* We observed a regular sequence of peaks of the aforementioned elemental ratios that are congruent with a sequence of plankton blooms of different species that occurs in the Trondheimsfjord. However, a quantification of the extent of the bloom is not possible, as there is no correlation of the peak height and the concentration of chlorophyll. An expected correlation between P/Ca ratios and growth lines, due to phosphorylated groups in these areas, had to be discarded.

Investigations on cold-water corals revealed a significant correlation between water-temperature and Na/Ca ratios. While the large variability complicates the usability of this system, we found that other organisms such as *Porites* sp. and *M. edulis* display a similar sensitivity as cold-water corals. This constant sensitivity among different organism groups might provide a way to reconstruct temperatures in the past on extinct organisms, when no species-specific calibration is possible. We suggest that temperature sensitive Na and/or Ca pumps control the Na/Ca ratio in the calcifying fluid and consequently in the precipitated carbonate. Mg/Ca and Sr/Ca ratios were not found to be controlled by temperature, salinity or pH.

Interesting results are gathered during the investigation of *H. sarcophaga*. This parasitic foraminifer displays significant compositional changes based on the host organism it infested. Sr/Ca ratios are significantly increased on specimen that infested the cold-water coral *D. pertusum*. We expect that the aragonite, which is naturally enriched in Sr, is

dissolved by the foraminifera and ingested to potentially satisfy Ca/DIC requirements. We also detect significant compositional variability in oxygen and carbon isotopes. While *A. excavata* appears to calcify close to the isotopic equilibrium, *H. sarcophaga* that infested *D. pertusum* show depleted $\delta^{18}O$ and $\delta^{13}C$ values, similar to the host. Again, we expect this to be a sign of uptake of host material by the parasite. The isotopic variability can also be caused by the different pH environments in the hosts, through changes of the extent of the hydration/hydroxylation reaction. We also found the progress of boring through the bivalve's shell to control Mn/Ca ratios. Higher Mn/Ca ratios in specimen with incomplete shell penetration can be explained with a change of the food source. Potentially the foraminifera feeds on the Mn and Fe-rich periostracum when it hasn't established access to the internal soft-body of the bivalve. The results display that a thorough knowledge of the investigated species for paleoenvironmental reconstructed is mandatory for reliable results. Based on our results reconstructions using $\delta^{18}O$ measured in *H. sarcophaga* can overestimate the temperature by 1°C when specimens from *D. pertusum* are used. Future studies should target further parasitic and predatory species to investigate if this is a common phenomenon.

In order to investigate the influence of different pH-regimes on the elemental composition of *H. sarcophaga* we also measured boron isotopes and B/Ca ratios. Similar to the previous results B/Ca ratios are significantly different in H. sarcophaga from different hosts. We expected to observe differences in the boron isotopic composition as well, due to the different pH-regimes of the host species. However, we did not observe significant differences. This might indicate that a transfer of body fluids from host to parasite is not accomplished. The results are also explainable with a proposed model that involves boric-acid diffusion. Gagnon et al, 2021 use this model to explain why foraminifera record the seawater pH in their boron isotopic composition despite their own ph-regulation mechanisms.

Despite biologically induced vital effects, preservation techniques can influence the chemical composition of sampled material. We investigated the influence of ethanol on Mg/Ca, Sr/Ca and Na/Ca ratios. We detect no influence on Sr/Ca ratios but Mg/Ca and Na6/Ca ratios decrease significantly after treatment time of six months. The ethanol probably preferentially dissolved areas rich in Mg and Na and releases loosely bound ions from the crystal lattice. These results showcase that proper sample treatment is mandatory for reliable results.

In summary, the gathered results showcase the problems and caveats of paleoenvironmental reconstructions using elemental ratios and isotopic compositions on marine biogenic carbonate producers. Vital effects are ubiquitous and knowledge of these effects is highly important to gain reliable information of past environments.

8.2 Deutsch

Diese Arbeit soll das Wissen über verschiedene geochemische Proxies in verschiedenen Spezies von Kaltwasser Korallenriffen erweitern. Die Untersuchungen an der Bivalve *A. excavata* decken sich mit den Ergebnissen von anderen Bivalvenspezies, dass Element Verhältnisse im Karbonat von Bivalven nur bedingt für Paleoumweltrekonstruktionen nutzbar sind. Unsere Untersuchungen zeigen das Temperatur und Salinität einen Einfluss auf die Variabilität von Mg/Ca, Sr/Ca und Na/Ca Verhältnissen haben, jedoch verhindern starke Vital Effekte die Nutzung als Proxy. Insbesondere eine mögliche Beeinflussung durch Stress-effekte stellt einen grundlegenden Befund dar und sollte in zukünftigen Studien weiter untersucht werden. Die Wachstumsinkremente von *A. excavata* werden von Gezeitenzyklen beeinflusst und könnten sich als nützlich für die Untersuchung von anderen Spezies erweisen, die von diesen Gezeitenzyklen abhängen. Dies betrifft zum Beispiel *Desmophyllum pertusum,* die durch die internen Wellen mit Nahrung versorgt werden (Kiriakoulakis et al., 2007; Mienis et al., 2007). Ba/Ca, Mn/Ca und P/Ca Verhältnisse zeigen eine regelmäßige Abfolge von Peaks die konsistent mit dem Auftreten von Blüten verschiedener Planktonarten sind. Jedoch gibt es keinen Zusammenhang zwischen der Ausbreitung und Stärke der Blüte und der Höhe der beobachteten Peaks, wodurch eine quantitative Rekonstruktion dieser Blüten nicht möglich ist. Weiterhin untersuchten wir P/Ca Verhältnisse auf ihre Variabilität in verschiedenen Wachstumsstrukturen der Muscheln. Eine mögliche Anreicherung von Phosphor-Gruppen in der Umgebung von Wachtumslinien konnte jedoch nicht festgestellt werden.

Unsere Untersuchung an Kaltwasserkorallen zeigen eine signifikante Korrelation zwischen Na/Ca Verhältnissen und der Wassertemperatur. Trotz dieser Korrelation, macht es die hohe Variabilität, die durch organisches Material, Wachstumsratenänderung und andere Vital Effekte ausgelöst wird, schwierig zuverlässige Ergebnisse zu erhalten. Dennoch könnte sich die Temperatursensitivität der Na/Ca Verhältnisse, die in ähnlicher Form auch in Warmwasserkorallen und der Muschel *M. edulis* zu finden ist, als nützlich erweisen um sie an ausgestorbenen Spezies zu verwenden, wenn keine spezies-spezifische Kalibration möglich ist. Diese Temperatursensitivität die in verschiedenen Spezies gleichermaßen vorkommt, könnte durch Natrium- oder Calciumpumpen bedingt sein, deren Aktivität durch die Wassertemperatur beeinflusst ist.

Die Foraminifere *H. sarcophaga* zeigt eine diverse Ausprägung eines Vitaleffektes, ausgelöst durch ihre parasitäre Lebensweise. In Abhängigkeit des Wirtes zeigt *H. sarcophaga* signifikante Unterschiede in der Element- und Isotopenzusammensetzung. Sr/Ca Verhältnisse sind signifikant erhöht in Individuen die auf *D. pertusum* lebten. Wahrscheinlich führt die Lösung des strontiumreichen Aragonit Skelets und anschließende Aufnahme der

entstandenen Lösungen durch *H. sarcophaga* zur Erhöhung der Sr/Ca Verhältnisse. Weiterhin gibt es auch Unterschiede in der Kohlenstoff- und Sauerstoffisotopie zwischen *H. sarcophaga* die auf *A. excavata* und *D. pertusum* lebten. Auch hier könnte die Signalweitergabe durch Aufnahme von gelöstem Wirt-Karbonat oder anderen internen Körperflüssigkeiten ausgelöst sein. Eine weitere Erklärung könnte in den unterschiedlich internen pH-Werten der des Wirtes liegen, da die Rate der Hydrations/Hydroxilations Reaktion pH abhängig ist. Weiterhin konnten wir Variationen der Mn/Ca Verhältnisse feststellen, diese sind jedoch nicht durch die jeweilige Host Spezies ausgelöst, sondern durch den Bohrfortschritt der Foraminifera. Wenn *H. sarcophaga* die Schale von *A excavata* noch nicht komplett durchbohrt hat, zeigt sie signifikant erhöhte Mn/Ca Verhältnisse. Dies ist wahrscheinlich durch eine Umstellung der Nahrungsversorgung zu erklären. Erst durch die vollständige Durchbohrung der Schale erhält die Foraminifere Zugang zum internen Weichkörper der Muschel, davor ernährt sie sich möglicherweise vom organischen Periostracum der Muscheln das sich auf der Schalen Außenseite befindet und reich an Mangan und Eisen ist. Diese Resultate zeigen das eine genaue Kenntnis der untersuchten Spezies sehr wichtig ist. Die unterschiedlichen Sauerstoffisotopen Werte würden in diesem Fall zu einer Überschätzung der rekonstruierten Wassertemperatur um 1°C führen.

Um zu testen ob unterschiedliche interne pH-Werte zu Variationen der Isotopie in *H. sarcophaga* führen haben wir zusätzlich Bor-isotope und B/Ca Verhältnisse gemessen. Jedoch konnten keine signifikanten Unterschiede in der Bor Isotopie festgestellt werden. Daher ist davon auszugehen das kein Transfer von Flüssigkeiten von Wirt zu Parasiten erfolgt oder dieser Transfer führt zu keiner pH Änderung in der Foraminifera. Eine weitere Erklärung ist die Diffusion von Borsäure durch Zellmembrane. Solch eine Diffusion, wurde von Gagnon et al., 2020 benutzt um die Bor-Isotopie in Foraminiferen zu erklären, die trotz biologischer pH Regulierungsmechanismen den pH-Wert des umgebenden Meerwassers aufzeichnet.

Neben biologischen Vitaleffekten können auch Preservationstechniken die chemische Zusammensetzung von Karbonaten beeinflussen. Dazu haben wir den Einfluss von Ethanol auf Mg/Ca, Sr/Ca und Na/Ca in verschiedenen marinen Karbonaten untersucht. Auswirkungen auf die Sr/Ca Verhältnisse konnten dabei nicht festgestellt werden, jedoch wurden Mg/Ca und Na/Ca Verhältnisse signifikant niedriger nach einer Preservationszeit von 6 Monaten. Dies liegt wahrscheinlich an der präferentiellen Auflösung von Mg und Na-reichem Karbonat.

Zusammenfassend zeigen unsere Ergebnisse die Probleme, die bei der Verwendung von Elementverhältnissen und Isotopie zur Rekonstruktion von Paläoumweltbedingungen

auftreten können. Vitaleffekte sind allgegenwärtig und die korrekte Bestimmung und Quantifizierung ist unerlässlich um solide Ergebnisse zu erhalten.

9 Outlook

9.1 Subsequent studies using laboratory cultivated bivalves.

The studies presented in this thesis are based on *in-situ* calibrated specimen. This technique, however has some mayor drawbacks compared to calibrations on specimen that were cultivated in the laboratory. The main point is the control over the water chemistry on longer time scales. *In-situ* calibrations have to rely mostly on water samples that are taken at the beginning and the end of the measurement period, especially with regards to deep-water organisms. Continuous sampling of water is just too expensive for bivalves that live outside of shallow water regions. The inability to take regular water samples for calibration limits the studies to environmental factors such as temperature, salinity and pH. However, several studies showed the relation of the E/Ca ratios in the surrounding water and the E/Ca ratio recorded in biogenic carbonate(LaVigne et al., 2011; Hauzer et al., 2018). This is especially important in bivalves were many internal processes around the biomineralization and controls on different E/Ca ratios are not fully understood.

Another point is the necessity for a reliable chronology to compare the geochemical results to the recorded environmental parameters. Constructing a reliable chronology in *A. excavata* turned out to be a big limitation due to poor visibility of growth increments, especially in the calcitic shell parts. This problem can be circumvented by catching the samples, marking them with e.g. Calcein or ^{14}C-labeling, and place them back in their natural habitat, to produce a clear mark to base the chronology on.

Another negative aspect of *in-situ* calibrations is the cost factor. The environmental information used in this study was recorded by two lander systems that were deployed for a 14 month period in close proximity to the investigated reefs. This is a very costly process, that involves buying/production of suitable landers, employment and regathering of the landers as well as sampling the investigated specimen (by means of ROV or manned submersibles such as JAGO). These processes are much cheaper feasible in a laboratory environment.

The mayor advantage of laboratory cultivation studies is that most external effects can be fully controlled and measured. Physical properties can be recorded automatically, regular water samples can be taken and factors such as predation events can be excluded. However, this full control can be also negative. If there is no access to local marine seawater (by means of deep-sea pumps), artificial seawater has to be prepared. This can lead to problems when organisms unknowingly rely on trace elements in this water that are not part

of the mixture. This could also lead to stress in the cultivated specimens which might be a factor in element incorporation (Wanamaker and Gillikin, 2019; Lorens and Bender, 1980).

Bivalves are generally considered to be difficult to cultivate in an aquarium, however this is only true when clean water in the aquarium shall be maintained (for aesthetic purposes). Bivalves need a constant food supply which can be only achieved in murky water. Apart from this caveat, bivalves are easily cultivated in aquaria. This is also true for *Acesta excavata*, they can easily survive in buckets of cool deep water without filtration or added food particles for at least two weeks (pers. Comment Solvin Zankl, 2020). An easy cultivation setup, that can be achieved with minimal effort and cost, will be presented here.

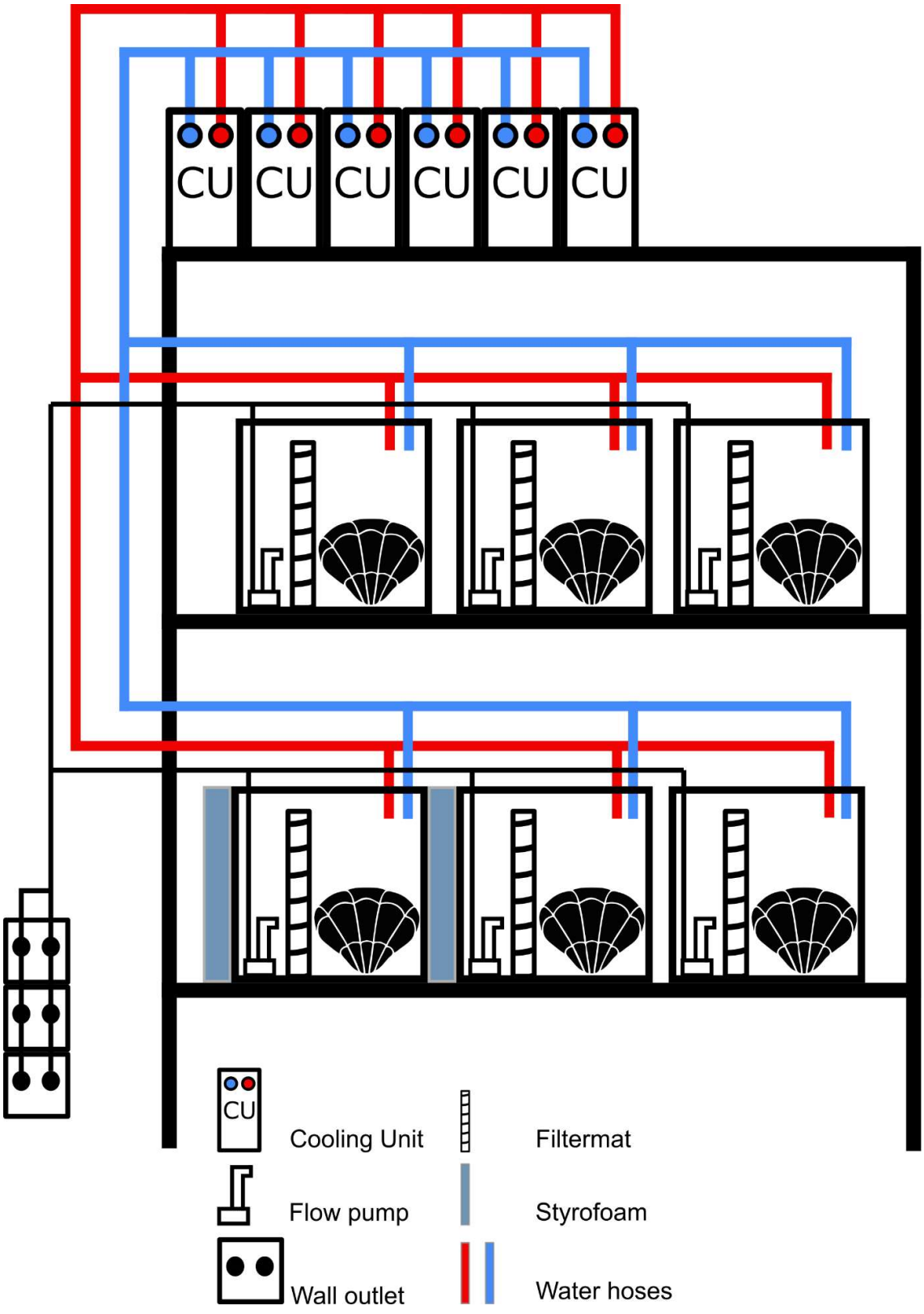

Figure 9-1 Schematic model of a cultivation setup with six tanks.

The space requirements are very low and can be achieved basically everywhere. For six cultivation containers that space required corresponds to 1 m². The footprint can be kept low by using heavy duty shelfs, ordering the tanks in several layers. Every tank needs three AC outlets but the actual power consumption is low (30 – 60 Watts/tank) so multiply sockets can be used, reducing the need to wall outlets to one per three tanks. The room itself should maintain a constant temperature and be equipped with a drain and water supply. Room isolation is not critical as Styrofoam boxes can be used to insulate the tanks.

The tank equipment depends to some extent on the species to be cultivated (cold/warm species, shallow/deep species). The most important point is the tank itself. Again, the size of the tank should be adjusted to the cultivated species and the experimental question but a mid-sized tank (40cm*40cm*40cm ~ 64L) can comply most requirements. A tank of this size can hold at least six *Ostrea edulis* (Rhodes et al., 1975) which is equal in size to *A. excavata*. This results in 36 possible organisms cultivatable in a six tank setup. Smaller bivalves, however, can be kept in a higher specimen density. Large filter systems are not needed for maintaining bivalves, as they depend on the particle load in the water for nutrition. Instead it is necessary to maximize the bio-chemical filtration while minimizing the physical filtration. This can be accomplished by using so-called “Hamburger Mattenfilter”. These filters consist of spongy filter mats that are located in the corner of the tank with a current pump behind them. The filter mats will be inhabited by microorganisms that perform the bio-chemical filtration (conversion of ammonia/nitrite to nitrate). Current pumps are necessary for each tank to ensure a constant flow rate that transports nutrient particles into the vicinity of the cultivated specimen. The flow rate needs to be adjusted to the cultivated species; some species prefer high flow rates, some species low flow rates. A specialized air supply is not strictly necessary but might be in species that depend on high oxygen concentrations. Temperature control is, however strictly necessary independent of the cultivated species. External cooling units are preferable as they can both heat and cool the water, but they are rather expensive. Without these units, temperate species cannot be cultivated unless the room is equipped with some sort of temperature control.

Depending on the experimental setup, tanks with equivalent temperature should be insulated with Styrofoam to minimize temperature variations and keep electrical cost at a minimum.

The monthly cost for a six tanks setup is 72€ ~ 12€/tank. The price is calculated with German electricity prices (0.3 cent/kW/h) and with constantly running filters and temperature control (not necessary with proper isolation). Additional cost is caused by the food necessary to cultivate the bivalves. There is specialized bivalve food available, but this does not reassemble the natural food sources. Live food such as Artemia larvae, *Brachionus* or Algal

mixtures (*Chaetoceros, Bellerochea* (Rodde et al., 1976)) is closer to the natural food sources and can be bought or cultivated alongside the bivalves.

Data logging can be done manually or automated with an Arduino/Raspberry Pi + temperature sensor (other kinds of sensors are available such as pH or conductivity). Ready-to-use solutions exist and offer a lot possibilities (automated feeding, complete datalogging including pH, temperature conductivity) but are rather expensive (100€ per tank).

All in all, the here presented setup would cost 200 €/tank consisting of the tank (50€), cooling unit (130 €), filter material (10€) and a current pump (10€). The prices can be decreased significantly by either choosing regular buckets instead of glass tanks and/or using heaters instead of cooling units (only warmwater species can be cultivated). Additionally, the items can be bought in large quantities, ultimately reducing the price per item. In addition to the presented costs, I suggest another 50€/tank for spare parts, hoses, and isolation material.

With the presented setup, a wide variety of different species can be cultivated and used for research questions

10 References

Adkins, J. F., Boyle, E. A., Curry, W. B., and Lutringer, A.: Stable isotopes in deep-sea corals and a new mechanism for “vital effects,” Geochimica et Cosmochimica Acta, 67, 1129–1143, https://doi.org/10.1016/S0016-7037(02)01203-6, 2003.

Affek, H. P., Bar-Matthews, M., Ayalon, A., Matthews, A., and Eiler, J. M.: Glacial/interglacial temperature variations in Soreq cave speleothems as recorded by “clumped isotope” thermometry, Geochimica et Cosmochimica Acta, https://doi.org/10.1016/j.gca.2008.06.031, 2008.

Alexander, S. P. and Delaca, T. E.: Feeding adaptations of the foraminiferan Cibicides refulgens living epizoically and parasitically on the Antarctic scallop Adamussium colbecki, Biological Bulletin, https://doi.org/10.2307/1541868, 1987.

Alfonso, J. A., Azocar, J., Labrecque, J. J., Garcia, B., Palacios, D., and Benzo, Z.: Trace metals in bivalves and seagrass collected from Venezuelan coastal sites, Revista de Biologia Tropical, 56, 215–222, https://doi.org/10.15517/rbt.v56i0.5588, 2008.

Allen, J. A.: The Ecology of Deep-Sea Molluscs, in: Ecology, Elsevier, 29–75, https://doi.org/10.1016/b978-0-12-751406-2.50009-x, 1983.

Ambrose, W. G., Panieri, G., Schneider, A., Plaza-Faverola, A., Carroll, M. L., Åström, E. K. L., Locke, W. L., and Carroll, J. L.: Bivalve shell horizons in seafloor pockmarks of the last glacial-interglacial transition: A thousand years of methane emissions in the Arctic Ocean, Geochemistry, Geophysics, Geosystems, 16, 4108–4129, https://doi.org/10.1002/2015GC005980, 2015.

Anagnostou, E., Sherrell, R. M., Gagnon, A., LaVigne, M., Field, M. P., and McDonough, W. F.: Seawater nutrient and carbonate ion concentrations recorded as P/Ca, Ba/Ca, and U/Ca in the deep-sea coral Desmophyllum dianthus, Geochimica et Cosmochimica Acta, 75, 2529–2543, https://doi.org/10.1016/j.gca.2011.02.019, 2011.

Anagnostou, E., Huang, K. F., You, C. F., Sikes, E. L., and Sherrell, R. M.: Evaluation of boron isotope ratio as a pH proxy in the deep sea coral Desmophyllum dianthus: Evidence of physiological pH adjustment, Earth and Planetary Science Letters, 349–350, 251–260, https://doi.org/10.1016/j.epsl.2012.07.006, 2012.

WoRMS - World Register of Marine Species - Acesta excavata (Fabricius, 1779): http://www.marinespecies.org/aphia.php?p=taxdetails&id=140232, last access: 31 August 2020.

WoRMS - World Register of Marine Species - Desmophyllum pertusum (Linnaeus, 1758): http://www.marinespecies.org/aphia.php?p=taxdetails&id=1245747, last access: 30 July 2021.

WoRMS - World Register of Marine Species - Hyrrokkin Cedhagen, 1994: http://www.marinespecies.org/aphia.php?p=taxdetails&id=556142, last access: 30 July 2021.

Babcock, R. C., Wills, B. L., and Simpson, C. J.: Mass spawning of corals on a high latitude coral reef, Coral Reefs, 13, 161–169, https://doi.org/10.1007/BF00301193, 1994.

Bajnai, D., Fiebig, J., Tomašových, A., Milner Garcia, S., Rollion-Bard, C., Raddatz, J., Löffler, N., Primo-Ramos, C., and Brand, U.: Assessing kinetic fractionation in brachiopod calcite using clumped isotopes, Scientific Reports, 8, 533, https://doi.org/10.1038/s41598-017-17353-7, 2018.

Bajnai, D., Guo, W., Spötl, C., Coplen, T. B., Methner, K., Löffler, N., Krsnik, E., Gischler, E., Hansen, M., Henkel, D., Price, G. D., Raddatz, J., Scholz, D., and Fiebig, J.: Dual clumped isotope thermometry resolves kinetic biases in carbonate formation temperatures, Nature Communications, 11, 4005, https://doi.org/10.1038/s41467-020-17501-0, 2020.

Ballesta-Artero, I., Zhao, L., Milano, S., Mertz-Kraus, R., Schöne, B. R., van der Meer, J., and Witbaard, R.: Environmental and biological factors influencing trace elemental and microstructural properties of Arctica islandica shells, Science of the Total Environment, 645, 913–923, https://doi.org/10.1016/j.scitotenv.2018.07.116, 2018.

Barats, A., Amouroux, D., Chauvaud, L., Pécheyran, C., Lorrain, A., Thébault, J., Church, T. M., and Donard, O. F. X.: High frequency Barium profiles in shells of the Great Scallop Pecten maximus: A methodical long-term and multi-site survey in Western Europe, Biogeosciences, 6, 157–170, https://doi.org/10.5194/bg-6-157-2009, 2009.

Barras, C., Duplessy, J.-C., Geslin, E., Michel, E., and Jorissen, F. J.: Calibration of δ 18 O of cultured benthic foraminiferal calcite as a function of temperature, Biogeosciences, 7, 1349–1356, https://doi.org/10.5194/bg-7-1349-2010, 2010.

Bemis, B. E., Spero, H. J., and Lea, W.: Reevaluation of the oxygen isotopic composition of planktonic foraminifera : Experimental results and revised paleotemperature equations for both species can be described by The O . relationships accurate with photosynthetic, 13, 150–160, 1998.

Bender, M. L., Klinkhammer, G. P., and Spencer, D. W.: Manganese in seawater and the marine manganese balance, Deep-Sea Research, 24, 799–812, https://doi.org/10.1016/0146-6291(77)90473-8, 1977.

Bentov, S., Brownlee, C., and Erez, J.: The role of seawater endocytosis in the biomineralization process in calcareous foraminifera, Proceedings of the National Academy of Sciences of the United States of America, 106, 21500–21504, https://doi.org/10.1073/pnas.0906636106, 2009.

Berelson, W., McManus, J., Coale, K., Johnson, K., Burdige, D., Kilgore, T., Colodner, D., Chavez, F., Kudela, R., and Boucher, J.: A time series of benthic flux measurements from Monterey Bay, CA, Continental Shelf Research, https://doi.org/10.1016/S0278-4343(03)00009-8, 2003.

Beuck, L., Correa, M. L., and Freiwald, A.: Biogeographical distribution of Hyrrokkin (Rosalinidae, Foraminifera) and its host-specific morphological and textural trace variability, in: Current Developments in Bioerosion, Springer Berlin Heidelberg, Berlin, Heidelberg, 329–360, https://doi.org/10.1007/978-3-540-77598-0_17, 2008.

Bigeleisen, J. and Mayer, M. G.: Calculation of Equilibrium Constants for Isotopic Exchange Reactions, The Journal of Chemical Physics, 15, 261–267, https://doi.org/10.1063/1.1746492, 1947.

Bijma, J., Spero, H. J., and Lea, D. W.: Reassessing Foraminiferal Stable Isotope Geochemistry: Impact of the Oceanic Carbonate System (Experimental Results), in: Use of Proxies in Paleoceanography, 489–512, https://doi.org/10.1007/978-3-642-58646-0_20, 1999.

Blamart, D., Rollion-bard, C., and Cuif, J.: Cold-Water Corals and Ecosystems, Cold-Water Corals and Ecosystems, https://doi.org/10.1007/3-540-27673-4, 2005.

Bourcier, M. and Zibrowius., H.: Note sur Lima excavata (Fabricius) pélécypod associé aux bancs coraux profonds. Société Zoologique de France, Bulletin 94(2):201-206. [Limidae], 1970.

Bourne, G. C.: Chap. 6. The Anthozoa. In: Lankester E.R. (ed), A Treatise on Zoology. Part II. The Porifera and Coelenterata. London, Adam & Charles Black., 1–84, 1900.

Brooke, S. and Järnegren, J.: Reproductive periodicity of the scleractinian coral *Lophelia pertusa* from the Trondheim Fjord, Norway, Marine Biology, 160, 139–153, https://doi.org/10.1007/s00227-012-2071-x, 2013.

Burnett, W. C., Bokuniewicz, H., Huettel, M., Moore, W. S., and Taniguchi, M.: Groundwater and pore water inputs to the coastal zone, https://doi.org/10.1023/B:BIOG.0000006066.21240.53, 2003.

Büscher, J.: Cold-water coral habitat characterisation and in situ physiological state analyses of four spatially distinct reefs in North- and mid-Norway-Cruise Report RV POSEIDON 525 [POS525], GEOMAR, Kiel, Germany, https://doi.org/10.3289/CR_POS525, 2018.

Büscher, J. V., Form, A. U., and Riebesell, U.: Interactive Effects of Ocean Acidification and Warming on Growth, Fitness and Survival of the Cold-Water Coral *Lophelia pertusa* under Different Food Availabilities, Frontiers in Marine Science, 4, 1–14, https://doi.org/10.3389/fmars.2017.00101, 2017.

Came, R. E., Eiler, J. M., Veizer, J., Azmy, K., Brand, U., and Weidman, C. R.: Coupling of surface temperatures and atmospheric CO2 concentrations during the Palaeozoic era, Nature, https://doi.org/10.1038/nature06085, 2007.

Carcassi, A.: Uteriore ritrovamento di Acesta excavata vivente in Mediterraneo., Bollettino Malacologico, 19, 264, 1983.

Cedhagen, T.: Taxonomy and biology of hyrrokkin sarcophaga gen. Et Sp. N., a parasitic foraminiferan (rosalinidae), Sarsia, 79, 65–82, https://doi.org/10.1080/00364827.1994.10413549, 1994.

Chauvaud, L. and Thébault, J.: What ' s Hiding Behind Ontogenetic δ 13 C Variations in Mollusk Shells ? New Insights from the Great Scallop (Pecten maximus), 211–220, https://doi.org/10.1007/s12237-010-9267-4, 2011.

Chauvaud, L., Helguen, L., Clavier, J., Pe, C., Thébault, J., L'Helguen, S., Barats, A., Jacquet, S., Pécheyran, C., and Amouroux, D.: Barium and molybdenum records in bivalve shells: Geochemical proxies for phytoplankton dynamics in coastal environments?, Limnology and Oceanography, 54, 1002–1014, 2009.

Cheng, Y. R. and Dai, C. F.: A bioeroding foraminifer, Hyrrokkin sarcophaga, on deepwater corals from the South China Sea, Coral Reefs, 35, 901, https://doi.org/10.1007/s00338-016-1447-7, 2016.

Chen, T., Yu, K., Li, S., Chen, T., and Shi, Q.: Anomalous Ba/Ca signals associated with low temperature stresses in Porites corals from Daya Bay, northern South China Sea, Journal of Environmental Sciences, 23, 1452–1459, https://doi.org/10.1016/S1001-0742(10)60606-7, 2011.

Chikaraishi, Y., Naraoka, H., and Poulson, S. R.: Hydrogen and carbon isotopic fractionations of lipid biosynthesis among terrestrial (C3, C4 and CAM) and aquatic plants, Phytochemistry, 65, 1369–1381, https://doi.org/10.1016/j.phytochem.2004.03.036, 2004.

Cléroux, C., Cortijo, E., Anand, P., Labeyrie, L., Bassinot, F., Caillon, N., and Duplessy, J. C.: Mg/Ca and Sr/Ca ratios in planktonic foraminifera: Proxies for upper water column temperature reconstruction, Paleoceanography, 23, https://doi.org/10.1029/2007PA001505, 2008.

Crenshaw, M. A.: The inorganic composition of molluscan extrapallial fluid, The Biological Bulletin, 143, 506–512, https://doi.org/10.2307/1540180, 1972.

Cuif, J.-P. and Dauphin, Y.: Microstructural and physico-chemical characterization of 'centers of calcification' in septa of some Recent scleractinian corals, Paläontologische Zeitschrift, 72, 257–269, https://doi.org/10.1007/bf02988357, 1998.

Cuif, J. P., Dauphin, Y. Y., Doucet, J., Salome, M., and Susini, J.: XANES mapping of organic sulfate in three scleractinian coral skeletons, Geochimica et Cosmochimica Acta, 67, 75–83, https://doi.org/10.1016/S0016-7037(02)01041-4, 2003.

Cusack, M., Dauphin, Y., Cuif, J. P., Salomé, M., Freer, A., and Yin, H.: Micro-XANES mapping of sulphur and its association with magnesium and phosphorus in the shell of the brachiopod, Terebratulina retusa, Chemical Geology, 253, 172–179, https://doi.org/10.1016/j.chemgeo.2008.05.007, 2008.

Dana, J. D.: Zoophytes. United States Exploring Expedition during the years 1838-1842, Lea and Blanchard, Philadelphia, 1846.

Dehairs, F., Baeyens, W., and Van Gansbeke, D.: Tight coupling between enrichment of iron and manganese in North Sea suspended matter and sedimentary redox processes: Evidence for seasonal variability, Estuarine, Coastal and Shelf Science, https://doi.org/10.1016/0272-7714(89)90080-2, 1989.

Dennis, K. J., Cochran, J. K., Landman, N. H., and Schrag, D. P.: The climate of the Late Cretaceous: New insights from the application of the carbonate clumped isotope thermometer to Western Interior Seaway macrofossil, Earth and Planetary Science Letters, 362, 51–65, https://doi.org/10.1016/j.epsl.2012.11.036, 2013.

Dodd, J. R.: Environmental control of strontium and magnesium in Mytilus, Geochimica et Cosmochimica Acta, 29, 385–398, https://doi.org/10.1016/0016-7037(65)90035-9, 1965.

D'Olivo, J. P., Sinclair, D. J., Rankenburg, K., and McCulloch, M. T.: A universal multi-trace element calibration for reconstructing sea surface temperatures from long-lived

Porites corals: Removing 'vital-effects,' Geochimica et Cosmochimica Acta, 239, 109–135, https://doi.org/10.1016/j.gca.2018.07.035, 2018.

Dullo, W. C., Flögel, S., and Rüggeberg, A.: Cold-water coral growth in relation to the hydrography of the Celtic and Nordic European continental margin, Marine Ecology Progress Series, 371, 165–176, https://doi.org/10.3354/meps07623, 2008.

Eagle, R. A., Eiler, J. M., Tripati, A. K., Ries, J. B., Freitas, P. S., Hiebenthal, C., Wanamaker, A. D., Taviani, M., Elliot, M., Marenssi, S., Nakamura, K., Ramirez, P., and Roy, K.: Climate of the Past Geoscientific Instrumentation Methods and Data Systems The influence of temperature and seawater carbonate saturation state on 13 C-18 O bond ordering in bivalve mollusks, Biogeosciences, 10, 4591–4606, https://doi.org/10.5194/bg-10-4591-2013, 2013.

Ehrenberg, C. G.: Beiträge zur physiologischen Kenntniss der Corallenthiere im allgemeinen, und besonders des rothen Meeres, nebst einem Versuche zur physiologischen Systematik derselben, Abhandlungen der Königlichen Akademie der Wissenschaften zu Berlin, 1, 1–156, 1834.

Eide, L. I.: Evidence of a topographically trapped vortex on the Norwegian continental shelf, Deep Sea Research Part A, Oceanographic Research Papers, 26, 601–621, https://doi.org/10.1016/0198-0149(79)90036-0, 1979.

Eiler, J. M.: "Clumped-isotope" geochemistry-The study of naturally-occurring, multiply-substituted isotopologues, Earth and Planetary Science Letters, https://doi.org/10.1016/j.epsl.2007.08.020, 2007.

El-Aneed, A., Cohen, A., and Banoub, J.: Mass spectrometry, review of the basics: Electrospray, MALDI, and commonly used mass analyzers, Applied Spectroscopy Reviews, 44, 210–230, https://doi.org/10.1080/05704920902717872, 2009.

Elliot, M., de Menocal, P. B., Linsley, B. K., Howe, S. S., Guilderson, T., and Quitmyer, I. R.: Late Holocene Environmental and Hydrologic Conditions in Northwestern Florida Derived from Seasonally Resolved Profiles of δ¹⁸O and Sr/Ca of Fossil Bivalves., AGUFM, 2002, PP72A-0429, 2002.

Elliot, M., Welsh, K., Chilcott, C., McCulloch, M., Chappell, J., and Ayling, B.: Profiles of trace elements and stable isotopes derived from giant long-lived *Tridacna gigas* bivalves: Potential applications in paleoclimate studies, Palaeogeography, Palaeoclimatology, Palaeoecology, 280, 132–142, https://doi.org/10.1016/j.palaeo.2009.06.007, 2009.

Epstein, S., Buchsbaum, R., Lowenstam, H. A., and Urey, H. C.: Revised carbonate-water isotopic temperature scale, Bulletin of the Geological Society of America, 64, 1315–1326, https://doi.org/10.1130/0016-7606(1953)64[1315:RCITS]2.0.CO;2, 1953.

Etayo-Cadavid, M. F., Andrus, C. F. T., Jones, K. B., and Hodgins, G. W. L.: Subseasonal variations in marine reservoir age from pre-bomb Donax obesulus and Protothaca asperrima shell carbonate, Chemical Geology, 526, 110–116, https://doi.org/10.1016/j.chemgeo.2018.07.001, 2019.

Feigl, F., Anger, V., and Koslow, R. H.: Spot Tests in Inorganic Analysis, Journal of The Electrochemical Society, 120, 261C, https://doi.org/10.1149/1.2403827, 1973.

Fiebig, J., Schöne, B. R., and Oschmann, W.: High-precision oxygen and carbon isotope analysis of very small (10-30 µg) amounts of carbonates using continuous flow isotope ratio mass spectrometry [2], https://doi.org/10.1002/rcm.2060, 2005.

Filipsson, H. L., Bernhard, J. M., Lincoln, S. A., and Mccorkle, D. C.: A culture-based calibration of benthic foraminiferal paleotemperature proxies: δ 18 O and Mg/Ca results, Biogeosciences, 7, 1335–1347, https://doi.org/10.5194/bg-7-1335-2010, 2010.

Finch, A. A. and Allison, N.: Mg structural state in coral aragonite and implications for the paleoenvironmental proxy, Geophysical Research Letters, 35, 1–5, https://doi.org/10.1029/2008GL033543, 2008.

Form, A. U., Büscher, J., Hissmann, K., Flögel, S., Wisshak, M., Rüggeberg, A., Hennige, S., Bennecke, S., Bannister, R., Schauer, J., and Fenske, M.: RV POSEIDON Cruise Report POS455 LORELEI Lophelia Reef Lander Expedition and Investigation, 1–29, https://doi.org/10.3289/CR_POS_455, 2014.

Form, A. U., Büscher, J., Hissmann, K., Flögel, S., Wisshak, M., Rüggenberg, A., Bannister, R., Kutti, T., Stapp, L., Bennecke, S., Küter, M., Nachtigall, K., Schauer, J., and Fenske, M.: RV POSEIDON Cruise Report POS473 LORELEI II LOphelia REef Lander Expedition and Investigation II, Tromsø-Bergen-Esbjerg, 15.08.-31.08.-04.09.2014, 25 pp. pp., https://doi.org/10.3289/CR_POS_473, 2015.

Foster, G. L.: Seawater pH, pCO2 and [CO2-3] variations in the Caribbean Sea over the last 130 kyr: A boron isotope and B/Ca study of planktic foraminifera, Earth and Planetary Science Letters, 271, 254–266, https://doi.org/10.1016/j.epsl.2008.04.015, 2008.

Foster, L. C., Finch, A. A., Allison, N., Andersson, C., and Clarke, L. J.: Mg in aragonitic bivalve shells: Seasonal variations and mode of incorporation in Arctica islandica, Chemical Geology, 254, 113–119, https://doi.org/10.1016/j.chemgeo.2008.06.007, 2008.

Freitas, P., Clarke, L. J., Kennedy, H., Richardson, C., and Abrantes, F.: Mg/Ca, Sr/Ca, and stable-isotope (δ18O and δ13C) ratio profiles from the fan mussel *Pinna nobilis*: Seasonal records and temperature relationships, Geochemistry, Geophysics, Geosystems, 6, https://doi.org/10.1029/2004GC000872, 2005.

Freitas, P. S., Clarke, L. J., Kennedy, H., Richardson, C. A., and Abrantes, F.: Environmental and biological controls on elemental (Mg/Ca, Sr/Ca and Mn/Ca) ratios in shells of the king scallop Pecten maximus, Geochimica et Cosmochimica Acta, 70, 5119–5133, https://doi.org/10.1016/j.gca.2006.07.029, 2006.

Freitas, P. S., Clarke, L. J., Kennedy, H. A., and Richardson, C. A.: Inter- and intra-specimen variability masks reliable temperature control on shell Mg/Ca ratios in laboratory- and field-cultured *Mytilus edulis* and *Pecten maximus* (bivalvia), Biogeosciences, 5, 1245–1258, https://doi.org/10.5194/bg-5-1245-2008, 2008.

Freitas, P. S., Clarke, L. J., Kennedy, H., and Richardson, C. A.: Ion microprobe assessment of the heterogeneity of Mg/Ca, Sr/Ca and Mn/Ca ratios in Pecten maximus and Mytilus edulis (bivalvia) shell calcite precipitated at constant temperature, Biogeosciences, 6, 1209–1227, https://doi.org/10.5194/bg-6-1209-2009, 2009.

Freiwald, A.: Reef-Forming Cold-Water Corals, in: Ocean Margin Systems, Springer Berlin Heidelberg, Berlin, Heidelberg, 365–385, https://doi.org/10.1007/978-3-662-05127-6_23, 2002.

Freiwald, A., Hühnerbach, V., Lindberg, B., Wilson, J. B., and Campbell, J.: The Sula Reef Complex, Norwegian shelf, Facies, https://doi.org/10.1007/bf02667712, 2002.

Gabitov, R. I., Sadekov, A., and Leinweber, A.: Crystal growth rate effect on Mg/Ca and Sr/Ca partitioning between calcite and fluid: An in situ approach, Chemical Geology, 367, 70–82, https://doi.org/10.1016/j.chemgeo.2013.12.019, 2014a.

Gabitov, R. I. I., Sadekov, A., and Leinweber, A.: Crystal growth rate effect on Mg/Ca and Sr/Ca partitioning between calcite and fluid: An in situ approach, Chemical Geology, 367, 70–82, https://doi.org/10.1016/j.chemgeo.2013.12.019, 2014b.

Gage, J. D.: Food inputs, utilization, carbon flow, and energetics, Ecosystems of Deep Oceans, 315–382, 2003.

Gagnon, A. C., Gothmann, A. M., Branson, O., Rae, J. W. B., and Stewart, J. A.: Controls on boron isotopes in a cold-water coral and the cost of resilience to ocean acidification, Earth and Planetary Science Letters, 554, https://doi.org/10.1016/j.epsl.2020.116662, 2021.

Gagnon, J. M. and Haedrich, R. L.: First record of the European Giant File Clam, Acesta excavata (Bivalvia: Pectinoidea: Limidae), in the Northwest Atlantic, Canadian Field-Naturalist, 117, 440–447, https://doi.org/10.22621/cfn.v117i3.748, 2003.

Gaillardet, J. and Allègre, C. J.: Boron isotopic compositions of corals: Seawater or diagenesis record?, Earth and Planetary Science Letters, 136, 665–676, https://doi.org/10.1016/0012-821X(95)00180-K, 1995.

Gass, S. E. and Roberts, J. M.: Growth and branching patterns of *Lophelia pertusa* (Scleractinia) from the North Sea, Journal of the Marine Biological Association of the United Kingdom, 91, 831–835, https://doi.org/10.1017/S002531541000055X, 2011.

Ghisotti, F.: Ritrivamente di *Acesta excavata* (Fabricius, 1779) vivente in Mediterraneo, Bollettino Malacologico, 15, 57–66, 1979.

Ghosh, P., Adkins, J., Affek, H., Balta, B., Guo, W., Schauble, E. A., Schrag, D., and Eiler, J. M.: 13C-18O bonds in carbonate minerals: A new kind of paleothermometer, Geochimica et Cosmochimica Acta, 70, 1439–1456, https://doi.org/10.1016/j.gca.2005.11.014, 2006.

Gillikin, D. P., Dehairs, F., Lorrain, A., Steenmans, D., Baeyens, W., and André, L.: Barium uptake into the shells of the common mussel (Mytilus edulis) and the potential for estuarine paleo-chemistry reconstruction, Geochimica et Cosmochimica Acta, 70, 395–407, https://doi.org/10.1016/j.gca.2005.09.015, 2006a.

Gillikin, D. P., Lorrain, A., Bouillon, S., Willenz, P., and Dehairs, F.: Stable carbon isotopic composition of Mytilus edulis shells: relation to metabolism, salinity, δ13CDIC and phytoplankton, Organic Geochemistry, 37, 1371–1382, https://doi.org/10.1016/j.orggeochem.2006.03.008, 2006b.

Gillikin, D. P., Lorrain, A., Meng, L., and Dehairs, F.: A large metabolic carbon contribution to the δ13C record in marine aragonitic bivalve shells, Geochimica et Cosmochimica Acta, 71, 2936–2946, https://doi.org/10.1016/j.gca.2007.04.003, 2007.

Gillikin, D. P., Lorrain, A., Paulet, Y. M., André, L., and Dehairs, F.: Synchronous barium peaks in high-resolution profiles of calcite and aragonite marine bivalve shells, Geo-Marine Letters, 28, 351–358, https://doi.org/10.1007/s00367-008-0111-9, 2008.

Glasby, G. P. and Schulz, H. D.: E(H), pH diagrams for Mn, Fe, Co, Ni, Cu and As under seawater conditions: Application of two new types of E(H), pH diagrams to the study of specific problems in marine geochemistry, Aquatic Geochemistry, https://doi.org/10.1023/A:1009663322718, 1999.

Glock, N., Eisenhauer, A., Liebetrau, V., Wiedenbeck, M., Hensen, C., and Nehrke, G.: EMP and SIMS studies on Mn/Ca and Fe/Ca systematics in benthic foraminifera from the Peruvian OMZ: A contribution to the identification of potential redox proxies and the impact of cleaning protocols, Biogeosciences, 9, 341–359, https://doi.org/10.5194/bg-9-341-2012, 2012.

Glover, E. D. and Sippel, R. F.: Synthesis of magnesium calcites, Geochimica et Cosmochimica Acta, 31, 603–613, https://doi.org/10.1016/0016-7037(67)90037-3, 1967.

Goewert, A., Surge, D., Carpenter, S. J., and Downing, J.: Oxygen and carbon isotope ratios of Lampsilis cardium (Unionidae) from two streams in agricultural watersheds of Iowa, USA, Palaeogeography, Palaeoclimatology, Palaeoecology, https://doi.org/10.1016/j.palaeo.2007.06.002, 2007.

Gordillo, S., Brey, T., Beyer, K., and Lomovasky, B. J.: Climatic and environmental changes during the middle to late Holocene in southern South America: A sclerochronological approach using the bivalve Retrotapes exalbidus (Dillwyn) from the beagle channel, Quaternary International, 377, 83–90, https://doi.org/10.1016/j.quaint.2014.12.036, 2015.

Gordon, C. M., Carr, R. A., and Larson, R. E.: the Influence of Environmental Factors on the Sodium and Manganese Content of Barnacle Shells, Limnology and Oceanography, 15, 461–466, https://doi.org/10.4319/lo.1970.15.3.0461, 1970.

Gray, W. R. and Evans, D.: Nonthermal Influences on Mg/Ca in Planktonic Foraminifera: A Review of Culture Studies and Application to the Last Glacial Maximum, Paleoceanography and Paleoclimatology, 34, 306–315, https://doi.org/10.1029/2018PA003517, 2019.

Groeneveld, J. and Filipsson, H. L.: Mg/Ca and Mn/Ca ratios in benthic foraminifera: the potential to reconstruct past variations in temperature and hypoxia in shelf regions, Biogeosciences, 10, 5125–5138, https://doi.org/10.5194/bg-10-5125-2013, 2013.

Guo, W., Mosenfelder, J. L., Goddard, W. A., and Eiler, J. M.: Isotopic fractionations associated with phosphoric acid digestion of carbonate minerals: Insights from first-principles theoretical modeling and clumped isotope measurements, Geochimica et Cosmochimica Acta, 73, 7203–7225, https://doi.org/10.1016/j.gca.2009.05.071, 2009.

Guo, X., Xu, B., Burnett, W. C., Yu, Z., Yang, S., Huang, X., Wang, F., Nan, H., Yao, P., and Sun, F.: A potential proxy for seasonal hypoxia: LA-ICP-MS Mn/Ca ratios in benthic foraminifera from the Yangtze River Estuary, Geochimica et Cosmochimica Acta, 245, 290–303, https://doi.org/10.1016/j.gca.2018.11.007, 2019.

sen Gupta, B. K.: Modern Foraminifera, https://doi.org/10.1007/0-306-48104-9, 2003.

Hadden, C. S., Loftis, K. M., and Cherkinsky, A.: Carbon Isotopes (δ13C and Δ14C) in Shell Carbonate, Conchiolin, and Soft Tissues in Eastern Oyster (Crassostrea Virginica), in: Radiocarbon, 1125–1137, https://doi.org/10.1017/RDC.2018.27, 2018.

Haeckel, E.: Systematische Phylogenie. Entwurf eines Natürlichen Systems der Organismen auf Grund ihrer Stammesgeschichte, xv+400 pp., 1894.

Haedrich, R. L. and Gagnon, J. M.: Rock wall fauna in a deep Newfoundland fiord, Continental Shelf Research, 11, 1199–1207, https://doi.org/10.1016/0278-4343(91)90097-P, 1991.

Hall, J. M. and Chan, L. H.: Ba/Ca in benthic foraminifera: Thermocline and middepth circulation in the North Atlantic during the last glaciation, Paleoceanography, 19, 1–13, https://doi.org/10.1029/2004PA001028, 2004a.

Hall, J. M. and Chan, L. H.: Ba/Ca in Neogloboquadrina pachyderma as an indicator of deglacial meltwater discharge into the western Arctic Ocean, Paleoceanography, 19, 1–9, https://doi.org/10.1029/2003PA000910, 2004b.

Hallmann, N., Schöne, B. R., Strom, A., and Fiebig, J.: An intractable climate archive - Sclerochronological and shell oxygen isotope analyses of the Pacific geoduck, Panopea abrupta (bivalve mollusk) from Protection Island (Washington State, USA), Palaeogeography, Palaeoclimatology, Palaeoecology, 269, 115–126, https://doi.org/10.1016/j.palaeo.2008.08.010, 2008.

Hallmann, N., Burchell, M., Schöne, B. R., Irvine, G. V., and Maxwell, D.: High-resolution sclerochronological analysis of the bivalve mollusk Saxidomus gigantea from Alaska and British Columbia: techniques for revealing environmental archives and archaeological seasonality, Journal of Archaeological Science, 36, 2353–2364, https://doi.org/10.1016/j.jas.2009.06.018, 2009.

Hall-Spencer, J. M. and Moore, P. G.: Limaria hians (Mollusca: Limacea): A neglected reef-forming keystone species, Aquatic Conservation: Marine and Freshwater Ecosystems, 10, 267–277, https://doi.org/10.1002/1099-0755(200007/08)10:4<267::AID-AQC407>3.0.CO;2-B, 2000.

Hammer, K. M., Kristiansen, E., and Zachariassen, K. E.: Physiological effects of hypercapnia in the deep-sea bivalve Acesta excavata (Fabricius, 1779) (Bivalvia; Limidae), Marine Environmental Research, 72, 135–142, https://doi.org/10.1016/j.marenvres.2011.07.002, 2011.

Hatschek, B.: Lehrbuch der Zoologie : eine morphologische Übersicht des Thierreiches zur Einführung in das Studium dieser Wissenschaft / von Berthold Hatschek., https://doi.org/10.5962/bhl.title.1381, 2011.

Hauzer, H., Evans, D., Müller, W., Rosenthal, Y., and Erez, J.: Calibration of Na partitioning in the calcitic foraminifer *Operculina ammonoides* under variable Ca concentration: Toward reconstructing past seawater composition, Earth and Planetary Science Letters, 497, 80–91, https://doi.org/10.1016/j.epsl.2018.06.004, 2018.

Hedges, K. J., Ludsin, S. A., and Fryer, B. J.: Effects of ethanol preservation on otolith microchemistry, Journal of Fish Biology, 64, 923–937, https://doi.org/10.1111/j.1095-8649.2004.00353.x, 2004.

Hédouin, L., Pringault, O., Bustamante, P., Fichez, R., and Warnau, M.: Validation of two tropical marine bivalves as bioindicators of mining contamination in the New Caledonia lagoon: Field transplantation experiments, Water Research, 45, 483–496, https://doi.org/10.1016/j.watres.2010.09.002, 2011.

Heinemann, A., Fietzke, J., Melzner, F., Böhm, F., Thomsen, J., Garbe-Schnberg, D., and Eisenhauer, A.: Conditions of Mytilus edulis extracellular body fluids and shell composition in a pH-treatment experiment: Acid-base status, trace elements and δ11B, Geochemistry, Geophysics, Geosystems, https://doi.org/10.1029/2011GC003790, 2012.

Hemming, N. G. and Hanson, G. N.: Boron isotopic composition and concentration in modern marine carbonates, Geochimica et Cosmochimica Acta, 56, 537–543, https://doi.org/10.1016/0016-7037(92)90151-8, 1992.

Henehan, M. J., Foster, G. L., Bostock, H. C., Greenop, R., Marshall, B. J., and Wilson, P. A.: A new boron isotope-pH calibration for Orbulina universa, with implications for understanding and accounting for 'vital effects,' Earth and Planetary Science Letters, 454, 282–292, https://doi.org/10.1016/J.EPSL.2016.09.024, 2016.

Henkes, G. A., Passey, B. H., Wanamaker, A. D., Grossman, E. L., Ambrose, W. G., and Carroll, M. L.: Carbonate clumped isotope compositions of modern marine mollusk and brachiopod shells, Geochimica et Cosmochimica Acta, 106, 307–325, https://doi.org/10.1016/j.gca.2012.12.020, 2013.

Henry, L.-A. and Roberts, J. M.: Global Biodiversity in Cold-Water Coral Reef Ecosystems, in: Marine Animal Forests, Springer International Publishing, Cham, 235–256, https://doi.org/10.1007/978-3-319-21012-4_6, 2017.

Hillaire-Marcel, Claude. and De Vernal, Anne.: Proxies in late cenozoic paleoceanography, Elsevier, 843 pp., 2007.

Hydes, D. J., Statham, P. J., and Burton, J. D.: A vertical profile of dissolved trace metals (Al, Cd, Cu, Mn, Ni) over the median valley of the mid Atlantic ridge, 43°N: Implications for Hydrothermal activity, Science of the Total Environment, The, https://doi.org/10.1016/0048-9697(86)90236-6, 1986.

Ingram, B. L., Conrad, M. E., and Ingle, J. C.: Stable isotope and salinity systematics in estuarine waters and carbonates: San Francisco Bay, Geochimica et Cosmochimica Acta, 60, 455–467, https://doi.org/10.1016/0016-7037(95)00398-3, 1996.

Ishikawa, M. and Ichikuni, M.: Uptake of sodium and potassium by calcite, Chemical Geology, 42, 137–146, https://doi.org/10.1016/0009-2541(84)90010-X, 1984.

Järnegren, J. and Altin, D.: Filtration and respiration of the deep living bivalve Acesta excavata (J.C. Fabricius, 1779) (Bivalvia; Limidae), Journal of Experimental Marine Biology and Ecology, 334, 122–129, https://doi.org/10.1016/j.jembe.2006.01.014, 2006.

Järnegren, J., Rapp, H. T., and Young, C. M.: Similar reproductive cycles and life-history traits in congeneric limid bivalves with different modes of nutrition, Marine Ecology, 28, 183–192, https://doi.org/10.1111/j.1439-0485.2006.00134.x, 2007.

Jensen, A. and Frederiksen, R.: The fauna associated with the bank-forming deepwater coral *lophelia pertusa* (scleractinaria) on the faroe shelf, Sarsia, 77, 53–69, https://doi.org/10.1080/00364827.1992.10413492, 1992.

Jones, D. S., Williams, D. F., and Arthur, M. A.: Growth history and ecology of the Atlantic surf clam, Spisula solidissima (Dillwyn), as revealed by stable isotopes and annual shell increments, Journal of Experimental Marine Biology and Ecology, 73, 225–242, https://doi.org/10.1016/0022-0981(83)90049-7, 1983.

Kanjilal, S.: Middle Callovian (Jurassic) Acesta Adams & Adams and Plagiostoma J. Sowerby (Limidae: Bivalvia) from the Habo Hill, district Kachchh, Gujarat: Their, 1990.

Katz, A.: The interaction of magnesium with calcite during crystal growth at 25-90°C and one atmosphere, Geochimica et Cosmochimica Acta, 37, 1563–1586, https://doi.org/10.1016/0016-7037(73)90091-4, 1973.

Khani, M. H., Pahlavanzadeh, H., and Alizadeh, K.: Biosorption of strontium from aqueous solution by fungus Aspergillus terreus, Environmental Science and Pollution Research, 19, 2408–2418, https://doi.org/10.1007/s11356-012-0753-z, 2012.

Kinsman, J. J. and Holland, H. D.: The co-precipitation of cations with CaCO3 - IV. The co-precipitation of Sr2+ with aragonite between 16" and 96°C, Geochimica et Cosmochimica Acta, 33, 1–17, https://doi.org/10.1016/0016-7037(69)90089-1, 1969.

Kiriakoulakis, K., Fisher, E., Wolff, G. A., Freiwald, A., Grehan, A., and Roberts, J. M.: Lipids and nitrogen isotopes of two deep-water corals from the North-East Atlantic: initial results and implications for their nutrition, in: Cold-Water Corals and Ecosystems, Springer-Verlag, Berlin/Heidelberg, 715–729, https://doi.org/10.1007/3-540-27673-4_37, 2005.

Kiriakoulakis, K., Freiwald, A., Fisher, E., and Wolff, G. A.: Organic matter quality and supply to deep-water coral/mound systems of the NW European Continental Margin, International Journal of Earth Sciences, 96, 159–170, https://doi.org/10.1007/s00531-006-0078-6, 2007.

Kitano, Y., Okumura, M., and Idogaki, M.: Incorporation of sodium, chloride and sulfate with calcium carbonate., GEOCHEMICAL JOURNAL, 9, 75–84, https://doi.org/10.2343/geochemj.9.75, 1975.

Klein, R. T., Lohmann, K. C., and Thayer, C. W.: Bivalve skeletons record sea-surface temperature and δ18O via Mg/Ca and18O/16O ratios, Geology, 24, 415–418, https://doi.org/10.1130/0091-7613(1996)024<0415:BSRSST>2.3.CO;2, 1996.

Klinkhammer, G. P. and McManus, J.: Dissolved manganese in the Columbia River estuary: Production in the water column, Geochimica et Cosmochimica Acta, https://doi.org/10.1016/S0016-7037(01)00650-0, 2001.

Koho, K. A., de Nooijer, L. J., and Reichart, G. J.: Combining benthic foraminiferal ecology and shell Mn/Ca to deconvolve past bottom water oxygenation and paleoproductivity, Geochimica et Cosmochimica Acta, 165, 294–306, https://doi.org/10.1016/J.GCA.2015.06.003, 2015.

Kristjánsdóttir, G. B., Lea, D. W., Jennings, A. E., Pak, D. K., and Belanger, C.: New spatial Mg/Ca-temperature calibrations for three Arctic, benthic foraminifera and reconstruction of north Iceland shelf temperature for the past 4000 years, Geochemistry, Geophysics, Geosystems, 8, https://doi.org/10.1029/2006GC001425, 2007.

Kubota, K., Shirai, K., Murakami-Sugihara, N., Seike, K., Minami, M., Nakamura, T., and Tanabe, K.: Bomb-14C Peak in the North Pacific Recorded in Long-Lived Bivalve Shells (Mercenaria stimpsoni), Journal of Geophysical Research: Oceans, 123, 2867–2881, https://doi.org/10.1002/2017JC013678, 2018.

Kunioka, D., Shirai, K., Takahata, N., Sano, Y., Toyofuku, T., and Ujiie, Y.: Microdistribution of Mg/Ca, Sr/Ca, and Ba/Ca ratios in Pulleniatina obliquiloculata test by using a NanoSIMS: Implication for the vital effect mechanism, Geochemistry, Geophysics, Geosystems, 7, n/a-n/a, https://doi.org/10.1029/2006GC001280, 2006.

Lampitt, R. S., Bett, B. J., Kiriakoulakis, K., Popova, E. E., Ragueneau, O., Vangriesheim, A., and Wolff, G. A.: Material supply to the abyssal seafloor in the northeast Atlantic, https://doi.org/10.1016/S0079-6611(01)00047-7, 2001.

Lamy, E.: Révision des Scrobiculariidae vivants du Muséum d'Histoire Naturelle de Paris, Journal de Conchyliologie, 61, 243–368, 1913.

Landing, W. M. and Bruland, K. W.: The contrasting biogeochemistry of manganese and iron in the Pacific ocean., Geochimica et Cosmochimica Acta, 51, 29–43, https://doi.org/10.1016/0016-7037(87)90004-4, 1987.

LaVigne, M., Matthews, K. A., Grottoli, A. G., Cobb, K. M., Anagnostou, E., Cabioch, G., and Sherrell, R. M.: Coral skeleton P/Ca proxy for seawater phosphate: Multi-colony calibration with a contemporaneous seawater phosphate record, Geochimica et Cosmochimica Acta, 74, 1282–1293, https://doi.org/10.1016/j.gca.2009.11.002, 2010.

LaVigne, M., Hill, T. M., Spero, H. J., and Guilderson, T. P.: Bamboo coral Ba/Ca: Calibration of a new deep ocean refractory nutrient proxy, Earth and Planetary Science Letters, 312, 506–515, https://doi.org/10.1016/j.epsl.2011.10.013, 2011.

Lazareth, C. E., Vander Putten, E., André, L., and Dehairs, F.: High-resolution trace element profiles in shells of the mangrove bivalve Isognomon ephippium: A record of environmental spatio-temporal variations?, Estuarine, Coastal and Shelf Science, 57, 1103–1114, https://doi.org/10.1016/S0272-7714(03)00013-1, 2003.

Lea, D. and Boyle, E.: Barium content of benthic foraminifera controlled by bottom-water composition, Nature, 338, 751–753, https://doi.org/10.1038/338751a0, 1989.

Lea, D. W. and Boyle, E. A.: Barium in planktonic foraminifera, Geochimica et Cosmochimica Acta, 55, 3321–3331, https://doi.org/10.1016/0016-7037(91)90491-M, 1991.

Lea, D. W., Mashiotta, T. A., and Spero, H. J.: Controls on magnesium and strontium uptake in planktonic foraminifera determined by live culturing, Geochimica et Cosmochimica Acta, 63, 2369–2379, https://doi.org/10.1016/S0016-7037(99)00197-0, 1999.

Lear, C., Elderfield, H., and Wilson, P.: Cenozoic {Deep-Sea} Temperatures and Global Ice Volumes from {Mg/Ca} in Benthic Foraminiferal Calcite, Science, 287, 269–272, https://doi.org/10.1126/science.287.5451.269, 2000.

Lear, C. H., Rosenthal, Y., and Slowey, N.: Benthic foraminiferal Mg/Ca-paleothermometry: A revised core-top calibration, Geochimica et Cosmochimica Acta, 66, 3375–3387, https://doi.org/10.1016/S0016-7037(02)00941-9, 2002.

Levin, L. A. and Bris, N. L.: The deep ocean under climate change, Science, 350, 766–768, https://doi.org/10.1126/science.aad0126, 2015.

Linnaeus, C.: Systema naturae per regna tria naturae: secundum classes, ordines, genera, species, cum characteribus, differentiis, synonymis, locis. Editio duodecima. 1. Regnum Animale. 1 & 2 Holmiae, Laurentii Salvii, 1758.

López Correa, M., Freiwald, A., Hall-Spencer, J., and Taviani, M.: Distribution and habitats of *Acesta excavata* (Bivalvia: Limidae) with new data on its shell ultrastructure, Cold-Water Corals and Ecosystems, 173–205, https://doi.org/10.1007/3-540-27673-4_9, 2005.

Lorens, R. B.: Sr, Cd, Mn and Co distribution coefficients in calcite as a function of calcite precipitation rate, Geochimica et Cosmochimica Acta, 45, 553–561, https://doi.org/10.1016/0016-7037(81)90188-5, 1981.

Lorens, R. B. and Bender, M. L.: The impact of solution chemistry on *Mytilus edulis* calcite and aragonite, Geochimica et Cosmochimica Acta, 44, 1265–1278, https://doi.org/10.1016/0016-7037(80)90087-3, 1980.

Lorrain, A., Paulet, Y. M., Chauvaud, L., Dunbar, R., Mucciarone, D., and Fontugne, M.: δ13C variation in scallop shells: Increasing metabolic carbon contribution with body size?, Geochimica et Cosmochimica Acta, https://doi.org/10.1016/j.gca.2004.01.025, 2004.

Lorrain, A., Gillikin, D. P., Paulet, Y. M., Chauvaud, L., le Mercier, A., Navez, J., and André, L.: Strong kinetic effects on Sr/Ca ratios in the calcitic bivalve Pecten maximus, Geology, 33, 965–968, https://doi.org/10.1130/G22048.1, 2005.

Mackensen, A. and Bickert, T.: Stable Carbon Isotopes in Benthic Foraminifera: Proxies for Deep and Bottom Water Circulation and New Production, Use of Proxies in Paleoceanography, 229–254, https://doi.org/10.1007/978-3-642-58646-0_9, 1999.

Madsen, F. J.: Marine Bivalvia, The Zoology of Iceland, 4, 1–116, https://doi.org/10.1071/IS03007, 1949.

Malatesta, A. and Zarlenga, F.: Northern guests in the Pleistocene Mediterranean Sea, Geologica Romana, 25, 91–154, 1986.

Marali, S., Schöne, B. R., Mertz-Kraus, R., Griffin, S. M., Wanamaker, A. D., Matras, U., and Butler, P. G.: Ba/Ca ratios in shells of Arctica islandica—Potential environmental

proxy and crossdating tool, Palaeogeography, Palaeoclimatology, Palaeoecology, 465, 347–361, https://doi.org/10.1016/j.palaeo.2015.12.018, 2017a.

Marali, S., Schöne, B. R., Mertz-Kraus, R., Griffin, S. M., Wanamaker, A. D., Butler, P. G., Holland, H. A., and Jochum, K. P.: Reproducibility of trace element time-series (Na/Ca, Mg/Ca, Mn/Ca, Sr/Ca, and Ba/Ca) within and between specimens of the bivalve *Arctica islandica* – A LA-ICP-MS line scan study, Palaeogeography, Palaeoclimatology, Palaeoecology, 484, 109–128, https://doi.org/10.1016/j.palaeo.2016.11.024, 2017b.

Mcconnaughey, T. A. and Gillikin, D. P.: Carbon isotopes in mollusk shell carbonates, 287–299, https://doi.org/10.1007/s12237-010-9267-4, 2008.

McConnaughey, T. A., Burdett, J., Whelan, J. F., and Paull, C. K.: Carbon isotopes in biological carbonates: Respiration and photosynthesis, Geochimica et Cosmochimica Acta, 61, 611–622, https://doi.org/10.1016/S0016-7037(96)00361-4, 1997.

McCulloch, M., Falter, J., Trotter, J., and Montagna, P.: Coral resilience to ocean acidification and global warming through pH up-regulation, Nature Climate Change, 2, 623–627, https://doi.org/10.1038/nclimate1473, 2012a.

McCulloch, M., Trotter, J., Montagna, P., Falter, J., Dunbar, R., Freiwald, A., Försterra, G., López Correa, M., Maier, C., Rüggeberg, A., and Taviani, M.: Resilience of cold-water scleractinian corals to ocean acidification: Boron isotopic systematics of pH and saturation state up-regulation, Geochimica et Cosmochimica Acta, 87, 21–34, https://doi.org/10.1016/j.gca.2012.03.027, 2012b.

McKenna, V. S. and Prell, W. L.: Calibration of the Mg/Ca of Globorotalia truncatulinoides (R) for the reconstruction of marine temperature gradients, Paleoceanography, 19, https://doi.org/10.1029/2000PA000604, 2004.

Mienis, F., de Stigter, H. C., White, M., Duineveld, G., de Haas, H., and van Weering, T. C. E.: Hydrodynamic controls on cold-water coral growth and carbonate-mound development at the SW and SE Rockall Trough Margin, NE Atlantic Ocean, Deep-Sea Research Part I: Oceanographic Research Papers, 54, 1655–1674, https://doi.org/10.1016/j.dsr.2007.05.013, 2007.

Mikkelsen, P. M. and Bieler, R.: Systematic revision of the western Atlantic file clams, Lima and Ctenoides (Bivalvia : Limoida : Limidae), Invertebrate Systematics, 17, 667, https://doi.org/10.1071/IS03007, 2003.

Mitsuguchi, T., Matsumoto, E., and Uchida, T.: Mg/Ca and Sr/Ca ratios of Porites coral skeleton: Evaluation of the effect of skeletal growth rate, Coral Reefs, 22, 381–388, https://doi.org/10.1007/s00338-003-0326-1, 2003.

Mook, W. G. and Vogel, J. C.: Isotopic equilibrium between shells and their environment, Science, 159, 874–875, https://doi.org/10.1126/science.159.3817.874, 1968.

Morse, J. W. and Bender, M. L.: Partition coefficients in calcite: Examination of factors influencing the validity of experimental results and their application to natural systems, Chemical Geology, 82, 265–277, https://doi.org/10.1016/0009-2541(90)90085-L, 1990.

Mortensen, P. B., Hovland, T., Fosså, J. H., and Furevik, D. M.: Distribution, abundance and size of *Lophelia pertusa* coral reefs in mid-Norway in relation to seabed characteristics, Journal of the Marine Biological Association of the United Kingdom, 81, 581–597, https://doi.org/10.1017/S002531540100426X, 2001.

Mucci, A. and Morse, J.: Chemistry of low-temperature abiotic calcites: Experimental studies on coprecipitation, stability, and fractionation, Rev. Aquat. Sci, 3, 217–254, 1990.

Mucci, A. and Morse, J. W.: The incorporation of Mg 2+ and Sr 2+ into calcite overgrowths: influences of growth rate and solution composition, Geochimica et Cosmochimica Acta, 47, 217–233, 1983.

Müller, W. and Fietzke, J.: The role of LA-ICP-MS in palaeoclimate research, Elements, 12, 329–334, https://doi.org/10.2113/gselements.12.5.329, 2016.

Naumann, M. S., Orejas, C., Wild, C., and Ferrier-Pages, C.: First evidence for zooplankton feeding sustaining key physiological processes in a scleractinian cold-water coral, Journal of Experimental Biology, 214, 3570–3576, https://doi.org/10.1242/jeb.061390, 2011.

Nehrke, G., Keul, N., Langer, G., de Nooijer, L. J., Bijma, J., and Meibom, A.: A new model for biomineralization and trace-element signatures of Foraminifera tests, Biogeosciences, https://doi.org/10.5194/bg-10-6759-2013, 2013.

Newton, A., Kohn, M. J., and Thunell, R. C.: Trace element (Mg, Sr, P, Ba and Cd) variability in single foraminifera and a possible new proxy for seawater phosphate, AGUFM, 2007, PP42A-06, 2007.

de Nooijer, L. J., Toyofuku, T., and Kitazato, H.: Foraminifera promote calcification by elevating their intracellular pH, Proceedings of the National Academy of Sciences of the United States of America, 106, 15374–15378, https://doi.org/10.1073/pnas.0904306106, 2009.

de Nooijer, L. J., Spero, H. J., Erez, J., Bijma, J., and Reichart, G. J.: Biomineralization in perforate foraminifera, Earth-Science Reviews, 135, 48–58, https://doi.org/10.1016/j.earscirev.2014.03.013, 2014.

Nürnberg, D., Bijma, J., and Hemleben, C.: Assessing the reliability of magnesium in foraminiferal calcite as a proxy for water mass temperatures, Geochimica et Cosmochimica Acta, 60, 803–814, https://doi.org/10.1016/0016-7037(95)00446-7, 1996.

Okumura, M. and Kitano, Y.: Coprecipitation of alkali metal ions with calcium carbonate, Geochimica et Cosmochimica Acta, 50, 49–58, https://doi.org/10.1016/0016-7037(86)90047-5, 1986.

O'Leary, M. H.: Carbon Isotopes in Photosynthesis, BioScience, 38, 328–336, https://doi.org/10.2307/1310735, 1988.

Olesik, J. W.: Elemental analysis using ICP-OES and ICP/MS, Analytical Chemistry, https://doi.org/10.1021/ac00001a001, 1991.

Oliver, P. G.: Adaptations of some deep-sea suspension-feeding bivalves (limopsis and bathyarca), Sarsia, 64, 33–36, https://doi.org/10.1080/00364827.1979.10411359, 1979.

O'Neil, D. D. and Gillikin, D. P.: Do freshwater mussel shells record road-salt pollution?, Scientific Reports, 4, 1–6, https://doi.org/10.1038/srep07168, 2014.

Oomori, T., Kaneshima, H., Maezato, Y., and Kitano, Y.: Distribution Coefficient of Mg2+ ions between calcite and solution at 10-50°C, Marine Chemistry, 20, 327–336, https://doi.org/10.1016/B978-044452228-3/50006-6, 1987.

Oron, S., Sadekov, A., Katz, T., and Goodman-Tchernov, B.: Benthic foraminifera geochemistry as a monitoring tool for heavy metal and phosphorus pollution — A post fish-farm removal case study, Marine Pollution Bulletin, 168, 112443, https://doi.org/10.1016/J.MARPOLBUL.2021.112443, 2021.

Owen, E. F., Wanamaker, A. D., Feindel, S. C., Schöne, B. R., and Rawson, P. D.: Stable carbon and oxygen isotope fractionation in bivalve (Placopecten magellanicus) larval aragonite, Geochimica et Cosmochimica Acta, 72, 4687–4698, https://doi.org/10.1016/j.gca.2008.06.029, 2008.

Owen, R., Kennedy, H., and Richardson, C.: Experimental investigation into partitioning of stable isotopes between scallop (Pecten maximus) shell calcite and sea water, Palaeogeography, Palaeoclimatology, Palaeoecology, 185, 163–174, https://doi.org/10.1016/S0031-0182(02)00297-3, 2002.

Peharda, M., Sironić, A., Markulin, K., Jozić, S., Borković, D., and Andersson, C.: The bivalve glycymeris pilosa as an archive of 14C in the Mediterranean sea, Radiocarbon, 61, 599–613, https://doi.org/10.1017/RDC.2018.146, 2019.

Personal Observation: Personal Observation, 2018.

Pigati, J. S.: On correcting 14C ages of gastropod shell carbonate for fractionation, in: Radiocarbon, https://doi.org/10.1017/S0033822200032203, 2002.

Van Plantinga, A. A. and Grossman, E. L.: Stable and clumped isotope sclerochronologies of mussels from the Brazos River, Texas (USA): Environmental and ecologic proxy, Chemical Geology, 502, 55–65, https://doi.org/10.1016/j.chemgeo.2018.10.012, 2018.

Poppe, G. and Goto, Y.: European Seashells: Polyplacophora, Caudofoveata, Solenogastra, Gastropoda, 1991.

Poulain, C., Gillikin, D. P., Thébault, J., Munaron, J. M., Bohn, M., Robert, R., Paulet, Y. M., and Lorrain, A.: An evaluation of Mg/Ca, Sr/Ca, and Ba/Ca ratios as environmental proxies in aragonite bivalve shells, Chemical Geology, 396, 42–50, https://doi.org/10.1016/j.chemgeo.2014.12.019, 2015.

Purton, L. M. A., Shields, G. A., Brasier, M. D., and Grime, G. W.: Metabolism controls Sr/Ca ratios in fossil aragonitic mollusks, Geology, 27, 1083–1086, https://doi.org/10.1130/0091-7613(1999)027<1083:MCSCRI>2.3.CO;2, 1999.

Putten, E. Vander, Dehairs, F., Keppens, E., and Baeyens, W.: High resolution distribution of trace elements in the calcite shell layer of modern Mytilus edulis: Environmental and biological controls, Geochimica et Cosmochimica Acta, 64, 997–1011, https://doi.org/10.1016/S0016-7037(99)00380-4, 2000.

Raddatz, J., Liebetrau, V., Rüggeberg, A., Hathorne, E., Krabbenhöft, A., Eisenhauer, A., Böhm, F., Vollstaedt, H., Fietzke, J., López Correa, M., Freiwald, A., and Dullo, W. C.: Stable Sr-isotope, Sr/Ca, Mg/Ca, Li/Ca and Mg/Li ratios in the scleractinian cold-water coral *Lophelia pertusa*, Chemical Geology, 352, 143–152, https://doi.org/10.1016/j.chemgeo.2013.06.013, 2013a.

Raddatz, J., Liebetrau, V., Trotter, J., Rüggeberg, A., Flögel, S., Dullo, W.-C., Eisenhauer, A., Voigt, S., and McCulloch, M.: Environmental constraints on Holocene cold-water coral reef growth off Norway: Insights from a multiproxy approach, Paleoceanography, 31, 1350–1367, https://doi.org/10.1002/2016PA002974, 2016.

Rae, J. W. B.: Boron Isotopes, edited by: Marschall, H. and Foster, G., Springer International Publishing, Cham, https://doi.org/10.1007/978-3-319-64666-4, 2018.

Rae, J. W. B., Foster, G. L., Schmidt, D. N., and Elliott, T.: Boron isotopes and B/Ca in benthic foraminifera: Proxies for the deep ocean carbonate system, Earth and Planetary Science Letters, 302, 403–413, https://doi.org/10.1016/j.epsl.2010.12.034, 2011.

Rhodes, E. W., Calabrese, A., Cable, W. D., and Landers, W. S.: The Development of Methods for Rearing the Coot Clam, Mulinia Lateralis, and Three Species of Coastal Bivalves in the Laboratory, in: Culture of Marine Invertebrate Animals, Springer US, 273–282, https://doi.org/10.1007/978-1-4615-8714-9_18, 1975.

De Ridder, F., Pintelon, R., Schoukens, J., Gillikin, D. P., André, L., Baeyens, W., de Brauwere, A., and Dehairs, F.: Decoding nonlinear growth rates in biogenic environmental archives, Geochemistry, Geophysics, Geosystems, 5, n/a-n/a, https://doi.org/10.1029/2004GC000771, 2004.

Rink, S., Kühl, M., Bijma, J., and Spero, H. J.: Microsensor studies of photosynthesis and respiration in the symbiotic foraminifer Orbulina universa, Marine Biology, 131, 583–595, https://doi.org/10.1007/s002270050350, 1998.

Rixhon, G., May, S. M., Engel, M., Mechernich, S., Schroeder-Ritzrau, A., Frank, N., Fohlmeister, J., Boulvain, F., Dunai, T., and Brückner, H.: Multiple dating approach (14C, 230Th/U and 36Cl) of tsunami-transported reef-top boulders on Bonaire (Leeward Antilles) – Current achievements and challenges, Marine Geology, 396, 100–113, https://doi.org/10.1016/j.margeo.2017.03.007, 2018.

Roberts, J. M., Wheeler, A., Freiwald, A., and Cairns, S.: Cold-Water Corals, Cambridge University Press, Cambridge, 1–350 pp., https://doi.org/10.1017/CBO9780511581588, 2009.

Rocchini, R.: Acesta excavata (Fabricius, 1779), nuovo ritrovamento in Mediterraneo, Bollettino Malacologico, 19, 83–84, 1983.

Rodde, K. M., Sunderlin, J. B., and Roels, O. A.: Experimental cultivation of Tapes japonica (Deshayes) (Bivalvia: Veneridae) in an artificial upwelling culture system, Aquaculture, 9, 203–215, https://doi.org/10.1016/0044-8486(76)90063-6, 1976.

Rogers, A. D.: The Biology of *Lophelia pertusa* (Linnaeus 1758) and Other Deep-Water Reef-Forming Corals and Impacts from Human Activities., International Review of Hydrobiology, 84, 315–406, https://doi.org/10.1002/iroh.199900032, 1999.

Rohling, E. J. and Cooke, S.: Carbonate Shells, c, 1998, 1998.

Rollion-Bard, C. and Blamart, D.: Possible controls on Li, Na, and Mg incorporation into aragonite coral skeletons, Chemical Geology, 396, 98–111, https://doi.org/10.1016/j.chemgeo.2014.12.011, 2015.

Rollion-Bard, C., Blamart, D., Cuif, J. P., and Dauphin, Y.: In situ measurements of oxygen isotopic composition in deep-sea coral, Lophelia pertusa: Re-examination of the

current geochemical models of biomineralization, Geochimica et Cosmochimica Acta, 74, 1338–1349, https://doi.org/10.1016/j.gca.2009.11.011, 2010.

Rosenthal, Y. and Katz, A.: The applicability of trace elements in freshwater shells for paleogeochemical studies, Chemical Geology, 78, 65–76, https://doi.org/10.1016/0009-2541(89)90052-1, 1989.

Rosenthal, Y., Lear, C. H., Oppo, D. W., and Linsley, B. K.: Temperature and carbonate ion effects on Mg/Ca and Sr/Ca ratios in benthic foraminifera: Aragonitic species Hoeglundina elegans, Paleoceanography, 21, n/a-n/a, https://doi.org/10.1029/2005PA001158, 2006.

Rucker, J. B. and Valentine, J. W.: Salinity response of trace element concentration in *Crassostrea virginica*, Nature, 190, 1099–1100, https://doi.org/10.1038/1901099a0, 1961.

Sadekov, A., Eggins, S. M., De Deckker, P., Ninnemann, U., Kuhnt, W., and Bassinot, F.: Surface and subsurface seawater temperature reconstruction using Mg/Ca microanalysis of planktonic foraminifera Globigerinoides ruber, Globigerinoides sacculifer, and Pulleniatina obliquiloculata, Paleoceanography, 24, https://doi.org/10.1029/2008PA001664, 2009.

Saenger, C., Affek, H. P., Felis, T., Thiagarajan, N., Lough, J. M., and Holcomb, M.: Carbonate clumped isotope variability in shallow water corals: Temperature dependence and growth-related vital effects, Geochimica et Cosmochimica Acta, 99, 224–242, https://doi.org/10.1016/j.gca.2012.09.035, 2012.

Schleinkofer, N., Raddatz, J., Freiwald, A., Evans, D., Beuck, L., Rüggeberg, A., and Liebetrau, V.: Environmental and biological controls on Na/Ca ratios in scleractinian cold-water corals, Biogeosciences, 16, 3565–3582, https://doi.org/10.5194/bg-16-3565-2019, 2019.

Schöne, B. and Surge, D. M.: Treatise Online no. 46: Part N, Revised, Volume 1, Chapter 14: Bivalve sclerochronology and geochemistry, Treatise Online, 0, https://doi.org/10.17161/to.v0i0.4297, 2012.

Schöne, B. R., Dunca, E., Fiebig, J., and Pfeiffer, M.: Mutvei's solution: An ideal agent for resolving microgrowth structures of biogenic carbonates, Palaeogeography, Palaeoclimatology, Palaeoecology, 228, 149–166, https://doi.org/10.1016/j.palaeo.2005.03.054, 2005.

Schöne, B. R., Zhang, Z., Jacob, D., Gillikin, D. P., Tütken, T., Garbe-Schönberg, D., McConnaughey, T., and Soldati, A.: Effect of organic matrices on the determination of the trace element chemistry (Mg, Sr, Mg/Ca, Sr/Ca) of aragonitic bivalve shells (*Arctica*

islandica) - Comparison of ICP-OES and LA-ICP-MS data, Geochemical Journal, 44, 23–37, https://doi.org/10.2343/geochemj.1.0045, 2010.

Schöne, B. R., Zhang, Z., Radermacher, P., Thébault, J., Jacob, D. E., Nunn, E. V., and Maurer, A. F.: Sr/Ca and Mg/Ca ratios of ontogenetically old, long-lived bivalve shells (*Arctica islandica*) and their function as paleotemperature proxies, Palaeogeography, Palaeoclimatology, Palaeoecology, 302, 52–64, https://doi.org/10.1016/j.palaeo.2010.03.016, 2011.

Schöne, B. R., Radermacher, P., Zhang, Z., and Jacob, D. E.: Crystal fabrics and element impurities (Sr/Ca, Mg/Ca, and Ba/Ca) in shells of *Arctica islandica*-Implications for paleoclimate reconstructions, Palaeogeography, Palaeoclimatology, Palaeoecology, 373, 50–59, https://doi.org/10.1016/j.palaeo.2011.05.013, 2013.

Schweizer, M., Bowser, S. S., Korsun, S., and Pawlowski, J.: Emendation of Cibicides Antarcticus (Saidova, 1975) Based on Molecular, Morphological, and ecological Data, The Journal of Foraminiferal Research, 42, 340–344, https://doi.org/10.2113/gsjfr.42.4.340, 2012.

Seguenza, G.: Studii stratigrafici sulla formazione pliocenica dell'Italia meridionale, 4 (1873): 29-45, 1 fig., pl. 1; 84–103, 2; 131- pp., 1873.

Seguenza, G.: Le formazioni terziarie nella provincia di Reggio (Calabria), Atti dell Accademia Nazionale dei Lincei.Classe di Scienze Fisiche, Matematiche e Naturali.Memorie.Sezione 3, 6, 3–443, 1880.

Spötl, C. and Mattey, D.: Stable isotope microsampling of speleothems for palaeoenvironmental studies: A comparison of microdrill, micromill and laser ablation techniques, Chemical Geology, 235, 48–58, https://doi.org/10.1016/j.chemgeo.2006.06.003, 2006.

Statham, P. J. and Burton, J. D.: Dissolved manganese in the North Atlantic Ocean, 0-35°N, Earth and Planetary Science Letters, https://doi.org/10.1016/0012-821X(86)90040-3, 1986.

Stecher, H. A., Krantz, D. E., Lord, C. J., Luther, G. W., and Bock, K. W.: Profiles of strontium and barium in Mercenaria mercenaria and Spisula solidissima shells, Geochimica et Cosmochimica Acta, 60, 3445–3456, https://doi.org/10.1016/0016-7037(96)00179-2, 1996.

Storm-Suke, A., Dempson, J. B., Caron, F., and Power, M.: Effects of formalin and ethanol preservation on otolith δ18O stable isotope signatures, Rapid Communications in Mass Spectrometry, 21, 503–508, https://doi.org/10.1002/rcm.2850, 2007.

Surge, D., Lohmann, K. C., and Dettman, D. L.: Controls on isotopic chemistry of the American oyster, Crassostrea virginica: Implications for growth patterns, Palaeogeography, Palaeoclimatology, Palaeoecology, 172, 283–296, https://doi.org/10.1016/S0031-0182(01)00303-0, 2001.

Surge, D. M. and Schöne, B. R.: Bivalve Sclerochronology, in: Encyclopedia of Scientific Dating Methods, edited by: Rink, W. J. and Thompson, J., Springer Netherlands, Dordrecht, 108–115, https://doi.org/10.1007/978-94-007-6304-3_165, 2015.

Takesue, R. K. and van Geen, A.: Mg/Ca, Sr/Ca, and stable isotopes in modern and Holocene *Protothaca staminea* shells from a northern California coastal upwelling region, Geochimica et Cosmochimica Acta, 68, 3845–3861, https://doi.org/10.1016/j.gca.2004.03.021, 2004.

Tanaka, K., Okaniwa, N., Miyaji, T., Murakami-Sugihara, N., Zhao, L., Tanabe, K., Schöne, B. R., and Shirai, K.: Microscale magnesium distribution in shell of the Mediterranean mussel Mytilus galloprovincialis: An example of multiple factors controlling Mg/Ca in biogenic calcite, Chemical Geology, 511, 0–1, https://doi.org/10.1016/j.chemgeo.2018.10.025, 2018.

Terreni, G. and Voliani, A.: New finding of Acesta excavata (Fabricius, 1779) in the Northern Tyrrhenian Sea, Conchiglia, 276, 13–14, 1995.

Thiagarajan, N., Adkins, J., and Eiler, J.: Carbonate clumped isotope thermometry of deep-sea corals and implications for vital effects, Geochimica et Cosmochimica Acta, 75, 4416–4425, https://doi.org/10.1016/j.gca.2011.05.004, 2011.

Thomas, J. and Gemming, T.: Analytische Transmissionselektronenmikroskopie, Springer Vienna, Vienna, https://doi.org/10.1007/978-3-7091-1440-7, 2013.

Tobin, T. S., Wilson, G. P., Eiler, J. M., and Hartman, J. H.: Environmental change across a terrestrial Cretaceous-Paleogene boundary section in eastern Montana, USA, constrained by carbonate clumped isotope paleothermometry, Geology, 42, 351–354, https://doi.org/10.1130/G35262.1, 2014.

Toyofuku, T., Matsuo, M. Y., de Nooijer, L. J., Nagai, Y., Kawada, S., Fujita, K., Reichart, G. J., Nomaki, H., Tsuchiya, M., Sakaguchi, H., and Kitazato, H.: Proton pumping accompanies calcification in foraminifera, Nature Communications, 8, 1–6, https://doi.org/10.1038/ncomms14145, 2017.

Tripati, A. K., Delaney, M. L., Zachos, J. C., Anderson, L. D., Kelly, D. C., and Elderfield, H.: Tropical sea-surface temperature reconstruction for the early Paleogene using Mg/Ca

ratios of planktonic foraminifera, Paleoceanography, 18, https://doi.org/10.1029/2003PA000937, 2003.

Tynan, S., Opdyke, B. N., Walczak, M., Eggins, S., and Dutton, A.: Assessment of Mg/Ca in Saccostrea glomerata (the Sydney rock oyster) shell as a potential temperature record, Palaeogeography, Palaeoclimatology, Palaeoecology, 484, 79–88, https://doi.org/10.1016/j.palaeo.2016.08.009, 2017.

Ullmann, C. V., Böhm, F., Rickaby, R. E. M., Wiechert, U., and Korte, C.: The Giant Pacific Oyster (Crassostrea gigas) as a modern analog for fossil ostreoids: Isotopic (Ca, O, C) and elemental (Mg/Ca, Sr/Ca, Mn/Ca) proxies, Geochemistry, Geophysics, Geosystems, 14, 4109–4120, https://doi.org/10.1002/ggge.20257, 2013.

Urey, H. C.: The thermodynamic properties of isotopic substances. Liversidge lecture, delivered before the Chemical Society in the Royal Institution on December 18th, 1946, Journal of the Chemical Society (Resumed), 562–581, https://doi.org/10.1039/jr9470000562, 1947.

Urey, H. C., Lowenstam, H. A., Epstein, S., and Mckinney, C. R.: Measurement of paleotemperatures and temperatures of the upper cretaceous of England, Denmark, and the southeastern United States, Bulletin of the Geological Society of America, 62, 399–416, https://doi.org/10.1130/0016-7606(1951)62[399:MOPATO]2.0.CO;2, 1951.

de Villiers, S., Shen, G. T., and Nelson, B. K.: The Sr/Ca-temperature relationship in coralline aragonite: Influence of variability in (Sr/Ca)Seawater and skeletal growth parameters, Geochimica et Cosmochimica Acta, 58, 197–208, https://doi.org/10.1016/0016-7037(94)90457-X, 1994.

de Villiers, S., Nelson, B. K., and Chivas, A.: Biological Control on Coral Sr/Ca and d18O Reconstructions of Sea Surface Temperatures, Science, 269, 1247–1249, 1995.

Wacker, U., Fiebig, J., Tödter, J., Schöne, B. R., Bahr, A., Friedrich, O., Tütken, T., Gischler, E., and Joachimski, M. M.: Empirical calibration of the clumped isotope paleothermometer using calcites of various origins, Geochimica et Cosmochimica Acta, 141, 127–144, https://doi.org/10.1016/j.gca.2014.06.004, 2014.

Walker, S. E., Hancock, L. G., and Bowser, S. S.: Diversity, biogeography, body size and fossil record of parasitic and suspected parasitic foraminifera: A review, Journal of Foraminiferal Research, 47, 34–55, https://doi.org/10.2113/gsjfr.47.1.34, 2017.

Waller, R. G. and Tyler, P. A.: The reproductive biology of two deep-water, reef-building scleractinians from the NE Atlantic Ocean, Coral Reefs, 24, 514–522, https://doi.org/10.1007/s00338-005-0501-7, 2005.

Wanamaker, A. D. and Gillikin, D. P.: Strontium, magnesium, and barium incorporation in aragonitic shells of juvenile *Arctica islandica*: Insights from temperature controlled experiments, Chemical Geology, 526, 117–129, https://doi.org/10.1016/j.chemgeo.2018.02.012, 2019.

Wanamaker, A. D., Kreutz, K. J., Wilson, T., Borns, H. W., Introne, D. S., and Feindel, S.: Experimentally determined Mg/Ca and Sr/Ca ratios in juvenile bivalve calcite for Mytilus edulis: Implications for paleotemperature reconstructions, Geo-Marine Letters, 28, 359–368, https://doi.org/10.1007/s00367-008-0112-8, 2008.

Wang, Z., Schauble, E. A., and Eiler, J. M.: Equilibrium thermodynamics of multiply substituted isotopologues of molecular gases, Geochimica et Cosmochimica Acta, https://doi.org/10.1016/j.gca.2004.05.039, 2004.

Watson, E. B.: Surface enrichment and trace-element uptake during crystal growth, Geochimica et Cosmochimica Acta, 60, 5013–5020, https://doi.org/10.1016/S0016-7037(96)00299-2, 1996.

Wheeler, A. P.: Mechanisms of Molluscan Shell Formation, in: Calcification in Biological Systems, CRC Press, 179–216, https://doi.org/10.1201/9781003068396-10, 2020.

White, A. F.: Sodium and potassium coprecipitation in aragonite, Geochimica et Cosmochimica Acta, 41, 613–625, https://doi.org/10.1016/0016-7037(77)90301-5, 1977.

Wienberg, C., Titschack, J., Freiwald, A., Frank, N., Lundälv, T., Taviani, M., Beuck, L., Schröder-Ritzrau, A., Krengel, T., and Hebbeln, D.: The giant Mauritanian cold-water coral mound province: Oxygen control on coral mound formation, Quaternary Science Reviews, 185, 135–152, https://doi.org/10.1016/j.quascirev.2018.02.012, 2018.

De Winter, N. J., Vellekoop, J., Vorsselmans, R., Golreihan, A., Soete, J., Petersen, S. V., Meyer, K. W., Casadio, S., Speijer, R. P., and Claeys, P.: An assessment of latest Cretaceous *Pycnodonte vesicularis* (Lamarck, 1806) shells as records for palaeoseasonality: A multi-proxy investigation, Climate of the Past, 14, 725–749, https://doi.org/10.5194/cp-14-725-2018, 2018.

Wit, J. C., De Nooijer, L. J., Wolthers, M., and Reichart, G. J.: A novel salinity proxy based on na incorporation into foraminiferal calcite, Biogeosciences, 10, 6375–6387, https://doi.org/10.5194/bg-10-6375-2013, 2013.

Yan, H., Shao, D., Wang, Y., and Sun, L.: Sr/Ca profile of long-lived Tridacna gigas bivalves from South China Sea: A new high-resolution SST proxy, Geochimica et Cosmochimica Acta, 112, 52–65, https://doi.org/10.1016/j.gca.2013.03.007, 2013.

Yan, H., Chen, J., and Xiao, J.: A review on bivalve shell, a tool for reconstruction of paleo-climate and paleo-environment, Chinese Journal of Geochemistry, 33, 310–315, https://doi.org/10.1007/s11631-014-0692-0, 2014.

Yan, L., Schöne, B. R., and Arkhipkin, A.: Eurhomalea exalbida (Bivalvia): A reliable recorder of climate in southern South America?, Palaeogeography, Palaeoclimatology, Palaeoecology, 350–352, 91–100, https://doi.org/10.1016/j.palaeo.2012.06.018, 2012.

Yoshimura, T., Tamenori, Y., Suzuki, A., Kawahata, H., Iwasaki, N., Hasegawa, H., Nguyen, L. T., Kuroyanagi, A., Yamazaki, T., Kuroda, J., and Ohkouchi, N.: Altervalent substitution of sodium for calcium in biogenic calcite and aragonite, Geochimica et Cosmochimica Acta, 202, 21–38, https://doi.org/10.1016/j.gca.2016.12.003, 2017.

Zeebe, R. E.: An explanation of the effect of seawater carbonate concentration on foraminiferal oxygen isotopes, Geochimica et Cosmochimica Acta, 63, 2001–2007, https://doi.org/10.1016/S0016-7037(99)00091-5, 1999.

Zhao, L., Schöne, B. R., Mertz-Kraus, R., and Yang, F.: Insights from sodium into the impacts of elevated pCO2 and temperature on bivalve shell formation, Journal of Experimental Marine Biology and Ecology, 486, 148–154, https://doi.org/10.1016/j.jembe.2016.10.009, 2017a.

Zhao, L., Schöne, B. R., Mertz-Kraus, R., and Yang, F.: Sodium provides unique insights into transgenerational effects of ocean acidification on bivalve shell formation, Science of the Total Environment, 577, 360–366, https://doi.org/10.1016/j.scitotenv.2016.10.200, 2017b.

11 Appendix

The following tables present the gathered data of the published studies. Data of unpublished work is not included to allow for publication at a later point.

11.1 Data (Chapter 3)

Table 11-1 Results of the ICP-OES measurements. Red values are identified as outliers and are not considered for further calculations. Species abbreviations stand for D = Desmophyllum pertusum, M = Madrepora oculata and C = Caryophylliid species. Sample names such as A1-A4 relate to multiple samples that derive from the same coral specimen/calice.

Sample name	Species	Na/Ca [mmol/mol]	Mg/Ca [mmol/mol]	Sr/Ca [mmol/mol]
A1 - A4	D	29.02	3.83	10.23

B1 - B2	D	24.87	3.17	9.91
C1 - C2	D	29.25	3.97	9.95
D1 – D4	D	27.57	3.94	10.01
E1 - E3	D	24.14	4.03	9.84
F1 – F4	D	24.61	3.56	10.05
G1 – G4	D	31.04	4.25	10.18
H1 – H3	D	23.93	3.62	10.21
I1 – I3	D	23.75	3.99	9.65
J1 – J2	D	21.2	2.45	10.35
K1 – K5	D	28.72	7.84	9.6
LO1	D	26.74	3.94	10
MSS1	D	26.85	5.41	10.03
MA1	M	25.18	3.73	10.47
MSM1	D	66.24	7.71	10.31
MSM2	D	30.17	6.38	10.42
MSM3	M	56.92	9.98	10.62
MSM4	D	25.43	3.04	10.22
ALB1	D	49.9	3.82	10.08
KRS1	C	45.84	4.37	9.94
KRS2	C	22.33	4.47	10.15
KRS3	C	20.91	4.73	9.46
KRS4	C	20.49	2.81	9.78
KRS5	C	20.78	3.49	10.36
L10-1	D	21.12	2.2	10
L2-1 – L2-2	D	24.61	3.04	10.11
L3-1 – L3-2	D	24.58	3.19	10.36
L5-1 – L5-2	D	23.43	3.1	10.39
L6-1 – L6-2	D	23.79	3.68	10.26
L7-1 – L7-2	D	25.45	3.49	10.41
L8-1 – L8-2	D	23.67	3.23	10.21
LR1 – LR6	D	27.18	3.34	10.31
LW1 – LW5	D	26.23	3.79	9.63
NL-1 – NL6	D	28.14	4.67	9.9
OS1 – OS6	D	24.81	5.73	9.7
P391-1 – P391-3	D	24.45	6.26	10.38
RL1-1 – RL1-4	D	21.32	3.03	10.27
RL4-1 – RL4-4	D	24.36	4.72	10.38
RL9-1 – RL9-5	D	22.68	3.41	10.26
SJ1 – SJ6	D	28.64	4.51	10.07
SJ2-1 – SJ2-4	D	29.38	5.37	10.42
TF1 – TF2	D	25.72	6.1	10.13
TF2-1 – TF2-6	D	21.42	3.78	10.2
EFC1 – EFC6	D	26.01	4.31	9.94
EFE1 – EFE4	D	27.1	3.8	10.31

11.2 Data (Chapter 4)

11.2.1 Measurement tracks perpendicular to shell surface

11.2.1.1 Sample 1R

Table 11-2 Results of LA-ICP-MS measurements on sample 1R. The measurement tracks are perpendicular to the shell surface, through all shell sections

Distance from Shell surface (outside) [mm]	Mg/Ca [mmol/mol]	Na/Ca [mmol/mol]	Sr/Ca [mmol/mol]
0.000	17.32	20.59	1.81
0.042	16.30	20.33	1.87
0.085	16.74	20.96	1.74
0.127	15.66	21.05	1.75
0.170	15.41	22.22	1.76
0.212	15.81	22.27	1.67
0.254	15.92	22.40	1.64
0.297	16.51	22.99	1.64

0.339	16.14	21.94	1.61
0.382	15.56	22.31	1.60
0.424	15.32	24.14	1.61
0.466	15.03	23.27	1.54
0.509	14.99	22.48	1.52
0.551	14.95	22.14	1.51
0.593	12.83	18.33	1.29
0.636	14.36	20.49	1.43
0.678	13.32	19.45	1.36
0.721	13.71	19.56	1.37
0.763	13.90	19.81	1.39
0.805	13.25	20.23	1.32
0.848	13.47	19.10	1.35
0.890	12.83	18.57	1.28
0.933	13.13	18.44	1.27
0.975	12.90	18.22	1.25
1.017	12.31	17.82	1.21
1.060	13.13	18.21	1.25
1.102	12.91	18.16	1.22
1.145	12.28	17.64	1.17
1.187	12.76	18.26	1.17
1.229	12.23	17.52	1.15
1.272	12.85	17.79	1.19
1.314	12.33	17.94	1.17
1.356	12.15	17.88	1.17
1.399	12.05	17.53	1.17
1.441	11.90	18.00	1.13
1.484	12.07	18.33	1.15
1.526	12.41	18.57	1.19
1.568	12.16	18.43	1.15
1.611	10.95	17.03	1.04
1.653	11.99	18.85	1.17
1.696	11.46	18.94	1.13
1.738	11.45	19.57	1.23
1.780	11.14	19.41	1.18
1.823	11.09	19.20	1.15
1.865	11.05	19.83	1.19
1.908	11.29	19.29	1.15
1.950	11.24	20.38	1.22
1.992	10.84	20.58	1.19
2.035	10.96	22.23	1.21
2.077	10.86	21.68	1.22
2.119	10.58	21.17	1.17
2.162	10.74	22.28	1.20
2.204	10.95	22.53	1.22
2.247	11.17	23.33	1.26
2.289	10.90	23.54	1.25

2.331	11.38	24.61	1.24
2.374	11.28	24.79	1.24
2.416	11.35	24.61	1.26
2.459	11.32	24.76	1.26
2.501	11.62	25.49	1.33
2.543	11.26	25.75	1.28
2.586	11.84	25.59	1.30
2.628	11.31	25.88	1.28
2.671	11.19	26.16	1.36
2.713	11.38	26.90	1.31
2.755	11.24	26.75	1.29
2.798	11.09	26.31	1.26
2.840	11.16	26.61	1.29
2.882	11.27	27.14	1.30
2.925	11.12	26.66	1.35
2.967	11.19	26.98	1.30
3.010	11.03	26.62	1.27
3.052	10.94	26.93	1.28
3.094	11.10	26.82	1.26
3.137	10.44	25.41	1.22
3.179	10.29	24.75	1.19
3.222	11.56	26.40	1.44
3.264	10.74	26.28	1.28
3.306	10.43	25.66	1.31
3.349	10.68	26.26	1.25
3.391	10.64	25.93	1.27
3.434	10.62	25.72	1.27
3.476	10.63	25.75	1.24
3.518	10.52	25.21	1.23
3.561	10.64	25.74	1.24
3.603	10.26	24.81	1.21
3.645	10.51	25.02	1.22
3.688	10.45	25.15	1.22
3.730	10.57	24.92	1.24
3.773	10.59	25.34	1.25
3.815	10.44	24.56	1.21
3.857	10.40	24.80	1.22
3.900	10.52	24.41	1.23
3.942	10.17	23.58	1.18
3.985	11.28	23.64	1.19
4.027	10.43	23.34	1.18
4.069	10.91	23.56	1.19
4.112	10.68	23.40	1.21
4.154	10.64	22.81	1.21
4.197	10.62	22.37	1.19
4.239	10.63	22.09	1.18
4.281	10.63	21.45	1.17

4.324	10.51	21.29	1.25
4.366	10.79	21.07	1.22
4.408	10.84	20.73	1.21
4.451	10.94	20.21	1.18
4.493	10.95	19.56	1.17
4.536	11.14	19.72	1.19
4.578	11.56	19.12	1.18
4.620	10.97	18.55	1.18
4.663	11.19	18.61	1.18
4.705	11.18	18.18	1.17
4.748	11.77	17.95	1.17
4.790	11.37	17.42	1.17
4.832	11.65	17.17	1.17
4.875	11.49	16.66	1.20
4.917	11.51	16.32	1.19
4.960	11.28	16.00	1.17
5.002	11.47	16.24	1.15
5.044	11.17	15.62	1.13
5.087	10.98	14.89	1.10
5.129	11.36	15.62	1.12
5.171	11.09	14.80	1.11
5.214	11.26	14.83	1.13
5.256	11.26	14.67	1.13
5.299	11.43	14.52	1.13
5.341	11.47	14.34	1.12
5.383	11.59	13.81	1.13
5.426	11.65	14.00	1.11
5.468	11.65	13.70	1.13
5.511	11.77	13.56	1.11
5.553	11.38	13.36	1.11
5.595	11.11	13.13	1.09
5.638	10.87	12.87	1.09
5.680	10.95	12.53	1.08
5.723	10.94	13.07	1.10
5.765	10.63	12.91	1.06
5.807	10.37	12.79	1.08
5.850	10.16	12.94	1.08
5.892	10.12	12.83	1.05
5.934	9.10	12.64	1.02
5.977	8.80	13.64	1.03
6.019	8.42	13.15	1.03
6.062	8.20	13.35	1.04
6.104	7.78	13.29	1.03
6.146	7.37	12.81	0.99
6.189	7.44	13.29	1.02
6.231	7.15	13.15	1.02
6.274	6.89	13.21	1.01

6.316	6.81	13.12	1.03
6.358	6.77	13.17	1.05
6.401	6.20	12.13	0.96
6.443	6.79	13.00	1.07
6.486	6.59	12.62	1.06
6.528	6.42	12.58	1.06
6.570	6.39	12.83	1.06
6.613	6.01	13.57	1.12
6.655	6.02	14.30	1.17
6.697	5.32	15.63	1.30
6.740	4.75	16.55	1.27
6.782	4.45	18.57	1.37
6.825	3.99	19.85	1.47
6.867	3.48	21.08	1.47
6.909	3.18	23.60	1.60
6.952	2.53	23.66	1.55
6.994	2.33	26.19	1.63
7.037	1.95	27.10	1.67
7.079	1.56	28.51	1.69
7.121	1.23	29.36	1.71
7.164	0.89	30.25	1.73
7.206	0.65	31.84	1.80
7.249	0.47	31.43	1.75
7.291	0.42	32.44	1.80
7.333	0.44	30.41	1.70
7.376	0.47	31.86	1.79
7.418	0.42	32.06	1.78
7.460	0.58	32.45	1.80
7.503	0.42	31.82	1.85
7.545	0.41	31.86	1.76
7.588	0.44	31.89	1.75
7.630	0.42	32.09	1.77
7.672	0.44	32.31	1.74
7.715	0.42	32.14	1.73
7.757	0.41	32.04	1.72
7.800	0.41	32.23	1.69
7.842	0.41	31.51	1.65
7.884	0.43	32.09	1.62
7.927	0.39	32.40	1.62
7.969	0.39	31.23	1.55
8.012	0.42	29.98	1.49
8.054	0.38	31.47	1.57
8.096	0.41	31.64	1.55
8.139	0.40	31.50	1.63
8.181	0.39	31.47	1.53
8.223	0.39	31.31	1.53
8.266	0.41	31.66	1.54

8.308	0.40	31.29	1.54
8.351	0.84	31.46	1.56
8.393	0.41	30.57	1.54
8.435	0.36	29.26	1.46
8.478	0.42	31.35	1.64
8.520	0.42	31.30	1.65
8.563	0.42	30.88	1.68
8.605	0.48	31.15	1.68
8.647	0.44	30.44	1.69
8.690	0.49	31.17	1.75
8.732	0.47	29.68	1.68
8.775	0.49	30.94	1.82
8.817	0.52	29.65	1.73
8.859	0.50	30.13	1.75
8.902	0.47	29.23	1.69
8.944	0.51	29.70	1.75
8.987	0.53	29.58	1.78
9.029	0.56	29.87	1.78
9.071	0.55	29.78	1.83
9.114	0.62	28.88	1.83
9.156	0.57	28.54	1.81
9.198	0.61	28.39	1.83
9.241	0.62	27.94	1.84
9.283	0.63	26.90	1.84
9.326	0.58	26.65	1.84

11.2.1.2 Sample 6R

Table 11-3 Results of LA-ICP-MS measurements on sample 6R. The measurement tracks are perpendicular to the shell surface, through all shell sections

Distance from Shell surface (outside) [mm]	Mg/Ca [mmol/mol]	Na/Ca [mmol/mol]	Sr/Ca [mmol/mol]
0.000	17.27	12.89	1.52
0.004	17.23	14.93	1.65
0.008	18.71	17.16	1.40
0.013	18.30	17.79	1.42
0.017	18.22	17.72	1.43
0.021	18.42	18.31	1.41
0.025	18.22	18.77	1.42
0.030	17.66	18.04	1.34
0.034	18.24	18.80	1.42
0.038	18.36	18.99	1.37
0.042	17.75	18.37	1.33
0.047	18.39	18.83	1.38
0.051	18.69	19.30	1.31
0.055	18.36	18.86	1.29

0.059	18.43	18.89	1.28
0.064	18.50	19.27	1.37
0.068	17.80	18.95	1.28
0.072	17.51	18.83	1.32
0.076	17.07	18.46	1.21
0.081	16.41	18.38	1.21
0.085	15.86	18.13	1.19
0.089	15.36	17.51	1.17
0.093	15.43	17.83	1.12
0.097	14.04	15.92	1.04
0.102	14.67	17.37	1.11
0.106	14.45	17.18	1.11
0.110	14.25	16.66	1.06
0.114	13.50	15.61	1.04
0.119	14.65	16.27	1.06
0.123	13.53	15.04	1.01
0.127	14.89	16.55	1.08
0.131	15.87	15.29	1.14
0.136	15.72	15.55	1.10
0.140	15.86	15.01	1.05
0.144	15.77	15.37	1.08
0.148	15.85	15.20	1.08
0.153	15.96	14.05	1.05
0.157	16.42	14.02	1.06
0.161	16.75	14.05	1.06
0.165	17.25	13.28	1.05
0.170	17.01	12.73	1.03
0.174	17.35	12.44	1.05
0.178	18.76	12.75	1.07
0.182	19.08	12.46	1.10
0.187	19.42	12.38	1.10
0.191	20.21	12.19	1.12
0.195	19.15	11.02	1.03
0.199	20.62	12.14	1.10
0.203	21.56	12.07	1.13
0.208	21.38	11.18	1.07
0.212	21.54	11.30	1.09
0.216	21.73	10.75	1.12
0.220	22.85	11.28	1.10
0.225	23.00	10.94	1.15
0.229	24.60	11.19	1.12
0.233	23.32	11.06	1.13
0.237	23.08	10.81	1.08
0.242	24.15	10.98	1.11
0.246	22.99	11.03	1.13
0.250	22.37	11.02	1.08
0.254	22.15	11.09	1.09

0.259	22.33	11.55	1.09
0.263	21.54	11.63	1.10
0.267	20.92	12.04	1.09
0.271	20.24	12.25	1.20
0.276	19.13	12.25	1.11
0.280	18.73	12.30	1.11
0.284	17.71	12.08	1.03
0.288	17.05	12.43	1.12
0.292	16.96	12.87	1.07
0.297	16.48	13.23	1.05
0.301	15.78	15.38	1.17
0.305	15.81	13.16	1.06
0.309	15.03	12.75	1.07
0.314	14.42	12.81	1.07
0.318	14.38	13.08	1.08
0.322	14.73	13.57	1.21
0.326	14.09	13.22	1.11
0.331	14.20	13.39	1.12
0.335	14.22	13.28	1.11
0.339	14.19	13.40	1.14
0.343	14.34	13.00	1.13
0.348	14.84	13.22	1.15
0.352	15.47	13.41	1.15
0.356	15.03	13.18	1.17
0.360	15.90	13.21	1.12
0.365	15.77	13.26	1.14
0.369	15.96	13.45	1.15
0.373	15.78	12.90	1.09
0.377	16.33	13.15	1.13
0.382	17.15	13.21	1.11
0.386	16.85	13.57	1.12
0.390	18.23	13.85	1.13
0.394	18.13	13.98	1.16
0.398	18.20	14.49	1.13
0.403	19.58	15.47	1.14
0.407	18.76	15.79	1.12
0.411	18.77	16.41	1.11
0.415	18.27	16.85	1.10
0.420	17.82	17.50	1.14
0.424	16.84	17.64	1.07
0.428	16.82	18.47	1.10
0.432	16.35	18.71	1.10
0.437	16.14	19.46	1.13
0.441	15.47	19.13	1.10
0.445	15.40	19.63	1.12
0.449	14.42	19.68	1.10
0.454	13.57	19.63	1.11

0.458	14.49	20.72	1.15
0.462	13.04	20.45	1.13
0.466	12.63	20.55	1.12
0.471	11.94	21.09	1.14
0.475	11.81	21.49	1.17
0.479	12.00	21.29	1.15
0.483	11.46	21.53	1.28
0.487	10.49	19.99	1.06
0.492	11.40	21.90	1.17
0.496	11.33	21.85	1.15
0.500	12.32	21.94	1.13
0.504	11.77	22.20	1.17
0.509	11.63	22.63	1.17
0.513	11.50	21.98	1.16
0.517	11.80	22.56	1.21
0.521	11.69	22.51	1.21
0.526	11.96	22.73	1.19
0.530	11.74	22.89	1.19
0.534	12.11	23.14	1.21
0.538	12.35	22.44	1.16
0.543	11.80	23.52	1.19
0.547	11.73	23.58	1.21
0.551	11.62	23.05	1.25
0.555	11.34	23.40	1.24
0.560	10.71	21.85	1.16
0.564	11.03	23.11	1.24
0.568	10.73	24.39	1.25
0.572	10.54	23.86	1.24
0.576	10.33	24.36	1.27
0.581	10.13	24.00	1.24
0.585	10.21	24.65	1.26
0.589	10.70	24.54	1.27
0.593	9.99	24.76	1.26
0.598	10.18	24.94	1.29
0.602	9.99	24.81	1.26
0.606	10.21	24.26	1.26
0.610	9.98	24.33	1.29
0.615	10.34	23.75	1.27
0.619	10.75	23.78	1.29
0.623	11.12	23.21	1.24
0.627	11.80	23.32	1.31
0.632	11.74	22.89	1.25
0.636	12.36	22.71	1.28
0.640	12.75	22.75	1.30
0.644	12.95	23.08	1.38
0.649	12.85	22.86	1.35
0.653	12.42	21.80	1.30

0.657	12.83	22.02	1.37
0.661	12.43	21.48	1.32
0.666	12.01	20.35	1.29
0.670	12.37	20.99	1.34
0.674	12.20	20.51	1.32
0.678	11.99	20.39	1.32
0.682	11.89	20.21	1.34
0.687	11.61	19.45	1.39
0.691	11.41	19.03	1.31
0.695	10.95	18.84	1.31
0.699	10.59	18.38	1.25
0.704	10.10	17.82	1.29
0.708	10.50	18.39	1.23
0.712	10.51	17.62	1.23
0.716	9.91	16.65	1.19
0.721	10.28	17.77	1.23
0.725	10.27	18.11	1.22
0.729	9.97	17.95	1.22
0.733	9.60	17.93	1.20
0.738	9.37	18.37	1.20
0.742	9.38	18.68	1.23
0.746	9.23	19.09	1.22
0.750	8.96	18.80	1.26
0.755	15.97	18.80	1.23
0.759	8.70	19.01	1.22
0.763	8.31	19.09	1.27
0.767	8.27	18.90	1.23
0.771	8.14	18.68	1.23
0.776	8.06	18.29	1.22
0.780	8.26	18.59	1.23
0.784	8.45	18.13	1.19
0.788	8.43	18.19	1.22
0.793	8.35	17.79	1.24
0.797	8.72	17.39	1.23
0.801	9.35	17.45	1.21
0.805	8.97	16.98	1.19
0.810	9.05	16.34	1.21
0.814	9.00	15.84	1.18
0.818	9.16	15.52	1.19
0.822	9.58	15.08	1.35
0.827	9.30	14.90	1.19
0.831	9.42	14.63	1.21
0.835	9.41	14.35	1.26
0.839	8.85	15.02	1.32
0.844	8.54	15.58	1.39
0.848	8.62	16.41	1.46
0.852	7.36	17.01	1.50

0.856	6.92	18.13	1.58
0.860	6.37	19.65	1.64
0.865	5.70	20.93	1.68
0.869	4.93	21.84	1.73
0.873	4.36	22.97	1.82
0.877	3.54	23.95	1.81
0.882	3.01	26.10	1.92
0.886	2.65	27.75	1.95
0.890	2.18	28.90	2.01
0.894	1.67	29.03	1.98
0.899	1.29	30.36	1.97
0.903	1.02	30.37	1.95
0.907	0.68	30.48	1.98
0.911	0.49	31.71	2.06
0.916	0.47	32.19	2.05
0.920	0.56	32.80	2.04
0.924	0.43	32.20	2.03
0.928	0.40	32.35	1.96
0.933	0.41	32.18	1.99
0.937	0.40	32.34	2.01
0.941	0.42	31.89	1.91
0.945	0.41	33.15	1.94
0.950	0.42	32.54	1.90
0.954	0.41	32.33	1.90
0.958	0.49	31.87	1.82
0.962	0.41	31.75	1.82
0.966	0.42	32.35	1.80
0.971	0.53	32.43	1.79
0.975	0.39	32.06	1.72
0.979	0.39	32.72	1.87
0.983	0.46	32.40	1.74
0.988	0.52	31.23	1.70
0.992	0.42	31.50	1.74
0.996	0.43	31.95	1.71
1.000	0.43	31.36	1.74
1.005	0.43	31.76	1.72
1.009	0.45	31.44	1.72
1.013	0.44	31.63	1.72
1.017	0.43	30.97	1.72
1.022	0.43	30.38	1.67
1.026	0.46	30.34	1.66
1.030	0.45	30.66	1.72
1.034	0.46	30.38	1.71
1.039	0.46	30.37	1.68
1.043	0.50	30.34	1.73
1.047	0.48	30.52	1.70
1.051	0.50	30.38	1.73

1.055	0.48	29.44	1.70
1.060	0.50	30.02	1.78
1.064	0.49	30.50	1.79
1.068	0.52	29.73	1.78
1.072	0.50	30.06	1.80
1.077	0.49	28.46	1.79
1.081	0.53	29.61	1.83
1.085	0.55	29.63	1.81
1.089	0.57	30.02	1.82
1.094	0.55	29.62	1.84
1.098	0.51	27.91	1.75
1.102	0.56	28.91	1.85
1.106	0.53	28.11	1.83
1.111	0.53	28.35	1.84
1.115	0.56	27.52	1.82
1.119	0.58	26.73	1.79
1.123	0.58	26.90	1.83
1.128	0.55	26.06	1.83
1.132	0.54	24.78	1.76
1.136	0.62	25.49	1.82

11.2.1.3 Sample 14R

Table 11-4 Results of LA-ICP-MS measurements on sample 14R. The measurement tracks are perpendicular to the shell surface, through all shell sections

Distance from Shell surface (outside) [mm]	Mg/Ca [mmol/mol]	Na/Ca [mmol/mol]	Sr/Ca [mmol/mol]
0.000	11.81	17.51	1.64
0.004	11.14	16.69	1.44
0.008	13.42	19.14	1.58
0.013	12.87	18.95	1.57
0.017	13.03	19.57	1.63
0.021	14.17	20.59	1.60
0.025	14.47	20.32	1.59
0.030	13.59	20.26	1.55
0.034	14.14	20.67	1.63
0.038	12.87	18.46	1.34
0.042	14.65	20.74	1.46
0.047	14.91	21.25	1.45
0.051	14.80	21.49	1.46
0.055	15.26	21.57	1.45
0.059	15.04	21.30	1.40
0.064	14.32	20.00	1.34
0.068	15.11	20.99	1.37
0.072	15.25	20.37	1.37
0.076	15.77	20.85	1.32
0.081	15.02	19.84	1.29
0.085	15.88	20.85	1.29
0.089	16.57	20.94	1.28

0.093	16.27	20.54	1.26
0.097	16.18	20.38	1.25
0.102	15.96	20.20	1.49
0.106	15.73	20.19	1.31
0.110	16.04	20.12	1.26
0.114	15.00	19.33	1.18
0.119	15.05	19.65	1.22
0.123	14.70	19.64	1.18
0.127	14.16	19.22	1.14
0.131	15.03	19.32	1.17
0.136	14.52	19.76	1.18
0.140	14.62	19.70	1.19
0.144	14.30	19.79	1.18
0.148	14.33	20.17	1.22
0.153	14.41	20.09	1.21
0.157	14.03	19.57	1.16
0.161	14.03	20.46	1.20
0.165	13.70	20.52	1.24
0.170	13.65	20.51	1.20
0.174	13.78	20.69	1.19
0.178	13.84	21.05	1.22
0.182	14.00	22.13	1.21
0.187	13.97	20.87	1.21
0.191	14.59	21.24	1.19
0.195	14.02	21.68	1.21
0.199	14.26	21.66	1.23
0.203	14.23	21.79	1.27
0.208	14.05	21.61	1.21
0.212	13.81	21.28	1.19
0.216	14.73	21.71	1.21
0.220	14.40	22.70	1.22
0.225	14.48	21.78	1.20
0.229	14.60	21.98	1.20
0.233	14.40	20.99	1.19
0.237	14.53	21.55	1.19
0.242	15.16	21.90	1.26
0.246	15.20	21.90	1.21
0.250	15.09	21.44	1.20
0.254	16.12	21.36	1.20
0.259	15.32	21.31	1.17
0.263	15.18	21.36	1.19
0.267	15.18	20.88	1.18
0.271	15.31	21.22	1.19
0.276	15.26	20.91	1.22
0.280	15.33	20.76	1.17
0.284	15.56	21.08	1.16
0.288	15.25	20.22	1.21

0.292	15.36	20.21	1.16
0.297	14.68	19.55	1.09
0.301	15.68	20.63	1.16
0.305	15.90	20.64	1.17
0.309	15.37	20.93	1.14
0.314	15.78	21.32	1.15
0.318	15.95	21.59	1.16
0.322	16.02	21.70	1.18
0.326	15.59	21.20	1.16
0.331	13.54	18.32	0.99
0.335	15.58	21.64	1.19
0.339	15.18	21.38	1.17
0.343	14.73	21.03	1.17
0.348	15.38	21.66	1.19
0.352	15.17	22.24	1.22
0.356	14.92	22.03	1.20
0.360	14.46	21.50	1.17
0.365	14.88	21.48	1.23
0.369	14.90	21.06	1.24
0.373	15.22	19.88	1.25
0.377	15.82	19.48	1.25
0.382	15.04	18.09	1.20
0.386	16.09	18.63	1.27
0.390	16.18	18.61	1.25
0.394	15.94	18.09	1.28
0.398	16.54	17.78	1.28
0.403	16.58	17.74	1.29
0.407	16.20	17.22	1.25
0.411	16.59	17.32	1.37
0.415	16.79	17.16	1.26
0.420	16.90	16.94	1.28
0.424	16.86	16.83	1.24
0.428	16.81	17.01	1.26
0.432	16.91	17.01	1.26
0.437	16.79	17.02	1.22
0.441	16.44	17.46	1.24
0.445	16.09	18.02	1.21
0.449	15.45	18.53	1.21
0.454	15.10	19.35	1.22
0.458	14.02	19.23	1.42
0.462	14.06	19.69	1.19
0.466	13.75	20.07	1.20
0.471	13.93	20.31	1.36
0.475	13.38	20.30	1.23
0.479	13.27	20.32	1.24
0.483	13.13	20.60	1.26
0.487	12.65	20.62	1.23

0.492	12.78	21.46	1.25
0.496	12.62	20.96	1.25
0.500	12.01	20.52	1.23
0.504	11.99	20.91	1.25
0.509	11.70	21.33	1.26
0.513	11.27	20.65	1.24
0.517	11.48	20.95	1.25
0.521	11.79	20.88	1.25
0.526	11.81	20.83	1.27
0.530	11.78	21.10	1.28
0.534	11.86	21.03	1.25
0.538	11.78	21.02	1.27
0.543	12.20	20.70	1.24
0.547	11.82	20.96	1.24
0.551	12.23	20.72	1.26
0.555	12.08	20.57	1.29
0.560	11.76	20.51	1.23
0.564	11.87	20.47	1.21
0.568	11.70	20.24	1.22
0.572	11.77	20.20	1.21
0.576	11.84	20.00	1.19
0.581	11.54	19.94	1.18
0.585	11.60	20.21	1.20
0.589	11.60	20.29	1.20
0.593	11.17	19.44	1.18
0.598	11.32	19.30	1.19
0.602	10.89	19.29	1.19
0.606	10.84	19.14	1.20
0.610	10.61	18.70	1.17
0.615	10.87	18.50	1.19
0.619	10.45	18.41	1.20
0.623	10.58	18.18	1.19
0.627	10.17	17.11	1.16
0.632	10.26	17.25	1.18
0.636	9.20	14.85	1.06
0.640	10.17	15.98	1.18
0.644	10.84	15.28	1.19
0.649	11.37	14.77	1.21
0.653	10.78	14.30	1.21
0.657	11.02	13.60	1.20
0.661	10.93	12.71	1.19
0.666	11.39	12.76	1.21
0.670	11.50	12.14	1.19
0.674	11.64	11.64	1.21
0.678	11.53	11.35	1.18
0.682	11.27	11.70	1.23
0.687	11.37	12.25	1.28

0.691	10.87	12.31	1.31
0.695	10.13	13.26	1.34
0.699	9.63	14.02	1.37
0.704	9.20	15.29	1.44
0.708	8.89	16.38	1.51
0.712	7.72	18.29	1.60
0.716	6.81	19.30	1.65
0.721	6.03	21.16	1.75
0.725	4.89	23.09	1.79
0.729	4.20	24.43	1.85
0.733	3.36	25.20	1.84
0.738	2.83	25.32	1.80
0.742	2.49	26.66	1.82
0.746	2.18	27.07	1.80
0.750	1.77	28.04	1.84
0.755	1.35	28.61	1.85
0.759	1.16	29.09	1.84
0.763	0.97	29.99	1.87
0.767	0.91	30.68	1.90
0.771	0.58	30.14	1.89
0.776	0.51	29.87	1.87
0.780	0.51	30.22	1.89
0.784	0.51	30.50	1.92
0.788	0.51	30.43	1.92
0.793	0.53	29.95	1.93
0.797	0.50	26.85	1.73
0.801	0.53	30.04	1.96
0.805	0.52	30.21	1.94
0.810	0.53	29.29	1.97
0.814	0.62	29.27	1.97
0.818	0.52	29.58	1.99
0.822	0.51	29.23	1.97
0.827	0.51	29.63	1.98
0.831	0.52	28.90	1.96
0.835	0.51	29.10	1.94
0.839	0.47	29.02	1.93
0.844	0.43	25.09	1.68
0.848	0.45	28.93	1.92
0.852	0.47	30.70	1.98
0.856	0.44	29.13	1.91
0.860	0.44	29.01	1.89
0.865	0.45	29.89	1.90
0.869	0.43	29.74	1.88
0.873	0.43	29.22	1.85
0.877	0.43	29.77	1.87
0.882	0.44	29.51	1.87
0.886	0.42	29.20	1.83

0.890	0.40	27.10	1.69
0.894	0.43	28.87	1.84
0.899	0.44	29.11	1.86
0.903	0.44	28.83	1.87
0.907	0.46	29.43	1.86
0.911	0.45	28.53	1.88
0.916	0.47	28.83	1.88
0.920	0.48	28.51	1.87
0.924	0.49	27.85	1.88
0.928	0.49	28.79	1.89
0.933	0.49	28.32	1.88
0.937	0.51	28.90	1.91
0.941	0.50	27.75	1.85
0.945	0.53	27.83	1.91
0.950	0.50	27.88	1.95
0.954	0.51	27.58	2.01
0.958	0.50	25.95	1.93
0.962	0.51	26.51	1.99
0.966	0.51	26.58	2.04
0.971	0.54	26.46	2.19
0.975	0.56	26.39	2.15
0.979	0.54	25.84	2.18
0.983	0.56	25.54	2.23
0.988	0.53	23.80	2.38
0.992	0.56	23.38	2.18
0.996	0.52	24.50	2.33
1.000	0.57	23.35	2.39
1.005	0.57	22.97	2.45
1.009	0.54	20.56	2.29

11.2.2 Measurement tracks along ontogenetic growth (fibrous layer)

The data presented here only shows a very small proportion of the measured data of one sample. The complete data set consists of ~ 40000 measurements. The data is openly accessible at https://doi.pangaea.de/10.1594/PANGAEA.930296

Table 11-5 LA-ICP-MS measurement results of the fibrous shell section along the ontogenetic growth (Sample 1R). Data is presented strongly reduced, the original data consists of 2515 data points.

Distance from commissure [mm]	Mg/Ca [mmol/mol]	Na/Ca [mmol/mol]	Sr/Ca [mmol/mol]
0.00	11.40	15.16	1.25
0.27	10.10	14.98	1.25
0.58	9.75	14.48	1.31
0.88	10.20	12.63	1.16
1.19	10.54	13.17	1.19
1.50	9.75	12.67	1.19
1.81	10.51	11.78	1.30
2.11	10.08	11.59	1.26
2.42	9.74	11.31	1.34

2.73	9.64	11.36	1.28
3.03	8.76	11.65	1.24
3.34	9.18	11.22	1.29
3.65	9.00	14.67	1.10
3.96	9.18	14.06	1.04
4.27	10.46	15.34	1.05
4.57	8.69	14.06	1.10
4.88	9.09	13.89	1.11
5.19	9.18	14.19	1.16
5.49	8.37	12.19	1.08
5.80	8.32	13.07	1.11
6.11	9.54	12.47	1.10
6.42	3.08	21.54	2.59
6.73	2.82	20.37	2.16
7.03	3.11	21.20	2.17
7.34	2.93	18.32	2.76
7.65	2.49	18.93	3.11
7.95	2.53	18.51	2.87
8.26	1.44	17.58	2.50
8.57	1.24	16.65	2.44
8.88	1.15	17.51	2.51
9.18	11.11	18.00	1.33
9.49	11.46	19.15	1.33
9.80	11.50	17.32	1.31
10.11	10.91	10.39	1.26
10.41	11.89	10.87	1.23
10.72	11.18	10.79	1.25
11.03	9.94	10.09	1.23
11.34	10.93	10.42	1.24
11.64	10.55	10.10	1.22
11.95	16.51	35.30	1.19
12.26	13.89	37.05	1.43
12.57	14.34	30.15	1.19
12.88	9.83	12.22	1.21
13.18	9.81	11.73	1.22
13.49	10.21	11.97	1.18
13.79	7.26	14.27	1.05
14.10	6.68	14.49	1.05
14.41	6.61	14.23	1.04
14.72	7.94	12.09	1.12
15.03	7.88	12.29	1.16
15.33	7.75	12.45	1.15
15.64	6.68	40.57	10.76
15.95	6.33	40.04	10.86
16.25	7.10	35.78	10.05
16.56	4.70	23.00	10.82

16.87	3.76	21.28	11.05
17.18	4.48	22.07	11.14
17.49	2.11	22.36	10.76

11.2.3 Measurement tracks along ontogenetic growth (microgranular layer)

The data presented here only shows a very small proportion of the measured data of one sample. The complete data set consists of ~ 40000 measurements. The data is openly accessible at https://doi.pangaea.de/10.1594/PANGAEA.930296

Table 11-6 LA-ICP-MS measurement results of the microgranular shell section along the ontogenetic growth (Sample 1R). Data is presented strongly reduced, the original data consists of 2515 data points.

Distance from commissure [mm]	Mg/Ca [mmol/mol]	Na/Ca [mmol/mol]	Sr/Ca [mmol/mol]
0.00	**0.15**	**0.25**	**0.02**
0.27	10.09	20.47	1.21
0.58	12.80	17.36	1.12
0.88	14.55	18.01	1.16
1.19	12.29	21.88	1.19
1.50	14.51	17.67	1.59
1.81	14.56	16.65	1.08
2.11	13.50	17.35	1.19
2.42	17.76	13.85	1.14
2.73	22.39	15.26	1.20
3.03	14.18	16.71	1.06
3.34	10.89	21.93	1.10
3.65	10.99	21.46	1.11
3.96	10.33	23.43	1.16
4.27	10.59	25.65	1.15
4.57	10.99	26.08	1.12
4.88	10.96	24.29	1.13
5.19	9.81	25.70	1.15
5.49	10.45	27.54	1.13
5.80	10.28	26.34	1.17
6.11	10.64	23.18	1.16
6.42	11.79	17.23	1.14
6.73	25.67	14.20	1.22
7.03	15.16	17.83	1.12
7.34	10.98	19.64	1.24
7.65	17.00	15.08	1.22
7.95	11.78	20.28	1.20
8.26	11.16	23.12	1.15
8.57	12.14	18.84	1.03
8.88	11.44	17.16	1.06
9.18	17.66	14.22	1.09
9.49	16.94	17.31	1.11
9.80	14.12	21.13	1.08

10.11	12.48	21.90	1.06
10.41	11.81	24.23	1.14
10.72	11.72	25.35	1.19
11.03	11.03	24.46	1.11
11.34	10.98	26.01	1.20
11.64	10.64	22.64	1.09
11.95	10.57	20.09	1.02
12.26	17.90	17.19	1.02
12.57	10.83	21.62	1.08
12.88	13.70	18.55	1.03
13.18	13.58	19.21	1.06
13.49	12.20	22.00	1.08
13.79	12.05	22.10	1.13
14.10	11.09	22.31	1.11
14.41	12.90	20.41	1.03
14.72	10.97	23.85	1.10
15.03	11.00	26.64	1.14
15.33	11.05	24.72	1.14
15.64	10.29	24.76	1.14
15.95	11.19	25.71	1.19
16.25	11.56	23.80	1.12
16.56	10.64	24.20	1.06
16.87	10.80	26.51	1.11
17.18	11.67	21.15	1.04

11.2.4 Effects of oxidative cleaning with H_2O_2

Only a small fraction of the data is reported here. Full dataset is available at https://doi.pangaea.de/10.1594/PANGAEA.930296

Table 11-7 LA-ICP-MS measurements of two samples before and after treatment with H_2O_2.

Before H2O2 Treatment								After H2O2 Treatment							
Sample 14R				Sample 6R				Sample 14R				Sample 6R			
Distance from commissure [mm]	Mg/Ca [mmol/mol]	Na/Ca [mmol/mol]	Sr/Ca [mmol/mol]	Distance from commissure [mm]	Mg/Ca [mmol/mol]	Na/Ca [mmol/mol]	Sr/Ca [mmol/mol]	Distance from commissure [mm]	Mg/Ca [mmol/mol]	Na/Ca [mmol/mol]	Sr/Ca [mmol/mol]	Distance from commissure [mm]	Mg/Ca [mmol/mol]	Na/Ca [mmol/mol]	Sr/Ca [mmol/mol]
0	20.7	1.13	11.26	0	26.29	1.56	15.09	0	24.63	1.26	10.91	0	27.56	1.32	11.89
0.01	20.81	1.16	12.14	0.01	27.88	1.52	14.73	0.01	24.72	1.29	10.11	0.01	27.16	1.27	11.95
0.03	22.68	1.26	13.04	0.03	27.23	1.52	14.15	0.01	24.39	1.25	10.21	0.01	26.53	1.25	11.98
0.04	24.35	1.3	13.89	0.04	26.86	1.37	13.77	0.02	24.6	1.27	10.99	0.02	25.48	1.22	11.68
0.06	25.53	1.33	14.18	0.06	27	1.4	13.73	0.03	25.29	1.3	10.85	0.03	26.16	1.24	12.2
0.07	26.73	1.34	14.71	0.07	28.53	1.39	14.81	0.04	25.32	1.27	10.94	0.04	24.31	1.27	12.3
0.08	25.66	1.32	14.7	0.08	27.52	1.44	13.94	0.04	25.73	1.3	11.35	0.04	24.65	1.18	12.16
0.1	25.66	1.33	15.77	0.1	25.67	1.28	13.14	0.05	25.26	1.29	11.87	0.05	23.21	1.15	12.31
0.11	23.83	1.25	15.56	0.11	26	1.29	13.23	0.06	25.63	1.29	11.77	0.06	22.99	1.13	12.3
0.13	22.64	1.25	15.66	0.13	25.87	1.25	13.55	0.06	24.66	1.26	11.84	0.06	22.37	1.13	12.75
0.14	22.25	1.26	15.73	0.14	26.4	1.29	13.8	0.07	25.6	1.27	11.86	0.07	21.57	1.08	11.88
0.16	21.72	1.24	15.95	0.16	24.87	1.23	14.22	0.08	25.06	1.28	12.42	0.08	22.33	1.14	12.95
0.17	21.48	1.23	15.91	0.17	22.28	1.27	14.75	0.09	24.87	1.26	12.15	0.09	21.94	1.13	12.58
0.18	21.37	1.24	16.12	0.18	18.74	1.1	11.75	0.09	24.2	1.24	12.17	0.09	21.42	1.17	12.87
0.2	21.33	1.24	16.42	0.2	19.38	1.09	14.51	0.1	23.84	1.23	12.11	0.1	21.14	1.16	12.64
0.21	20.98	1.24	16.53	0.21	19.77	1.13	13.65	0.11	23.49	1.23	12.44	0.11	20.59	1.16	12.88
0.23	20.67	1.24	16.83	0.23	19.94	1.09	14.05	0.11	24.04	1.24	13.16	0.11	20.6	1.12	13.04
0.24	20.65	1.24	16.87	0.24	19.33	1.13	13.29	0.12	23.04	1.23	12.77	0.12	20.55	1.13	12.64

0.25	19.98	1.22	17.08	0.25	17.31	1.13	13.7	0.13	23.17	1.23	12.74	0.13	19.05	1.09	12.27
0.27	19.37	1.22	17.43	0.27	18.92	1.14	14.91	0.14	21.98	1.22	12.57	0.14	19.71	1.13	12.41
0.28	19.08	1.22	17.83	0.28	17.49	1.06	13.61	0.14	22.48	1.23	12.84	0.14	18.39	1.11	13.24
0.3	18.3	1.22	18.4	0.3	16.98	1.05	13.44	0.15	21.25	1.18	13.01	0.15	19.51	1.11	12.22
0.31	17.62	1.2	18.72	0.31	16.2	1.07	13.58	0.16	22.2	1.24	13.01	0.16	18.37	1.11	12.75
0.32	16.74	1.2	19.24	0.32	16.4	1.09	13.55	0.16	21.87	1.2	13.11	0.16	17.95	1.1	12.42
0.34	16.17	1.18	19.4	0.34	14.6	1.03	13.02	0.17	22.15	1.22	13.85	0.17	17.87	1.09	13.05
0.35	15.11	1.17	19.89	0.35	15.46	1.11	13.96	0.18	21.4	1.22	13.58	0.18	17.79	1.14	13.21
0.37	14.37	1.14	20.52	0.37	15.84	1.13	14.61	0.19	20.97	1.21	13.44	0.19	18.06	1.13	13.14
0.38	13.6	1.13	20.48	0.38	14.44	1.03	15.76	0.19	21.12	1.22	13.54	0.19	17.77	1.15	13.11
0.4	12.84	1.12	20.73	0.4	14.64	1.09	15.01	0.2	20.83	1.23	14.22	0.2	17.04	1.12	12.9
0.41	12.29	1.11	20.59	0.41	14.11	1.08	14.34	0.21	20.39	1.2	14.32	0.21	16.82	1.09	12.94
0.42	11.94	1.09	20.84	0.42	15.78	1.17	16.44	0.21	20.01	1.2	13.72	0.21	17.74	1.17	14.01
0.44	11.57	1.09	20.82	0.44	15.03	1.11	16.51	0.22	20.01	1.21	14.62	0.22	17.73	1.15	13.38
0.45	11.66	1.12	20.73	0.45	15.29	1.22	17.74	0.23	19.34	1.21	14.56	0.23	17.25	1.18	13.87
0.47	11.34	1.08	20.51	0.47	13.47	1.09	16.41	0.24	19.19	1.2	14.54	0.24	17.65	1.16	13.49
0.48	11.27	1.1	21.08	0.48	12.92	1.08	14.66	0.24	18.61	1.2	15.25	0.24	17.5	1.19	13.83
0.49	11.12	1.1	20.65	0.49	14.05	1.14	16.03	0.25	17.88	1.18	15.32	0.25	17.32	1.18	14.26
0.51	10.8	1.09	20.22	0.51	15.28	1.28	18.7	0.26	17.9	1.18	15.29	0.26	18.37	1.23	14.76
0.52	10.76	1.1	20.42	0.52	14.95	1.21	15.96	0.26	16.64	1.16	15.93	0.26	17.54	1.21	14.29
0.54	10.64	1.11	20.28	0.54	14.54	1.1	16.09	0.27	16.77	1.16	15.88	0.27	17.55	1.28	14.17
0.55	10.51	1.11	20.28	0.55	15.9	1.2	17.1	0.28	16.01	1.15	16.87	0.28	17.22	1.23	14.56
0.57	10.41	1.1	20.21	0.57	14.93	1.13	17.04	0.29	15.89	1.16	16.84	0.29	16.52	1.2	14.57
0.58	10.3	1.1	20.29	0.58	14.47	1.2	16.62	0.29	14.61	1.12	17.05	0.29	17.02	1.22	15.49
0.59	10.26	1.12	20.37	0.59	14.73	1.26	16.53	0.3	14.68	1.14	17.23	0.3	18.32	1.28	15.33
0.61	10.11	1.11	20.12	0.61	13.57	1.14	16.18	0.31	13.74	1.1	17.15	0.31	18.66	1.28	16.11
0.62	10.08	1.14	20.59	0.62	14.53	1.14	17.52	0.31	13.97	1.1	17.22	0.31	17.25	1.27	15.62
0.64	10.19	1.16	20.73	0.64	13.91	1.11	16.84	0.32	13.26	1.12	16.8	0.32	17.4	1.26	15.85
0.65	9.98	1.13	20.6	0.65	13	1.02	15.8	0.33	13.26	1.12	16.73	0.33	17.03	1.23	15.2

0.66	9.94	1.15	20.36	0.66	14.21	1.06	16.73	0.34	12.68	1.08	16.37	0.34	18.4	1.33	16.58
0.68	10.15	1.14	20.49	0.68	12.99	1.06	15.23	0.34	12.12	1.08	16.82	0.34	17.86	1.26	17.14
0.69	9.75	1.16	20.28	0.69	12.77	1.22	15.37	0.35	12.26	1.08	16.7	0.35	17.9	1.28	16.89
0.71	9.73	1.14	20.41	0.71	14.5	1.06	16.99	0.36	12.35	1.09	16.94	0.36	16.93	1.18	15.83
0.72	9.54	1.14	20.07	0.72	13.13	1.16	14.7	0.36	12.44	1.09	16.54	0.36	17.57	1.25	16.29
0.73	9.57	1.17	20.36	0.73	12.56	1.1	15.26	0.37	12.77	1.12	17.44	0.37	17.98	1.22	16.8
0.75	9.67	1.14	20.28	0.75	12.97	1.13	15.23	0.38	11.94	1.1	16.25	0.38	17.64	1.32	16.3
0.76	9.81	1.16	20.42	0.76	12.57	1.03	14.66	0.39	12.05	1.09	17.12	0.39	17.33	1.22	16.04
0.78	10	1.15	20.45	0.78	12.02	1.17	14.99	0.39	11.92	1.09	16.71	0.39	16.99	1.23	15.61
0.79	9.93	1.14	20.35	0.79	12.97	1.09	15.44	0.4	11.57	1.08	16.85	0.4	17.23	1.21	15.89
0.81	10.14	1.14	20.28	0.81	12.51	1.1	14.79	0.41	11.44	1.08	16.08	0.41	17.26	1.24	16.21
0.82	10.49	1.17	20.26	0.82	12.88	1.09	15.23	0.41	11.33	1.11	16.6	0.41	17.7	1.25	16.73
0.83	11.34	1.16	20.03	0.83	11.74	0.94	13.59	0.42	11.29	1.09	16.48	0.42	17.21	1.22	16.13
0.85	11.32	1.17	20.17	0.85	12.3	1.29	16.44	0.43	11.28	1.1	16.81	0.43	16.54	1.18	15.65
0.86	11.62	1.15	20.03	0.86	12.23	1.25	15.62	0.44	11.35	1.09	16.56	0.44	17.95	1.2	16.22
0.88	11.53	1.16	19.85	0.88	12.67	1.15	16.15	0.44	11.21	1.08	16.52	0.44	16.51	1.15	15.76
0.89	11.72	1.15	19.66	0.89	12.82	1.16	16.38	0.45	11.01	1.1	16.76	0.45	16.8	1.21	15.64
0.9	12.04	1.16	19.31	0.9	11.97	1.02	15.03	0.46	11.65	1.14	17.27	0.46	16.22	1.19	16.03
0.92	11.91	1.16	19.27	0.92	12.82	1.13	16.71	0.46	11.25	1.11	16.17	0.46	16.62	1.13	15.53
0.93	11.85	1.16	18.83	0.93	12.59	1.11	15.1	0.47	10.83	1.13	16.32	0.47	16.2	1.13	15.46
0.95	11.88	1.15	18.37	0.95	12.05	1.03	15	0.48	10.67	1.11	16.36	0.48	15.54	1.14	15.09
0.96	12.02	1.15	18.38	0.96	11.9	1.09	14.85	0.49	10.7	1.12	16.28	0.49	16.6	1.19	15.75
0.97	12.02	1.16	18.11	0.97	11.78	0.99	14.13	0.49	11.01	1.15	16.56	0.49	15.76	1.16	15.09
0.99	12.38	1.14	17.94	0.99	12.8	1.26	15.45	0.5	10.71	1.14	16.31	0.5	14.85	1.14	14.85
1	12.81	1.14	17.25	1	12.47	1.11	15.13	0.51	10.63	1.13	16.26	0.51	15.43	1.13	15.48
1.02	13.8	1.16	17.12	1.02	12.83	1.09	15.92	0.51	10.59	1.13	16.18	0.51	15.04	1.11	14.61
1.03	15.23	1.17	16.79	1.03	12.73	1.24	15.1	0.52	10.84	1.14	16.19	0.52	15.76	1.14	15.04
1.05	16.33	1.22	16.21	1.05	13.09	1.06	14.95	0.53	10.51	1.13	16.2	0.53	14.68	1.1	14.48
1.06	17.54	1.2	15.78	1.06	12.12	1.12	16.47	0.54	10.53	1.16	16.92	0.54	15.58	1.11	14.7

1.07	19.68	1.26	15.64	1.07	14.17	1.19	16.68	0.54	10.68	1.16	16.84	0.54	15.21	1.1	14.33
1.09	21.26	1.29	15.39	1.09	12.7	1.22	14.52	0.55	10.59	1.16	16.43	0.55	15.18	1.17	14.79
1.1	22.59	1.31	14.94	1.1	12.28	1.13	15.71	0.56	10.61	1.18	15.91	0.56	14.77	1.11	14.42
1.12	23.76	1.33	14.7	1.12	13.37	1.16	15.58	0.56	10.56	1.16	16.43	0.56	15.08	1.11	14.76
1.13	25.05	1.36	14.82	1.13	12.48	1.19	15.58	0.57	10.6	1.13	16.01	0.57	14.59	1.11	14.53
1.14	25.47	1.35	14.63	1.14	12.19	1.16	14.48	0.58	10.4	1.14	16.3	0.58	14.72	1.13	14.36
1.16	26.26	1.37	14.76	1.16	12.88	1.08	14.38	0.59	10.5	1.15	16.27	0.59	14.63	1.11	14.7
1.17	26.18	1.38	14.66	1.17	12.41	1.2	14.68	0.59	10.16	1.14	15.91	0.59	15.23	1.11	14.74
1.19	25.9	1.35	15.12	1.19	11.78	1.13	14.34	0.6	10.68	1.13	16.15	0.6	15.55	1.15	14.86
1.2	25.97	1.37	15.6	1.2	11.97	1.13	15.31	0.61	10.79	1.15	16.35	0.61	14.64	1.17	14.61
1.22	25.33	1.34	15.51	1.22	12.5	1.34	14.49	0.61	10.97	1.16	16.46	0.61	15.51	1.13	14.57
1.23	24.31	1.35	16.42	1.23	12.61	1.18	15.31	0.62	10.81	1.14	16.34	0.62	15.29	1.18	14.7
1.24	23.15	1.29	16.38	1.24	12.94	1.12	15.88	0.63	10.95	1.14	15.81	0.63	14.99	1.1	14.41
1.26	22.23	1.28	17.04	1.26	12.65	1.24	15.66	0.64	10.88	1.14	15.6	0.64	15.89	1.14	14.85
1.27	21.54	1.24	17.48	1.27	12.34	1.14	14.55	0.64	11.62	1.14	16.32	0.64	15.89	1.17	15.21
1.29	20.67	1.24	17.89	1.29	12.61	1.17	15.92	0.65	11.5	1.14	15.6	0.65	15.43	1.14	14.46
1.3	19.73	1.22	18.04	1.3	13.08	1.3	16.14	0.66	12.24	1.13	15.89	0.66	15.13	1.12	14.89
1.31	18.92	1.19	17.97	1.31	12.86	1.2	15.62	0.66	11.4	1.14	15.55	0.66	16	1.16	14.94
1.33	18.83	1.2	18.61	1.33	13.31	1.26	15.75	0.67	11.79	1.15	15.92	0.67	15.21	1.16	14.8
1.34	17.98	1.17	18.53	1.34	13.34	1.27	15.49	0.68	11.75	1.13	15.66	0.68	15.43	1.19	14.97

11.3 Data (Chapter 5)

11.3.1 EPMA

Table 11-8 EPMA measurements of Sample 11R and 1.2. Measurements are conducted in different sections. Biv A = Bivalve aragonite; Biv C = Bivalve calcite; Biv R = Bivalve callus region; Foram B = Foraminfera on Bivalve; f = fluorescent; nf = non-fluorescent

Sample	Section	Mg/Ca [mmol/mol]	Sr/Ca [mmol/mol]	Na/Ca [mmol/mol]	S/Ca [mmol/mol]	Ca [wt%]	Layer
11R_p1	Biv R	1.05	2.45	25.50	1.21	38.20	nf
11R_p2	Biv R	0.84	2.39	25.73	1.40	38.56	nf
11R_p3	Biv R	0.91	2.13	25.90	1.21	38.56	nf
11R_p4	Biv R	3.48	5.10	24.14	2.40	38.03	nf
11R_p5	Biv R	2.27	9.00	18.50	2.77	38.06	f
11R_p6	Biv R	3.60	3.96	26.81	2.24	38.11	nf
11R_p7	Biv A	1.18	1.38	21.85	1.97	38.44	
11R_p8	Biv C	8.77	0.82	10.78	1.98	38.87	
11R_p9	Biv C	9.85	0.95	13.47	1.30	38.56	
11R_p10	Foram B	61.21	2.41	15.40	5.95	36.87	
11R_p11	Foram B	71.88	2.71	16.67	6.66	36.52	
11R_p12	Foram B	53.37	2.81	17.58	2.10	37.45	
11R_p13	Foram B	64.19	2.31	15.02	3.98	36.71	
11R_p14	Foram B	26.79	1.88	11.78	0.63	37.99	
11R_p15	Foram B	36.60	2.27	13.25	1.03	37.39	
11R_p16	Biv C	13.65	0.92	13.47	1.74	38.85	
11R_p17	Biv C	11.68	0.87	18.28	1.31	37.93	
11R_p18	Biv C	10.32	0.76	15.86	1.23	38.52	
11R_p19	Biv A	0.43	1.24	23.81	1.91	38.51	
11R_p20	Biv R	3.27	6.30	23.12	4.06	37.41	f
11R_p21	Biv R	3.37	7.91	22.23	4.36	37.35	f
1.2_P1	Biv C	7.97	1.12	16.07	2.99	38.22	
1.2_P2	Biv C	9.18	0.90	20.17	2.26	37.75	
1.2_P3	Biv C	11.37	0.94	19.42	4.02	38.66	
1.2_P4	Biv C	8.21	0.90	13.03	2.23	38.11	
1.2_P5	Biv A		1.61	22.59	2.13	38.08	
1.2_P6	Biv A	1.44	1.83	17.31	2.17	38.25	
1.2_P7	Biv A	0.25	1.24	21.56	1.97	38.38	
1.2_P8	Biv A		1.23	20.58	1.36	38.30	
1.2_P9	Biv A	0.91	1.75	19.80	2.37	38.45	
1.2_P10	Biv A	0.76	1.75	19.57	1.89	38.57	
1.2_P11	Biv R	4.87	7.84	34.92	11.08	36.85	f
1.2_P12	Biv R	3.49	7.08	26.06	3.65	37.23	nf
1.2_P13	Biv R	5.61	7.09	25.26	3.31	37.01	nf
1.2_P14	Biv R	6.69	5.46	26.34	7.87	36.82	f
1.2_P15	Biv R	5.49	8.23	28.70	5.94	37.06	f
1.2_P16	Biv R	5.16	5.49	28.54	2.47	37.66	nf
1.2_P17	Biv R	4.53	5.94	27.76	2.64	37.65	nf
1.2_P18	Foram B	56.57	2.13	14.30	3.42	37.44	

1.2_P19	Foram B	33.44	2.44	15.84	0.97	37.89	
1.2_P20	Foram B	41.42	2.28	14.93	1.70	37.66	
1.2_P21	Foram B	80.60	2.85	17.17	9.38	36.76	
1.2_P22	Foram B	27.71	2.31	13.04	0.60	38.41	
1.2_P23	Foram B	24.21	2.12	15.85	0.41	37.89	
1.2_P24	Foram B	29.25	2.48	14.17	1.43	37.51	
1.2_P25	Foram B	51.90	2.86	18.20	5.76	37.36	
1.2_P26	Foram B	31.58	2.23	12.59	1.31	37.79	
1.2_P27	Foram B	29.72	1.94	10.47	0.50	38.01	
11R Line	Biv C	7.98	0.74	9.94	1.48	39.28	
11R Line	Biv C	7.25	0.80	9.64	2.02	38.83	
11R Line	Biv A	0.26	1.60	24.64	1.55	38.18	
11R Line	Biv A	0.30	1.65	25.23	1.87	38.00	
11R Line	Biv A	0.16	1.60	24.53	1.63	38.27	
11R Line	Biv A	0.25	1.36	22.81	1.86	38.11	
11R Line	Biv A	0.64	1.50	22.66	1.82	38.35	
11R Line	Biv A	1.46	1.75	20.59	2.27	38.35	
11R Line	Biv R	2.63	6.37	19.21	4.70	36.95	f
11R_p22	Biv R	2.82	7.65	22.01	3.49	37.56	f

11.3.2 ICP-OES

Table 11-9 ICP-OES measurements of *H. sarcophaga* from different hosts and measurements of the according host species. acesta/o = Acesta without shell penetration, acesta/m = Acesta with shell penetration.

Sample	Mg/Ca	Na/Ca	Sr/Ca	Mn/Ca	Material	Host	Organism
O1_2	43.74	13.69	2.43	0.08	calcite	acesta/o	*H. sarcophaga*
O2_2	33.56	12.97	2.10	0.05	calcite	acesta/o	*H. sarcophaga*
O3_2	33.35	13.31	2.28	0.04	calcite	acesta/o	*H. sarcophaga*
O4_2	43.17	20.19	2.45	0.08	calcite	acesta/o	*H. sarcophaga*
O5_2	35.98	23.20	1.08	0.11	calcite	acesta/o	*H. sarcophaga*
O6_2	45.10	23.23	1.21	0.13	calcite	acesta/o	*H. sarcophaga*
O7_2	42.30	14.73	2.30	0.04	calcite	acesta/o	*H. sarcophaga*
O8_2	44.38	13.65	2.34	0.05	calcite	acesta/o	*H. sarcophaga*
O9_2	51.74	20.86	2.49	0.08	calcite	acesta/o	*H. sarcophaga*
O10_2	53.20	19.81	2.52	0.10	calcite	acesta/o	*H. sarcophaga*
M1_2	43.66	15.40	2.50	0.04	calcite	acesta/m	*H. sarcophaga*
M2_2	53.47	17.18	2.54	0.02	calcite	acesta/m	*H. sarcophaga*
M3_2	45.01	13.53	2.12	0.01	calcite	acesta/m	*H. sarcophaga*
M4_2	53.05	17.31	2.56	0.01	calcite	acesta/m	*H. sarcophaga*
M5_2	35.15	14.67	2.26	0.03	calcite	acesta/m	*H.*

							sarcophaga
M6_2	49.68	17.83	2.44	0.02	calcite	acesta/m	*H. sarcophaga*
M7_2	41.98	14.65	2.39	0.01	calcite	acesta/m	*H. sarcophaga*
M8_2	50.51	18.16	2.49	0.02	calcite	acesta/m	*H. sarcophaga*
M9_2	34.57	12.39	2.21	0.01	calcite	acesta/m	*H. sarcophaga*
M10_2	36.91	12.97	2.17	0.01	calcite	acesta/m	*H. sarcophaga*
L1_2	43.11	17.03	4.10	0.01	calcite	lophelia	*H. sarcophaga*
L2_2	38.78	16.39	3.61	0.00	calcite	lophelia	*H. sarcophaga*
L3_2	42.51	16.41	4.05	0.01	calcite	lophelia	*H. sarcophaga*
L4_2	45.65	15.57	3.43	0.03	calcite	lophelia	*H. sarcophaga*
L5_2	37.15	12.63	3.98	0.00	calcite	lophelia	*H. sarcophaga*
L6_2	31.98	12.46	4.49	0.00	calcite	lophelia	*H. sarcophaga*
L7_2	36.37	17.57	3.30	0.01	calcite	lophelia	*H. sarcophaga*
L8_2	53.27	18.06	2.54	0.02	calcite	lophelia	*H. sarcophaga*
L9_2	52.26	15.36	2.42	0.01	calcite	lophelia	*H. sarcophaga*
L10_2	43.39	13.19	3.12	0.01	calcite	lophelia	*H. sarcophaga*
lophelia	3.14	29.92	10.21		aragonite	host Desmophyllum	*D. pertusum*
lophelia	4.13	28.98	10.17		aragonite	host Desmophyllum	*D. pertusum*
lophelia	3.87	27.66	10.18		aragonite	host Desmophyllum	*D. pertusum*
lophelia	4.17	29.51	10.35		aragonite	host Desmophyllum	*D. pertusum*
lophelia	3.88	28.22	9.94		aragonite	host Desmophyllum	*D. pertusum*
lophelia	4.05	30.29	9.97		aragonite	host Desmophyllum	*D. pertusum*
lophelia	4.35	31.24	10.30		aragonite	host Desmophyllum	*D. pertusum*
lophelia	4.03	30.34	10.26		aragonite	host Desmophyllum	*D. pertusum*
lophelia	4.39	31.54	10.19		aragonite	host Desmophyllum	*D. pertusum*
lophelia	6.06	27.85	10.35		aragonite	host Desmophyllum	*D. pertusum*
lophelia	8.61	30.12	9.60		aragonite	host Desmophyllum	*D. pertusum*
lophelia	8.83	28.58	9.38		aragonite	host Desmophyllum	*D. pertusum*
lophelia	2.20	21.12	10.00		aragonite	host Desmophyllum	*D. pertusum*
lophelia	3.25	24.61	10.05		aragonite	host Desmophyllum	*D. pertusum*
lophelia	3.55	25.79	10.30		aragonite	host Desmophyllum	*D. pertusum*
lophelia	2.83	23.37	10.43		aragonite	host Desmophyllum	*D. pertusum*
lophelia	3.22	24.11	10.52		aragonite	host Desmophyllum	*D. pertusum*
lophelia	2.97	22.75	10.27		aragonite	host Desmophyllum	*D. pertusum*
lophelia	3.83	22.71	10.30		aragonite	host Desmophyllum	*D. pertusum*
lophelia	3.54	24.88	10.22		aragonite	host Desmophyllum	*D. pertusum*
lophelia	3.49	25.32	10.38		aragonite	host Desmophyllum	*D. pertusum*
lophelia	3.48	25.58	10.44		aragonite	host Desmophyllum	*D. pertusum*
lophelia	3.18	24.10	10.06		aragonite	host Desmophyllum	*D. pertusum*
lophelia	3.28	23.24	10.36		aragonite	host Desmophyllum	*D. pertusum*
lophelia	2.74	26.31	10.42		aragonite	host Desmophyllum	*D. pertusum*
lophelia	3.46	27.49	10.25		aragonite	host Desmophyllum	*D. pertusum*

lophelia	3.62	30.38	10.23		aragonite	host Desmophyllum	*D. pertusum*
lophelia	3.72	26.31	10.11		aragonite	host Desmophyllum	*D. pertusum*
lophelia	3.18	25.42	10.33		aragonite	host Desmophyllum	*D. pertusum*
lophelia	3.14	25.88	10.16		aragonite	host Desmophyllum	*D. pertusum*
lophelia	4.12	26.77	10.10		aragonite	host Desmophyllum	*D. pertusum*
lophelia	4.12	26.04	10.06		aragonite	host Desmophyllum	*D. pertusum*
lophelia	6.06	27.27	10.35		aragonite	host Desmophyllum	*D. pertusum*
lophelia	4.22	27.90	8.95		aragonite	host Desmophyllum	*D. pertusum*
lophelia	4.10	27.74	9.96		aragonite	host Desmophyllum	*D. pertusum*
lophelia	4.31	29.65	10.02		aragonite	host Desmophyllum	*D. pertusum*
lophelia	4.43	24.41	9.43		aragonite	host Desmophyllum	*D. pertusum*
lophelia	4.29	24.85	10.03		aragonite	host Desmophyllum	*D. pertusum*
lophelia	4.50	25.64	9.69		aragonite	host Desmophyllum	*D. pertusum*
lophelia	8.02	24.12	9.77		aragonite	host Desmophyllum	*D. pertusum*
lophelia	7.30	23.43	9.18		aragonite	host Desmophyllum	*D. pertusum*
lophelia	5.83	26.43	10.11		aragonite	host Desmophyllum	*D. pertusum*
lophelia	6.77	25.05	10.18		aragonite	host Desmophyllum	*D. pertusum*
lophelia	2.86	20.53	10.25		aragonite	host Desmophyllum	*D. pertusum*
lophelia	2.99	21.42	10.33		aragonite	host Desmophyllum	*D. pertusum*
9R	20.71	18.30	1.44	0.09	calcite	host Acesta	*A. excavata*
9R	23.74	22.33	1.42	0.11	calcite	host Acesta	*A. excavata*
9R	27.48	17.36	1.36	0.11	calcite	host Acesta	*A. excavata*
9R	22.98	17.64	1.37	0.10	calcite	host Acesta	*A. excavata*
9R	21.90	16.81	1.41	0.11	calcite	host Acesta	*A. excavata*
9R	20.77	17.88	1.38	0.13	calcite	host Acesta	*A. excavata*
9R	22.91	19.55	1.34	0.08	calcite	host Acesta	*A. excavata*
9R	30.84	14.43	1.43	0.11	calcite	host Acesta	*A. excavata*
9R	24.79	14.57	1.27	0.09	calcite	host Acesta	*A. excavata*
9R	23.51	16.36	1.26	0.10	calcite	host Acesta	*A. excavata*
9R	26.11	19.23	1.32	0.10	calcite	host Acesta	*A. excavata*
9R	23.36	17.54	1.25	0.11	calcite	host Acesta	*A. excavata*
9R	18.20	19.59	1.29	0.10	calcite	host Acesta	*A. excavata*
9R	18.25	21.02	1.25	0.10	calcite	host Acesta	*A. excavata*
9R	25.50	22.23	1.21	0.13	calcite	host Acesta	*A. excavata*
11R	21.57	22.03	1.35	0.09	calcite	host Acesta	*A. excavata*
11R	17.06	19.83	1.31	0.16	calcite	host Acesta	*A. excavata*
11R	16.70	19.21	1.25	0.16	calcite	host Acesta	*A. excavata*
11R	20.73	17.76	1.23	0.08	calcite	host Acesta	*A. excavata*
11R	19.85	13.06	1.28	0.15	calcite	host Acesta	*A. excavata*
11R	22.16	15.90	1.28	0.15	calcite	host Acesta	*A. excavata*
11R	23.94	12.17	1.19	0.17	calcite	host Acesta	*A. excavata*
11R	19.31	15.50	1.13	0.17	calcite	host Acesta	*A. excavata*
11R	15.91	18.92	1.23	0.18	calcite	host Acesta	*A. excavata*
11R	17.95	16.05	1.12	0.13	calcite	host Acesta	*A. excavata*
11R	14.27	16.15	1.12	0.12	calcite	host Acesta	*A. excavata*
11R	12.00	20.70	1.13	0.12	calcite	host Acesta	*A. excavata*
11R	13.40	18.86	1.18	0.13	calcite	host Acesta	*A. excavata*

11R	15.72	9.75	1.15	0.11	calcite	host Acesta	*A. excavata*
11R	13.39	55.62	1.06	0.12	calcite	host Acesta	*A. excavata*
12R	16.23	9.78	1.22	0.13	calcite	host Acesta	*A. excavata*
12R	15.82	21.49	1.28	0.14	calcite	host Acesta	*A. excavata*
12R	12.58	16.56	1.21	0.14	calcite	host Acesta	*A. excavata*
12R	18.90	20.04	1.10	0.15	calcite	host Acesta	*A. excavata*
12R	13.95	22.07	1.15	0.13	calcite	host Acesta	*A. excavata*
12R	16.57	21.54	1.22	0.15	calcite	host Acesta	*A. excavata*
12R	18.13	13.97	1.20	0.14	calcite	host Acesta	*A. excavata*
12R	14.08	15.02	1.04	0.17	calcite	host Acesta	*A. excavata*
12R	16.38	22.86	1.02	0.14	calcite	host Acesta	*A. excavata*
12R	14.37	20.80	1.04	0.17	calcite	host Acesta	*A. excavata*
12R	12.03	31.54	1.06	0.18	calcite	host Acesta	*A. excavata*
12R	16.85	25.93	0.99	0.20	calcite	host Acesta	*A. excavata*
12R	14.67	33.50	1.00	0.15	calcite	host Acesta	*A. excavata*
12R	15.24	28.05	0.97	0.14	calcite	host Acesta	*A. excavata*
SHA3	4.37		10.56	0.01	aragonite	host Desmophyllum	*A. excavata*
SHA3	4.36		10.71	0.01	aragonite	host Desmophyllum	*A. excavata*
SHA9	3.93		10.30	0.01	aragonite	host Desmophyllum	*A. excavata*
SHA9`	3.93		10.24	0.01	aragonite	host Desmophyllum	*A. excavata*
SHA19	4.25		10.38	0.01	aragonite	host Desmophyllum	*A. excavata*
SHA19´	4.24		10.37	0.01	aragonite	host Desmophyllum	*A. excavata*

11.3.3 MS

Table 11-10 Oxygen- and carbon isotopic composition of *H. sarcophaga* from different hosts and the according hosts as well as from the ambient seawater. acesta/o = Acesta without shell penetration, acesta/m = Acesta with shell penetration.

ID	$\delta^{13}C$	$\delta^{18}O$	material	host	organism
O1	-0.52	1.77	calcite	acesta/o	*H. sarcophaga*
O2	-0.43	2.11	calcite	acesta/o	*H. sarcophaga*
O3	0.45	1.82	calcite	acesta/o	*H. sarcophaga*
O4	-0.03	1.93	calcite	acesta/o	*H. sarcophaga*
O5	-1.06	1.47	calcite	acesta/o	*H. sarcophaga*
O6	-0.92	1.59	calcite	acesta/o	*H. sarcophaga*
O7	-0.91	1.54	calcite	acesta/o	*H. sarcophaga*
O8	-0.56	1.88	calcite	acesta/o	*H. sarcophaga*
O9	-0.41	2.13	calcite	acesta/o	*H. sarcophaga*
M1	-0.11	1.76	calcite	acesta/m	*H. sarcophaga*
M2	0.12	1.96	calcite	acesta/m	*H. sarcophaga*
M3	-1.40	1.23	calcite	acesta/m	*H. sarcophaga*
M4	-0.60	1.67	calcite	acesta/m	*H.*

					sarcophaga
M5	-0.43	1.76	calcite	acesta/m	*H. sarcophaga*
M6	-0.06	1.79	calcite	acesta/m	*H. sarcophaga*
M7	-0.25	1.60	calcite	acesta/m	*H. sarcophaga*
M8	0.03	1.96	calcite	acesta/m	*H. sarcophaga*
M9	-0.67	1.85	calcite	acesta/m	*H. sarcophaga*
L1	-4.67	1.64	calcite	Desmophyllum	*H. sarcophaga*
L2	-5.00	0.99	calcite	Desmophyllum	*H. sarcophaga*
L3	-3.33	1.56	calcite	Desmophyllum	*H. sarcophaga*
L4	-3.67	1.75	calcite	Desmophyllum	*H. sarcophaga*
L5	-3.15	1.64	calcite	Desmophyllum	*H. sarcophaga*
L6	-3.65	1.52	calcite	Desmophyllum	*H. sarcophaga*
L7	-3.22	1.62	calcite	Desmophyllum	*H. sarcophaga*
L8	-3.74	1.30	calcite	Desmophyllum	*H. sarcophaga*
L9	-2.90	1.54	calcite	Desmophyllum	*H. sarcophaga*
L10	-2.76	1.51	calcite	Desmophyllum	*H. sarcophaga*
a1-3	0.30	1.93	calcite		*A. excavata*
a2-3	0.40	1.99	calcite		*A. excavata*
a3-3	0.44	1.92	calcite		*A. excavata*
a4-3	0.42	1.87	calcite		*A. excavata*
a5-3	0.34	1.65	calcite		*A. excavata*
a6-3	0.41	1.88	calcite		*A. excavata*
a7-3	0.38	2.02	calcite		*A. excavata*
a8-3	0.24	1.96	calcite		*A. excavata*
a9-3	0.27	1.89	calcite		*A. excavata*
a11-3	0.22	1.93	calcite		*A. excavata*
a12-3	0.35	1.92	calcite		*A. excavata*
a13-3	0.26	1.86	calcite		*A. excavata*
a14-3	-0.04	1.90	calcite		*A. excavata*
a15-3	0.18	1.97	calcite		*A. excavata*
a16-3	-0.03	2.01	calcite		*A. excavata*
a17-3	0.09	2.00	calcite		*A. excavata*
a18-3	-0.03	1.95	calcite		*A. excavata*
a19-3	0.06	1.91	calcite		*A. excavata*
a20-3	-0.11	1.98	calcite		*A. excavata*
a21-3	0.00	1.96	calcite		*A. excavata*
b1-3	0.72	1.90	calcite		*A. excavata*
b2-3	0.62	1.83	calcite		*A. excavata*
b3-3	0.58	1.80	calcite		*A. excavata*
b4-3	0.50	1.52	calcite		*A. excavata*
b5-3	0.72	1.75	calcite		*A. excavata*
b6-3	0.76	1.82	calcite		*A. excavata*

b7-3	0.70	1.85	calcite	*A. excavata*
b8-3	0.63	1.88	calcite	*A. excavata*
b9-3	0.53	1.82	calcite	*A. excavata*
b10-3	0.54	1.84	calcite	*A. excavata*
b11-3	0.55	1.80	calcite	*A. excavata*
b12-3	0.44	1.93	calcite	*A. excavata*
b13-3	0.48	1.82	calcite	*A. excavata*
b14-3	0.49	1.91	calcite	*A. excavata*
b15-3	0.35	1.81	calcite	*A. excavata*
b16-3	0.42	1.91	calcite	*A. excavata*
b17-3	0.25	1.90	calcite	*A. excavata*
b18-3	0.31	1.84	calcite	*A. excavata*
b19-3	0.34	1.87	calcite	*A. excavata*
b20-3	0.20	1.99	calcite	*A. excavata*
c1-3	0.82	1.95	calcite	*A. excavata*
c2-3	0.76	1.79	calcite	*A. excavata*
c3-3	0.74	2.04	calcite	*A. excavata*
c4-3	0.61	1.89	calcite	*A. excavata*
c5-3	0.68	1.86	calcite	*A. excavata*
c6-3	0.32	1.83	calcite	*A. excavata*
c7-3	0.48	1.90	calcite	*A. excavata*
c8-3	0.37	1.84	calcite	*A. excavata*
c9-3	0.31	1.80	calcite	*A. excavata*
c10-3	0.68	1.84	calcite	*A. excavata*
c11-3	0.69	1.96	calcite	*A. excavata*
c12-3	0.72	1.95	calcite	*A. excavata*
c13-3	0.68	1.91	calcite	*A. excavata*
c14-3	0.90	1.84	calcite	*A. excavata*
c15-3	1.03	1.81	calcite	*A. excavata*
c16-3	0.85	2.09	calcite	*A. excavata*
c17-3	0.82	1.96	calcite	*A. excavata*
c18-3	0.81	1.84	calcite	*A. excavata*
c19-3	1.04	1.86	calcite	*A. excavata*
c20-3	0.97	1.92	calcite	*A. excavata*
c21-3	0.84	2.14	calcite	*A. excavata*
c22-3	0.66	2.02	calcite	*A. excavata*
c23-3	0.75	2.09	calcite	*A. excavata*
1-1-1	-6.63	-1.27	aragonite	*D. pertusum*
1-1-2	-5.42	-0.78	aragonite	*D. pertusum*
1-1-4	-7.54	-1.02	aragonite	*D. pertusum*
1-1-5	-6.35	-1.14	aragonite	*D. pertusum*
1-2-2	-6.79	-1.47	aragonite	*D. pertusum*
1-2-5	-7.71	-1.87	aragonite	*D. pertusum*
1-3-1	-7.17	-1.45	aragonite	*D. pertusum*
1-3-2	-5.97	-1.21	aragonite	*D. pertusum*
1-3-4	-6.01	-0.69	aragonite	*D. pertusum*
2-1-1	-4.14	0.37	aragonite	*D. pertusum*

2-1-2	-5.67	-0.85	aragonite	*D. pertusum*
2-1-3	-5.96	-0.95	aragonite	*D. pertusum*
2-1-4	-5.43	0.00	aragonite	*D. pertusum*
2-2-1	-3.79	-0.04	aragonite	*D. pertusum*
2-2-2	-3.29	0.54	aragonite	*D. pertusum*
2-2-3	-6.68	-1.51	aragonite	*D. pertusum*
2-2-5	-7.19	-1.59	aragonite	*D. pertusum*
2-2-6	-7.54	-1.79	aragonite	*D. pertusum*
2-2-7	-5.09	-0.19	aragonite	*D. pertusum*
2-3-1	-3.97	-0.23	aragonite	*D. pertusum*
2-3-2	-5.34	-0.88	aragonite	*D. pertusum*
2-3-3	-5.39	-0.64	aragonite	*D. pertusum*
2-3-4	-6.22	-1.06	aragonite	*D. pertusum*
2-3-5	-7.05	-1.11	aragonite	*D. pertusum*
3-1-1	-6.37	-1.03	aragonite	*D. pertusum*
3-1-2	-6.49	-0.88	aragonite	*D. pertusum*
3-1-3	-7.15	-0.98	aragonite	*D. pertusum*
3-1-4	-8.89	-1.93	aragonite	*D. pertusum*
3-1-5	-7.91	-1.19	aragonite	*D. pertusum*
3-2-2	-6.82	-0.94	aragonite	*D. pertusum*
3-2-3	-8.08	-1.45	aragonite	*D. pertusum*
3-2-4	-8.23	-1.43	aragonite	*D. pertusum*
3-2-5	-5.89	0.34	aragonite	*D. pertusum*
3-3-1	-7.08	-0.82	aragonite	*D. pertusum*
3-3-4	-7.45	-0.91	aragonite	*D. pertusum*
3-3-5	-9.14	-1.90	aragonite	*D. pertusum*
3-3-6	-9.40	-1.00	aragonite	*D. pertusum*
2-1-6	-7.47	-1.93	aragonite	*D. pertusum*
1-1-6	-6.85	-1.73	aragonite	*D. pertusum*
1-2-6	-7.67	-1.82	aragonite	*D. pertusum*
1-3-6	-6.57	-0.92	aragonite	*D. pertusum*
Water Nord	0.36	0.18	water	water
Water Nord	0.38	0.26	water	water
Water Nord	0.36	0.27	water	water

11.4 Data (Chapter 6)

11.4.1 Carbonate

Table 11-11 Results of ICP-OES measurements on different organisms after ethanol preservation.

Sample	Species	Time in ethanol [months]	Mg/Ca [mmol/mol]	Na/Ca [mmol/mol]	Sr/Ca [mmol/mol]
2107	*Chlamys islandica*	0	11.40	15.16	1.25
2107	*Chlamys islandica*	0	10.10	14.98	1.25
2107	*Chlamys islandica*	0	9.75	14.48	1.31
2107	*Chlamys islandica*	3	10.20	12.63	1.16
2107	*Chlamys islandica*	3	10.54	13.17	1.19

2107	*Chlamys islandica*	3	9.75	12.67	1.19
2107	*Chlamys islandica*	4,5	10.51	11.78	1.30
2107	*Chlamys islandica*	4,5	10.08	11.59	1.26
2107	*Chlamys islandica*	4,5	9.74	11.31	1.34
2107	*Chlamys islandica*	6	9.64	11.36	1.28
2107	*Chlamys islandica*	6	8.76	11.65	1.24
2107	*Chlamys islandica*	6	9.18	11.22	1.29
B1	*Delectopecten vitreus*	0	9.00	14.67	1.10
B1	*Delectopecten vitreus*	0	9.18	14.06	1.04
B1	*Delectopecten vitreus*	0	10.46	15.34	1.05
B1	*Delectopecten vitreus*	1,5	8.69	14.06	1.10
B1	*Delectopecten vitreus*	1,5	9.09	13.89	1.11
B1	*Delectopecten vitreus*	1,5	9.18	14.19	1.16
B1	*Delectopecten vitreus*	3	8.37	12.19	1.08
B1	*Delectopecten vitreus*	3	8.32	13.07	1.11
B1	*Delectopecten vitreus*	3	9.54	12.47	1.10
B2	*Acesta excavata*	0	3.08	21.54	2.59
B2	*Acesta excavata*	0	2.82	20.37	2.16
B2	*Acesta excavata*	0	3.11	21.20	2.17
B2	*Acesta excavata*	1,5	2.93	18.32	2.76
B2	*Acesta excavata*	1,5	2.49	18.93	3.11
B2	*Acesta excavata*	1,5	2.53	18.51	2.87
B2	*Acesta excavata*	3	1.44	17.58	2.50
B2	*Acesta excavata*	3	1.24	16.65	2.44
B2	*Acesta excavata*	3	1.15	17.51	2.51
B3	*Chlamys islandica*	0	11.11	18.00	1.33
B3	*Chlamys islandica*	0	11.46	19.15	1.33
B3	*Chlamys islandica*	0	11.50	17.32	1.31
B3	*Chlamys islandica*	1,5	10.91	10.39	1.26
B3	*Chlamys islandica*	1,5	11.89	10.87	1.23
B3	*Chlamys islandica*	1,5	11.18	10.79	1.25
B3	*Chlamys islandica*	3	9.94	10.09	1.23
B3	*Chlamys islandica*	3	10.93	10.42	1.24
B3	*Chlamys islandica*	3	10.55	10.10	1.22
B4	*Delectopecten vitreus*	0	16.51	35.30	1.19
B4	*Delectopecten vitreus*	0	13.89	37.05	1.43
B4	*Delectopecten vitreus*	0	14.34	30.15	1.19
B4	*Delectopecten vitreus*	3	9.83	12.22	1.21
B4	*Delectopecten vitreus*	3	9.81	11.73	1.22
B4	*Delectopecten vitreus*	3	10.21	11.97	1.18
B4	*Delectopecten vitreus*	4,5	7.26	14.27	1.05

B4	*Delectopecten vitreus*	4,5	6.68	14.49	1.05
B4	*Delectopecten vitreus*	4,5	6.61	14.23	1.04
B4	*Delectopecten vitreus*	6	7.94	12.09	1.12
B4	*Delectopecten vitreus*	6	7.88	12.29	1.16
B4	*Delectopecten vitreus*	6	7.75	12.45	1.15
E1	*Enallopsammia rostrata*	0	6.68	40.57	10.76
E1	*Enallopsammia rostrata*	0	6.33	40.04	10.86
E1	*Enallopsammia rostrata*	0	7.10	35.78	10.05
E1	*Enallopsammia rostrata*	1,5	4.70	23.00	10.82
E1	*Enallopsammia rostrata*	1,5	3.76	21.28	11.05
E1	*Enallopsammia rostrata*	1,5	4.48	22.07	11.14
E1	*Enallopsammia rostrata*	3	2.11	22.36	10.76
E1	*Enallopsammia rostrata*	3	1.91	21.72	10.51
E1	*Enallopsammia rostrata*	3	1.83	21.96	10.84
Lo1	*Desmophyllum pertusum*	0	5.18	24.99	10.14
Lo1	*Desmophyllum pertusum*	0	4.89	27.91	10.17
Lo1	*Desmophyllum pertusum*	0	4.99	26.79	10.80
Lo1	*Desmophyllum pertusum*	1,5	3.89	23.36	10.21
Lo1	*Desmophyllum pertusum*	1,5	4.32	22.74	10.36
Lo1	*Desmophyllum pertusum*	1,5	4.45	23.02	10.22
Lo1	*Desmophyllum pertusum*	3	3.25	23.92	10.38
Lo1	*Desmophyllum pertusum*	3	3.21	21.50	10.49
Lo1	*Desmophyllum pertusum*	3	3.00	21.51	10.55
H1	*Hyrrokkin sarcophaga*	0	54.89	35.18	2.23
H1	*Hyrrokkin sarcophaga*	0	43.62	33.10	2.16
H1	*Hyrrokkin sarcophaga*	0	49.39	37.30	2.20
H1	*Hyrrokkin sarcophaga*	1,5	50.47	29.54	2.86
H1	*Hyrrokkin sarcophaga*	1,5	50.50	26.31	2.52
H1	*Hyrrokkin sarcophaga*	1,5	51.92	32.36	2.51
H1	*Hyrrokkin sarcophaga*	3	48.33	20.11	2.39
H1	*Hyrrokkin sarcophaga*	3	47.58	22.27	2.28
H1	*Hyrrokkin sarcophaga*	3	50.70	23.01	2.33
616	*Madrepora oculata*	0	4.77	23.78	10.26
616	*Madrepora oculata*	0	4.42	24.13	10.64
616	*Madrepora oculata*	0	4.92	23.77	10.55

616	*Madrepora oculata*	1,5	3.58	23.11	10.53
616	*Madrepora oculata*	1,5	3.58	22.53	10.29
616	*Madrepora oculata*	1,5	3.75	23.40	10.59
616	*Madrepora oculata*	3	2.81	22.43	10.50
616	*Madrepora oculata*	3	2.97	23.40	10.75
616	*Madrepora oculata*	3	2.73	22.05	10.55
1668	*Acesta excavata*	0	12.02	20.58	1.08
1668	*Acesta excavata*	0	10.87	21.11	1.07
1668	*Acesta excavata*	0	11.44	22.09	1.08
1668	*Acesta excavata*	3	10.47	17.62	1.12
1668	*Acesta excavata*	3	10.91	17.05	1.08
1668	*Acesta excavata*	3	10.79	17.61	1.09
1668	*Acesta excavata*	4,5	10.79	16.13	1.19
1668	*Acesta excavata*	4,5	10.10	17.24	1.14
1668	*Acesta excavata*	4,5	9.19	16.97	1.10
1668	*Acesta excavata*	6	9.67	16.54	1.10
1668	*Acesta excavata*	6	8.65	15.87	1.04
1668	*Acesta excavata*	6	8.88	14.69	1.07
2106	*Arctica islandica*	0	1.05	19.62	2.40
2106	*Arctica islandica*	0	1.38	20.09	2.49
2106	*Arctica islandica*	0	1.73	19.57	2.56
2106	*Arctica islandica*	1,5	1.04	18.79	2.60
2106	*Arctica islandica*	1,5	1.14	19.30	2.52
2106	*Arctica islandica*	1,5	1.08	18.96	2.50
2106	*Arctica islandica*	3	0.57	18.80	2.53
2106	*Arctica islandica*	3	0.35	18.16	2.62
2106	*Arctica islandica*	3	0.48	17.97	2.56

11.4.2 Ethanol

Table 11-12 Elemental concentration of Mg, Na and Sr in preservation ethanol.

Sample	Mg [mg/l]	Na [mg/l]	Sr [mg/l]
1668	5543	49832	21
2106	462	1223	260
2107	931	15055	0
616	6889	35271	1700
B1	801	7065	0
B2	0	0	0
B3	1093	15085	0
B4	186	1396	0
E1	12251	264056	0
H1	1785	33978	90
Lo1	4917	40048	277